Optical Transmitters and Receivers (OTR)

When: Tue 08:00–09:30 8L
Fri 09:45–11:15 8L
Fri 11:30–12:15 13T (begin 30.10.15)

Where: Bldg. 30.10 Room 3.42 (L+T)

Lecturer: Prof. Dr. Wolfgang Freude
Tutors: Juned N. Kemal, M.Sc.
Pablo Marin Palomo, M.Sc.
Heiner Zwickel, M.Sc.

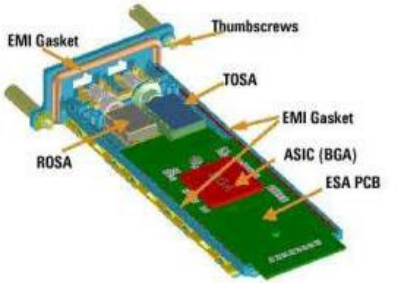

Contents:

- Optical communication concepts
- Transmitters
  - Light sources
  - Modulators
- Optical amplifiers
- Receivers
  - Pin photodiode
  - Noise
  - Detection errors

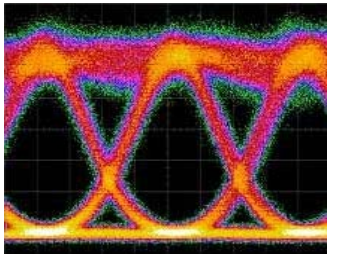

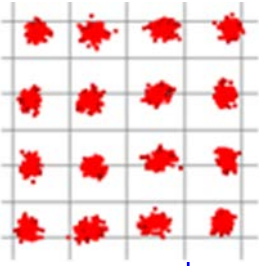

Lectures (Room 3.42, Build. 30.10)

PI avoid unnecessary emails.
However, I am more than ready for Q&A.

1.	Tue	20.10.15 08:00	
2.	Fri	23.10.15 09:45	
3.	Tue	03.11.15 08:00	
4.	Fri	06.11.15 09:45	
5.	Tue	10.11.15 08:00	
6.	Fri	13.11.15 09:45	
A.	Tue	17.11.15 08:00	Q&A 1
B.	Fri	20.11.15 09:45	Q&A 2
7.	Tue	24.11.15 08:00	
8.	Fri	27.11.15 09:45	
9.	Tue	01.12.15 08:00	
10.	Fri	04.12.15 09:45	
11.	Tue	08.12.15 08:00	
12.	Fri	11.12.15 09:45	
C.	Tue	15.12.15 08:00	Q&A 3
D.	Fri	18.12.15 09:45	Q&A 4
13.	Tue	12.01.16 08:00	
14.	Fri	15.01.16 09:45	
15.	Tue	19.01.16 08:00	
16.	Fri	22.01.16 09:45	
E.	Tue	26.01.16 08:00	Q&A 5
F.	Fri	29.01.16 09:45	Q&A 6

Tutorial (Room 3.42, Build. 30.10)

First Fri 30.10.15 11:30–12:15

Last Fri 05.02.16 11:30–12:15

Total of 13 tutorials

Lab Tour OTR, FPC, etc. (IPQ)

- Fri 29.01.16 11:30–13:00

Examinations (in my office)

1. Wed 03.02.16 13:00–19:00
2. Wed 10.02.16 13:00–19:00
3. *Normally* once a month

LECTURE 1

Introduction

Why optical communications?

- Based on inexpensive extremely broadband glass fibres
- Fast transmitters with semiconductor lasers
- Fast receivers with semiconductor photodetectors
- Optical broadband amplifiers available

Lightwave technology developed over the last 40 years has greatly infuenced our needs for communication. Resources made accessible in the World Wide Web (WWW) have changed our attitude towards information acquisition, which is being regarded as an everyday's necessity, and even as a natural right for everybody. Today's undersea and underground optical cables provide large-capacity links carrying more than 90 % of the communication traffic.

Communication With Light

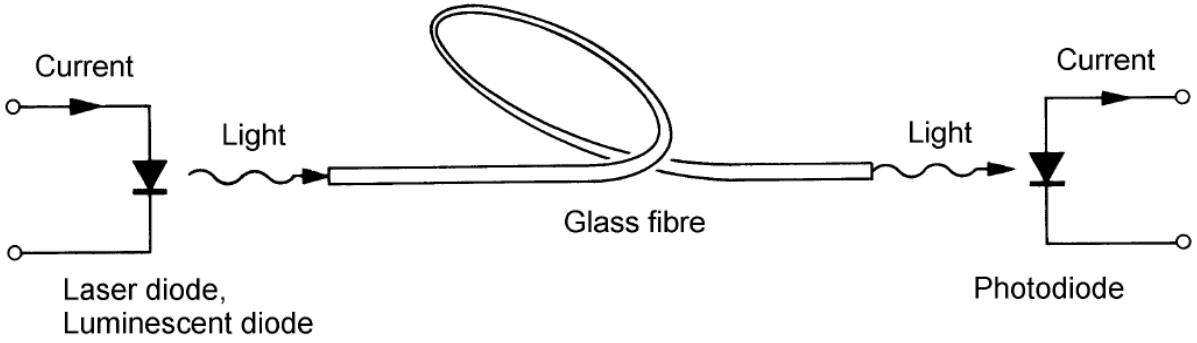

Fig. 1.1. Optical point-to-point transmission link with an intensity-modulated carrier centered at a wavelength λ and direct (incoherent) detection

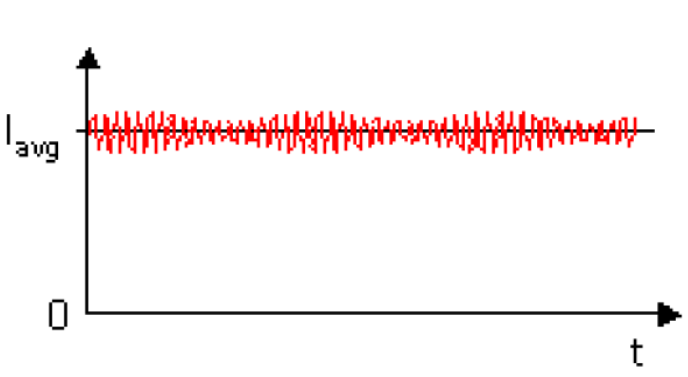

(a) Analogue intensity modulation

(b) Digital intensity modulation with TDM

Fig. 1.2. Modulation formats (a) Analogue intensity modulation around an operating point I_{avg} (b) Digital intensity modulation between an off (I_0) and an on value (I_1). For a 4-channel *t*ime *d*ivision *m*ultiplexing scheme (TDM) individual transmission time slots $1 \ldots 4$ are assigned to each data source

A World-Wide Optical Network

World-wide network "world-wide web"
(WWW, web = spider web)

- Satellite wireless communication (ViaSat-1)
  Bandwidth 1.25 GHz, distance $2 \times 36\,000$ km $\rightarrow$ 240 ms delay
  Downlink-Ku carrier 11.7...12.95 GHz, rel. bandwidth $1.25/12.325 \approx 10\,\%$
  Downlink-Ka band 27...40 GHz, 72 lobes à 1.9 Gbit/s, data rate 134 Gbit/s

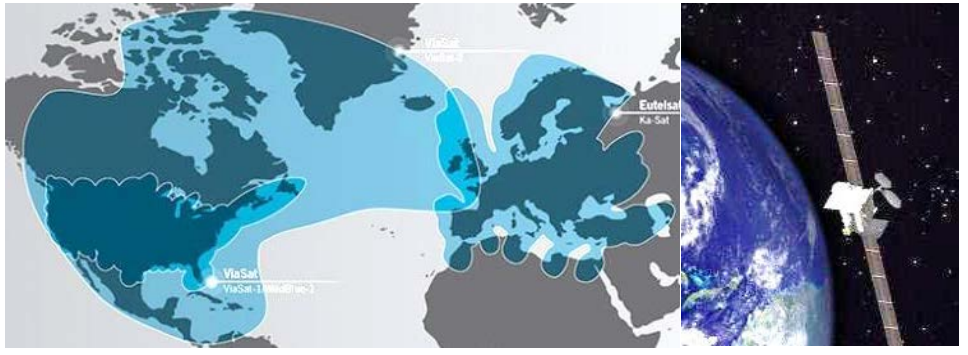

https://www.viasat.com/broadband-satellite-networks/high-capacity-satellite-system

http://www.dailytech.com/Sabotage+Still+Not+Ruled+Out+in+Undersea+Cable+Cuts/article10779.htm

- Submarine cable with glass fibres
  Bandwidth 10 THz, distance 10 000 km $\rightarrow$ 50 ms delay
  Optical carriers 190...200 THz, relative bandwidth $10/195 \approx 5\,\%$
  8 fibre pairs à 100 Gbit/s, data rate 1.6 Tbit/s

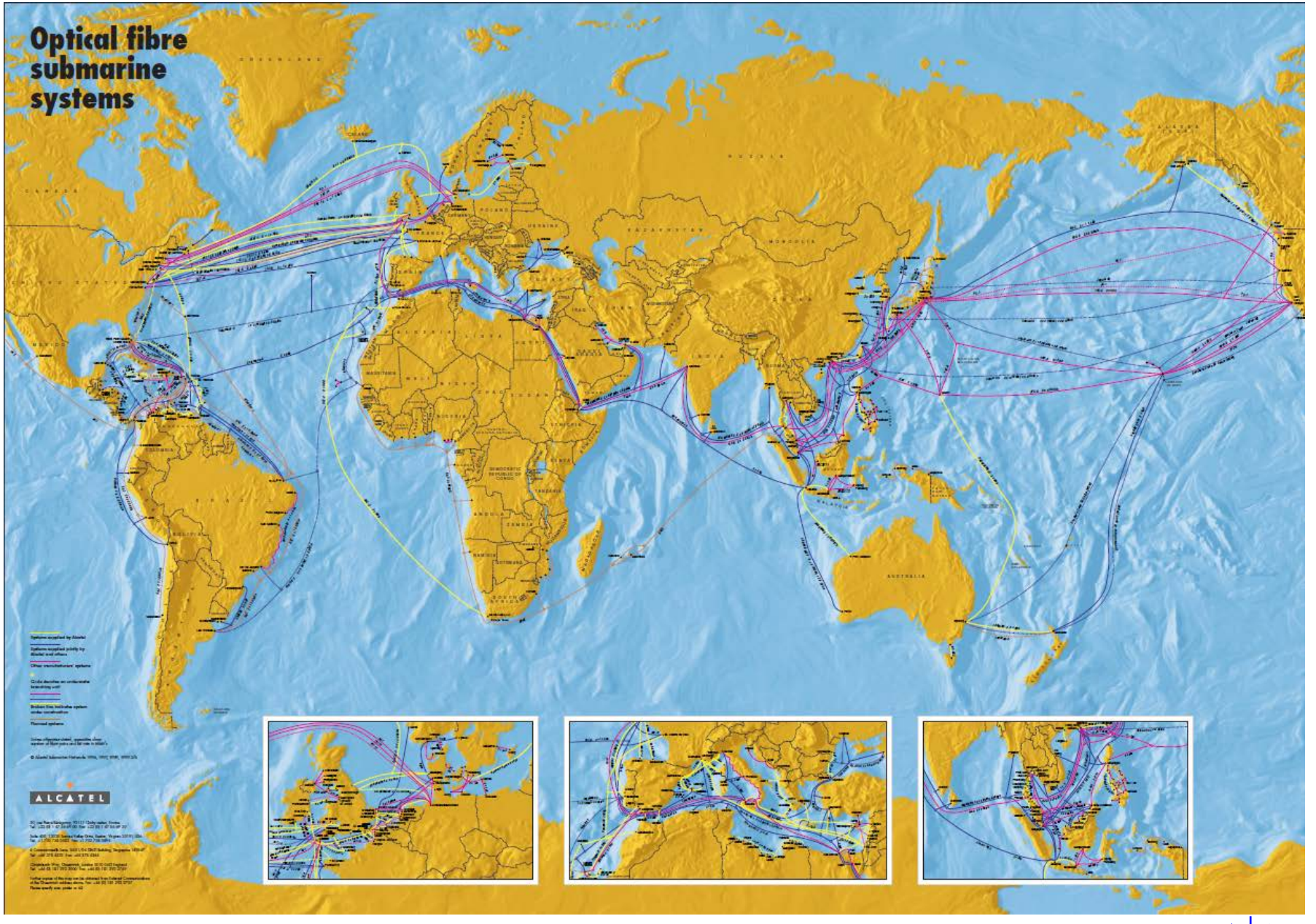
Optical fibre submarine systems
ALCATEL

Submarine Cable Map (2013)

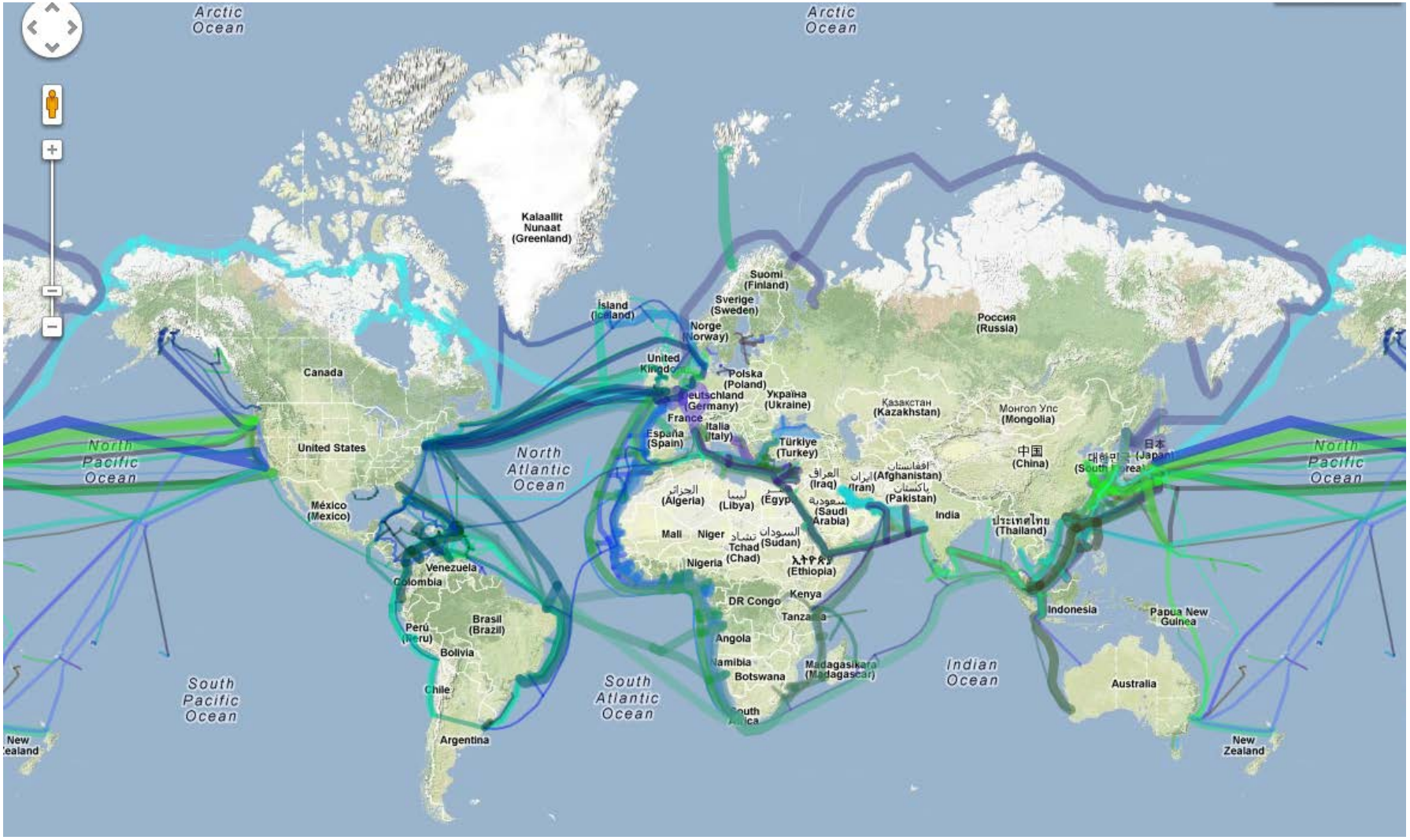

http://www.cablemap.info/

Submarine Cable Map (2014)

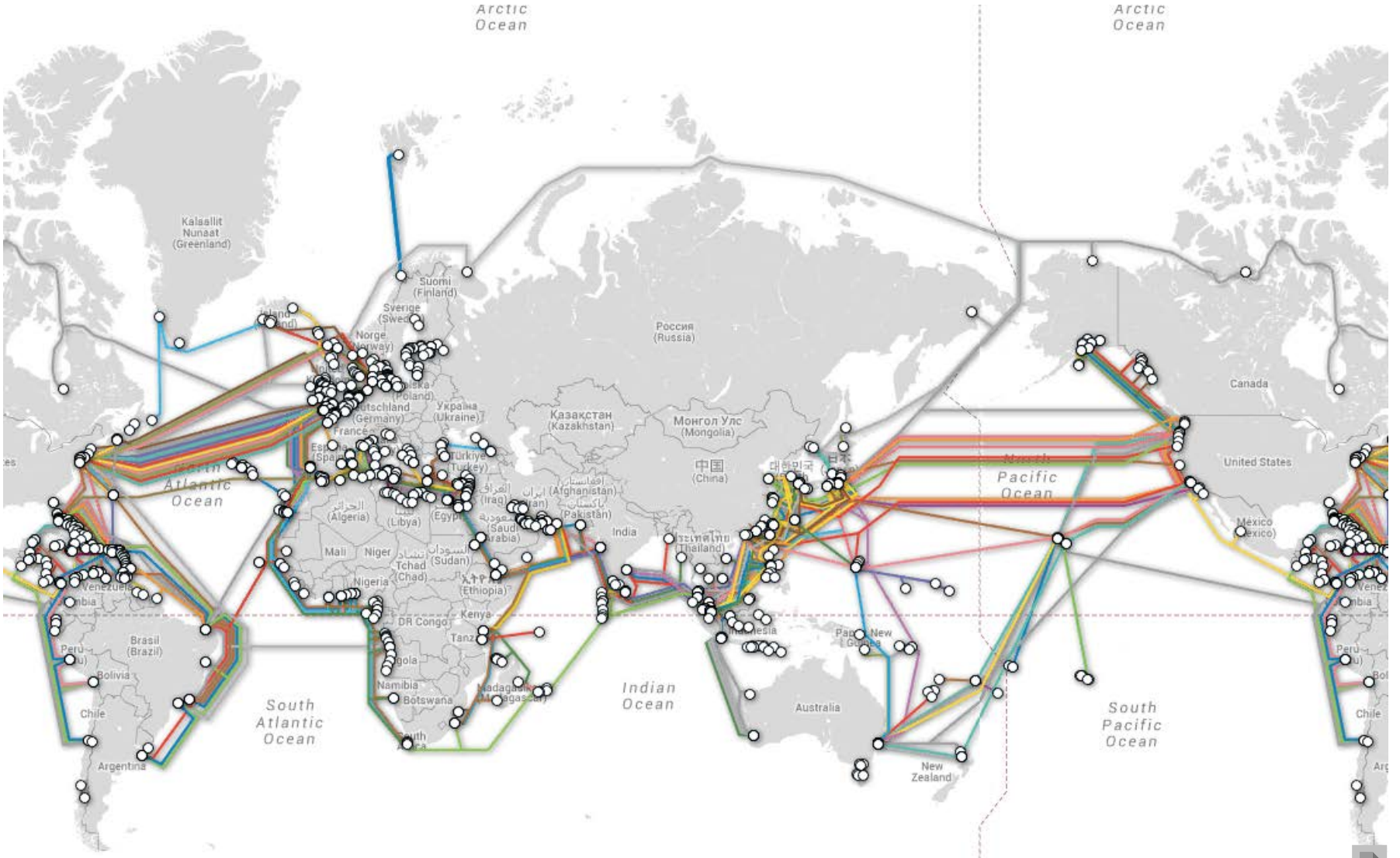

http://www.submarinecablemap.com/#/

Submarine Cable Map (2015)

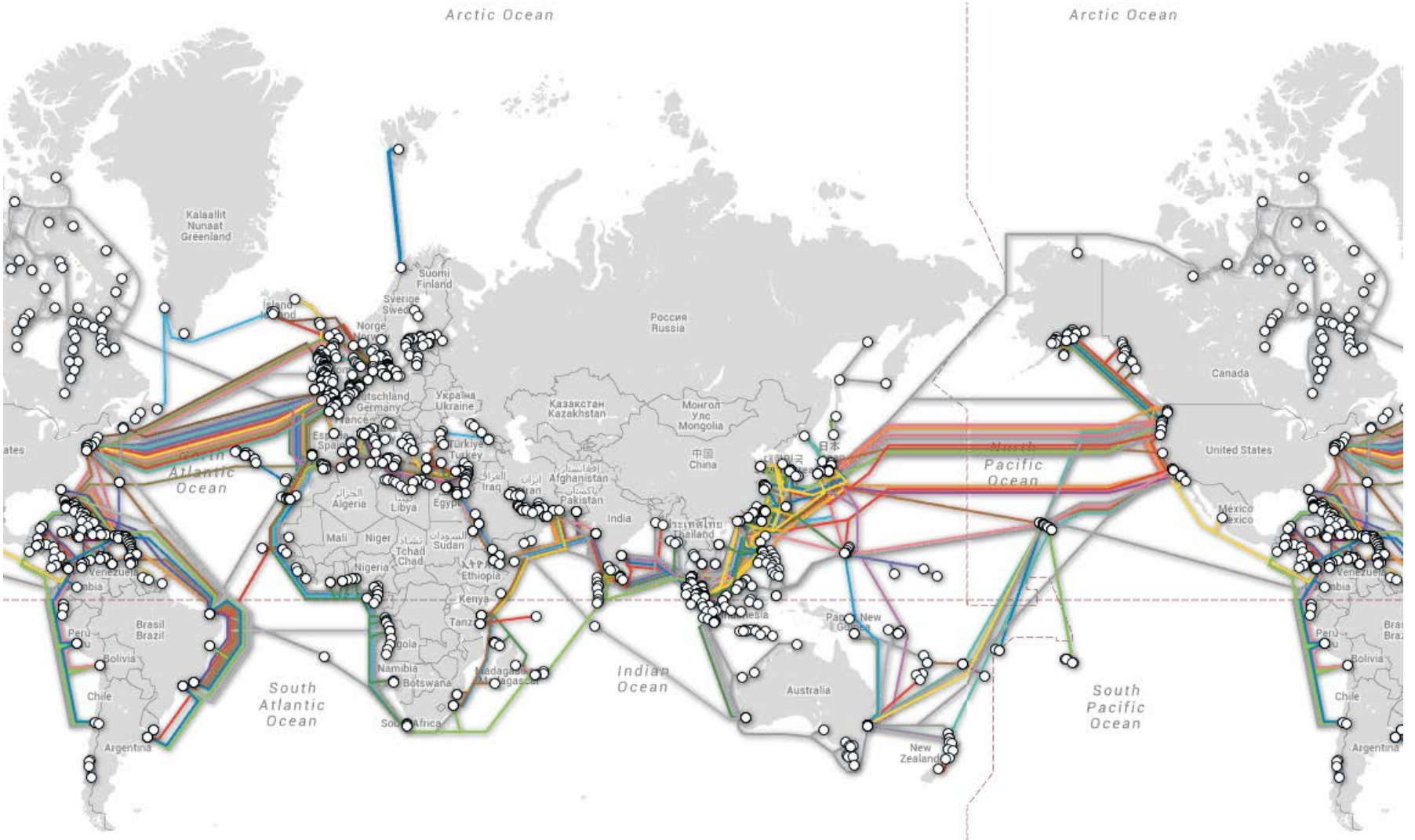

http://www.submarinecablemap.com/#/

Submarine Communication Systems — Laying the Cable

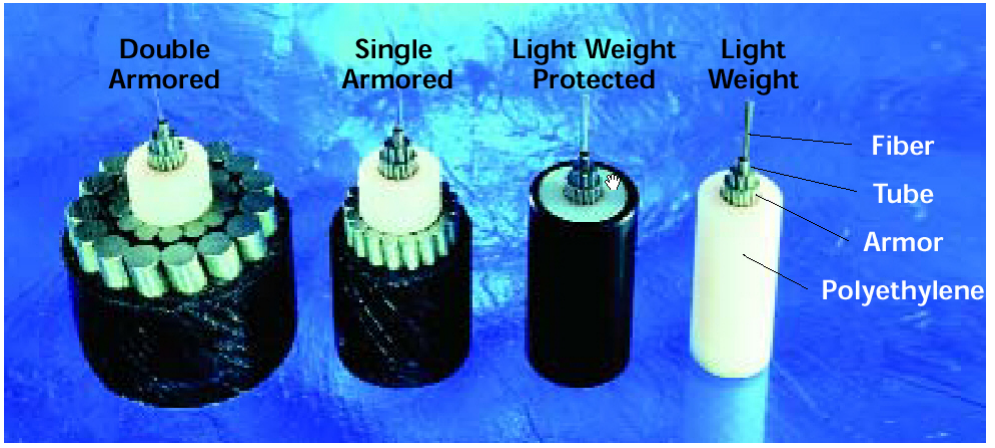

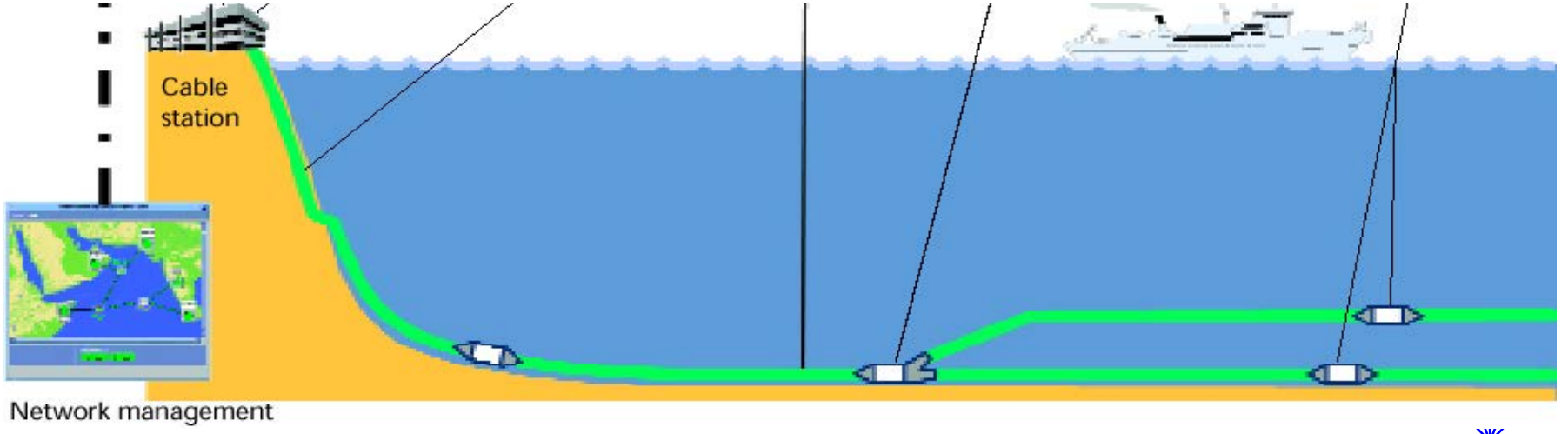

Submarine Communications Cable

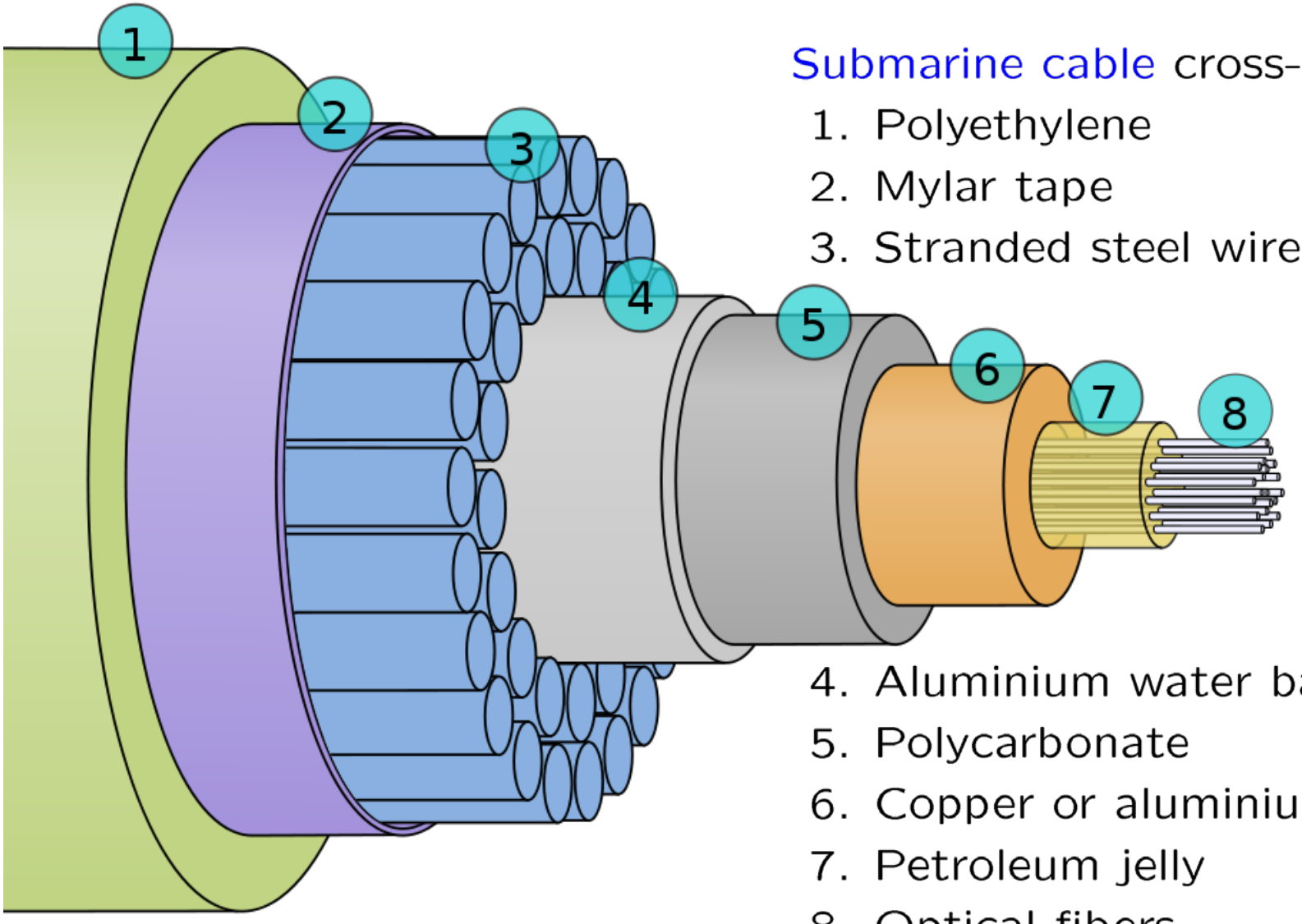

Submarine cable cross-section:

1. Polyethylene
2. Mylar tape
3. Stranded steel wires
4. Aluminium water barrier
5. Polycarbonate
6. Copper or aluminium tube
7. Petroleum jelly
8. Optical fibers

http://en.wikipedia.org/wiki/Submarine_communications_cable

Optical Network Infrastructure — Abbreviations & Buzz Words

SONET Synchronous optical network (ANSI)
American National Standards Institute
SDH Synchroneous digital hierachy (ITU)
International Telecommunication Union

WDM/TDM fiber links

Backbone ISP POP, CO

AP MAN/LAN Access Point

WDM Wavelength division multip.
TDM Time division multiplexing
PON Passive optical network
FTTx Fibre to the $x = $ C, B, H
for Cabinet, Curb,
Building, Home

MAN Metropolitan area net.
LAN Local area network
AP Access point
ISP Internet service provdr
POP Post office protocol
CO Central office

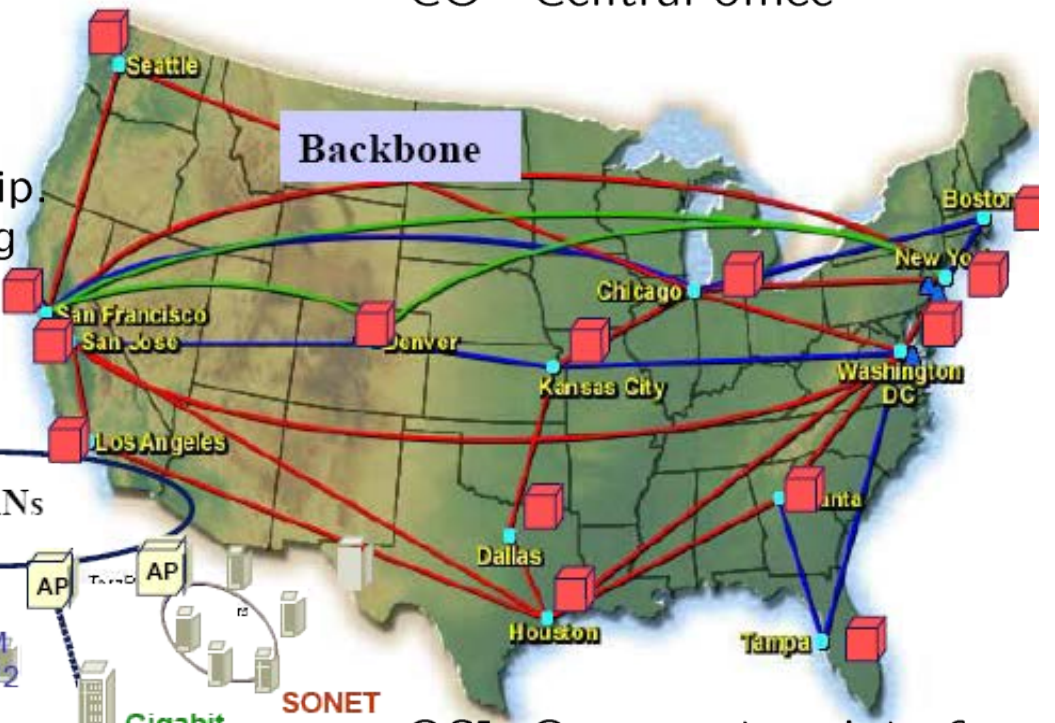

OSI Open system interface
Ethernet from "luminiferous aether" (or "ether")

An Optical Network the Size of a Football Ground

Data centres (Google, Facebook, Microsoft, Apple, . . .)

- Size of a data centre, for example YouTube

  100 h video files / min uploaded in May 2013 → 375 PB

  Volume increases by 185 TB / d, annual growth rate is 70 %.

  540 TB storage per rack & increase for 1 a → 1 200 racks,

  good for 30 000 servers including mass storage of 632 PB.

  1 200 racks require an area of 30 m × 100 m = 3 000 m^2.

http://www.autonomoussystem.net/ — Posted 1st July 2013 by Nathan Owens

Facebook´s data center in Luleå, Sweden: On-line 06/2013

Luleå ['lu:leo:]

An Optical Network the Size of a Football Ground — Interior

- Internal data network with high-density data traffic
  Server connected by switches with $30\,000 \times 3 = 90\,000$ 10 G-ports,
  i. e., by 90 000 cables, each with a capacity of 10 Gbit/s.
  The aggregate internal data rate amounts to 900 Tbit/s.

http://www.autonomoussystem.net/

An Optical Network the Size of a Football Ground — Interior

- Internal data network with high-density data traffic

  Server connected by switches with $30\,000 \times 3 = 90\,000$ 10 G-ports,

  i. e., by 90 000 cables, each with a capacity of 10 Gbit/s.

  The aggregate internal data rate amounts to 900 Tbit/s.

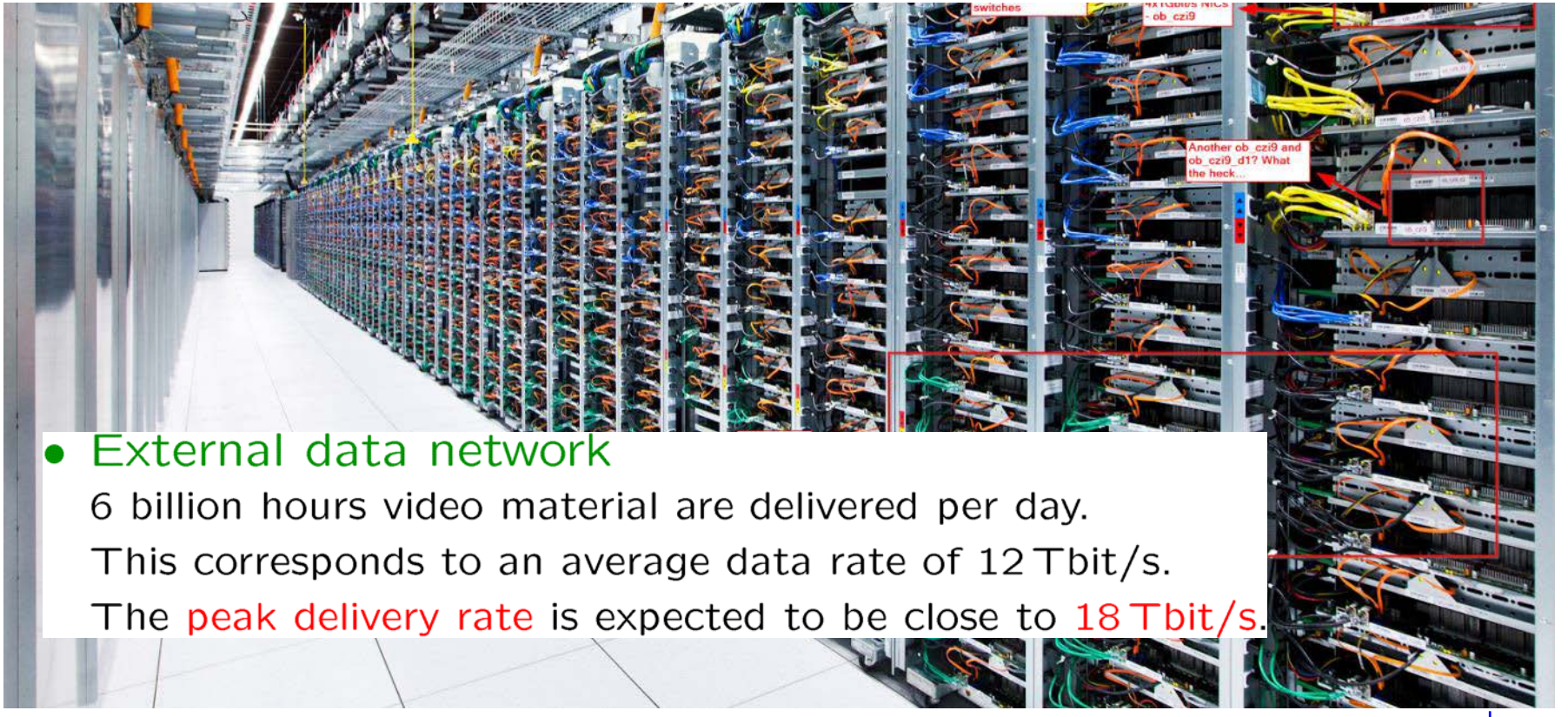

- External data network

  6 billion hours video material are delivered per day.

  This corresponds to an average data rate of 12 Tbit/s.

  The peak delivery rate is expected to be close to 18 Tbit/s.

A Board and Chip-wide Optical Network

Problem today:
Processing power of computer limited by bandwidth and energy re-quirements of electrical con-nections

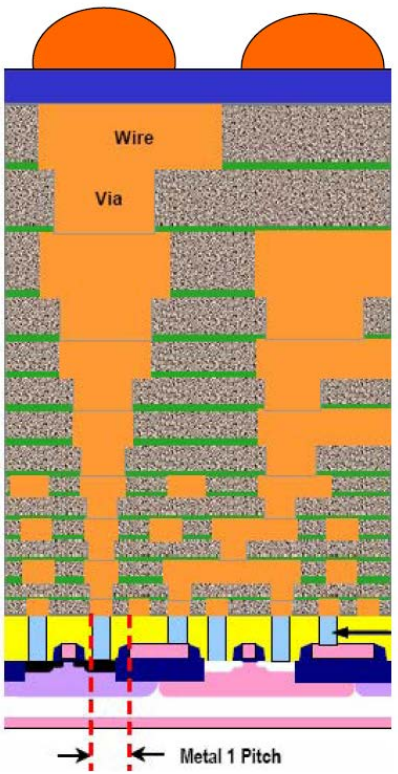

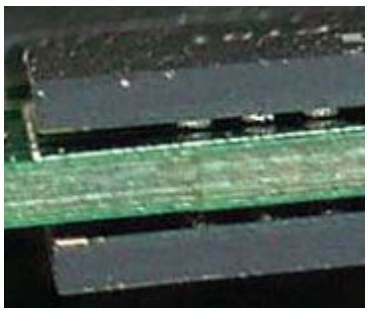

The perspective:
10 TFlops on a 3D chip

Logical plane: 300 cores
Photonic plane: 70 Tbit/s

On-chip and from/to chip with routing and switching on the chip

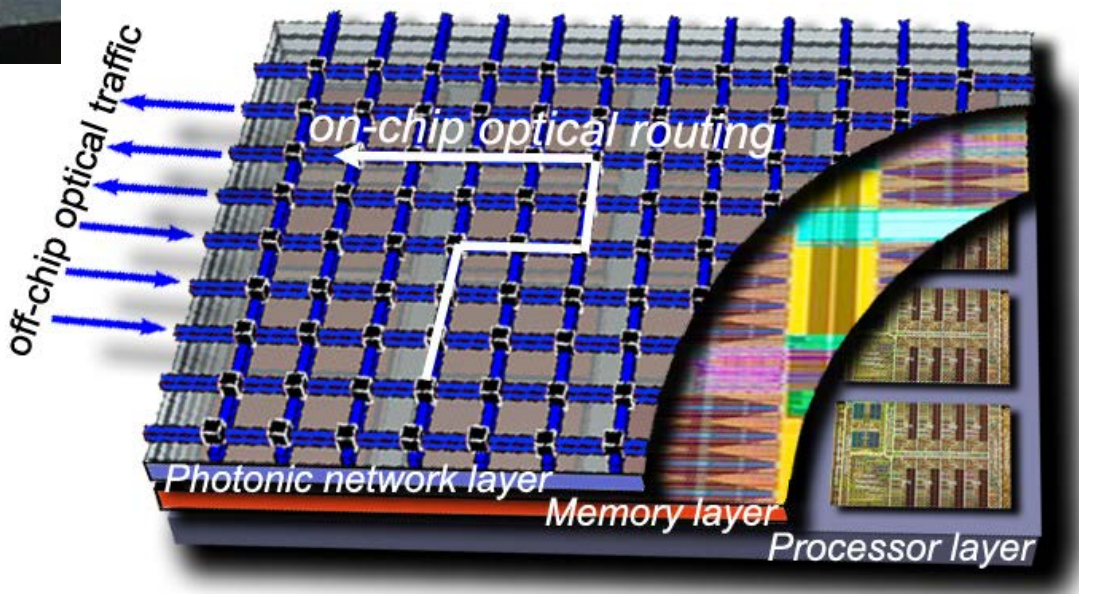

http://en.wikipedia.org/wiki/Ball_grid_array

http://domino.research.ibm.com/comm/research_projects.nsf/pages/photonics.index.html

Manfred Börner — Worldwide First Patent (Telefunken, 1966)

Als Übertragungsmedium werden sogenannte Lichtwellenleiter verwendet. Diese bestehen aus meist innenverspiegelten Hohlrohren, längs deren Achse optische Führungen in Form von Linsen, sei es aus Glas, sei es aus Gasverteilungen, angeordnet sind, die den Laserstrahl auf die Achse des einige Zentimeter im Durchmesser betragenden Hohlrohres zentrieren.

BUNDESREPUBLIK DEUTSCHLAND

DEUTSCHES PATENTAMT

PATENTSCHRIFT 1254 513

Int. Cl.: F 21 q
G 02 f; G 08 b; H 04 b

Deutsche Kl.: 74 d - 8/02

Nummer: 1 254 513
Aktenzeichen: T 32812 IX d/74 d
Anmeldetag: 21. Dezember 1966
Auslegetag: 16. November 1967
Ausgabetag: 16. Mai 1968

Patentschrift stimmt mit der Auslegeschrift überein

1

Die Erfindung betrifft ein mehrstufiges Übertragungssystem für in Pulscodemodulation dargestellte Nachrichten, bei dem jede Übertragungsstufe Laserorgane als Sender, fotoempfindliche Organe als Empfänger und Impulsaufbereitungseinrichtungen, welche durch die vom zugehörigen Empfänger decodierten Signalimpulse gesteuert werden, enthält und zwischen den Stufen eine geschlossene Übertragungsstrecke vorgesehen ist.

Der Laser hat in letzter Zeit dank seiner Breitbandigkeit, infolge der er einen theoretisch idealen Übertragungsträger darstellen könnte, mehr und mehr an Interesse für einen Einsatz zur Nachrichtenübertragung gefunden. Bisher sind an Übertragungssystemen auf Laserbasis im wesentlichen zwei ver-

Mehrstufiges Übertragungssystem für in Pulscodemodulation dargestellte Nachrichten

Patentiert für:
Telefunken
Patentverwertungsgesellschaft m. b. H.,
Ulm/Donau, Elisabethenstr. 3

Als Erfinder benannt:
Dipl.-Phys. Dr. rer. nat. Manfred Börner,
Ulm/Donau

Patent novelty:

a) Die sendenden Laserorgane sind Halbleiterlaser, vorzugsweise Halbleiterinjektionslaser;

b) die fotoempfindlichen Empfänger sind Halbleiterfotodioden;

c) die Impulsaufbereitungseinrichtungen sind Halbleiterschaltungen;

d) die Übertragungsstrecke besteht aus Lichtwellenfaserleitern.

Optical Communication in the 70s

TECHNIK DER SPIEGEL, Nr. 25/1973

Puls im Glas

Mit Laser-Licht und optischen Fasern könnte ein neuartiges Nachrichtennetz aufgebaut werden. Es wäre leistungsfähiger als alle bisherigen Kabel- und Funksysteme.

Der „Quantensprung in einen völlig neuen Bereich ultrafeiner Kurzwellen-Übertragung", meinte das US-Wirtschaftsmagazin „Fortune", werde wohl noch „innerhalb dieser Dekade" geprobt werden. Ein solches System, das Bild und Ton in Form von Lichtimpulsen übermittelt, könnte auf einer Leitung in jeder Sekunde rund eine Milliarde Informationseinheiten (bit) verarbeiten; das entspräche dem Redefluß von gleichzeitig 20 000 Telephongesprächen.

AEÜ ARCHIV FÜR ELEKTRONIK UND ÜBERTRAGUNGSTECHNIK
ELECTRONICS AND COMMUNICATION
Band 32 (1978), pp. 105–110

Monomode Operation of Direct Modulated GaAlAs DHS Injection Lasers from 260 Mbit/s up to 1.4 Gbit/s

by Wolfgang Freude*
Report from the Institut für Hochfrequenztechnik und Quantenelektronik, Universität Karlsruhe

Monomode emission of DHS lasers with stripe-geometry is demonstrated for 260 Mbit/s, 1.25 Gbit/s, and 1.4 Gbit/s. No structural difference between the cw spectra and the spectra during modulation can be observed for a defined range of operating parameters.
Numerical studies confirm the measured time dependence of the light output at high bit rates.

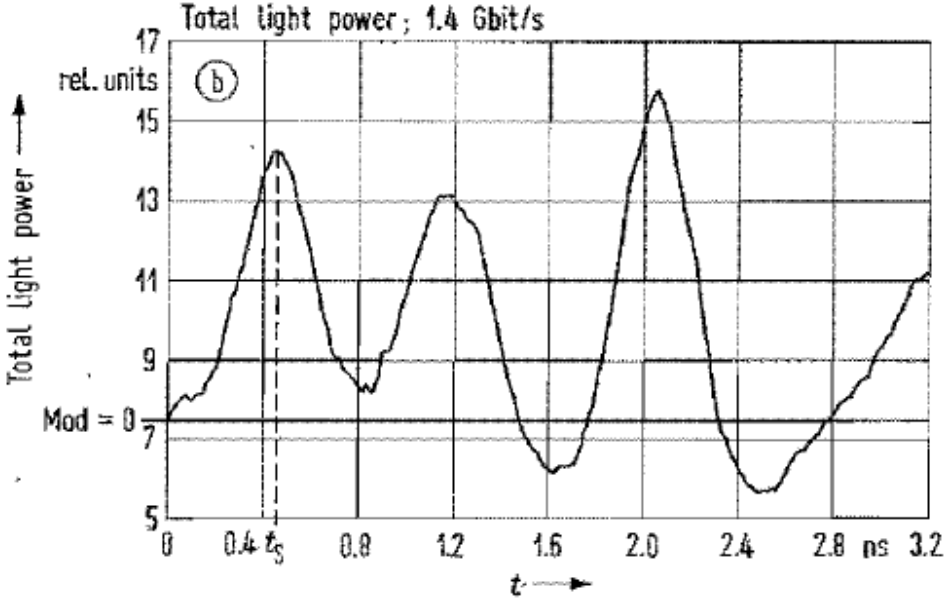

Optical Data Transmission

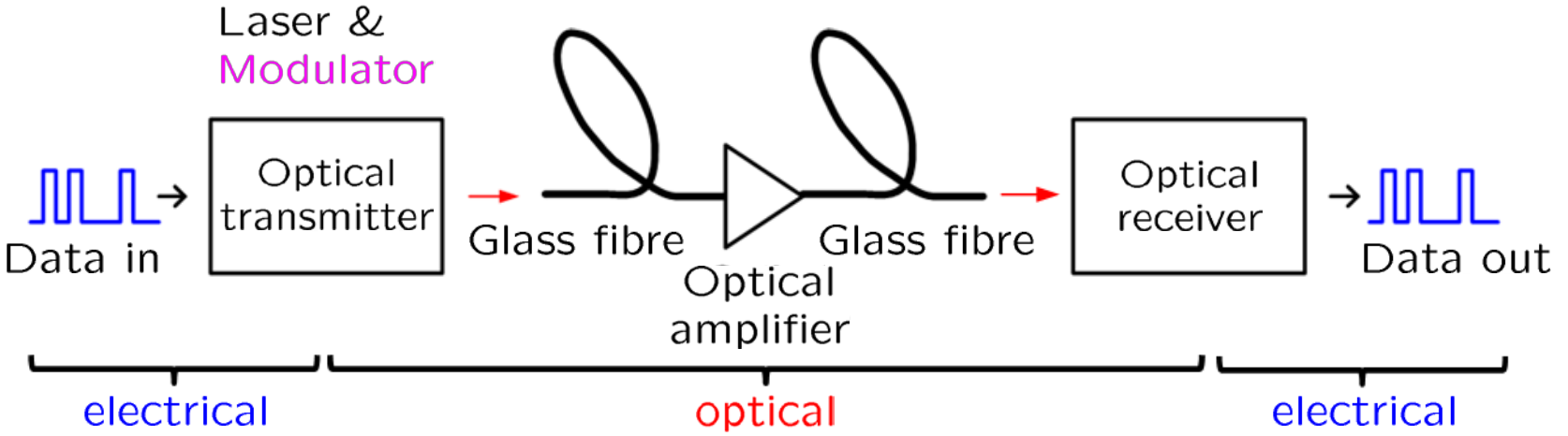

Advantages of optical communication:

- Large transmission capacity**:** Fibre bandwidth 250…190 THz = 60 THz

  Bitrates of typical services:

  Voice 64 kbit/s (compressed < 10 kbit/s)
  Picture (TV) 140 Mbit/s (compressed 2…6 Mbit/s)

  Bitrates for transmission media:

  Twisted pair 6 Mbit/s (6 km); Koaxialkabel 650 Mbit/s (1.5 km)
  Optical fibre > 100 Tbit/s (10 billion ISDN, 20 million TV)

- Large transmission length through low fibre attenuation:

  Minimal 0.15 dB/km @ ¸ = 1.55 µm,
  (50 % transmission for a fibre length of *L* = 20 km)

Charles Kuen Kao
Pioneering low-loss fibres
Nobel prize 2009

Light Guidance by Total Internal Reflection or by Index Gradient

Snell's law (1621, by Willebrord van Roijen Snell, also called Snellius, ⋆1580 †1626, Dutch astronomer and mathematician)

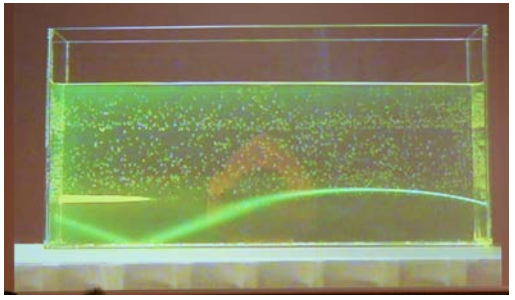

Water with sugar solution acts as graded-index light guide.

Gießen, H.: Öffentliche Vorlesung über Tarnkappen im Mercedes Museum am 22.7.2008. http://www.pi4.uni-stuttgart.de/

Total internal reflection (TIR) at transition from optically denser medium (larger refractive index n_1) to medium with lesser density (smaller refractive index $n_2 < n_1$)

http://en.wikipedia.org/wiki/File:Total_internal_reflection_of_Chelonia_mydas_.jpg

http://en.wikipedia.org/wiki/File:TIR_in_PMMA.jpg

Light Guidance by Total Internal Reflection

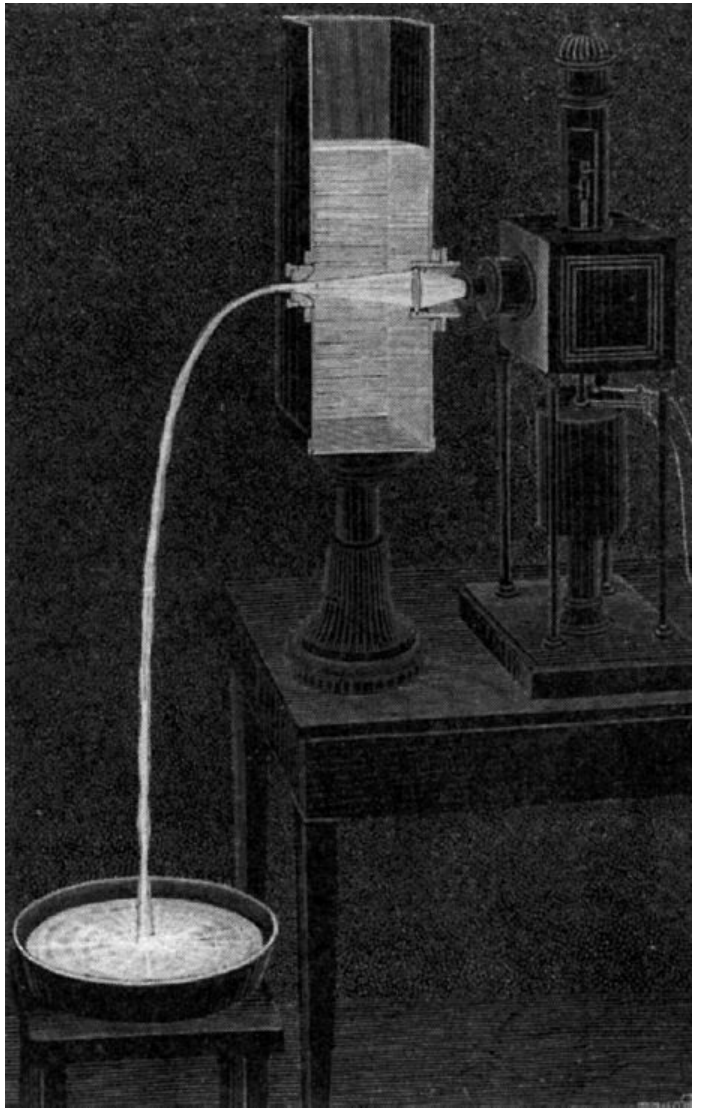

Colladon described 1842 a "light fountain" or a "light pipe".

Video demonstration

Jean-Daniel Colladon, Swiss physicist, ⋆Genf 15.12.1802, †30.06.1893).

Comptes rendus, J. Franz. Akademie der Wissenschaften (1842).

Others:

Auguste A. de la Rive (arc discharge)

Jacques Babinet (candle & glass bottle)

John Tyndall (1870, shows light guidance by total internal reflection)

Fibre Types

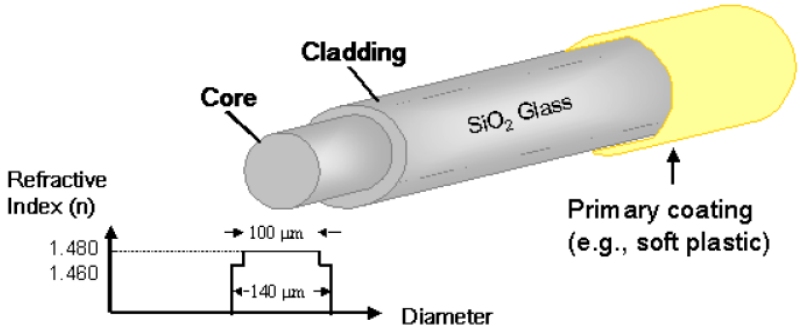

(a) Multimode fibre with step-index profile

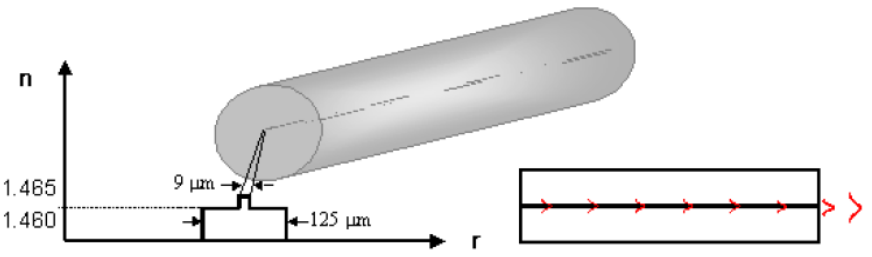

(b) Single-mode fibre with step-index profile

Fig. 1.3. Fibre types with step-shaped refractive index profile comprising a higher-index core and a lower-index cladding (a) Fat-core step-index multimode fibre with a relative refractive index difference $\Delta \approx 1.3\,\%$ (b) Long-haul step-index single-mode communication fibre with $\Delta \approx 0.33\,\%$

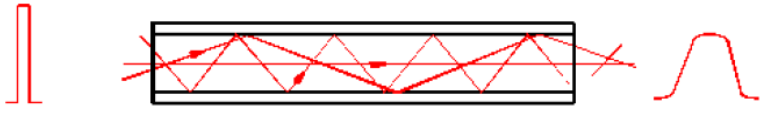

(a) Multimode fibre with step-index profile

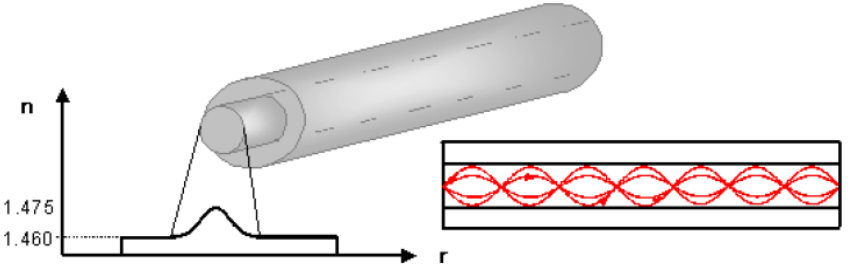

(b) Multimode fibre with graded-index profile

Fig. 1.4. Intermodal dispersion for multimode fibres. (a) Step-index profile with significant group delay differences (b) Graded-index profile, where geometrical path length differences are compensated by radial variations in the refractive index

Chromatic Dispersion

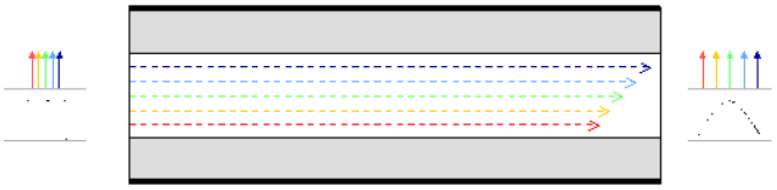

(a) Chromatic dispersion in a single-mode fibre

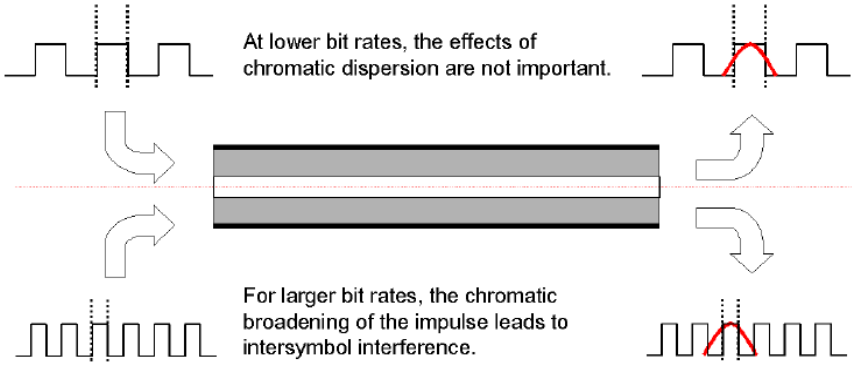

(b) Group delay dispersion and intersymbol interference

Fig. 1.5. Group delay dispersion and bit error probability (bit error rate BER). (a) Different wavelengths ("colours", therefore "chromatic") inside the same mode propagate with different velocities, thereby increasing the output impulse width (b) Broadening of the transmitted impulse leads to bit detection errors

Optical Wavelength Division Multiplexing (WDM)

- Internet: Need for bandwidth B

- Optical transmission systems

  fibres: $B \approx 65$ THz (450 nm)

  amplifiers: $B \approx 10$ THz (80 nm)

  wavelength division multiplexing

  channels: $\Delta f \approx 5, 10, 25, 50, 100$ GHz

  capacity: 40 Gbit/s × 100 ch = 4 Tbit/s

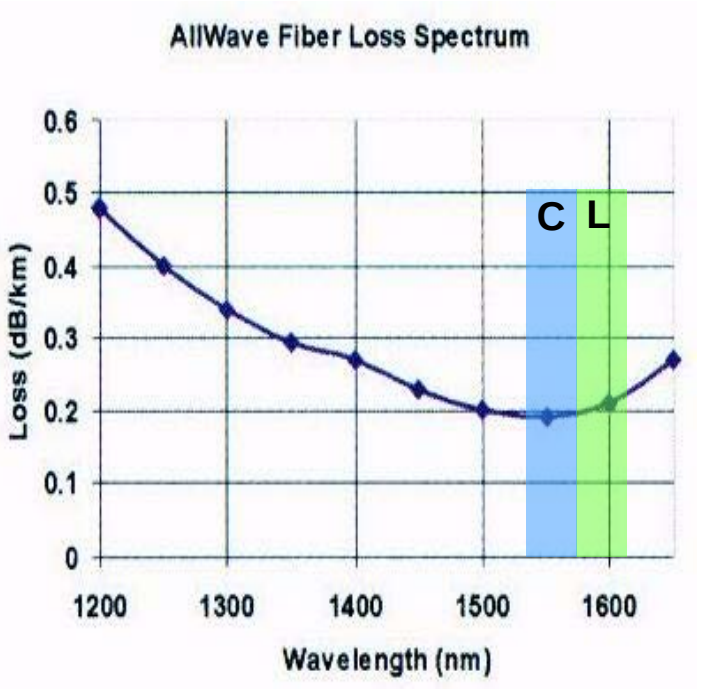

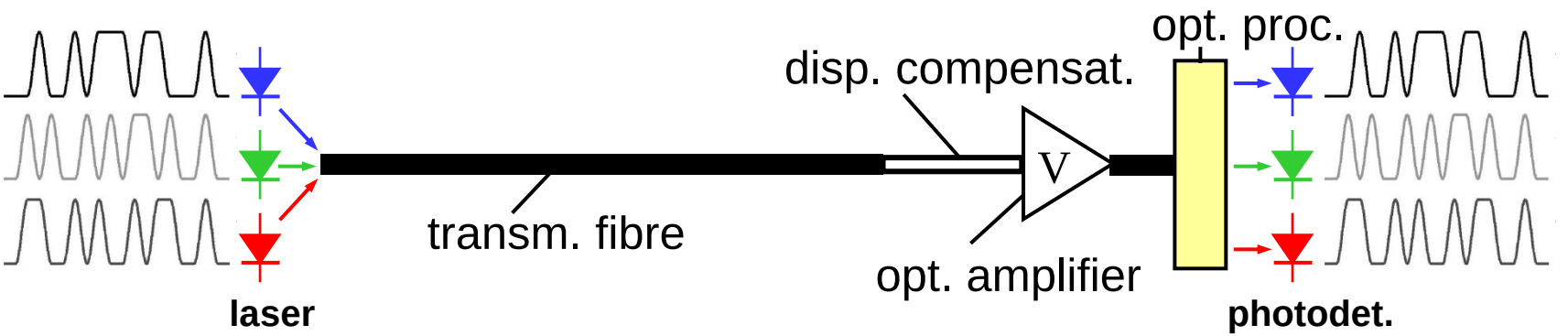

Wavelength Division Multiplexing

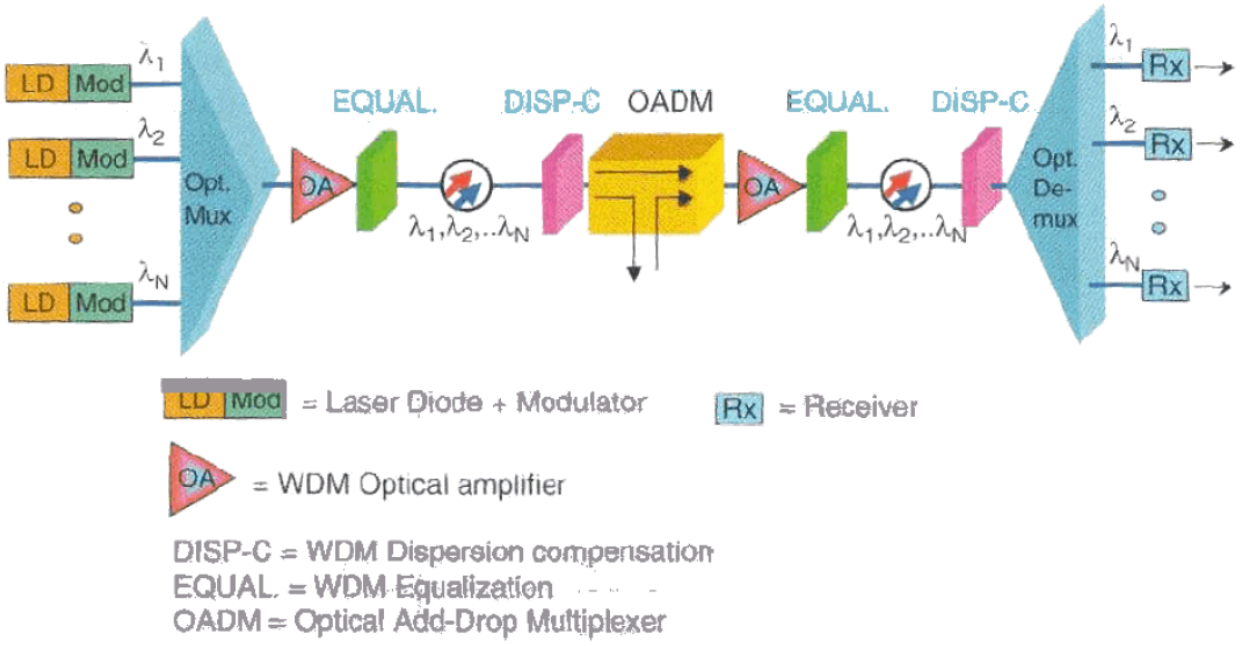

Fig. 1.6. Wavelength division multiplexing transmission scheme. The path from LD MOD(λ_i) to Rx(λ_i) corresponds to the simplified point-to-point transmission depicted in Fig. 1.1. [after Fig. iii on Page xxiv in reference Footnote 10 on Page 4]

Standard ITU Channel Grid

CH	Frequency(THz)	Wavelength(nm	CH	Frequency(GHz)	Wavelength(nm)
15	191.500	1,565.4961	44	194,400	1,542.1425
16	191.600	1,564.6790	45	194.500	1,541.3496
17	191.700	1,563.8628	46	194,600	1,540.5576
18	191.800	1,563.0475	47	194.700	1,539.7663
19	191.900	1,562.2329	48	194.800	1,538.9759
20	192.000	1,561.4193	49	194.900	1,538.1863
21	192.100	1,560.6065	50	195,000	1,537.3974
22	192.200	1,559.7945	51	195.100	1,536.6094
23	192.300	1,558.9834	52	195.200	1,535.8222
24	192.400	1,558.1731	53	195.300	1,535.0358
25	192.500	1,557.3636	54	195.400	1,534.2503
26	192.600	1,556.5550	55	195.500	1,533.4655
27	192.700	1,555.7473	56	195.600	1,532.6815
28	192.800	1,554.9404	57	195.700	1,531.8983
29	192.900	1,554.1343	58	195.800	1,531.1159
30	193.000	1,553.3290	59	195.900	1,530.3344
31	193.100	1,552.5246	60	196.000	1,529.5536
32	193.200	1,551.7210	61	196.100	1,528.7736
33	193.300	1,550.9183	62	196,200	1,527.9944
34	193.400	1,550.1163	63	196.300	1,527.2160
35	193.500	1,549.3153	64	196.400	1,526.4384
36	193.600	1,548.5150	65	196.500	1,525.6616
37	193.700	1,547.7155	66	196.600	1,524.8856
38	193.800	1,546.9169	67	196.700	1,524.1103
39	193.900	1,546.1191	68	196.800	1,523.3359
40	194.000	1,545.3222	69	196.900	1,522.5622
41	194.100	1,544.5260	70	197.000	1,521.7893
42	194.200	1,543.7307	71	197.100	1,521.0200
43	194.300	1,542.9362	72	197.200	1,520.2500

Reference frequency: 195 THz

Basic grid: 100 GHz (≈ 0.79 nm)

Subdivisions: 50 GHz or 25 GHz

LECTURE 2

12.8Tbit/s Transmission of 160 PDM-QPSK (160x2x40Gbit/s) Channels with Coherent Detection over 2,550km

Gabriel Charlet[1], Jérémie Renaudier[1], Haik Mardoyan[1], Oriol Bertran Pardo[1], Frédéric Cérou[2], Patrice Tran[1], Sébastien Bigo[1]

1 : Alcatel-Lucent, Research and Innovation, Centre de Villarceaux, 91620, Nozay, France,

2 : IRISA/INRIA de Rennes, Campus universitaire de Beaulieu, 35042 Rennes, France

Gabriel.Charlet@alcatel-lucent.fr

ECOC'07 PDP 1.6

Abstract: *A 12.8Tbit/s ultra-high capacity transmission is demonstrated over an ultra-long distance of 2,550km thanks to coherent detection and powerful signal processing against chromatic dispersion, PMD and narrow optical filtering.*

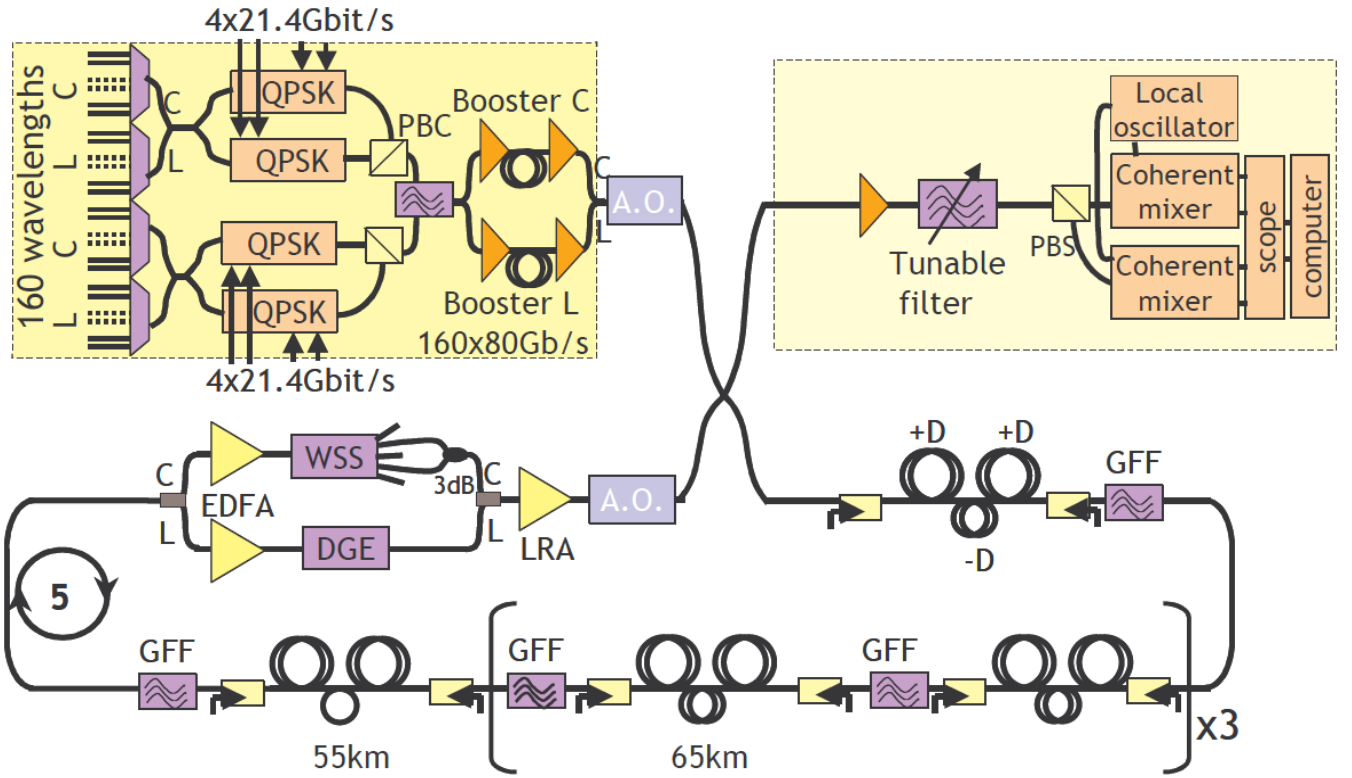

25.6-Tb/s C+L-Band Transmission of Polarization-Multiplexed RZ-DQPSK Signals

A. H. Gnauck[(1)], G. Charlet[(2)], P. Tran[(2)], P. J. Winzer[(1)], C. R. Doerr[(1)], J. C. Centanni[(1)], E. C. Burrows[(1)], T. Kawanishi[(3)],T. Sakamoto[(3)], and K. Higuma[(4)]

(1) Alcatel-Lucent, Bell Labs, Holmdel, New Jersey 07733, USA, Email: gnauck@lucent.com
(2) Alcatel-Lucent, Research and Innovation, Centre de Villarceaux, Route de Villejust, 91620 NOZAY, France
(3) National Inst. of Information and Communications Technologies (NICT), 4-2-1 Nukui-Kita, Koganei, Tokyo 184-8795, Japan
(4) Sumitomo Osaka Cement, 585 Toyotomi, Funabashi, Chiba 274-8601, Japan

OFC'07 PDP 19

Abstract: We demonstrate record 25.6-Tb/s transmission over 240 km using 160 WDM channels on a 50-GHz grid in the C+L bands. Each channel contains two polarization-multiplexed 85.4-Gb/s RZ-DQPSK signals, yielding a spectral efficiency of 3.2 b/s/Hz in each band.

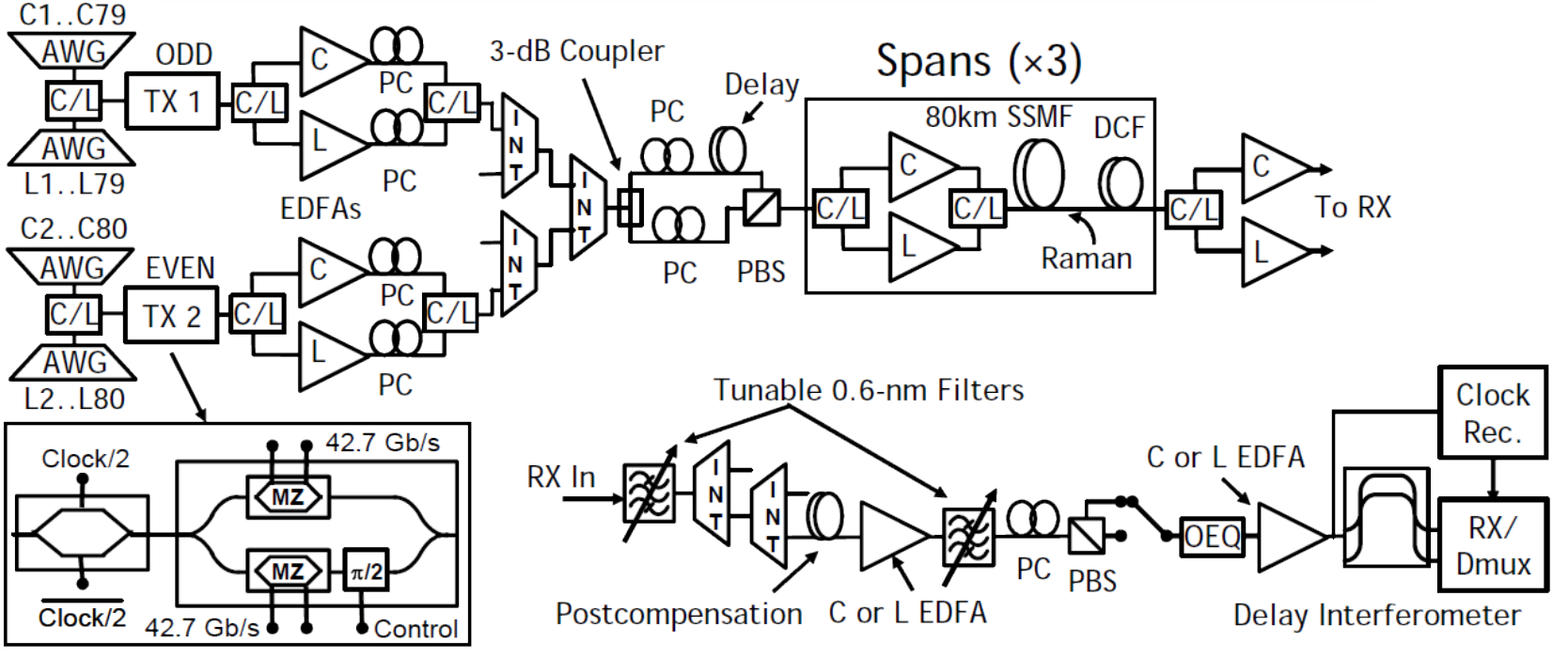

Fig. 1. Experimental setup. AWG: Arrayed Waveguide Grating Router. C/L: C-band/L-band splitter or combiner. INT: 50GHz/100GHz interleaver or de-interleaver. PC: Polarization controller. PBS: Polarization beamsplitter. OEQ: Optical equalizer.

32-bit/s/Hz Spectral Efficiency WDM Transmission over 177-km Few-Mode Fiber

R. Ryf[1], S. Randel[1], N. K. Fontaine[1], M. Montoliu[1,2], E. Burrows[1], S. Corteselli[1], S. Chandrasekhar[1], A. H. Gnauck[1], C. Xie[1], R.-J. Essiambre[1], P. J. Winzer[1], R. Delbue[3], P. Pupalaikis[3], A. Sureka[3], Y. Sun[4], L. Grüner-Nielsen[5], R. V. Jensen[5], and R. Lingle, Jr.[4]

[1]*Bell Laboratories, Alcatel-Lucent, 791 Holmdel-Keyport Rd, Holmdel, NJ, 07733, USA.*
[2]*Universitat Politècnica de Catalunya (ETSETB), Barcelona, Spain*
[3]*LeCroy Corporation, 700 Chestnut Ridge Road, Chestnut Ridge, NY 10977, USA*
[4]*OFS, 2000 Northeast Expressway, Norcross, GA 30071, USA*
[5]*OFS Fitel Denmark, Priorparken 680, 2605 Brondby, Denmark.*

Roland.Ryf@alcatel-lucent.com

Aggregate capacity: 24.6 Tbit/s in BW 800 GHz.

OFC'13 PDP 5A.1

Abstract: We transmit 32 WDM channels over 12 spatial and polarization modes of 177 km few-mode fiber at a record spectral efficiency of 32 bit/s/Hz. The transmitted signals are strongly coupled and recovered using 12×12 multiple-input multiple-output digital signal

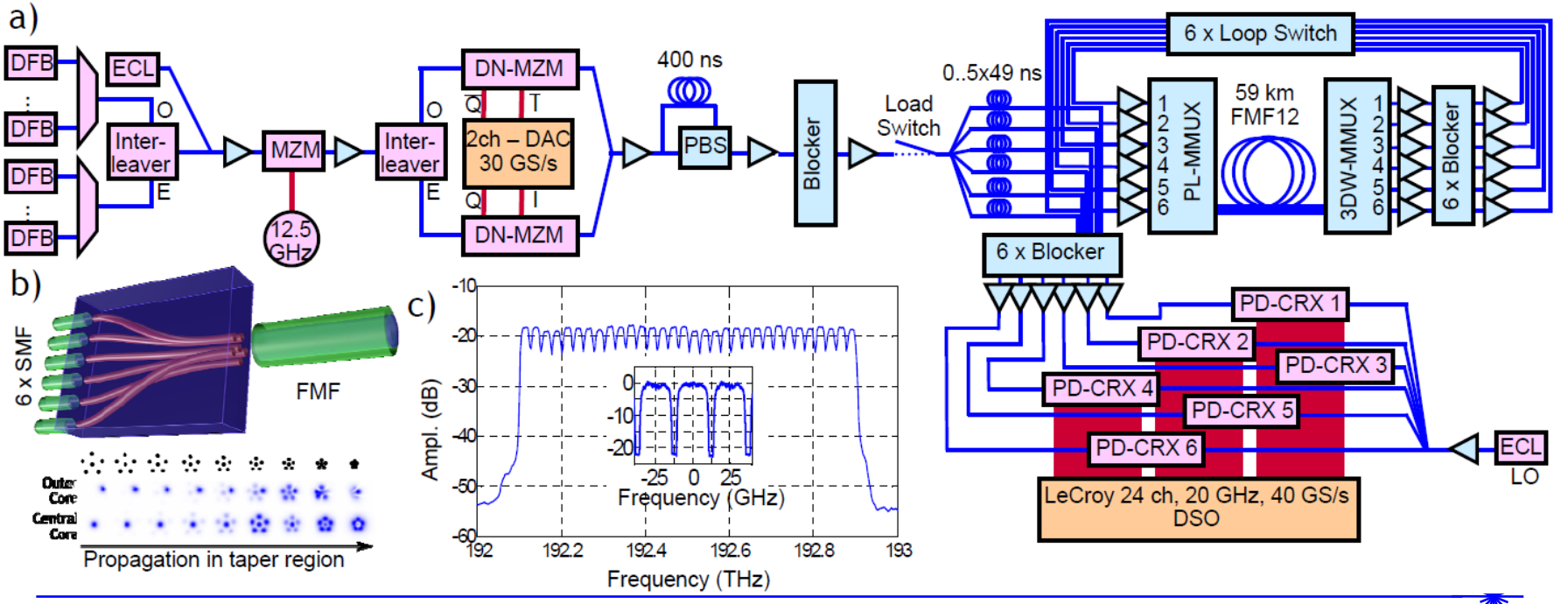

The Logarithmic Scale

dB = $10 \log_{10} (P_1 / P_0)$

0 dB	= 1
+ 0.1 dB	= 1.023 (+2.3%)
+ 3 dB	= 2
+ 5 dB	= 3
+ 10 dB	= 10
-3 dB	= 0.5
-10 dB	= 0.1
-20 dB	= 0.01
-30 dB	= 0.001

dBm = $10 \log_{10} (P / 1\ mW)$

0 dBm	= 1 mW
3 dBm	= 2 mW
5 dBm	= 3 mW
10 dBm	= 10 mW
20 dBm	= 100 mW
-3 dBm	= 0.5 mW
-10 dBm	= 100 μW
-30 dBm	= 1 μW
-60 dBm	= 1 nW

Optical Power

Power (P):

– *Transmitter: typ. -6 to +17 dBm (0.25 to 50 mW)*

– *Receiver: typ. -3 to -35 dBm (500 down to 0.3 µW)*

– *Optical Amplifier: typ. +3 to +20 dBm (2 to 100 mW)*

Laser safety

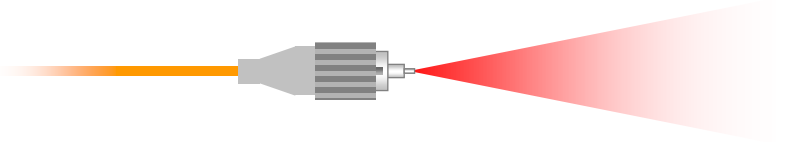

– International standard: IEC 825-1

– United States (FDA): 21 CFR 1040.10

– Both standards consider **class I** safe under reasonable forseeable conditions of operation (e.g., without using optical instruments, such as lenses or microscopes)

Notation and formulae

Time	t	(1)
Frequency f, wavelength λ, vacuum speed of light c	$f = \frac{c}{\lambda}\,, \qquad c = 2.997\,924\,58 \times 10^8\,\mathrm{m/s}$	(2)
Angular frequency ω, vacuum propagation constant k_0	$\omega = 2\pi f\,, \qquad k_0 = \frac{\omega}{c} = \frac{2\pi}{\lambda}$	(3)
Cartesian spatial coordin. & spatial (angular) frequencies	$x, y, z \quad \& \quad \xi, \eta, \zeta \quad (k_x = 2\pi\xi,\ k_y = 2\pi\eta,\ k_z = 2\pi\zeta)$	(4)
Imaginary unit	$\mathrm{j} = \sqrt{-1}$	(5)
Complex conjugate of $u = p + \mathrm{j}\,q$ (p, q real)	$u^* = p - \mathrm{j}\,q$	(6)
Adding to u its complex conjugate u^*	$u + u^* = 2\Re\{u\}\,, \quad u - u^* = \mathrm{j}\,2\Im\{u\}$	(7)
Plane wave propagating in medium with refractive index n, vacuum speed of light c	$\exp[\mathrm{j}\,(\omega t - (k_x x + k_y y + k_z z))]\,,$ $k_x^2 + k_x^2 + k_z^2 = n^2 k_0^2 = n^2\,\omega^2 / c^2$	(8)
Plane wave propagating in $+z$-direction, propagation constant $\beta \geq 0$, and effective index n_e	$\exp[\mathrm{j}\,(\omega t - \beta z)]\,, \qquad n_e = \frac{\beta}{k_0}$	(9)
Kronecker symbol $\delta_{m\,m'}$, $m, m' \in \mathbb{Z}$	$\delta_{m\,m'} = \begin{cases} 1 \text{ for } m = m' \\ 0 \text{ else} \end{cases}$	(10)
Dirac function $\delta(t)$	$\Psi(0) = \int_{-\infty}^{+\infty} \delta(t)\,\Psi(t)\,\mathrm{d}t, \quad \delta(t) = \lim_{k\to\infty} \int_{-k}^{+k} \mathrm{e}^{\pm \mathrm{j}\,2\pi f t}\,\mathrm{d}f$ $\delta(t) = 0 \text{ for } t \neq 0$	(11)
Heaviside function $H(t)$	$\int_0^{+\infty} \Psi(t)\,\mathrm{d}t = \int_{-\infty}^{+\infty} H(t)\,\Psi(t)\,\mathrm{d}t,$ $H(t) = \begin{cases} 1 \text{ for } t > 0 \\ 0 \text{ for } t < 0 \end{cases}$	(12)
rect-function $\mathrm{rect}\left(\frac{t}{T}\right)$	$\int_{-T/2}^{+T/2} \Psi(t)\,\mathrm{d}z = \int_{-\infty}^{+\infty} \mathrm{rect}\left(\frac{t}{T}\right)\Psi(t)\,\mathrm{d}t,$ $\mathrm{rect}\left(\frac{t}{T}\right) = \begin{cases} 1 \text{ for } \lvert t\rvert < T/2 \\ 0 \text{ for } \lvert t\rvert > T/2 \end{cases}$	(13)
sinc-function $\mathrm{sinc}\left(\frac{t}{T}\right)$	$\mathrm{sinc}\left(\frac{t}{T}\right) = \begin{cases} 1 & \text{for } t = 0 \\ \frac{\sin(\pi t/T)}{\pi t/T} & \text{else} \end{cases}$	(14)
triang-function $\mathrm{triang}\left(\frac{t}{T}\right) = \frac{1}{T}\,\mathrm{rect}\left(\frac{t}{T}\right) * \mathrm{rect}\left(\frac{t}{T}\right)$	$\mathrm{triang}\left(\frac{t}{T}\right) = \begin{cases} 1 - \lvert t\rvert/T & \text{for } \lvert t\rvert \leq T \\ 0 & \text{else} \end{cases}$	(15)

Notation and Formulae (2)

Continuous Fourier transform (FT, $\breve{\Psi}(f) = \mathcal{F}\{\Psi(t)\}$)	$\breve{\Psi}(f) = \int_{-\infty}^{+\infty} \Psi(t)\, \mathrm{e}^{-\mathrm{j}\,2\pi f t}\, \mathrm{d}t$, if $\Psi(t)$ real: $\breve{\Psi}(f) = \breve{\Psi}^*(-f)$	(16)
Continuous inverse FT (IFT, $\Psi(t) = \mathcal{F}^{-1}\{\breve{\Psi}(f)\}$)	$\Psi(t) = \int_{-\infty}^{+\infty} \breve{\Psi}(f)\, \mathrm{e}^{+\mathrm{j}\,2\pi f t}\, \mathrm{d}f$	(17)
Power spectrum $\Theta_\Psi(f) := \mathcal{F}\{\vartheta_\Psi(t)\}$ Autocorrelation function (ACF) $\vartheta_\Psi(t) := \mathcal{F}^{-1}\{\Theta_\Psi(f)\}$	$\Theta_\Psi(f) = \left\lvert\breve{\Psi}(f)\right\rvert^2$, one-sided power spectrum: $2\Theta_\Psi(f)$ for $f > 0$ and real $\Psi(t)$	(18)
Continuous spatial Fourier transform (SFT)	$\widetilde{\Psi}(\xi,\eta) = \iint_{-\infty}^{+\infty} \Psi(x,y) \exp[+\mathrm{j}(\xi x + \eta y)]\, \mathrm{d}x\, \mathrm{d}y$	(19)
Continuous spatial inverse FT (SIFT)	$\Psi(x,y) = \iint_{-\infty}^{+\infty} \widetilde{\Psi}(\xi,\eta) \exp[-\mathrm{j}(\xi x + \eta y)]\, \mathrm{d}\xi\, \mathrm{d}\eta$	(20)
FT of rect-function	$\int_{-\infty}^{+\infty} \mathrm{rect}\left(\frac{t}{T}\right) \mathrm{e}^{-\mathrm{j}\,2\pi f t}\, \mathrm{d}t = T\,\mathrm{sinc}(fT)$	(21)
FT of sinc-function	$\int_{-\infty}^{+\infty} \mathrm{sinc}\left(\frac{t}{T}\right) \mathrm{e}^{-\mathrm{j}\,2\pi f t}\, \mathrm{d}t = T\,\mathrm{rect}(fT)$	(22)
FT of triang-function	$\int_{-\infty}^{+\infty} \mathrm{triang}\left(\frac{t}{T}\right) \mathrm{e}^{-\mathrm{j}\,2\pi f t}\, \mathrm{d}t = T\,\mathrm{sinc}^2(fT)$	(23)
Inner product	$(\Psi_1 \cdot \Psi_2) \equiv \langle \Psi_1 \mid \Psi_2 \rangle = \int_{-\infty}^{+\infty} \Psi_1^*(t')\, \Psi_2(t')\, \mathrm{d}t'$	(24)
Convolution	$(\Psi_1 * \Psi_2)(t) := \int_{-\infty}^{+\infty} \Psi_1(t')\, \Psi_2(t-t')\, \mathrm{d}t' = \int_{-\infty}^{+\infty} \breve{\Psi}_1(f)\, \breve{\Psi}_2(f)\, \mathrm{e}^{\mathrm{j}\,2\pi f t}\, \mathrm{d}f$	(25)
Cross-correlation function $\vartheta_{\Psi_1\Psi_2}(t) := (\Psi_1 \otimes \Psi_2)(t)$ Cross power spectrum $\Theta_{\Psi_1\Psi_2}(f) := \mathcal{F}\left\{\vartheta_{\Psi_1\Psi_2}(t)\right\}$	$(\Psi_1 \otimes \Psi_2)(t) := \int_{-\infty}^{+\infty} \Psi_1(t')\, \Psi_2^*(t'-t)\, \mathrm{d}t' = \int_{-\infty}^{+\infty} \breve{\Psi}_1(f)\, \breve{\Psi}_2^*(f)\, \mathrm{e}^{\mathrm{j}\,2\pi f t}\, \mathrm{d}f$	(26)
$\cos x + \cos y$ & $\sin x + \sin y$	$2\cos\frac{x-y}{2}\cos\frac{x+y}{2}$ & $2\cos\frac{x-y}{2}\sin\frac{x+y}{2}$	(27)
$\cos x \cos y$ $(+)$, $\sin x \sin y$ $(-)$ & $\sin x \cos y$	$\frac{1}{2}[\cos(x-y) \pm \cos(x+y)]$ & $\frac{1}{2}[\sin(x-y) + \sin(x+y)]$	(28)
$a\cos x + b\sin x = \Re\left\{\sqrt{a^2+b^2}\,\mathrm{e}^{-\mathrm{j}\arctan(b/a)}\,\mathrm{e}^{\mathrm{j}\,x}\right\}$	$\sqrt{a^2+b^2}\cos\left(x - \arctan\frac{b}{a}\right) = \sqrt{a^2+b^2}\sin\left(x + \arctan\frac{a}{b}\right)$	(29)
Logarithms and their bases, $\log_a x = \frac{\log_b x}{\log_b a}$	$\lg x = \log_{10} x$, $\ln x = \log_{\mathrm{e}} x$, $\mathrm{lb}\, x = \log_2 x$	(30)
Power and amplitude ratios a and $b = \sqrt{a}$ in dB	$a_{\mathrm{dB}} = 10\lg a = 20\lg b$	(31)

Organization of Course

1. Introduction
2. Communications concepts (information theory, modulation)
3. Optical transmitters (lasers, modulators, implementation)
4. Optical amplifiers (SOA, EDFA)
5. Optical receivers (PD, noise, direct and coherent Rx)
6. Optical communication systems (impairments, noise figure, shaping)

Photonics: Basic Components

Probe, laser bar, fibre — glass fibres — photodiode, eye of a needle

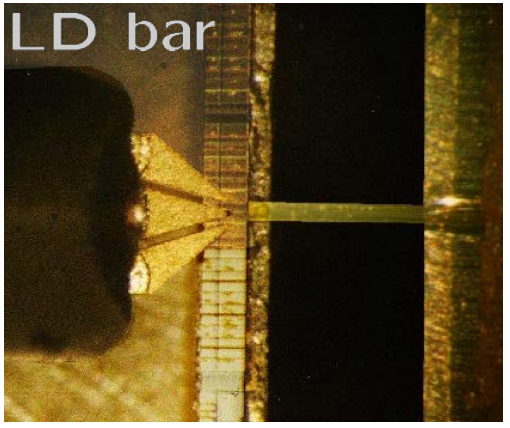

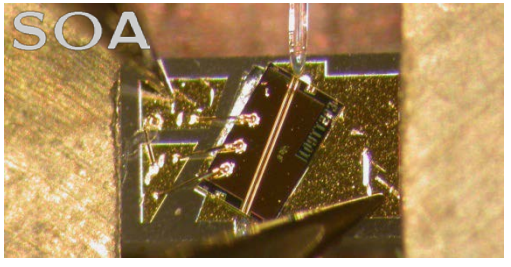

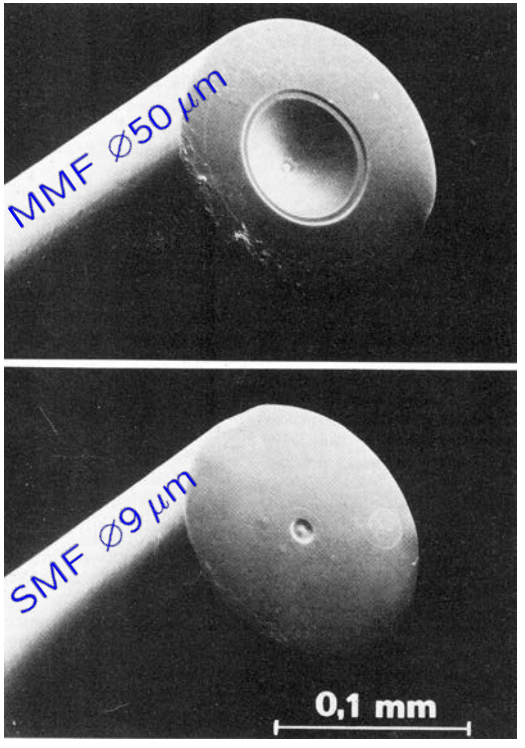

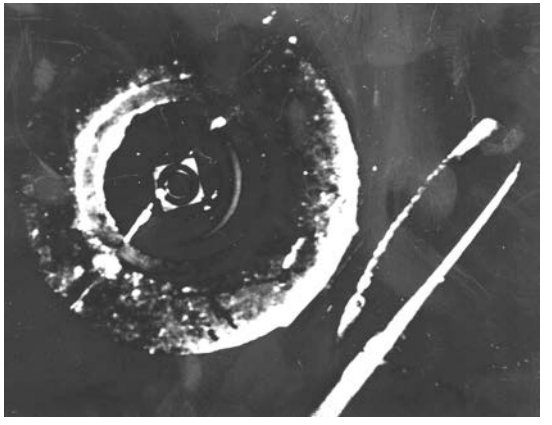

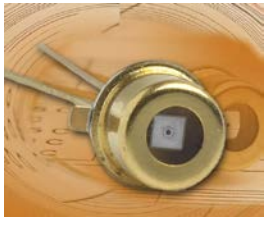

Multimode fibre

$2a = 65\,\mu\text{m}$

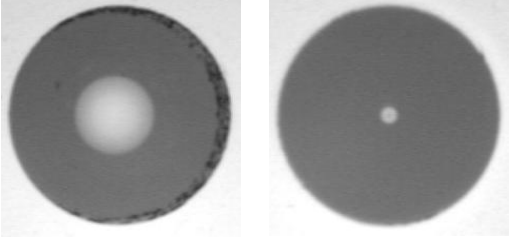

Single-mode fibre

$2a = 9\,\mu\text{m}$

Advantages and Shortcomings of Optical Communication (1)

Data transmission capacity

Obviously, optical communication systems can replace conventional electrical systems only, if there is some advantage to be gained, which justifies the additional expenses of a twofold conversion current-light and light-current. Some important advantages of optical signal transport are:

- Large transmission capacity because of high carrier frequency near $f_O = 200\,\mathrm{THz}$, large fibre bandwidth in the order of $(250 \ldots 190)\,\mathrm{THz} = 60\,\mathrm{THz}$
- Low fibre loss, about $2.2, 0.35, 0.15\,\mathrm{dB/km}$ at $\lambda = 0.85, 1.3, 1.55\,\mu\mathrm{m}$, i. e., down to 3 dB loss for a fibre length of $L = 20\,\mathrm{km}$ corresponding to a power attenuation by a factor of only 2
- Immunity to interference because of the high carrier frequency, and because of the strong confinement of the light inside the fibre

Three milestones of lightwave technology are especially noteworthy. Following an earlier suggestion,[19,20] the first *low-loss fibres* were produced[21] in 1970 reducing the loss from 1 000 dB / km to below 20 dB / km. Further progress[22] resulted by 1979 in a loss of only 0.2 dB / km near $\lambda = 1.55\,\mu\mathrm{m}$. The ultimate low loss[23] of 0.154 dB / km for fibres with a silica (SiO_2) core and a F-doped cladding is limited only by the amorphous structure of silica (Rayleigh scattering) and was reached in 1986.

Although *semiconductor lasers* were first made[24] in 1962, their use became practical only after 1970 when GaAs lasers operating continuously at room temperature were available[25].

Finally, it was only after the invention and perfection of the *Er-doped fibre amplifier*[26] (EDFA) in 1986 that optical communication became so powerful as it is today.

In recent years, with the increasing demand in transmission capacity, new frontiers have opened by the re-invention of *coherent optical communications*, which had formerly been regarded as too complicated and as obsolete in view of the availability of EDFA.

Advantages and Shortcomings of Optical Communication (2)

Planck's law for spectral black-body radiance ($\frac{\mathrm{W}}{\mathrm{sr\,m^2\,Hz}}, \frac{\mathrm{W}}{\mathrm{sr\,m^2\,\mu m}}$):

$$B_f(f,T) = 2\frac{f^2}{c^2}\frac{hf}{\mathrm{e}^{hf/(kT)}-1},$$

$$B_\lambda(\lambda,T) = 2\frac{c}{\lambda^4}\frac{hc/\lambda}{\mathrm{e}^{(hc/\lambda)/(kT)}-1},$$

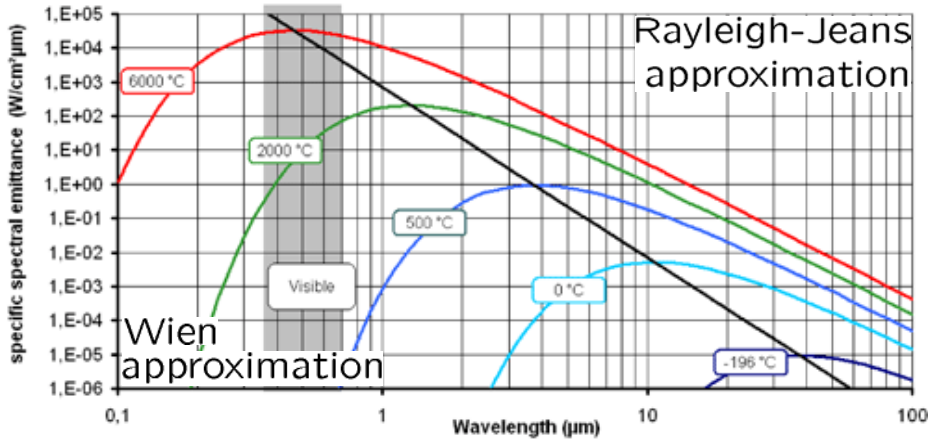

http://www.infratec.co.uk/thermography/thermography-knowledge/theory.html

Reception sensitivity

Optical communications has also shortcomings as compared to electrical transmission. Electrical reception is limited by thermal noise with a power $P_v = kT_0B$ (Boltzmann's constant k, room temperature $T_0 = 293\,\mathrm{K}$, signal bandwidth B), see Eq. (5.54) on Page 124. Optical systems, however, are limited by quantum noise with an equivalent noise power $P_{\mathrm{qu}} = 2hf_OB$ (Planck's constant h, optical carrier frequency f_O), see Eq. (5.81) on Page 132. With the received electrical and optical signal powers P_{el} and P_{op}, we find the respective signal-to-noise power ratios $\mathrm{SNR_{el}}$ and $\mathrm{SNR_{op}}$. For equal SNR we see that electrical reception is by far more sensitive ($kT_0 = 25\,\mathrm{meV}$, $hf_O = 1\,\mathrm{eV}$ at $f_O = 242\,\mathrm{THz}$, $\lambda_O = 1.24\,\mu\mathrm{m}$),

$$\mathrm{SNR_{el}} = \frac{P_{\mathrm{el}}}{kT_0B}\,, \quad \mathrm{SNR_{op}} = \frac{P_{\mathrm{op}}}{2hf_OB}\,, \quad \frac{P_{\mathrm{el}}}{P_{\mathrm{op}}} = \frac{kT_0}{2hf_O} \ll 1\,, \quad \left.\frac{P_{\mathrm{el}}}{P_{\mathrm{op}}}\right|_{\mathrm{dB}} \approx 10\lg\frac{25\,\mathrm{meV}}{2\,\mathrm{eV}} = -19\,\mathrm{dB}\,. \quad (1.3)$$

Advantages and Shortcomings of Optical Communication (3)

Transmission spans

Practical spans without amplification are about $L = 70\,\mathrm{km}$

Why?

Why need amplifiers be distributed along a transmission distance?

Due to attenuation in the transmitting fibre the optical signal decays exponentially with the transmission span. Practical spans without amplification are about 70 km. Why are the spans so short?

A transatlantic transmission from New York to London experiences an attenuation of about 1 400 dB (7 000 km @ 0.2 dB / km). Thus, for receiving one photon in London we have to inject 10^{140} photons into the optical fibre end in New York. If all the mass of our sun ($m_{\text{sun}} = 2 \times 10^{33}$ g) having an energy equivalent of $W_{\text{sun}} = mc^2 = 1.8 \times 10^{47}$ Ws could be converted into photons with a photon energy $hf = 6 \times 10^{-34}\,\text{Ws}^2 \times 200\,\text{THz} = 1.2 \times 10^{-19}$ Ws, we had generated 1.5×10^{66} photons at a wavelength of 1.55 μm ($f \approx 200$ THz), and could bridge a span with 660 dB loss, corresponding to a transmission distance of 3 300 km only. For a direct transmission New York – London we thus had to evaporate $10^{140}/10^{66} = 10^{74}$ suns.

Calculations stimulated by an oral presentation of N. J. Doran (S. K. Turitsyn, M. P. Fedoruk, N. J. Doran and W. Forysiak: Optical soliton transmission in fiber lines with short-scale dispersion management. 25th European Conf. on Optical Communication (ECOC'99), Nice, France, September 26–30, 1999)

Why need amplifiers be distributed along a transmission distance?

10^{74} suns are quite a bit. The (observable) universe is estimated to have an extension of 14×10^9 light years. Its mean density is supposed to be $3 \times 10^{-30}\,\mathrm{g/cm^3}$ (http://curious.astro.cornell.edu/question.php?number=342).

So, the universe's mass (comprising not only suns) is $m_{\mathrm{univ}} = 7 \times 10^{54}\,\mathrm{g}$, and its energy equivalent is $W_{\mathrm{univ}} = m_{\mathrm{univ}} c^2 = 6 \times 10^{68}\,\mathrm{Ws}$ corresponding to 4.7×10^{87} photons at a wavelength of $1.55\,\mu\mathrm{m}$.

If we are able to receive one photon then the maximum span will be $877\,\mathrm{dB}/(0.2\,\mathrm{dB/km}) = 4\,385\,\mathrm{km}$.

However, for bridging the distance New York – London in one go we had to burn $10^{140}/10^{87} = 10^{53}$ universes!

How come — NY supernova not visible in London? Spherical $\sim (bL)^2$, fibre $\sim \exp(\alpha L)$:

$$a_{\text{free space}}/\,\mathrm{dB} \sim 10\lg\left[(bL)^2\right] = 20\lg(bL)$$

$$a_{\text{fibre}}/\,\mathrm{dB} = 10\lg\left[\exp(\alpha L)\right] = 4.34(\alpha L)$$

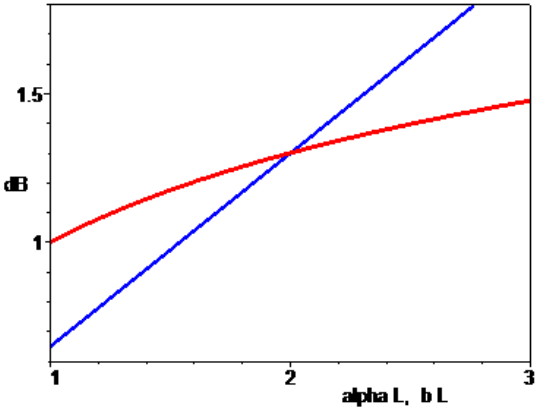

Universe's mass calculations and web address contributed by Dipl.-Phys. Jan Brückner, DFG Research Training Group 786 "Mixed Fields and Nonlinear Interactions" (http://www.gkmf.uni-karlsruhe.de), Karlsruhe, Germany, June 23, 2005

LECTURE 3

Optical Communication Concepts

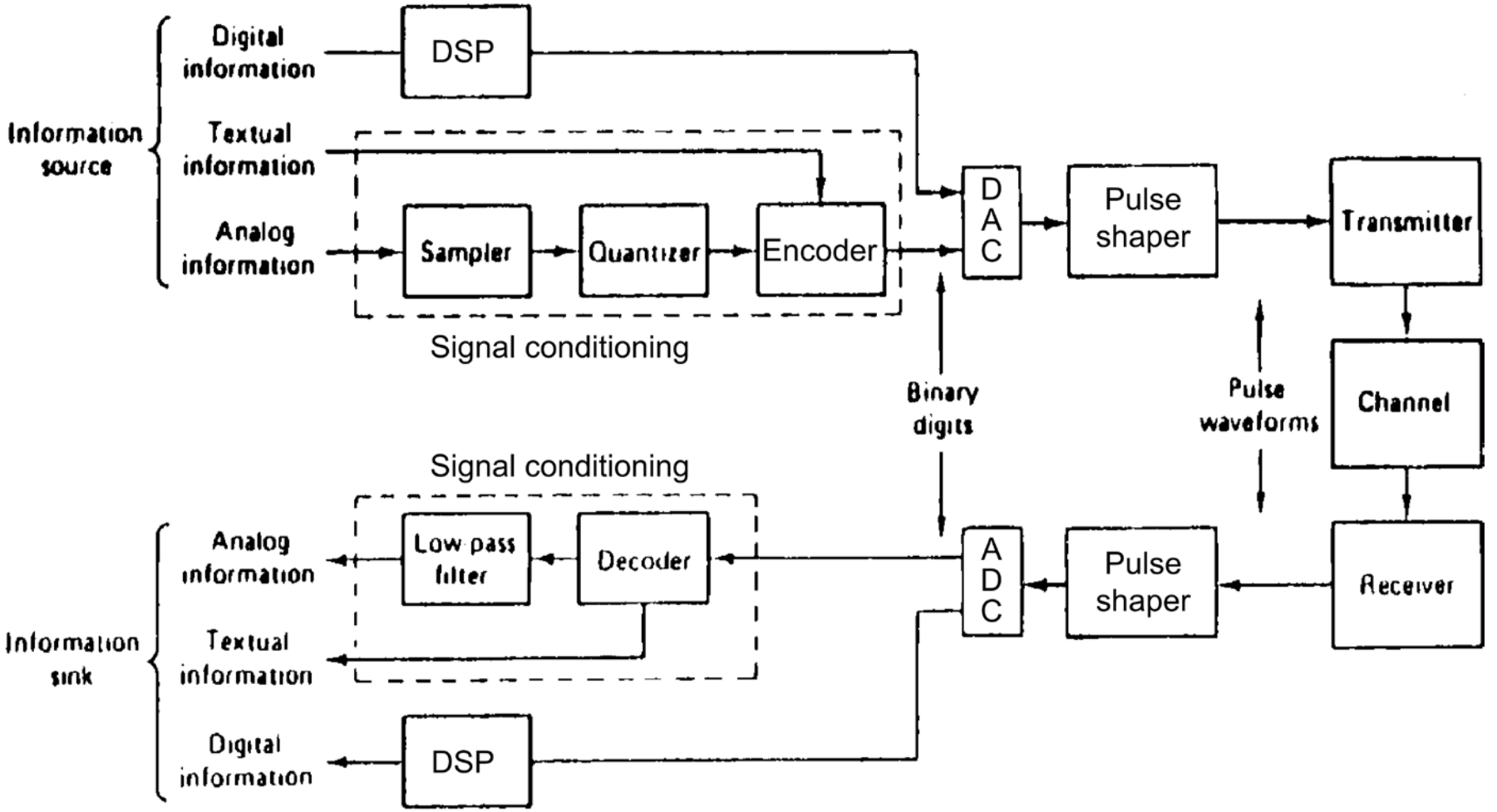

Signal Conditioning

Sampling, Nyquist Frequency and Interpolation

Sampling function $\sigma(t)$ is self-reciprocal in Fourier space $\bar{\sigma}(f)$:

$$\sigma(t) = T_s \sum_{i=-\infty}^{+\infty} \delta(t - iT_s) = \sum_{i=-\infty}^{+\infty} \exp\left(\mathrm{j}\, 2\pi\, i\, \frac{t}{T_s}\right),$$

$$\bar{\sigma}(f) = \sum_{i=-\infty}^{+\infty} \delta(f - iF_s), \qquad F_s = 1/T_s$$

Function $\Psi(t)$ bandlimited, baseband spectra on periodic carriers:

$$\bar{\Psi}(f) = \int_{-\infty}^{+\infty} \Psi(t) \exp\left(-\mathrm{j}\, 2\pi\, ft\right) \mathrm{d}t\,, \quad \bar{\Psi}(|f| > B) = 0$$

$\Psi(t)$ sampled with Nyquist frequency B at intervals $T_s = 1/(2B)$, discrete $\Psi_s(t) = \sigma(t)\,\Psi(t)$ at positions $t = t_i = i/(2B)$ result:

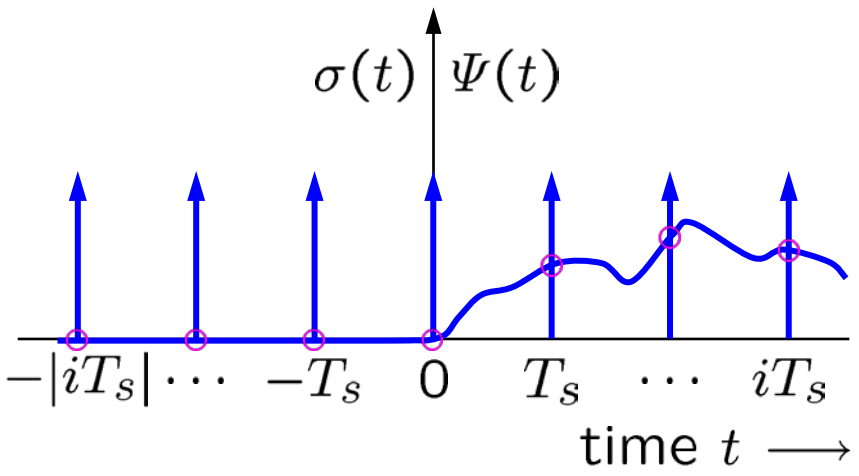

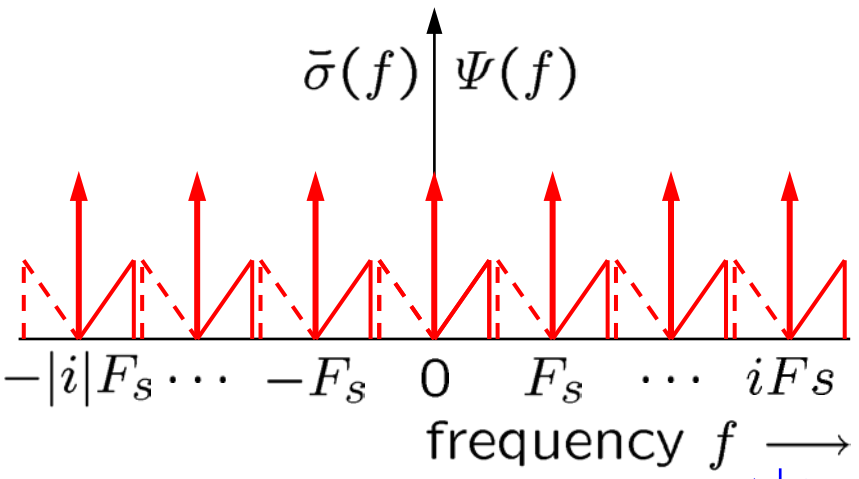

Sampling, Nyquist Frequency and Interpolation

Reconstruction of $\Psi(t)$ from real sampled data $\Psi(i(2B))$ by filtering with ideal lowpass (transm. 1 in band $|f| < B$, 0 outside), i. e., with interpolation recipe (convolution, no *linear* interpolat.):

$$\Psi(t) = \sum_{i=-\infty}^{+\infty} \Psi(iT_s) \frac{\sin(\pi(t - iT_s)2B)}{\pi(t - iT_s)2B}, \quad T_s = \frac{1}{2B}, \quad F_s = \frac{1}{T_s}$$

Oversampling needed for real-world filter.

Undersampling leads to aliasing errors!

Sideband overlap ($F_s < 2B$) for $T_s > \frac{1}{2B}$ → "aliasing" errors in $\Psi(t)$

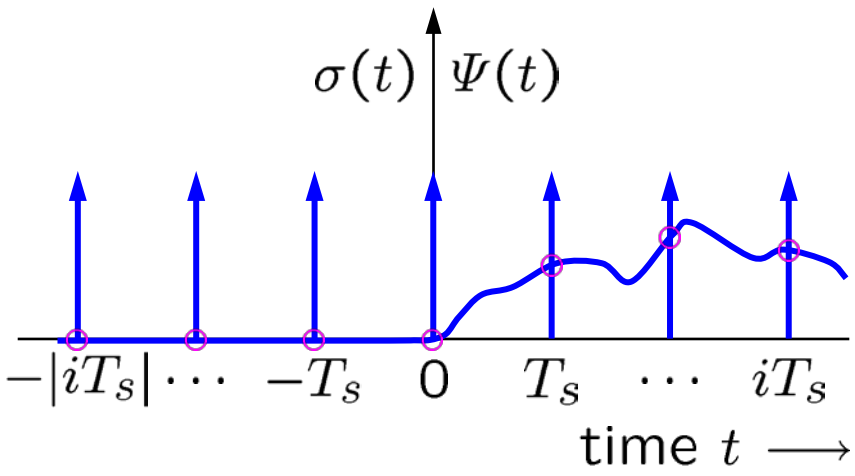

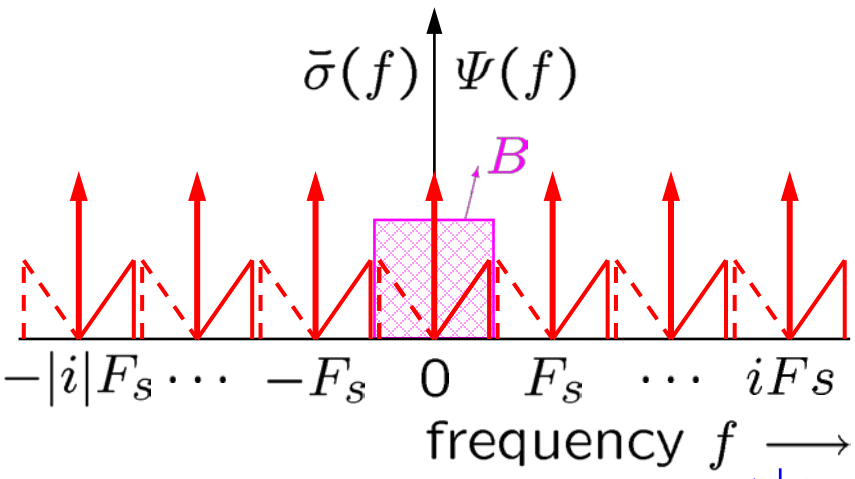

Quantization (1)

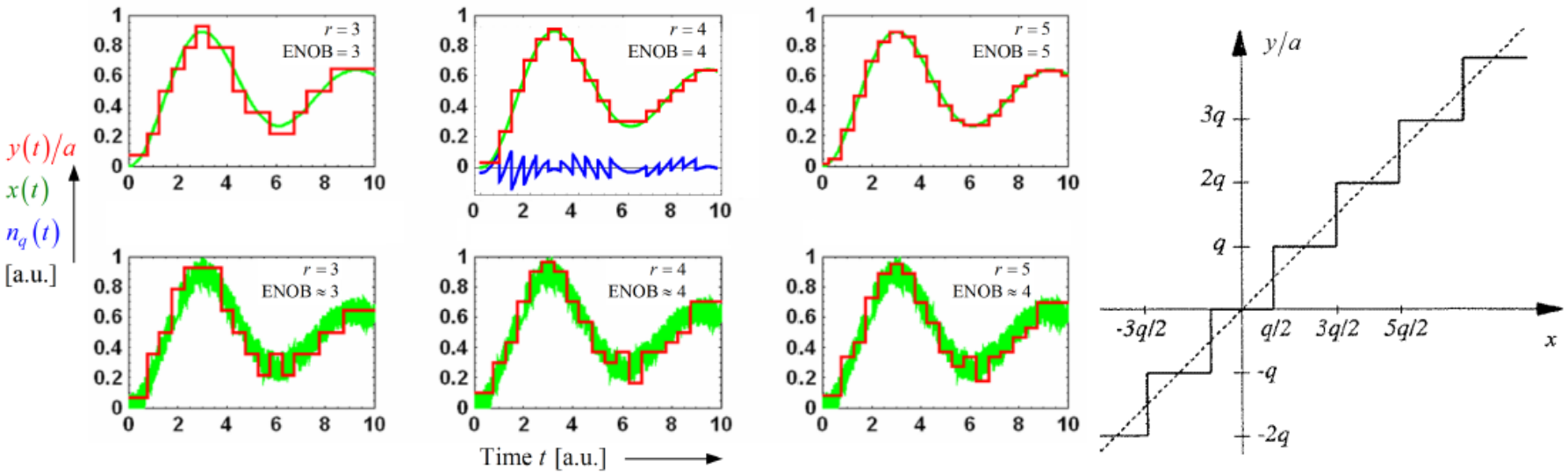

Quantization For quantization, the effective signal span $\sqrt{P_S}$ has to be covered with a number of M discrete quantization levels (not necessarily equidistantly spaced) such that one can assign one out of M discrete values to each sampling point. Clearly, this procedure leads to additional inaccuracies named quantization noise[6], see Appendix B.2.3 on Page 192 ff., Eq. (B.42b). The logarithmic signal-to-noise power ratio due to quantizing a sinusoidal signal by an analogue-to-digital converter (ADC) with r bit and $M = 2^r \gg 1$ levels is approximately, according to Appendix B.2.3, Eq. (B.43) on Page 193,

$$\mathrm{SNR}_{q,\mathrm{dB}}^{(\sin)} = 6.02\,r + 1.76\,, \qquad r_e = \mathrm{ENOB} = \frac{\mathrm{SNDR}_{q,\mathrm{dB}}}{6.02} - 0.293\,. \tag{2.5}$$

The presence of noise decreases the effective number of bits (ENOB) from the physical value r to a smaller effective value $r_e = \mathrm{ENOB}$. Again, Eq. (2.5) can be used, if $\mathrm{SNR}_{q,\mathrm{dB}}^{(\sin)}$ is now interpreted as the signal-to-noise-and-distortion power ratio $\mathrm{SNDR}_{q,\mathrm{dB}}$ at the input of the ADC, and r is replaced by $r_e = \mathrm{ENOB}$.

Quantization (2)

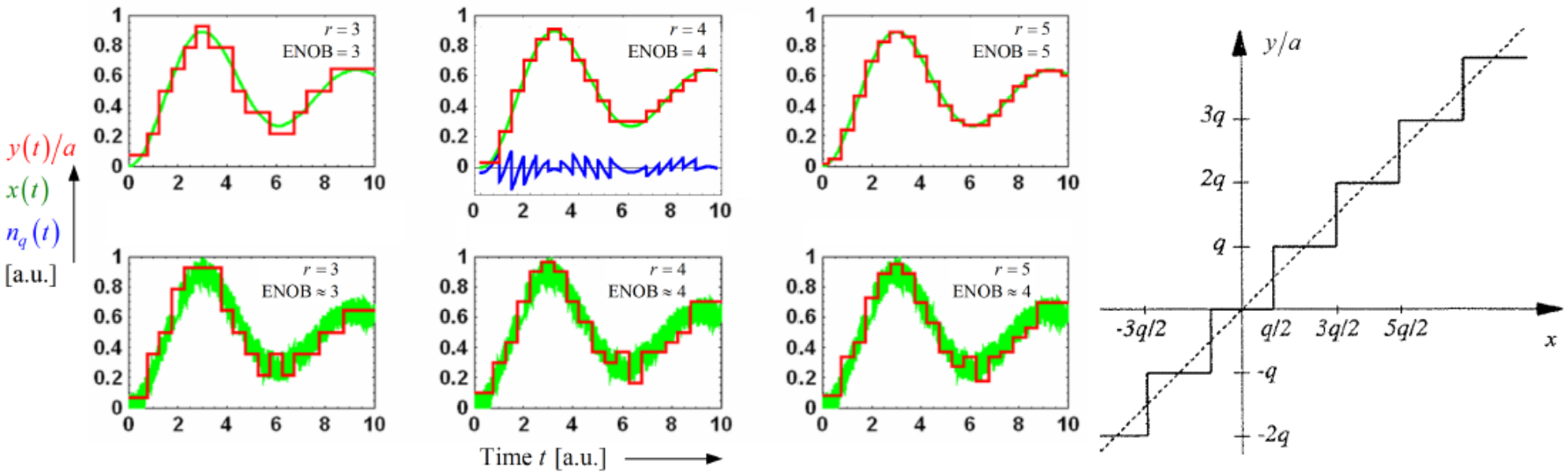

Fig. 2.3. Quantization, noise and effective number of bits (ENOB) in an analogue-to-digital converter (ADC). Input $x(t)$, down-scaled quantized output $y(t)/a$ and quantization error (quantization noise) $n_q(t)$ as a function of time t. The quantity a is the average slope of the ADC, $\mathbf{y} = a\,\mathbf{x}$. **Upper row:** Quantization of noiseless signal $x(t)$ with $r = \{3, 4, 5\}$ bit and $M = 2^r$ levels. The larger r becomes, the better the down-scaled quantized output $y(t)/a$ approximates the input $x(t)$ (clearly visible for $t = \{0 \ldots 1, 5 \ldots 7, 9 \ldots 10\}$). **Lower row:** Quantization of the signal $x(t)$ superimposed by noise.

It makes no sense to choose $M = 2^r$ so large that the resulting quantization noise with RMS value σ_{n_q}, see Eq. (B.42b), becomes much smaller then the noise which comes along with the signal. If the step size $q \approx \sqrt{P_R}$ between levels is chosen to be of the order of the signal's noise $\sqrt{P_R}$, the quantization noise $\sigma_{n_q} = q/\sqrt{12} \approx \frac{1}{3}q$ is of the order of the signal's noise $\sqrt{P_R}$. Therefore a coarse estimate of the proper number of levels is $M = 1 + \sqrt{P_S}/\sqrt{P_R}$ (one more level than intervals), a number which is intimately connected to the signal-to-noise power ratio (SNR),

$$\gamma \equiv \mathrm{SNR} := \frac{P_S}{P_R}, \qquad \gamma_{\mathrm{dB}} = 10\lg(\gamma), \qquad M = 1 + \sqrt{\gamma}, \quad M^2 = 1 + \gamma + 2\sqrt{\gamma} \approx 1 + \gamma. \tag{2.6}$$

Quantization and Coding

The quantization noise is of the order of the signal's noise having power P_R if the steps between levels are chosen to be of the order $\sqrt{P_R}$. Therefore a coarse estimate of the proper number of levels is $M = 1 + \sqrt{P_S}/\sqrt{P_R}$ (one more level than intervals), a number which is intimately connected to the signal-to-noise power ratio (SNR),

$$\gamma \equiv \mathrm{SNR} := \frac{P_S}{P_R}, \qquad \gamma_{\mathrm{dB}} = 10\lg(\gamma), \qquad M = 1 + \sqrt{\gamma}, \quad M^2 = 1 + \gamma + 2\sqrt{\gamma} \approx 1 + \gamma. \tag{2.6}$$

Coding Number of bits r needed to code each sample is related to the number of quantized signal levels M of Eq. (2.6):

$$M = b_l^r, \qquad r = \log_{b_l} M \qquad \Longrightarrow \qquad r \approx \frac{10\lg\sqrt{1+\gamma}}{10\lg 2} \approx 3.32 \times \frac{\gamma_{\mathrm{dB}}}{2} \quad \text{for } b_l = 2,\ \gamma \gg 1\,. \tag{2.7}$$

The resulting temporal bit sequence of logical 1 and 0 is known as a binary pulse code modulation (PCM). For transmission, the PCM signal has to be encoded in a sequence of symbols made up of discrete values of a physical quantity, e. g., a sequence of binary impulses $p(t)$ with amplitudes $a_n = 0, 1$. For $b_l = 2$, the PCM bit rate R_b is a multiple r of the sampling rate F_s,

$$R_b = rF_s, \quad R_b = F_s \log_2 M \qquad \text{for } b_l = 2. \tag{2.8}$$

An example for binary PCM is telephone voice transmission with $B = 3.4\,\mathrm{kHz}$, where $r = 8$ and $F_s = 8\,\mathrm{kHz}$ with $R_b = 8\,F_s = 64\,\mathrm{kbit/s}$ are common. The circuitry responsible for converting analog electrical signals to digital data and vice versa is known as *co*der / *dec*oder (CODEC). A CODEC translates each sampled value into its binary representation.

Coding

Forward error correction (FEC) With increasing computing power, a redundancy transmission scheme becomes possible, where codes are transmitted which allow an error correction at the receiver side. For an optical communication channel at 40 Gbit/s the bit error probability (BER) performance of moderate-length nonbinary low-density parity-check (LDP) codes[8,9,10,11] is as follows (RS stands for Reed-Solomon):

First generation FEC Hard-decision block code, typically RS(255, 239) with a 6.69 % overhead. For an output BER $= 10^{-13}$, the RS code yields a net coding gain (see below) of about 6 dB.

Second generation FEC Hard-decision concatenated codes combined with interleaving and iterative decoding techniques to improve the FEC capability. The ITU-T G.975.1 standard has defined eight second-generation FEC algorithms with 6.69 % overhead. As an example, an LDP(29136, 27 315) code[12] achieves a coding gain of 9.4 dB at an output BER $= 10^{-15}$, starting from a pre-FEC BER $= 4.45 \times 10^{-3}$.

Third generation FEC Soft-decision[13] FEC (SD-FEC) with turbo product and LDP codes are especially necessary for 100G long-haul transmission equipment. Coherent receiving technology in optical communication systems and the rapid growth in computing power enables soft-decision FEC. For an output BER $= 10^{-15}$ with 15 . . . 20 % overhead, soft-decision FEC yields a net coding gain of 11 dB. An FEC scheme[14] with 15 % overhead and an input pre-FEC BER $= (1.8 \ldots 2) \times 10^{-2}$ effectively prevents line errors.

Without going into coding details, these examples demonstrates the potential of the technique: A coding gain of about 10 dB means that 10 dB less power can be received for a final BER $= 10^{-15}$ than without FEC. This allows a raw BER of the order of 10^{-4}. The price is that a data rate of, e. g., 40 Gbit/s increases to a line rate of 43 Gbit/s with a redundancy overhead of about 7 %.

Bit Rate

Bit rate The minimum PCM bit rate ($b_l = 2$) resulting from analogue-to-digital conversion of a bandwidth-limited real-valued signal (sampling rate $F_s = 2B$, number of quantized signal levels M) for a signal-to-noise power ratio γ as in Eq. (2.6) is[15,16]

$$R_b = rF_s = 2B\log_2 M = B\log_2\left(M^2\right) \quad \text{(for a real-valued band-limited signal)},$$

$$R_b \approx B\log_2(1+\gamma) = B\frac{10\log_{10}(1+\gamma)}{10\log_{10}2} \approx 3.32\times B\,\gamma_{\mathrm{dB}} \quad \text{for } \gamma \gg 1\,. \tag{2.9}$$

If a real signal with bandwidth B is sampled with a rate $F_s = 2B$, quantized with multiple levels M, and encoded with symbols representing r bit each, the symbol rate[17] equals the sampling rate, $R_s = F_s$ (unit Bd)[18], and is smaller than the bit rate R_b by a factor of r. Depending on the shape of the pulses, the occupied spectral passband width $\mathcal{B}$ around an optical carrier changes. When signalling with a sequence of real-valued sinc-shaped so-called Nyquist pulses $\sum_{i=-\infty}^{+\infty}\Psi(iT_s)\,\mathrm{sinc}(t/T_s - i)$ as in Eq. (2.3), the required spectral passband width $\mathcal{B} = 2B$ is minimum as compared to other pulse shapes. If the Nyquist pulses are in addition complex-valued, the required spectral passband width is $\mathcal{B} = B$, and we find

$$R_s = F_s = \frac{R_b}{r}, \quad \text{sinc-pulses with spectral width } \mathcal{B} = F_s = \begin{cases} 2B & \text{(real symbols)} \\ B & \text{(complex symbols)} \end{cases}. \tag{2.10}$$

Real signal $\Psi_c(t) = 2\Psi(t)\cos\omega_0 t$: Carrier sidebands are correlated, $\bar{\Psi}(f) = \bar{\Psi}^*(-f)$:

$$\bar{\Psi}_c(f) = \int_{-\infty}^{+\infty}\Psi(t)\left(\mathrm{e}^{\mathrm{j}2\pi f_0 t} + \mathrm{e}^{-\mathrm{j}2\pi f_0 t}\right)\mathrm{e}^{-\mathrm{j}2\pi f t}\,\mathrm{d}t = \bar{\Psi}(f-f_0) + \bar{\Psi}(f+f_0) = \bar{\Psi}(f-f_0) + \bar{\Psi}^*(-f+f_0) = \bar{\Psi}_c^*(-f)$$

Changing the base of the logarithm of x from a to b:

$\log_a x = y\log_b x, \quad x = a^{y\log_b x}, \quad \log_b x = \log_b\left(a^{y\log_b x}\right) = y\log_b x\,\log_b a \quad \rightarrow \quad y = 1/\log_b a,$

$\log_b x = \log_b a\,\log_a x.$ Example: $\log_{10} x = \log_{10} 2\,\log_2 x = 0.301\times\log_2 x, \quad \log_2 x = 3.32\times\log_{10} x.$

LECTURE 4

Orthogonal Functions

Inner product: $$(\Psi_1 \cdot \Psi_2) \equiv \langle \Psi_1 | \Psi_2 \rangle = \int_{-\infty}^{+\infty} \Psi_1^* \left(t'\right) \Psi_2 \left(t'\right) \mathrm{d}t'$$

$$= \int_{-\infty}^{+\infty} \bar{\Psi}_1^* \left(f'\right) \bar{\Psi}_2 \left(f'\right) \mathrm{d}f'$$

$$\frac{1}{T} \int_{-\infty}^{+\infty} \mathrm{rect}\left(\frac{t}{T} - m\right) \mathrm{rect}\left(\frac{t}{T} - m'\right) \mathrm{d}t = \delta_{mm'},$$

$$\frac{1}{T} \int_{-\infty}^{+\infty} \mathrm{sinc}\left(\frac{t}{T} - m\right) \mathrm{sinc}\left(\frac{t}{T} - m'\right) \mathrm{d}t = \delta_{mm'},$$

$$\frac{1}{T} \int_{T_0 - T/2}^{T_0 + T/2} \exp\left(+\mathrm{j}2\pi m \frac{t}{T}\right) \exp\left(-\mathrm{j}2\pi m' \frac{t}{T}\right) \mathrm{d}t = \delta_{mm'},$$

$$\frac{1}{F} \int_{F_0 - F}^{F_0 + F} \cos\left(\frac{\pi}{2} \frac{f}{F}\right) \exp\left(+\mathrm{j}2\pi m \frac{f}{F}\right) \cos\left(\frac{\pi}{2} \frac{f}{F}\right) \exp\left(-\mathrm{j}2\pi m' \frac{f}{F}\right) \mathrm{d}f = \delta_{mm'}.$$

$$\frac{1}{N} \sum_{n=0}^{N-1} \exp\left(+\mathrm{j}2\pi \frac{\nu n}{N}\right) \exp\left(-\mathrm{j}2\pi \frac{\nu' n}{N}\right) = \delta_{\nu\nu'}$$

Leuthold, J.; Freude, W.: 'Optical OFDM and Nyquist Multiplexing'. In: Kaminow, I. P.; Li, Tingye; Willner, A. E. (Eds.): 'Optical Fiber Telecommunications VI B. Systems and Networks', 6th Ed. Elsevier (Imprint: Academic Press), Amsterdam 2013, Chapter 9, pp. 381–432

Orthogonality, Modulation, Multiplexing, and Coding

Signal orthogonality: Receiving signal 1 independent of signal 2.

Mod Amplitude (AM), phase (PM), frequency (FM) modulation
Intensity (IM), pulse position modulation (PPM)

Multiplexing (MUX) orthogonal signals allows transmission in a shared medium (i. e., air for wireless).

MUX technologies (digital/analogue, base/carrier band, P2P/MP):

Space Space division (directions, cables, fibres, modes)
Multiple input – multiple output (MIMO)

Time Time division (TDM, disjoint time slots)
Orthog. time division (OTDM, orthog. impulses, Nyquist-WDM)

Freq Wavelength division (WDM/FDM, disjoint λ-slots/f-slots)
Orthog. frequency division (OFDM, orthog. carriers)

Pol Polarization division (PDM, orthog. polarizations)

Code Code division multiple access (CDMA)

Coding (FEC): BER$=1.9\times10^{-2}$ reduced to 10^{-15} (25 % overhead)

T. Mizuochi: Recent progress in forward error correction and its interplay with transmission impairments. IEEE J. Sel. Topics Quantum Electron.12 (2006) 544–554

Time and Frequency **M**ultiplexing (**T**DM, O**T**DM, O**F**DM, **W**DM)

Time **D**ivision Orth. **T**ime **D**iv. Orth. **F**req. **D**iv. **W**avelength **D**iv.

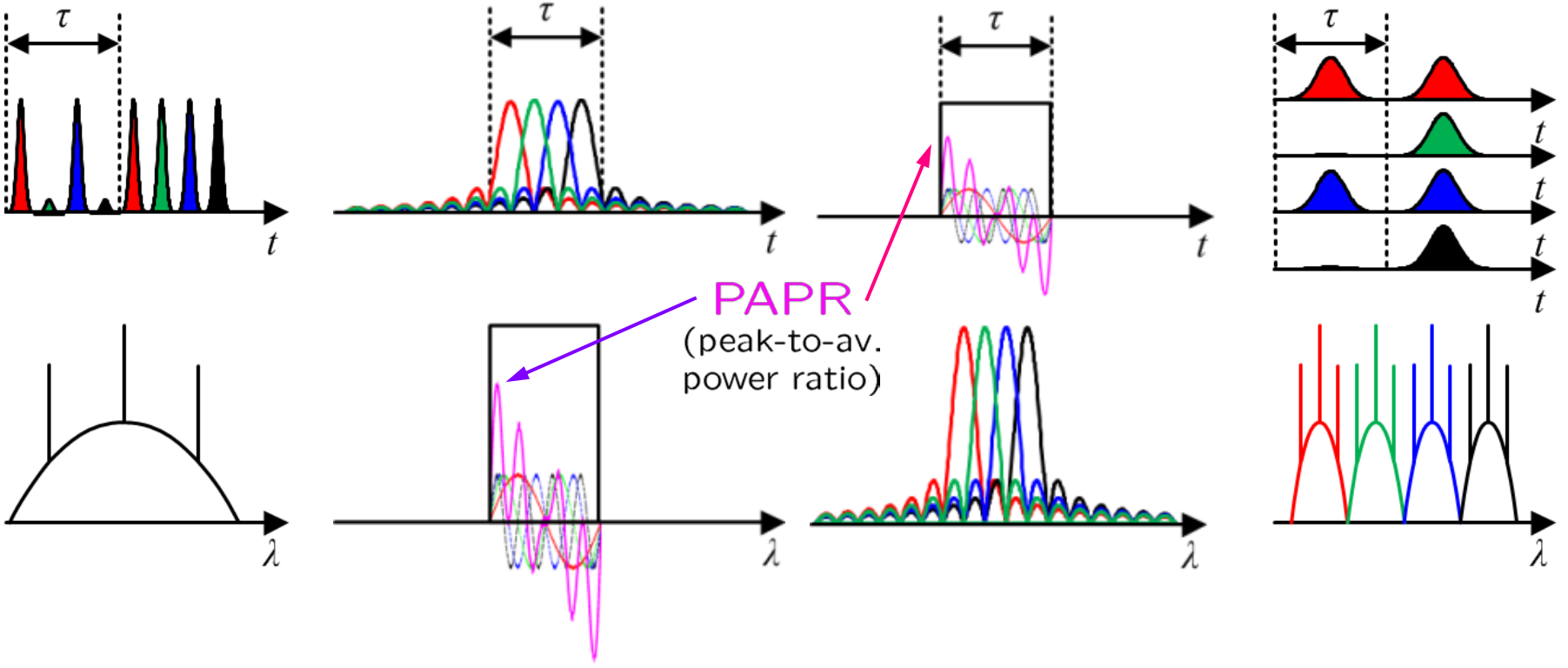

Symbol rate N/τ.
N ch in time slot τ,
broad spectrum
TDM

Symbol rate $1/\tau$.
N overlapping
sinc-impulses
OTM, Nyquist-WDM

Symbol rate $1/\tau$.
N overlapping
sinc-spectra
OFDM

Symbol rate $1/\tau$.
N adjacent
carrier spectra
WDM

Fundamentals of Wave Propagation

Maxwell's Equations

$$\operatorname{curl}\vec{H}=\frac{\partial\vec{D}}{\partial t}\,,\qquad \operatorname{curl}\vec{E}=-\frac{\partial\vec{B}}{\partial t}\,,$$

$$\operatorname{div}\vec{D}=0\,,\qquad \operatorname{div}\vec{B}=0\,,$$

$$\vec{D}=\epsilon_0\vec{E}+\vec{P}\,,\qquad \vec{B}=\mu_0\vec{H}$$

Fourier Transform

$$\Psi(t)=\int_{-\infty}^{+\infty}\bar{\Psi}(f)\,\mathrm{e}^{+\mathrm{j}\,2\pi f t}\,\mathrm{d}f,\qquad \bar{\Psi}(f)=\int_{-\infty}^{+\infty}\Psi(t)\,\mathrm{e}^{-\mathrm{j}\,2\pi f t}\,\mathrm{d}t$$

Coordinates — Homogeneous Medium — Wave Equation

$$\mathrm{d}F = \mathrm{d}x\ \mathrm{d}y = r\mathrm{d}r\,\mathrm{d}\varphi\,,$$
$$x = d\sin\gamma\cos\Phi\,,$$
$$y = d\sin\gamma\sin\Phi\,,$$
$$z = d\cos\gamma\,,$$
$$\frac{\partial(x,y)}{\partial(\gamma,\Phi)} = d^2\cos\gamma\sin\gamma\,,$$
$$\mathrm{d}\Omega = \sin\gamma\,\mathrm{d}\gamma\,\mathrm{d}\Phi\,.$$

For Cartesian coordinates only ($q = x, y, z$):

$$\Psi(t,x,y,z) = E_q(t,x,y,z), H_q(t,x,y,z),$$
$$\Psi(t,r,\varphi,z) = E_z(t,r,\varphi,z), H_z(t,r,\varphi,z),$$
$$\nabla^2\Psi(t,\vec{r}) = \frac{n^2}{c^2}\frac{\partial^2}{\partial t^2}\Psi(t,\vec{r}).$$

Weak inhomogeneity:

$$\frac{|\Delta n|_\lambda}{n} \ll 1\,, \qquad \frac{|\Delta(\mathrm{grad}\,n)|_\lambda}{|\mathrm{grad}\,n|} \ll 1$$

$$\Rightarrow \qquad \nabla^2\Psi(t,\vec{r}) = \frac{n^2(r)}{c^2}\frac{\partial^2}{\partial t^2}\Psi(t,\vec{r})$$

Propagating Mode in a Waveguide

Fundamental modal field $\Psi(t,z) := \Psi(t,\vec{r})$ (equivalent plane wave propagating in $+z$-direction with waveguide's propagation constant $\beta(\omega) = n_e(\omega)\, k_0$ (propagation constant in vacuum $k_0 = \omega/c$, equivalent modal refractive index $n_e = \beta/k_0 = \sqrt{\epsilon_{r\,\mathrm{eff}}}$), calculated from an eigenfunction analysis.

Solution $\Psi(t,z)$, Fourier transform $\bar{\Psi}(f,z)$:

$$\Psi(t,z) = a(t)\, \mathrm{e}^{\mathrm{j}[\omega_0 t - \beta(\omega_0) z]},$$

$$\bar{\Psi}(f,z) = \bar{a}(f - f_0)\, \mathrm{e}^{-\mathrm{j}\,\beta(\omega_0) z}$$

Solution ansatz: Carrier wave $\exp(\mathrm{j}\,\omega_0 t)$ with angular frequency $\omega_0 = 2\pi f_0$, modulated with complex amplitude $a(t)$, varies slowly on scale of optical carrier's period $1/f_0$.

Fibre nonlinearities referred to later on.

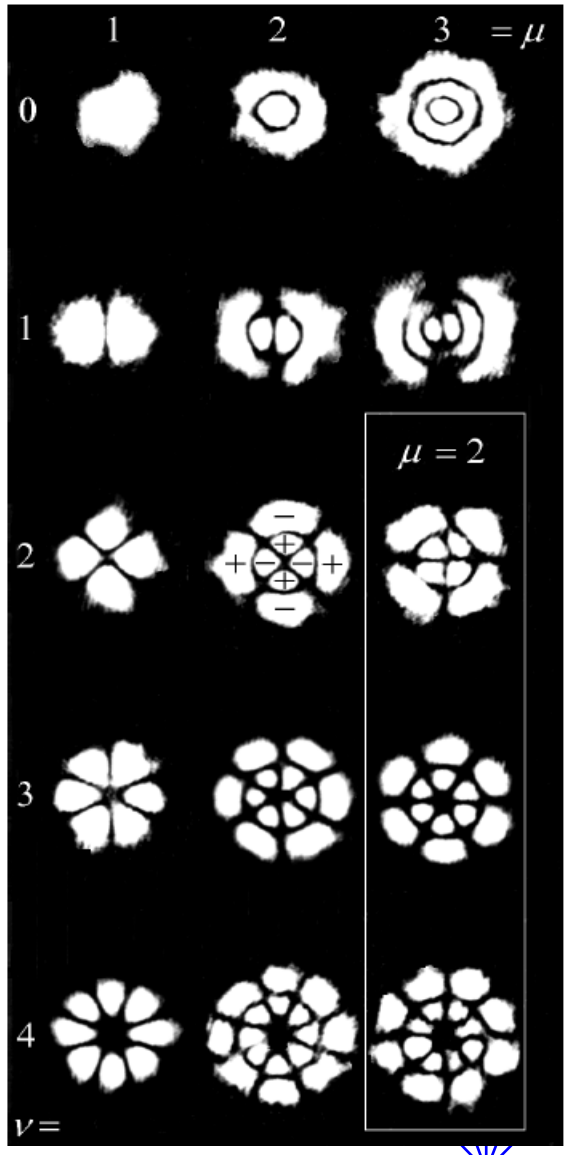

Optical Fibre Channel (1)

The fundamendal-mode transfer function $\breve{h}_c(f) := \breve{h}(f, L)$ of a weakly guiding fibre with length L is defined by the ratio of the Fourier transforms of the fields at output $z = L$ and input $z = 0$ of the fibre. The (analytic) transfer function $\breve{h}_c(f)$ and the associated (causal) real impulse response $h_c(t)$ are

$$\breve{h}_c(f) := \breve{h}(f, L) = \frac{\breve{\Psi}(f, L)}{\breve{\Psi}(f, 0)} = \mathrm{e}^{-\mathrm{j}\,\beta(\omega)L}, \quad \beta(\omega) = -\beta(-\omega); \quad h_c(t) = \int_{-\infty}^{+\infty} \breve{h}_c(f)\,\mathrm{e}^{\mathrm{j}\,2\pi f t}\,\mathrm{d}f. \tag{2.12}$$

Instead of the propagation constant β, the effective refractive index n_e of the propagating mode is frequently used; the normalized frequency parameter V combines the quantities core radius a, angular frequency ω, core refractive index n_1, cladding refractive index n_2, and relative refractive index difference Δ,

$$n_e = \frac{\beta}{k_0}, \qquad k_0 = \frac{\omega}{c} = \frac{2\pi}{\lambda}, \qquad V = a k_0 n_1 \sqrt{2\Delta}, \qquad \Delta = \frac{n_1^2 - n_2^2}{2n_1^2} \underset{\Delta \ll 1}{\approx} \frac{n_1 - n_2}{n_1}. \tag{2.13}$$

For narrow-banded optical spectra it is useful to expand $\beta(\omega)$ in a Taylor series around the carrier frequency $f_0 = c/\lambda_0 = \omega_0/(2\pi)$ and retain terms up to third order, that is,

$$\beta(\omega) \approx \beta_0^{(0)} + (\omega - \omega_0)\beta_0^{(1)} + \frac{(\omega - \omega_0)^2}{2!}\,\beta_0^{(2)} + \frac{(\omega - \omega_0)^3}{3!}\,\beta_0^{(3)}, \tag{2.14}$$

$$\beta_0^{(i)} = \left.\frac{\mathrm{d}^i \beta(\omega)}{\mathrm{d}\omega^i}\right|_{\omega=\omega_0}, \quad \beta_0 := \beta_0^{(0)}, \quad \Delta\omega = \omega - \omega_0\,, \quad \Delta f = \Delta\omega/(2\pi).$$

Optical Fibre Channel (2)

We identify the modal phase velocity v_p, the group velocity v_g and the group delay t_g (propagation length $z = L$, group refractive index n_g), which is related to the first-order chromatic dispersion C and its derivatives (e. g., D), Eq. (2.17),

$$v_p = \frac{\omega_0}{\beta_0^{(0)}}, \qquad v_g^{-1} = \frac{t_g}{L} = \frac{n_g}{c} = \beta_0^{(1)}, \qquad \frac{1}{L}\frac{\mathrm{d}t_g}{\mathrm{d}\omega} = \beta_0^{(2)}, \qquad \frac{1}{L}\frac{\mathrm{d}^2 t_g}{\mathrm{d}\omega^2} = \beta_0^{(3)}. \tag{2.15}$$

The length-related group delay time difference $\Delta t_g/L$ of two signals propagating in the same fundamental mode at optical carriers, which differ in λ by $\Delta\lambda$, can be approximately written as (step-index fibre with core radius a, core refractive index n_1, cladding refractive index n_2, $V = ak_0\sqrt{n_1^2 - n_2^2}$, $B \approx (\beta - n_2 k_0)/(n_1 k_0 - n_2 k_0)$, $k_0 = \omega/c$)

$$\Delta t_g/L = \left[t_g(\lambda + \Delta\lambda) - t_g(\lambda)\right]/L = C\Delta\lambda = (M + W)\Delta\lambda\,,$$

$$M = M_s = \underbrace{\frac{1}{c}\frac{\mathrm{d}n_{sg}}{\mathrm{d}\lambda}}_{\substack{\text{material}\\ \text{dispersion}}} \quad (s = 1 \text{ or } 2), \; W = -\frac{n_{1g} - n_{2g}}{c\lambda}\underbrace{V\frac{\mathrm{d}^2(VB)}{\mathrm{d}V^2}}_{\substack{\text{dispersion}\\ \text{factor}}} \tag{2.16}$$

Optical Fibre Channel (3)

The first-order material dispersion coefficients in core (M_1) and cladding ($M_2 \approx M_1$) are assumed to be of similar value. The chromatic dispersion is expressed by the first-order coefficient C (unit ps / (km nm)) for a fixed reference wavelength λ_1. We extend Eq. (2.16) by one more term and define a second-order dispersion coefficient D (unit ps / (km nm^2)),

$$\Delta t_g/L = C\,\Delta\lambda + D\,(\Delta\lambda)^2 + \ldots, \qquad C = M + W, \tag{2.17a}$$

$$C = \frac{1}{L}\frac{\mathrm{d}\,t_g}{\mathrm{d}\lambda} = -\frac{2\pi c}{\lambda_0^2}\beta_0^{(2)}\,, \tag{2.17b}$$

$$C(\lambda_C) = 0\,, \qquad \lambda_C \text{ first-order dispersion zero wavelength}, \tag{2.17c}$$

$$D = \frac{1}{L}\frac{1}{2}\frac{\mathrm{d}^2 t_g}{\mathrm{d}\lambda^2} = \Big(\frac{2\pi c}{\lambda_0^2}\Big)^2\beta_0^{(3)} + \frac{4\pi c}{\lambda_0^3}\beta_0^{(2)}\,. \tag{2.17d}$$

When for a certain reference wavelength $\lambda_1 = \lambda_C$ the first-order chromatic dispersion C becomes zero, the total dispersion is determined by the second-order dispersion coefficient D.

With a slight re-ordering of Eq. (2.17a) we can define a wavelength-dependent chromatic dispersion factor $C_\lambda(\lambda) = C + D\,\Delta\lambda$ which is approximated by a straight line near the reference wavelength λ_1,

$$\Delta t_g/L = C_\lambda(\lambda)\,\Delta\lambda = (C + D\,\Delta\lambda)\,\Delta\lambda = C\,\Delta\lambda + D\,(\Delta\lambda)^2\,, \quad D = \frac{\mathrm{d}C_\lambda(\lambda)}{\mathrm{d}\lambda}\,. \tag{2.17e}$$

Comparing D in Eq. (2.17a), (2.17e) could lead to confusion because of the factor 1/2. In Eq. (2.17a), the dispersion *coefficients* $C \equiv C(\lambda_1)$, $D \equiv D(\lambda_1)$ are constants of the Taylor expansion for the function $t_{gm}(\lambda)$ at a certain reference wavelength $\lambda = \lambda_1$. Therefore, $\mathrm{d}C(\lambda_1)/\mathrm{d}\lambda = 0$ holds by definition, and $D(\lambda_1) \neq \mathrm{d}C(\lambda_1)/\mathrm{d}\lambda$. On the other hand, the dispersion *function* $C_\lambda(\lambda)$ may be linearly expanded, and its so-called dispersion slope $D = \mathrm{d}C_\lambda(\lambda)/\mathrm{d}\lambda|_{\lambda_1}$ is then well defined.

Propagation in a Nonlinear Fibre

$$\nabla^2\Psi(t,\vec{r}) = \frac{n^2(r)}{c^2}\frac{\partial^2}{\partial t^2}\Psi(t,\vec{r})$$

$$A(T,z) := a(t,z)$$

retarded time frame $T = T(t,z) := t - \beta_0^{(1)} z = t - z/v_g$

$$\frac{\partial A(T,z)}{\partial z} = \mathrm{j}\,\frac{\beta_0^{(2)}}{2}\frac{\partial^2 A(T,z)}{\partial T^2} - \mathrm{j}\,\gamma\,|A(T,z)|^2\,A(T,z) - \frac{\alpha}{2}A(T,z) \qquad \gamma = \Re\{\bar{\gamma}\} = \frac{n_2^I k_0}{A_{\mathrm{eff}}} \quad (2.21)$$

In general, a simple transfer function as in Eq. (2.12) cannot be specified. In the case of zero linear attenuation $\alpha = 0$, Eq. (2.21), (A.34) resembles the well-known Schrödinger[21] equation of quantum mechanics with a nonlinear (quadratic) potential term $\mathrm{j}\,\gamma\,|A(T,z)|^2\,A(T,z)$. Thus, it is called the *nonlinear Schrödinger equation*[22,23] (NLSE). If during the propagation of a light signal its loss is continuously compensated by gain, then the power loss constant can be set actually to zero, $\alpha = 0$. For including random perturbations by, e. g., ASE noise of optical amplifiers, a random field[24] $-\mathrm{j}\,N_{\mathrm{ASE}}(T,z)$ can be added on the right-hand side of Eq. (2.21), (A.34).

The parameters of a standard single-mode fibre[25] (SSMF) are listed in Table 2.1. For the definition of symbols and their context see also Appendix A.4 on Page 177 ff.

Parameter	Symbol	SSMF data
Chromatic dispersion	C	$17\ \frac{\mathrm{ps}}{\mathrm{km\ nm}}$
Dispersion slope	D	$0.07\ \frac{\mathrm{ps}}{\mathrm{km\ nm^2}}$
Attenuation factor per length	a/L	$0.2\ \frac{\mathrm{dB}}{\mathrm{km}}$
Nonlinear refractive index	n_2^I	$2.5\times10^{-20}\ \frac{\mathrm{m^2}}{\mathrm{W}}$
Effective area	A_{eff}	$80\,\mu\mathrm{m}$
Nonlinear coefficient	γ	$1.27\,\mathrm{W^{-1}\,km^{-1}}$
Operating wavelength	λ_0	$1.55\,\mu\mathrm{m}$
Operating frequency	f_0	$193.41\,\mathrm{THz}$

Table 2.1. Standard single-mode fibre (SSMF) parameters

Channel Capacity and Spectral Efficiency (1)

Limiting channel capacity The theoretical limiting (maximum) channel capacity C (unit bit/s) per polarization for error-free signal transmission, which can be reached only with arbitrarily complex encoding techniques, is Real sign. $M=1+\sqrt{\gamma}$ $M^2 \approx 1+\gamma$ $R_b = rF_s = 2B\log_2 M$

$$C = \mathcal{B}\log_2\left(1+\frac{P_s}{P_r}\right) = \mathcal{B}\log_2(1+\gamma), \qquad \gamma \equiv \mathrm{SNR} := \frac{P_s}{P_r}. \qquad R_b \approx B\log_2(1+\gamma) \quad B=\tfrac{1}{2}\mathcal{B} \tag{2.22}$$

It is obvious that for a constant C the channel's SNR and its bandwidth $\mathcal{B}$ can be exchanged: The more elaborate the coding is, the less channel bandwidth $\mathcal{B}$ is required, but the higher the channel's SNR must be. This is also true for the spectral efficiency which is discussed in the following.

Spectral efficiency If we want to know how many information bits we can transmit per polarization during an observation time $\mathcal{T}$, we have to calculate the so-called spectral efficiency $\mathrm{SE} = C\mathcal{T} = \mathcal{B}\mathcal{T}\log_2(1+\gamma)$ (unit bit/s/Hz; in fact, this "unit" represents a number of bits and is therefore dimensionless). The shortest possible observation time for a complex symbol is $\mathcal{T} = 1/\mathcal{B}$ as specified by the sampling theorem Eq. (2.4) on Page 15. Thus, the limiting (maximum) spectral efficiency $C' = C/\mathcal{B}$ for an AWGN channel describes the maximum number of information bits to be transmitted during the minimum observation time $\mathcal{T} = 1/\mathcal{B}$. For a small SNR an approximation can be given, and we find

$$C' = \frac{C}{\mathcal{B}} = \log_2(1+\gamma), \qquad \gamma = 2^{C'} - 1, \tag{2.23}$$

$$C' \approx \frac{1}{\ln 2}\left(\gamma - \frac{1}{2}\gamma^2\right) \quad \text{for } \gamma \ll 1. \qquad C'_{\mathrm{pract}} = \frac{B\log_2(1+\gamma)}{\mathcal{B}} = \frac{B}{\mathcal{B}}C'. \tag{2.24}$$

However, if the observation time $\mathcal{T} = 1/B$ becomes longer, i. e., if the actual signal bandwidth $B < \mathcal{B}$ is chosen to be smaller than the channel bandwidth $\mathcal{B}$ so that the signal's information capacity (bit rate) is only $B\log_2(1+\gamma)$, then the practical spectral efficiency C'_{pract} results,

LECTURE 5

Channel Capacity and Spectral Efficiency (2)

We define the energy per symbol by dividing the signal power by the symbol rate, $W_s = P_s/R_s = P_s/\mathcal{B}$, and the energy per bit by relating the energy per symbol to the number of bits C' that are transmitted per symbol, $W_b = W_s/C'$. With these definitions, we write the SNR γ and the SNR per bit γ_b in different forms,

$$\gamma \equiv \mathrm{SNR} := \frac{P_s}{P_r} = \frac{P_s}{N_0\mathcal{B}} = \frac{W_s}{N_0}, \qquad W_s = \frac{P_s}{\mathcal{B}}, \tag{2.26}$$

$$\gamma_b \equiv \mathrm{SNR}_b := \frac{W_b}{N_0} = \frac{\gamma}{C'} = \frac{2^{C'}-1}{C'}, \qquad W_b = N_{Pb}\,hf_0 = \frac{W_s}{C'}. \tag{2.27}$$

The energy per bit W_b divided by the energy per photon hf_0 equals the number of photons per bit N_{Pb}. If we had minimum-uncertainty quantum fluctuations only, $N_0 = N_{0\,\mathrm{qu}} = w_O = hf_0$, SNR_b would correspond to the photon number per bit, $\gamma_b = N_{Pb}$. For the limits of large and small spectral efficiencies we find[36] from Eq. (2.27)

$$\gamma_b \equiv \mathrm{SNR}_b = \begin{cases} 2^{C'}/C' & \text{for } C' \gg 1\,, \\ \dfrac{1+C'\ln 2+\frac{1}{2}(C'\ln 2)^2-1}{C'} = \ln 2\left(1+\frac{1}{2}C'\ln 2\right) & \text{for } C' \ll 1\,. \end{cases} \tag{2.28}$$

$2^{C'} = \mathrm{e}^{C'\ln 2} = 1+\ldots$

The SNR per bit assumes a minimum value $\gamma_b^{(\min)} = \ln 2 \approx 0.693$, $\gamma_{b\,\mathrm{dB}}^{(\min)} = 10\lg(\ln 2) = -1.58\,\mathrm{dB}$ for a spectral efficiency of $C' \to 0$. This result is plausible and means that a minimum energy per bit is needed to transmit information over an AWGN channel with an ever so small spectral efficiency. The channel capacity $C = \mathcal{B}C'$ would then approach zero if not for an unphysical channel bandwidth $\mathcal{B} \to \infty$. From the first order approximation Eq. (2.28), the spectral efficiency can be written as

$$C' \approx \frac{2}{(\ln 2)^2}\left(\gamma_b - \gamma_b^{(\min)}\right) \approx 4.16 \times (\gamma_b - 0.693) \quad \text{for } C' \ll 1\,. \tag{2.29}$$

Channel Capacity and Spectral Efficiency (3)

If the channel bandwidth $\mathcal{B}$ increases, the channel capacity increases indefinitely according to Eq. (2.23). However, this assumes that the SNR remains constant. This is not true in practice because the noise power spectral density N_0 is essentially frequency-independent. In this case, the limiting channel capacity Eq. (2.22) and the limiting spectral efficiency Eq. (2.23) can be re-written,

$$C = \mathcal{B}\log_2\left(1+\frac{P_s}{N_0\mathcal{B}}\right) = \frac{\mathcal{B}}{\ln 2}\ln\left(1+\frac{P_s}{N_0\mathcal{B}}\right), \quad \ln(1+x)\approx x \text{ for } -1<x\leq+1 \tag{2.30}$$

$$\lim_{\mathcal{B}\to\infty} C = \frac{1}{\ln 2}\frac{P_s}{N_0} \approx 1.44\times\frac{P_s}{N_0}, \qquad \lim_{\mathcal{B}\to\infty} C' = \frac{1}{\ln 2}\frac{W_s}{N_0} \approx 1.44\times\frac{W_s}{N_0}, \tag{2.31}$$

$$C' = \log_2\left(1+\frac{P_s}{N_0\mathcal{B}}\right) = \log_2\left(1+\frac{W_s}{N_0}\right) = \log_2\left(1+\frac{C'W_b}{N_0}\right) = \log_2\left(1+C'\gamma_b\right), \tag{2.32}$$

$$\gamma_b = \frac{2^{C'}-1}{C'}, \quad \text{for quantum limit, } N_{Pb} = \frac{W_b}{N_0} \text{ and } N_0 = hf_0\text{: } N_{Pb} = \gamma_b\,. \tag{2.33}$$

The spectral efficiency C' as a function of the SNR_b along with various approximations of C' are displayed[37,38] in Fig. 2.4(a). This type of graph is especially useful, if different modulation formats are to be compared[39]. Figure 2.4(b) shows that for minimum SNR_b requirements a modulation format like pulse position modulation (PPM) should be preferred (sensitivity-constrained), e. g., for deep-space wireless communication where a few photons per bit $N_{Pb} = \mathrm{SNR}_b$ must suffice. This comes at the cost of a low spectral efficiency. Alternatively, a modulation format with highest spectral efficiency could be chosen, e. g., phase-shift keying with 64 different phases (64PSK), which would be suitable for long-haul communication over fibres with a densely crowded spectrum (capacity-constrained). This comes at the cost of more stringent SNR_b-requirements, i. e., larger transmitting powers. A selection of modulation formats will be explained in more detail in Sect. 2.4 on Page 31.

Channel Capacity and Spectral Efficiency (4)

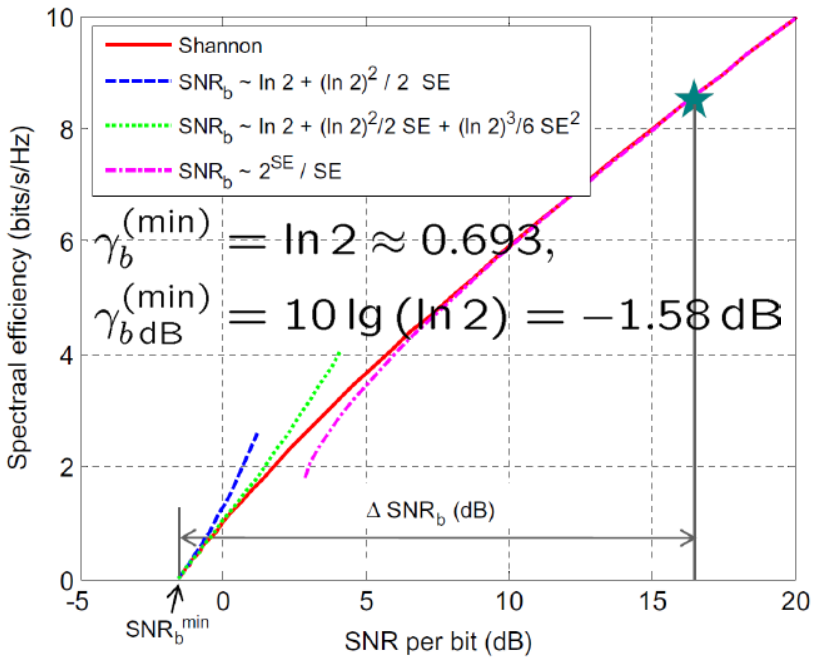

(a) Limiting spectral efficiency SE $\equiv C'$ as a function of SNR per bit SNR_b [after Fig. 1.4 of Ref. 25 on Page 20]

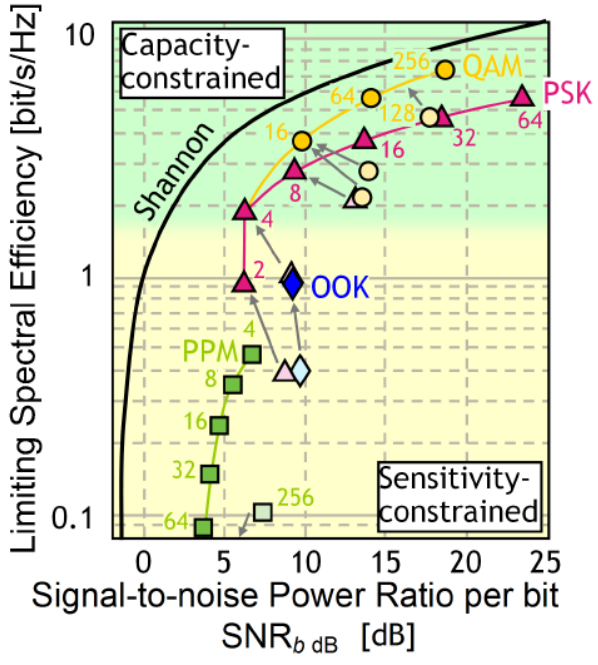

(b) Spectral efficiency of various modulation formats [after Ref. 39 on Page 23]

Fig. 2.4. Shannon limit for the spectral efficiency $C' \equiv \mathrm{SE}$ in one polarization as a function of the signal-to-noise power ratio per bit $\mathrm{SNR}_{b\,\mathrm{dB}} = 10\lg(\mathrm{SNR}_b)$. For the quantum-limited case, $N_0 = hf_0$ in Eq. (2.33), the SNR_b corresponds to the number of photons per bit. (a) The inset gives a few approximations to $\mathrm{SNR}_b(C')$ of Eq. (2.27). The SNR_b, at which a specifically chosen system operates (marked with ★), is related to the minimum $\mathrm{SNR}_b^{(\mathrm{min})}$ and expressed in dB, $\Delta\,\mathrm{SNR}_{b\,\mathrm{dB}} = \mathrm{SNR}_{b\,\mathrm{dB}} - \mathrm{SNR}_{b\,\mathrm{dB}}^{(\mathrm{min})}$. (b) Trade-off between spectral efficiency and sensitivity (small SNR_b) of various modulation formats limited by AWGN. Modulation formats (bright: theoretical limits; faint: experimental results) for a 7 % overhead code at a pre-FEC BER $= 2 \times 10^{-3}$ (squares: (256,64,32,16,8,4)PPM; triangles: (2,4,8,16,32,64)PSK; circles: (4,16,64,128,256)QAM; 4PSK $\equiv$ QPSK $\widehat{=}$ 4QAM; diamonds: OOK)

Nonlinear Shannon Limit

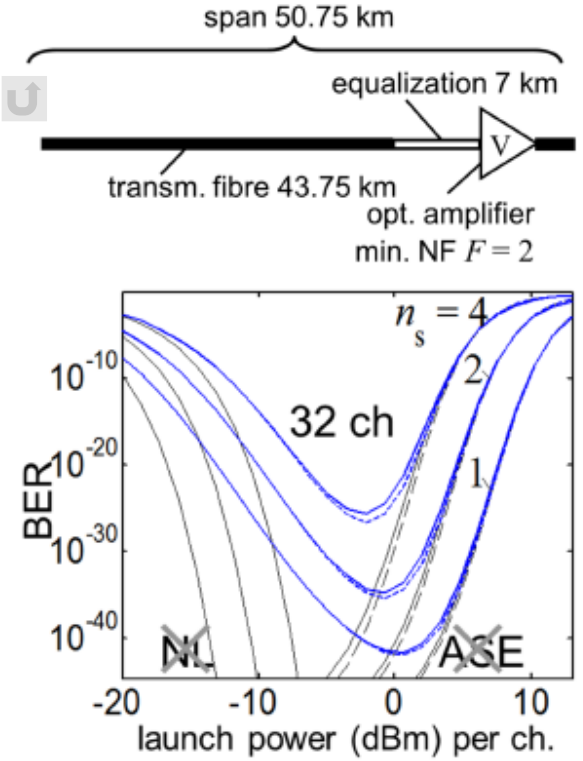

(a) Span setup and BER simulations for 32 WDM channels and $n_s = 1 \ldots 4$ spans [after Ref. 24 on Page 21]

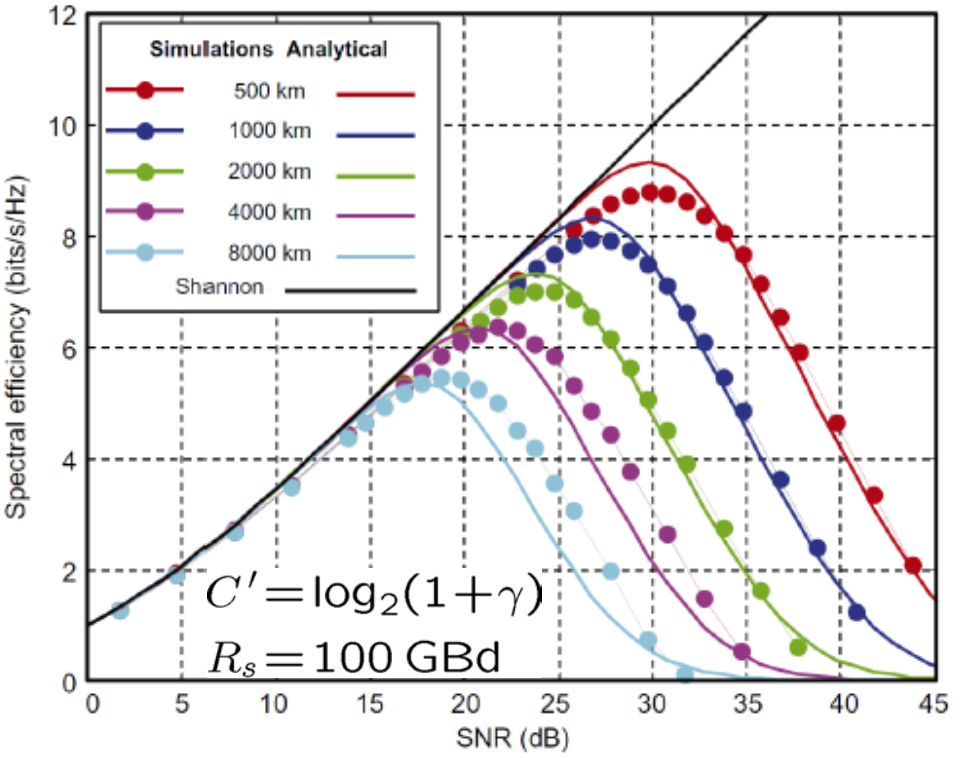

(b) Limiting spectral efficiency simulations for 5 WDM channels separated by $\Delta f = 100$ GHz and span lengths as specified in the inset [after Fig. 1.10 of Ref. 16 on Page 18, Fig. 4 of Ref. 25 on Page 22]

Fig. 2.4. Simulation of BER as a function of launch power per channel, and simulation of spectral efficiency as a function of SNR $\equiv \gamma$ for nonlinear WDM systems with various transmission distances. (a) BER vs. channel power for 32 WDM channels. Non-return-to-zero (NRZ) data with bit rate 40 Gbit, channel grid spacing 100 GHz, pseudo-random bit sequence (PRBS) with 1 024 bit length per channel, 0.45 mW power per channel, one optical amplifier per span with a theoretically minimum noise figure $F = 2$ (inversion factor $n_{sp} = 1$). Solid lines (——) include dispersion slope ($\beta_0^{(3)}$), self-steepening and Raman effect, broken lines (– – –), (— —) do not include the aforementioned types of nonlinearities. Solid-line asymptotes (——) without nonlinearities ~~NL~~ and without ~~ASE~~ noise, respectively. The BER numbers are not representative

Modulation and Mixing

Modulation is a fundamentally nonlinear process where two or more temporal signals interact.
Here, interaction of electromagnetic fields only.
The signals' spectra can be located at widely different or at rather similar centre frequencies.
Modulation: Baseband signal covering $0 \ldots 100\,\mathrm{GHz}$ interacts with carrier at widely different frequency $193.41\,\mathrm{THz}$ (vacuum wavelength $1.55\,\mu\mathrm{m}$).
Mixing: Signals interact, the spectra of which are centred at comparable frequencies (at $193.41\,\mathrm{THz}$ ($1.55\,\mu\mathrm{m}$) and $2 \times 193.41\,\mathrm{THz} = 386.82\,\mathrm{THz}$ ($0.775\,\mu\mathrm{m}$).

Multiplicative and Additive Mixing

Lowest-order nonlinearity is a product term of the contributing temporal signals.

Multiplicative mixing is a physical process which actually multiplies two quantities, $s_1(t)\,s_2(t)$ (voltage $s_1(t)$ applied between source and gate of a FET, $s_2(t)$ controls source-drain voltage).

Additive mixing first superimposes $s_1(t) + s_2(t)$, then applies a nonlinear operation (e. g., squaring) to the sum,

$$[s_1(t) + s_2(t)]^2 = s_1^2(t) + s_2^2(t) + 2\overbrace{s_1(t)\,s_2(t)}^{\text{mixing}}$$

Obviously, there is a mixing term, namely the product $s_1(t)\,s_2(t)$.

Analytic Signal, Phasor, IQ-(De)modulator, Heterodyne-Tx/Rx

Analytic complex time signal: $\underline{s}(t) = s_r(t) + \mathrm{j}\, s_i(t) = \underline{a}(t)\, \mathrm{e}^{\mathrm{j}\,\omega_0 t}$

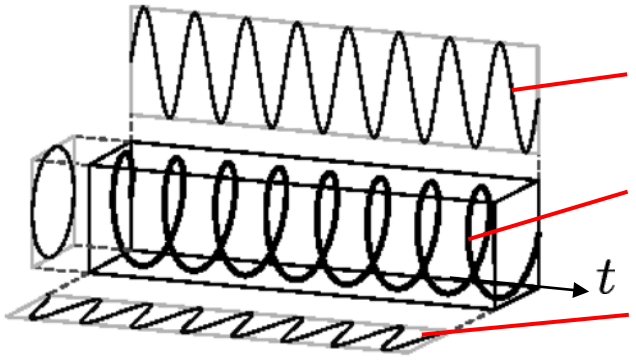

$s_i(t) = \sin(\omega_0 t)$

$\underline{s}(t) = \exp(\mathrm{j}\,\omega_0 t) = s_r(t) + \mathrm{j}\, s_i(t)$

$s_r(t) = \cos(\omega_0 t)$

IQ-modulator (mixer):

Signal direction for

Tx ($\sum$ = "diff"): $\longrightarrow$

Rx ($\sum$ = "split"): $\longleftarrow$

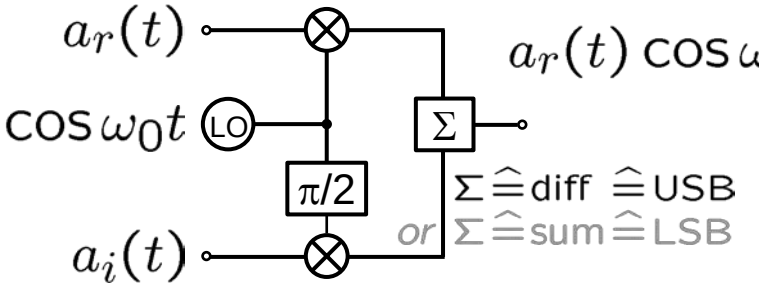

$a_r(t)\cos\omega_0 t - a_i(t)\sin\omega_0 t = \Re\left\{\underline{a}(t)\, \mathrm{e}^{\mathrm{j}\,\omega_0 t}\right\}$

Recipe for transmission and reception of $\Re\left\{\underline{a}(t)\, \mathrm{e}^{\mathrm{j}\,\omega_0 t}\right\}$:

- Modulate carrier $\cos\omega_0 t$ with real part $a_r(t)$ (in-phase I)
- Modulate carrier $\sin\omega_0 t$ with imag. part $a_i(t)$ (quadrature Q)
- Superimpose both orthogonal contributions
- Reception of $a_r(t), a_i(t)$ by mixing with cc LO: $\exp(-\mathrm{j}\,\omega_0 t)$

Transmission and Reception of a Complex Signal

A physical channel can transmit only physical quantities, i. e., signals that are measurable, e. g., with a voltmeter. The natural choice is then to map these signals to numbers which are real in the mathematical sense. However, at the transmitter, two independent data streams can be regarded as real and imaginary part of a complex signal, and both its real constituents can be transmitted. On reception, real and imaginary parts can be recombined to form a complex number. In this sense a channel is able to transmit also complex data signals.

We start with the real signal $s_r(t)$ from Eq. (2.38). A simple trigonometric manipulation leads to the definition of in-phase signal[48] $I(t)$ and quadrature signal $Q(t)$, which now serve as the representatives of the encoded data instead of amplitude $\hat{a}(t)$ and phase $\varphi(t)$,

$$\begin{aligned} s_r(t) &= \Re\left\{\hat{a}(t)\,\mathrm{e}^{\mathrm{j}\,\varphi(t)}\,\mathrm{e}^{\mathrm{j}\,\omega_0 t}\right\} = \hat{a}(t)\cos\left[\omega_0 t+\varphi(t)\right] = \hat{a}(t)\cos\varphi(t)\cos\omega_0 t - \hat{a}(t)\sin\varphi(t)\sin\omega_0 t \\ &= I(t)\cos(\omega_0 t) - Q(t)\sin(\omega_0 t) \quad \text{for } I(t)=\hat{a}(t)\cos\varphi(t),\ Q(t)=\hat{a}(t)\sin\varphi(t), \qquad (2.43) \\ \hat{a}(t) &= \sqrt{I^2(t)+Q^2(t)}, \qquad \tan\varphi(t) = \frac{Q(t)}{I(t)}. \end{aligned}$$

The naming of $I(t)$ and $Q(t)$ is derived from the fact that the real part $\hat{a}\cos\varphi$ of the complex amplitude $\hat{a}\,\mathrm{e}^{\mathrm{j}\,\varphi}$ is in phase with the carrier phasor[49] $\mathrm{e}^{\mathrm{j}\,\omega_0 t}$ of $\cos(\omega_0 t)$, while the imaginary part $\hat{a}\sin\varphi$ is in phase with the carrier phasor $-\mathrm{j}\,\mathrm{e}^{\mathrm{j}\,\omega_0 t} = \mathrm{e}^{\mathrm{j}(\omega_0 t-\pi/2)}$ of $\sin(\omega_0 t)$ that points at right angles ("is in quadrature") with respect to the phasor of $\cos(\omega_0 t)$, see also Fig. 2.6 on Page 27.

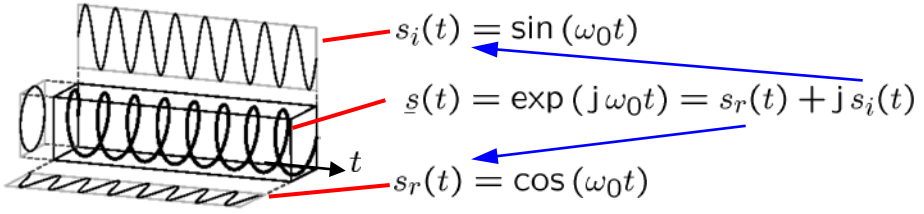

Spectrum of IQ-Modulator Output Signal

Spectrum of IQ-modulator output signal The real IQ-modulator output $s_r(t) = \Re\{a(t)\,\mathrm{e}^{\mathrm{j}\,\omega_0 t}\}$ in Fig. 2.7(a) and Eq. (2.44) has the spectrum

$$\breve{s}_r(f) = \int_{-\infty}^{+\infty} \tfrac{1}{2}\left(a(t)\,\mathrm{e}^{\mathrm{j}\,2\pi f_0 t} + a^*(t)\,\mathrm{e}^{-\mathrm{j}\,2\pi f_0 t}\right)\mathrm{e}^{-\mathrm{j}\,2\pi f t}\,\mathrm{d}t = \tfrac{1}{2}\breve{a}(f - f_0) + \tfrac{1}{2}\breve{a}^*(-(f + f_0)). \quad (2.45a)$$

The band-limited baseband spectrum $\breve{a}(|f| > B) = 0$ of the complex modulation signal $a(t)$ in Eq. (2.45a) is shifted to the positive carrier frequency f_0, and in inverted and complex conjugate form also to $-f_0$.

Alternatively, we may use the second form of Eq. (2.44), $s_r(t) = a_r(t)\cos\omega_0 t - a_i(t)\sin\omega_0 t$, and find for the IQ-modulator output spectrum

$$\begin{aligned}\breve{s}_r(f) &= \int_{-\infty}^{+\infty} (a_r(t)\cos\omega_0 t - a_i(t)\sin\omega_0 t)\,\mathrm{e}^{-\mathrm{j}\,2\pi f t}\,\mathrm{d}t = \breve{s}_r^*(-f) \\ &= \tfrac{1}{2}\big(\breve{a}_r(f - f_0) + \mathrm{j}\,\breve{a}_i(f - f_0)\big) + \tfrac{1}{2}\big(\breve{a}_r(f + f_0) - \mathrm{j}\,\breve{a}_i(f + f_0)\big). \quad (2.45b)\end{aligned}$$

The baseband spectra $\breve{a}_{r,i}(f) = \breve{a}_{r,i}^*(-f)$ of the real signals $a_{r,i}(t)$ have a *lowpass* bandwidth $B < f_0$ and comprise correlated positive and negative frequency components in a range $-B < f \le +B$. After shifting these spectra to the respective carrier frequencies $\pm f_0$, the *passband* spectra of real and imaginary part $\breve{a}_{r,i}(f \mp f_0)$ span a range $-B \pm f_0 < f \le +B \pm f_0$ *and overlay each other.*

It is obvious that the composite spectra $\breve{a}(f - f_0) = \breve{a}_r(f - f_0) + \mathrm{j}\,\breve{a}_i(f - f_0)$ and $\breve{a}^*(-(f + f_0)) = \breve{a}_r(f + f_0) - \mathrm{j}\,\breve{a}_i(f + f_0)$ likewise span a range of $2B$ centred at $\pm f_0$, but cannot be separated simply in contributions belonging to $\breve{a}_r(f \mp f_0)$ and $\breve{a}_i(f \mp f_0)$. Incoherent square-law detection would not not help. Instead, we must rely on the fact that $\pm\mathrm{j}\,\breve{a}_i(f \pm f_0)$ and $\breve{a}_r(f \mp f_0)$ are orthogonal to each other (all phases are shifted by $\pi/2$), a property which can be exploited with an IQ-demodulator Fig. 2.7(b) that operates with orthogonal LO signals, see Eq. (2.47).

LECTURE 6

Single-Sideband Modulation

Single-sideband modulation Let a real data signal $m(t)$ modulate the subcarrier $e^{j\omega_a t}$ having an angular frequency ω_a. The spectral width B_m of $\breve{m}(f)$ is assumed to be limited to $B_m < f_a$. Then the real part $a_r(t)$ and the imaginary part $a_i(t)$ of the analytic signal $\underline{a}(t) = m(t)\, e^{j\omega_a t}$ are related by a Hilbert transform Eq. (2.40a) on Page 27.

When an IQ-modulator Fig. 2.7(a) is fed with $a_r(t) = m(t)\cos\omega_a t$ and $a_i(t) = m(t)\sin\omega_a t$, a single-sideband (SSB) spectrum is generated: After subtracting the mixer outputs as assumed in Fig. 2.7(a), only the upper sideband (USB) signal $m_{\mathrm{USB}}(t) = m(t)\cos(\omega_0 + \omega_a)t$ appears at the output, because the lower sidebands cancel.

If the two mixer outputs are added, the lower side band (LSB) $m_{\mathrm{LSB}}(t) = m(t)\cos(\omega_0 - \omega_a)t$ is generated, because the upper sidebands cancel. The modulated subcarrier $\underline{a}(t)$ and its (causal) spectrum $\breve{a}(f)$ as well as the generated (non-causal) USB spectrum $\breve{m}_{\mathrm{USB}}(f)$ and LSB spectrum $\breve{m}_{\mathrm{LSB}}(f)$ can be written as

$$\underline{a}(t) = a_r(t) + j\, a_i(t) = m(t)\,(\cos\omega_a t + j\sin\omega_a t) \quad \text{for } m(t) \text{ real}, \tag{2.46a}$$

$$\breve{a}(f) = \breve{m}(f - f_a) \quad \text{causal if spectral width of } \breve{m}(f) \text{ is } B_m < f_a, \tag{2.46b}$$

$$\breve{m}_{\mathrm{USB}}(f) = \tfrac{1}{2}\left[\breve{m}(f - (f_0 + f_a)) + \breve{m}(f + (f_0 + f_a))\right], \tag{2.46c}$$

$$\breve{m}_{\mathrm{LSB}}(f) = \tfrac{1}{2}\left[\breve{m}(f - (f_0 - f_a)) + \breve{m}(f + (f_0 - f_a))\right]. \tag{2.46d}$$

If in contrast to the assumption in Eq. (2.46a) the quantities $a_r(t)$ and $a_i(t)$ represent independent data, the associated USB and LSB spectra are also independent and cannot cancel, see Eq. (2.45c).

IQ-Demodulator — Heterodyne and Homodyne Reception

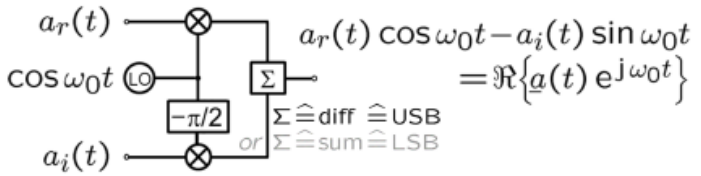

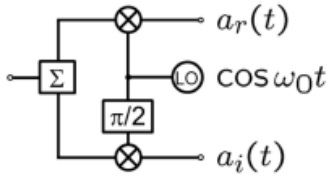

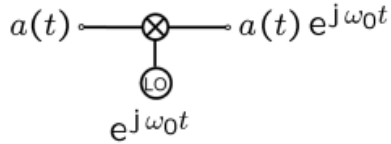

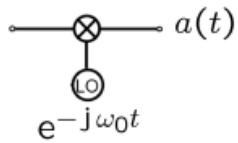

IQ-demodulator An IQ-demodulator is seen in Fig. 2.7(b). It recovers a complex data signal $a(t) = a_r(t) + \mathrm{j}\,a_i(t)$ with real part $a_r(t)$ and imaginary part $a_i(t)$, which were modulated on two orthogonal carriers $\cos\omega_0 t$ and $\sin\omega_0 t$. The incoming signal is split (symbol Σ). The local oscillator (LO) supplies orthogonal carriers $\cos\omega_0 t$ and $-\sin\omega_0 t$ to the two mixers, the in-phase (I) and quadrature outputs (Q) of which are

$$2I(t) = 2\left[a_r(t)\cos\omega_0 t - a_i(t)\sin\omega_0 t\right]\cos\omega_0 t = a_r(t)\left(1+\cos 2\omega_0 t\right) - a_i(t)\sin 2\omega_0 t\,, \qquad (2.47a)$$

$$2Q(t) = -2\left[a_r(t)\cos\omega_0 t - a_i(t)\sin\omega_0 t\right]\sin\omega_0 t = a_i(t)\left(1-\cos 2\omega_0 t\right) - a_r(t)\sin 2\omega_0 t\,. \qquad (2.47b)$$

When filters remove the carrier harmonics at $2f_0$ (or if they are not generated from the beginning, in case the mixers are realized by photodetectors), the receiver recovers the transmitted signals,

$$2I(t) = a_r(t)\,, \qquad 2Q(t) = a_i(t)\,. \qquad (2.47c)$$

The schematic Fig. 2.7(d) has the same functionality, but uses a complex mixer and complex quantities for convenience. It is important to note that on reception the complex conjugate of the transmitting carrier serves as a LO, otherwise the quadrature component changes sign, $2Q(t) = -a_i(t)$.
The type of reception as discussed in Fig. 2.7, where a receiver LO has the same frequency as and is (implicitly) phase-locked to the transmitter, is called homodyne[50] reception. The transmitted signal is directly transfered to the baseband. If transmitter and LO frequencies differ, $f_0 - f_0' \neq 0$, we speak of heterodyne[51] reception.

Analogue Modulation — Amplitude Modulation

$$\Psi(t) = s(t)\cos\omega_0 t:\quad \bar{\Psi}(f) = \int_{-\infty}^{+\infty} s(t)\,\mathrm{e}^{-\mathrm{j}2\pi(f-f_0)t}\,\mathrm{d}t + \int_{-\infty}^{+\infty} s(t)\,\mathrm{e}^{-\mathrm{j}2\pi(f+f_0)t}\,\mathrm{d}t,$$

$$(s(t)\ \text{real})\quad \bar{\Psi}^*(f) = \int_{-\infty}^{+\infty} s(t)\,\mathrm{e}^{\ \mathrm{j}2\pi(f-f_0)t}\,\mathrm{d}t + \int_{-\infty}^{+\infty} s(t)\,\mathrm{e}^{\ \mathrm{j}2\pi(f+f_0)t}\,\mathrm{d}t,$$

$$\bar{\Psi}^*(-f) = \int_{-\infty}^{+\infty} s(t)\,\mathrm{e}^{-\mathrm{j}2\pi(f+f_0)t}\,\mathrm{d}t + \int_{-\infty}^{+\infty} s(t)\,\mathrm{e}^{-\mathrm{j}2\pi(f-f_0)t}\,\mathrm{d}t = \bar{\Psi}(f)$$

The spectrum $\breve{s}_{\mathrm{AM}\,r}(f)$ of the real part $s_{\mathrm{AM}\,r}(t)$ of the modulated analytic carrier $\underline{s}_{\mathrm{AM}}(t)$, and th
modulation spectra $\breve{m}(f-f_0)$, $\breve{m}(f+f_0)$ of the positive real band-limited modulation signal r

$$\breve{s}_{\mathrm{AM}\,r}(f) = \tfrac{1}{2}\hat{a}\,[\breve{m}(f-f_0) + \breve{m}(f+f_0)] = \breve{s}^*_{\mathrm{AM}\,r}(-f)\,,$$

$$\breve{m}(f-f_0) = \breve{m}(f-f_0)|_{0<f<+f_0} + \breve{m}(f-f_0)|_{f>+f_0}$$

$$= \underbrace{\breve{m}^*(-f+f_0)|_{0<f<+f_0}}_{\mathrm{LSB}\,(f-f_0)} + \underbrace{\breve{m}(f-f_0)|_{f>+f_0}}_{\mathrm{USB}\,(f-f_0)} = \breve{m}^*(-f+f_0)\,,$$

(Kehrlage) inverse (freq.) position — (Gleichlage) regular (freq.) position

$$\breve{m}(f+f_0) = \breve{m}(f+f_0)|_{f<-f_0} + \breve{m}(f+f_0)|_{0>f>-f_0}$$

$$= \underbrace{\breve{m}(f+f_0)|_{f<-f_0}}_{\mathrm{LSB}\,(f+f_0)} + \underbrace{\breve{m}^*(-f-f_0)|_{0>f>-f_0}}_{\mathrm{USB}\,(f+f_0)} = \breve{m}^*(-f-f_0)\,.$$

Upper sideband (USB) and lower sideband (LSB) are related and carry the same information as can be seen from $\mathrm{USB}\,(f \mp f_0) = \mathrm{LSB}^*(-f \pm f_0)$.

Analogue Modulation — Sinusoidal Amplitude Modulation

For definiteness, we now assume a real sinusoidal modulation $m(t) = 1 + m\cos\omega_a t$ with angular frequency $\omega_a = 2\pi f_a$ and a constant modulation index $0 < m < 1$. For the modulated analytic signal $\underline{s}_{\mathrm{AM}}(t)$, its real part $s_{\mathrm{AM}\,r}(t)$ and the one-sided power spectrum $2\left|\breve{s}_{\mathrm{AM}\,r}(f)\right|^2 = 2\Theta_{s\,\mathrm{AM}}(f)$ we find

$$
\begin{aligned}
\underline{s}_{\mathrm{AM}}(t) &= \hat{a}\,m(t)\,\mathrm{e}^{\mathrm{j}\,\omega_0 t} = \hat{a}\,(1 + m\cos\omega_a t)\,\mathrm{e}^{\mathrm{j}\,\omega_0 t}, \qquad 0 < m(t) < 1, \\
&= \hat{a}\left[1 + \tfrac{1}{2}m\left(\mathrm{e}^{\mathrm{j}\,\omega_a t} + \mathrm{e}^{-\mathrm{j}\,\omega_a t}\right)\right]\mathrm{e}^{\mathrm{j}\,\omega_0 t} = \hat{a}\left[\mathrm{e}^{\mathrm{j}\,\omega_0 t} + \tfrac{1}{2}m\left(\mathrm{e}^{\mathrm{j}(\omega_0+\omega_a)t} + \mathrm{e}^{\mathrm{j}(\omega_0-\omega_a)t}\right)\right], \\
s_{\mathrm{AM}\,r}(t) &= \hat{a}\,(1 + m\cos\omega_a t)\cos\omega_0 t \\
&= \hat{a}\left[\cos\omega_0 t + \tfrac{1}{2}m\left(\cos(\omega_0 - \omega_a)\,t + \cos(\omega_0 + \omega_a)\,t\right)\right], \\
2\Theta_{s\,\mathrm{AM}}(f) &:= 2\left|\breve{s}_{\mathrm{AM}\,r}(f)\right|^2 \\
&= \tfrac{1}{2}\hat{a}^2\left\{\delta(f - f_0) + \tfrac{1}{4}m^2\left[\underbrace{\delta(f - (f_0 - f_a))}_{\text{“LSB”}} + \underbrace{\delta(f - (f_0 + f_a))}_{\text{“USB”}}\right]\right\} \quad \text{for } f > 0\,.
\end{aligned}
$$

Figure 2.7(a) displays the phasors of Eq. (2.47a). A schematic (one-sided) power spectrum similar to Eq. (2.47c), but for a non-sinusiodal modulation spectrum extending from frequency f_{a1} to f_{a2}, is to be seen in Fig. 2.7(b). The AM carrier at frequency f_0 contributes a minimum of $\frac{1}{1+2\times(1/4)} = \frac{2}{3}$ of the total spectral power for a maximum modulation index $m = 1$, Eq. (2.47c). This transmitter power could be saved if the carrier is suppressed and at the receiver re-supplied for detection.

Analogue Modulation — Amplitude Modulation

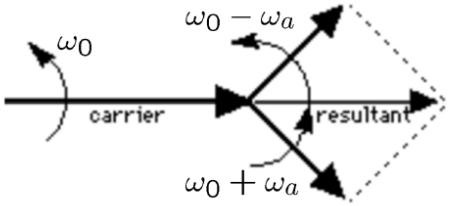

(a) Phasor diagram for a sinusoidal AM. The resultant is in phase with the carrier.

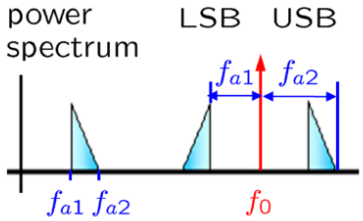

(b) One-sided power spectrum for AM with a baseband spectrum $f_{a1} \ldots f_{a2}$

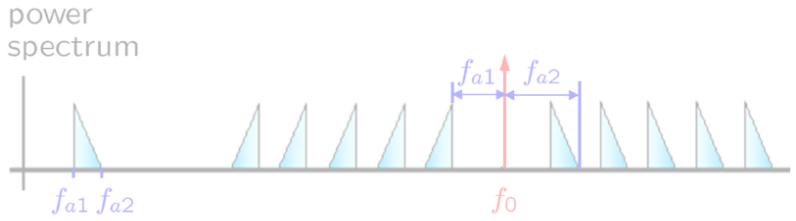

(c) One-sided power spectrum for IM. Power detection recovers the baseband spectrum $f_{a1} \ldots f_{a2}$. In contrast to (b), the IM-spectrum is infinitely extended.

Analogue amplitude modulation (AM) and intensity modulation (IM) with real modulation signals. (a) Phasors in the complex plane (see Footnote 45 on Page 26, origin located at the base point of the carrier phasor) for sinusoidal AM according to Eq. (2.46a). All phasors rotate counter-clockwise (ccw, in the mathematical positive sense). The carrier phasor, the upper sideband (USB) phasor and the lower sideband (LSB) phasor rotate with angular velocities ω_0, $\omega_0 + \omega_a$ and $\omega_0 - \omega_a$, respectively. If the observer rotates with the carrier, the USB phasor would seemingly rotate ccw with angular velocity ω_a, while the LSB phasor would seemingly rotate clockwise (cw) with the same angular velocity ω_a. (b) One-sided schematic AM power spectrum for a non-sinusoidal baseband modulation spectrum extending from frequency f_{a1} to f_{a2}. Upper and lower sidebands are related by $\mathrm{USB}(f) = \mathrm{LSB}^*(-f)$

Analogue Modulation — CS Sinusoidal Amplitude Modulation

Carrier-suppressed double-sideband modulation

With the carrier suppressed, the modulation function is $m(t) = m\cos\omega_a t$ in the case of sinusoidal modulation. This cannot be called AM any more, because $-1 \leq m(t) \leq +1$ holds as opposed to the requirement Eq. (2.47a). Instead, we talk of carrier-suppressed double-sideband (CS-DSB) modulation. Because only the sidebands remain, the resulting time function results from the superposition

$$s_{\text{CS-DSB}\,r}(t) = \tfrac{1}{2}\hat{a}\,m\left(\cos\left(\omega_0 - \omega_a\right)t + \cos\left(\omega_0 + \omega_a\right)t\right) = \hat{a}\,m\cos\omega_a t\cos\omega_0 t\,,$$

which resembles $s_{\text{AM}\,r}(t)$. At the zeros of the modulation function $m(t)$ the phase of the carrier $\hat{a}\cos\omega_0 t$ jumps by π. Such a linear superposition of signals with different frequencies is called a beat signal.

Analogue Modulation — Intensity Modulation

modulation signal $m(t) = \sqrt{p_m(t)}$ is assumed to vary slowly on the scale of a carrier period $1/f_0$. The intensity-modulated signal $s_{\mathrm{IM}\,r}(t)$ along with its modulated intensity $\langle s^2_{\mathrm{IM}\,r}\rangle(t)$ then reads

$$s_{\mathrm{IM}\,r}(t) = \hat{a}\sqrt{p_m(t)}\cos\omega_0 t, \quad \langle s^2_{\mathrm{IM}\,r}\rangle(t) = \tfrac{1}{2}\hat{a}^2 p_m(t), \quad \text{slowly varying positive real } p_m(t). \tag{2.51}$$

For a sinusoidal intensity modulation $p(t) = 1 + p_m\cos\omega_a t$ with $\omega_a \ll \omega_0$ and a small modulation index $p_m \ll 1$, the modulated signal $s_{\mathrm{IM}\,r}(t)$ can be expanded in a series,

$$\begin{aligned}
s_{\mathrm{IM}\,r}(t) &= \sqrt{1 + p_m\cos(\omega_a t)}\,\hat{a}\cos(\omega_0 t)\\
&\approx \left\{1 + \tfrac{p_m}{2}\cos(\omega_a t) - \tfrac{p_m^2}{8}\cos^2(\omega_a t) + \ldots\right\}\hat{a}\cos(\omega_0 t)\\
&\approx \quad \left\{1 - \tfrac{p_m^2}{16} + \ldots\right\}\hat{a}\ \cos\ (\omega_0 t)\\
&\quad + \left\{\tfrac{p}{4} + \tfrac{3p_m^3}{128} + \ldots\right\}\hat{a}\left\{\cos\left[(\omega_0 - \ \omega_a)\,t\right] + \cos\left[(\omega_0 + \ \omega_a)\,t\right]\right\}\\
&\quad + \left\{-\tfrac{p_m^2}{32} + \ldots\right\}\hat{a}\left\{\cos\left[(\omega_0 - 2\omega_a)\,t\right] + \cos\left[(\omega_0 + 2\omega_a)\,t\right]\right\}\\
&\quad + \left\{\tfrac{p_m^3}{128} + \ldots\right\}\hat{a}\left\{\cos\left[(\omega_0 - 3\omega_a)\,t\right] + \cos\left[(\omega_0 + 3\omega_a)\,t\right]\right\} + \ldots
\end{aligned} \tag{2.52}$$

A schematic (one-sided) power spectrum $2\langle|\breve{s}_{\mathrm{IM}\,r}(f)|^2\rangle$ of a non-sinusiodal modulation spectrum extending from frequency f_{a1} to f_{a2} is to be seen in Fig. 2.8(c). Basically, the spectrum is infinitely extended. If no frequency-dependent time or phase delays modify the partial spectra differently during transmission (due to, e. g., chromatic dispersion in a fibre), the receiver's photodetector current Eq. (1.1) on Page 2 exactly recovers the IM in the photocurrent, $i(t) \sim \langle s^2_{\mathrm{IM}\,r}\rangle(t) = \tfrac{1}{2}\hat{a}^2(1 + p_m\cos\omega_a t)$.

Analogue Modulation — Amplitude and Intensity Modulation

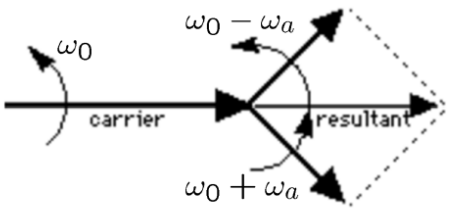

(a) Phasor diagram for a sinusoidal AM. The resultant is in phase with the carrier.

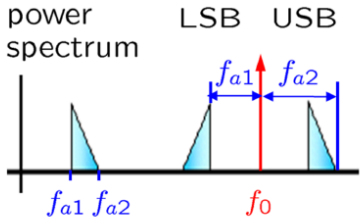

(b) One-sided power spectrum for AM with a baseband spectrum $f_{a1} \ldots f_{a2}$

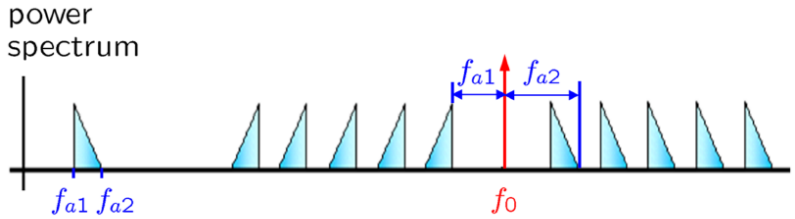

(c) One-sided power spectrum for IM. Power detection recovers the baseband spectrum $f_{a1} \ldots f_{a2}$. In contrast to (b), the IM-spectrum is infinitely extended.

Analogue amplitude modulation (AM) and intensity modulation (IM) with real modulation signals. (a) Phasors in the complex plane (see Footnote 45 on Page 26, origin located at the base point of the carrier phasor) for sinusoidal AM according to Eq. (2.46a). All phasors rotate counter-clockwise (ccw, in the mathematical positive sense). The carrier phasor, the upper sideband (USB) phasor and the lower sideband (LSB) phasor rotate with angular velocities ω_0, $\omega_0 + \omega_a$ and $\omega_0 - \omega_a$, respectively. If the observer rotates with the carrier, the USB phasor would seemingly rotate ccw with angular velocity ω_a, while the LSB phasor would seemingly rotate clockwise (cw) with the same angular velocity ω_a. (b) One-sided schematic AM power spectrum for a non-sinusoidal baseband modulation spectrum extending from frequency f_{a1} to f_{a2}. Upper and lower sidebands are related by $\mathrm{USB}(f) = \mathrm{LSB}^*(-f)$ (c) One-sided schematic IM spectrum for a non-sinusoidal baseband modulation spectrum extending from frequency f_{a1} to f_{a2}. Because the *power* $\langle s^2_{\mathrm{IM}\,r} \rangle (t)$ is modulated in proportion to a modulation signal $1 + p_m(t)$, the *amplitude* depends on the square-root of the modulating signal $\sqrt{1 + p_m(t)}$, so that the spectrum is infinitely extended.

Angle Modulation — Phase Modulation

If the angle of a carrier phasor $\hat{a}\,\mathrm{e}^{\mathrm{j}\,\omega_0 t}$ is changed, we talk of angle modulation. For definiteness, we assume again a real sinusoidal modulation $\eta\,(t) = \eta \sin \omega_a t$ with angular frequency $\omega_a = 2\pi f_a$ and a constant angle modulation index η,

$$\underline{s}_{\mathrm{PM}}\,(t) = \hat{a}\,\mathrm{e}^{\mathrm{j}[\omega_0 t + \eta(t)]} = \hat{a}\,\mathrm{e}^{\mathrm{j}(\omega_0 t + \eta \sin \omega_a t)} = \hat{a} \sum_{n=-\infty}^{+\infty} \mathrm{J}_n(\eta)\,\mathrm{e}^{\mathrm{j}[\omega_0 + n\omega_a]t}, \quad \mathrm{J}_{-n}(\eta) = (-1)^n\,\mathrm{J}_n(\eta), \tag{2.53a}$$

$$\begin{aligned} s_{\mathrm{PM}}\,(t) = \Re\left\{\underline{s}_{\mathrm{PM}}\,(t)\right\} = \hat{a}\big[\,&\mathrm{J}_0\,(\eta)\cos\omega_0 t - \mathrm{J}_1\,(\eta)\left[\sin\left(\omega_0+\omega_a\right)t + \sin\left(\omega_0-\omega_a\right)t\right] \\ &- \mathrm{J}_2\,(\eta)\left[\cos\left(\omega_0+2\omega_a\right)t + \cos\left(\omega_0-2\omega_a\right)t\right] + \mathrm{J}_3\,(\eta)\left[\sin\left(\omega_0+3\omega_a\right)t + \sin\left(\omega_0-3\omega_a\right)t\right] \pm \ldots\big]. \end{aligned} \tag{2.53b}$$

The exponential can be expanded in terms of Bessel functions[51] $\mathrm{J}_n(\eta)$ of the first kind and order n. Remarkably, the Bessel functions of negative odd order n have the opposite sign of their companions with positive order, $\mathrm{J}_{-n}(\eta) = (-1)^n\,\mathrm{J}_n(\eta)$.

For small-signal angle modulation, where $\eta \ll 1$ holds, the expansion Eq. (2.53a) reduces to three Bessel terms that can be further simplified[52] to resemble the case of AM, Eq. (2.49a) on Page 32 and Fig. 2.8(a),

$$\begin{aligned} \underline{s}_{\mathrm{PM}}\,(t) &\approx \hat{a}\left[\mathrm{J}_0(\eta)\,\mathrm{e}^{\mathrm{j}\,\omega_0 t} + \mathrm{J}_1(\eta)\left(\mathrm{e}^{\mathrm{j}(\omega_0+\omega_a)t} - \mathrm{e}^{\mathrm{j}(\omega_0-\omega_a)t}\right)\right] \\ &\approx \hat{a}\left[\mathrm{e}^{\mathrm{j}\,\omega_0 t} + \tfrac{1}{2}\eta\left(\mathrm{e}^{\mathrm{j}(\omega_0+\omega_a)t} - \mathrm{e}^{\mathrm{j}(\omega_0-\omega_a)t}\right)\right] \qquad \text{for } \eta \ll 1\,. \end{aligned} \tag{2.54}$$

A sinusoidal angle modulation can be interpreted either as a phase modulation as in Eq. (2.53a), or as a frequency modulation (FM), because the instantaneous frequency is $\mathrm{d}\eta\,(t)/\,\mathrm{d}t = \eta\,\omega_a \cos\omega_a t$. Introducing the frequency peak deviation $\Delta\omega = 2\pi\Delta f = \eta\,\omega_a$, i. e., the maximum deviation of the instantaneous frequency from the carrier frequency f_0, we write the FM signal

$$\underline{s}_{\mathrm{FM}}\,(t) = \hat{a}\,\mathrm{e}^{\mathrm{j}\left(\omega_0 + \frac{\mathrm{d}\eta(t)}{\mathrm{d}t}\right)t} = \hat{a}\,\mathrm{e}^{\mathrm{j}(\omega_0 + \Delta\omega\cos\omega_a t)t}, \qquad \Delta\omega = 2\pi\Delta f = \eta\,\omega_a. \tag{2.55}$$

Angle Modulation — Phase and Frequency Modulation

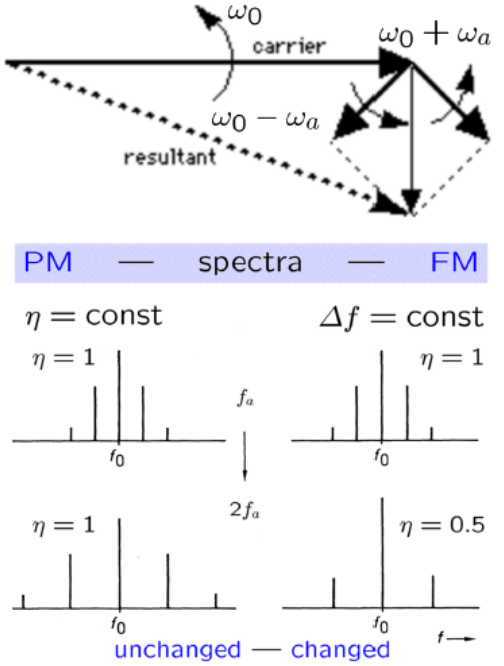

(a) Sinusoidal small-signal angle modulation [top] and power spectra for PM and FM [bottom]

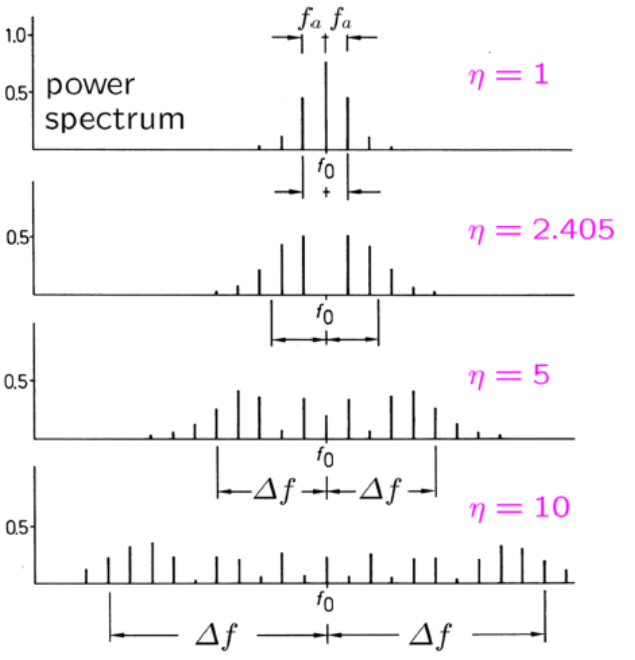

(b) Wideband FM for different modulation indices η. The carrier disappears for $\eta = 2.405$. The bandwidth is of order $2\Delta f = 2\eta f_a$.

Angle modulation. Small-signal phasor diagram and one-sided power spectra. The height of the lines represents the area of the associated spectral δ-functions. (a)-[top] Phasors for small-signal sinusoidal angle modulation with $\eta \ll 1$. All phasors rotate counter-clockwise (ccw). The carrier phasor, the upper sideband (USB) phasor and the lower sideband (LSB) phasor rotate with angular velocities ω_0, $\omega_0+\omega_a$ and $\omega_0-\omega_a$, respectively. If the observer rotates with the carrier, the USB phasor would seemingly rotate ccw with angular velocity ω_a, while the LSB phasor would seemingly rotate clockwise (cw) with the same angular velocity ω_a. (a)-[bottom] One-sided power spectra for phase modulation (PM) with constant modulation index $\eta = \text{const}$, and for frequency modulation (FM) with constant frequency peak deviation $\Delta f = \eta f_a$. (b) One-sided power spectra for sinusoidal frequency modulation (FM) with different modulation indeces η. The carrier disappears for $\eta = 2.405$. A bandwidth estimate for wideband angle modulation and a fixed modulating signal bandwidth $B = f_{a\,\max}$ is $B_{\text{angle}} = 2\,(\eta + 2)\,B = 2\Delta f + 4B$.

Single-Sideband Generation and Vestigial Sideband Filtering

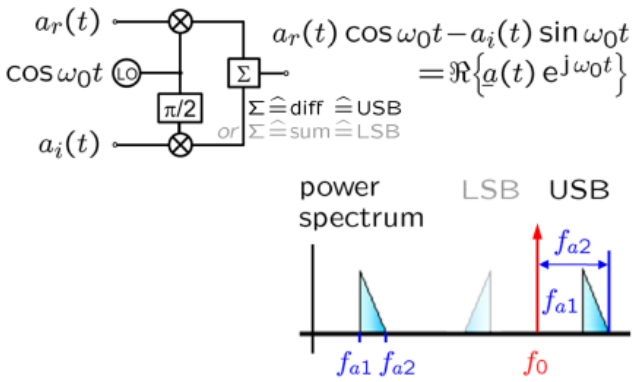

(a) IQ-modulator for single-sideband (SSB) generation (USB, Σ ≙ diff ≙ subtract) [top], and one-sided power spectrum [bottom]

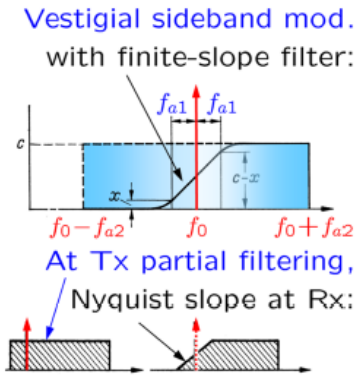

(b) Vestigial sideband (VSB) filtering suppresses redundant spectral parts.

Analogue single-sideband (SSB) generation with an IQ-modulator, and with vestigial sideband (VSB) filtering. (a)-[top] IQ-modulator of Fig. 2.6(a) on Page 27 for SSB generation. The modulator input quantities $a_r(t)$ and $a_i(t)$ are real and imaginary part of an analytic signal $\underline{a}(t) = m(t)(\cos\omega_a t + j\sin\omega_a t)$, see Eq. (2.45a) on Page 2.45a. The LO frequency is f_0. (a)-[bottom] The power spectrum $|\breve{a}(f)|^2$ extends from f_{a1} to f_{a2}. If Σ means subtraction (Σ ≙ diff ≙ USB), the upper sideband USB is generated. If Σ means addition (Σ ≙ sum ≙ LSB), the lower sideband LSB results. The carrier is suppressed. For demodulation, a LO at frequency f_0 must be added at the receiver. (b) Vestigial sideband filtering. (b)-[top] If most of the, e. g., LSB is cut off by a transmitter (Tx) filter, the spectral width is reduced as in (b)-[bottom left], but the information is preserved in the USB. As a consequence, the practical spectral efficiency C'_{pract} in Eq. (2.25) on Page 21) increases considerably. (b)-[bottom right] At the receiver, a filter with a so-called Nyquist slope weighs amplitude and phase of the vestigial LSB such that after downconversion with a LO at f_0 the baseband spectrum reproduces the original USB.

Analogue and Digital Modulation — Synopsis

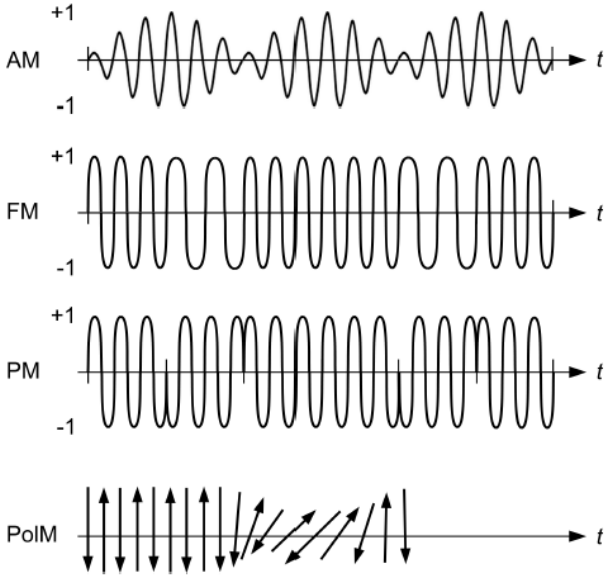

(a) Temporal signal shapes for analogue modulation formats

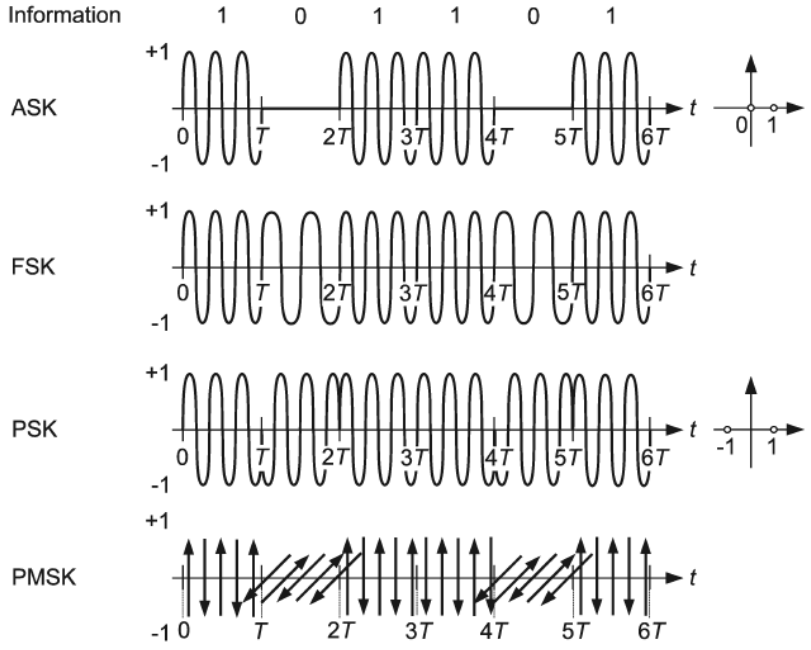

(b) Temporal signal shapes for digital modulation formats. The quantity T stands for the symbol period.

Fig. 2.11. Signal shapes for various analogue and digital modulation formats. (a) Schematic time dependency of signals with various analogue modulation formats. (AM) sinusoidal amplitude modulation with modulation index $0 < m < 1$. (FM) rectangular 2-frequency modulation (this analogue FM example happens to be identical to (b)-FSK). (PM) rectangular 2-phase modulation (this analogue PM example happens to be identical to (b)-PSK). (PolM) sinusoidal polarization-mode modulation. (b) Schematic time dependency of signals with various digital modulation formats. (ASK) amplitude-shift keying. (FSK) frequency-shift keying. (PSK) phase-shift keying. (PMSK) polarization mode-shift keying. To the right of the ASK and PSK curves the respective constellation diagrams are depicted, using the convention as described in Footnote 26 on Page 21 (Q-component or imaginary part on vertical axis, I-component or real part on horizontal axis). [Modified from Ref. † on the Preface page]

LECTURE 7

Digital Modulation Formats

ASK Modulation Formats (1)

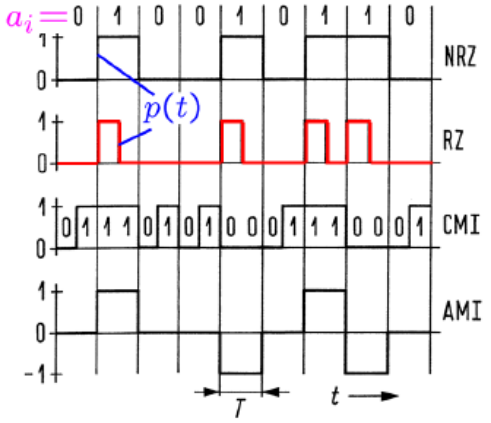

(a) Temporal signal shapes for ASK modulation formats

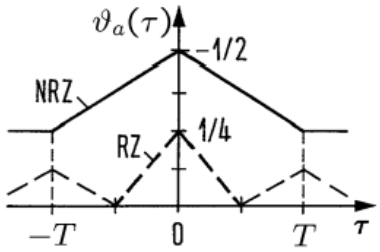

(b) Autocorrelation functions for NRZ and RZ

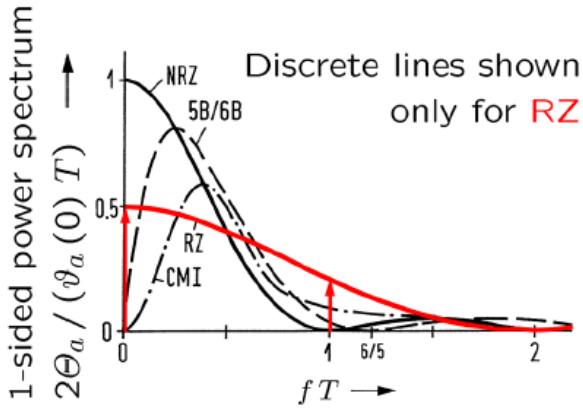

(c) Spectra for random bit sequences encoded with different modulation formats

Amplitude-shift keying (ASK) formats, autocorrelation functions of random non-return-to-zero (NRZ) and return-to-zero (RZ) data, and one-sided power spectra for some modulation formats. (a) Binary data $a_i \in \{0, 1\}$, encoded with the formats NRZ, RZ, coded mark inversion (CMI), and alternate mark inversion (AMI, a pseudo-ternary code). Physical pulse shapes $p(t)$ are rect-functions. (b) Autocorrelation functions (ACF) $\vartheta_a(\tau)$ for NRZ and RZ random sequences (c) One-sided normalized power spectra for random data sequences encoded with the formats NRZ, RZ, 5B/6B, and CMI. Discrete lines are only drawn for the RZ format.

ASK Modulation Formats (2)

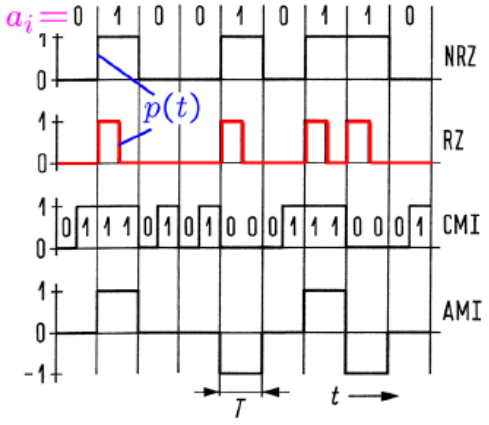

(a) Temporal signal shapes for ASK modulation formats

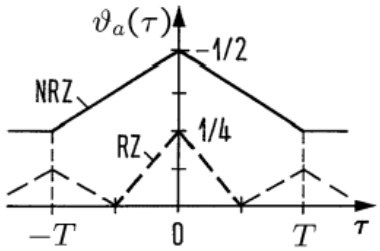

(b) Autocorrelation functions for NRZ and RZ

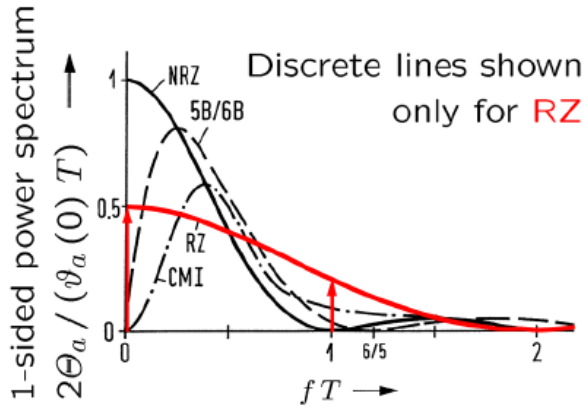

(c) Spectra for random bit sequences encoded with different modulation formats

Amplitude-shift keying (ASK) formats, autocorrelation functions of random non-return-to-zero (NRZ) and return-to-zero (RZ) data, and one-sided power spectra for some modulation formats. (a) Binary data $a_i \in \{0, 1\}$, encoded with the formats NRZ, RZ, coded mark inversion (CMI), and alternate mark inversion (AMI, a pseudo-ternary code). Physical pulse shapes $p(t)$ are rect-functions. (b) Autocorrelation functions (ACF) $\vartheta_a(\tau)$ for NRZ and RZ random sequences (c) One-sided normalized power spectra for random data sequences encoded with the formats NRZ, RZ, 5B/6B, and CMI. Discrete lines are only drawn for the RZ format.

In Fig. 2.11(b) the auto-correlation functions $\vartheta_a(\tau) = \overline{a(t+\tau)a(t)}$ (ACF, Table 1.3 on Page 9) for rectangularly shaped binary NRZ and RZ random sequences with equal distribution of logical 1 and 0 are constructed. The maximum $\vartheta_a(0) = \overline{a(t)^2}$ amounts to $1/2$ (NRZ) and $1/4$ (RZ), respectively. This corresponds to the probability $1/2$ (NRZ) and $1/4$ (RZ), respectively, to measure $a(t) = 1$ at any point of time. For the NRZ format and $|\tau| \geq T$, the joint probability for the events $a(t+\tau) = 1$ and $a(t) = 1$ is $1/4$, and therefore $\vartheta_a(|\tau| \geq T) = 1/4$ holds.

ASK Modulation Formats (3)

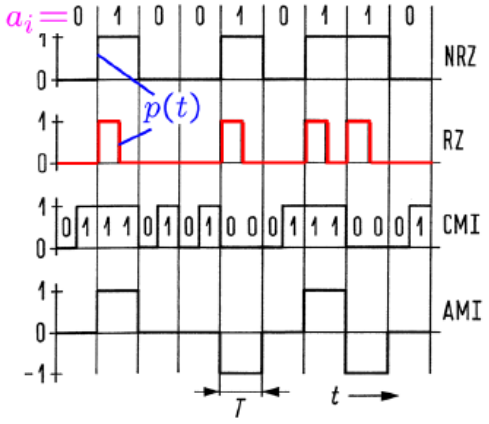

(a) Temporal signal shapes for ASK modulation formats

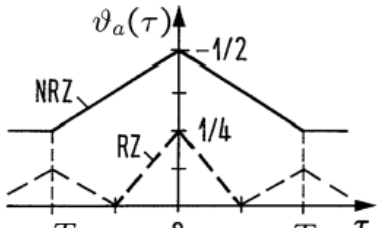

(b) Autocorrelation functions for NRZ and RZ

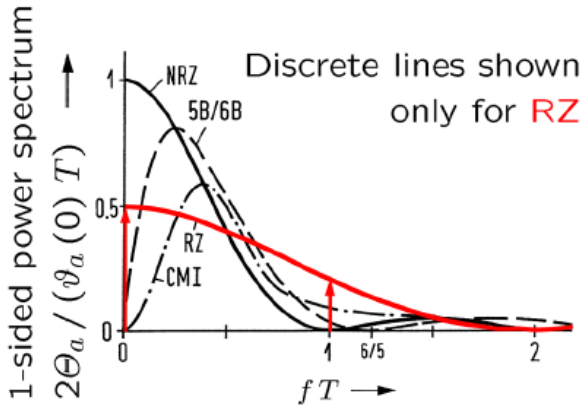

(c) Spectra for random bit sequences encoded with different modulation formats

For the RZ format and $|\tau| = (i - 1/2)\,T$ $(i = 0, \pm 1, \pm 2, \ldots)$, each logical 1 is opposed to a logical 0, and we have $\vartheta_a\,(|(i - 1/2)\,T|) = 0$. With an analogous reasoning as with NRZ, we conclude that the relative extrema $1/8$ of the RZ ACF are reached for $|\tau| = iT$ $(i \neq 0)$. Between the lower and upper corners of the NRZ and RZ ACF, the function $\vartheta_a(\tau)$ changes linearly.

For the ACF $\vartheta_a(\tau)$ and for the associated two-sided power spectrum $\Theta_a\,(f)$ of a binary NRZ random sequence we find, see Table 1.3 on Page 9,

$$\vartheta_{a\,\mathrm{NRZ}}\,(\tau) = \frac{1}{4}\begin{cases} 2 - \dfrac{|\tau|}{T}, & |\tau| \le T \\ 1\,, & |\tau| \ge T \end{cases}, \qquad \Theta_{a\,\mathrm{NRZ}}\,(f) = \frac{T}{4}\,\mathrm{sinc}^2(fT) + \frac{1}{4}\delta\,(f)\,. \tag{2.58}$$

All other discrete lines that could be expected fall on zeros of the sinc-function $\mathrm{sinc}^2(fT)$ and therefore do not show up. Spectra of NRZ test patterns (which could represent a code transmitting more than one bit per symbol) are nicely derived in an Application Note .

Digital Modulation Formats — Synopsis

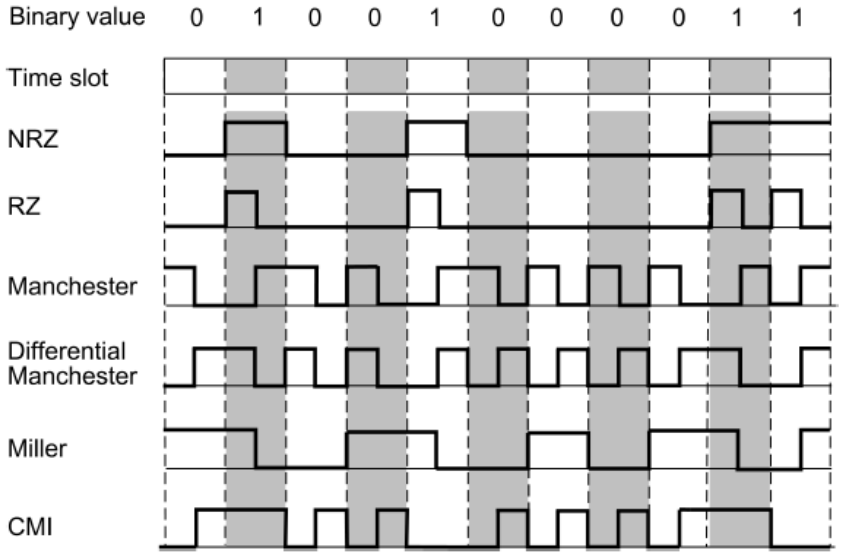

(a) Temporal signal shapes for unipolar ASK. The signal's polarity is always positive.

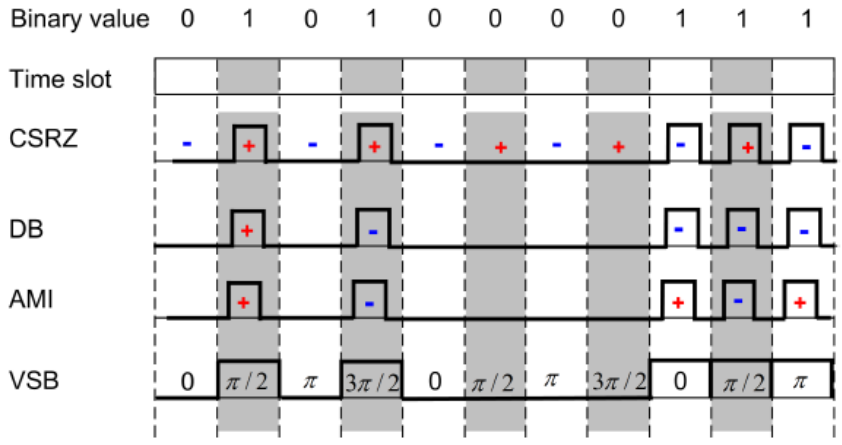

(b) Temporal signal shapes for bipolar ASK. The signal's polarity is marked by a negative (−) or a positive sign (+)

NRZ Non-return to zero. Logical 0 is a space (low level of physical signal), logical 1 is a mark (high level of physical signal). A string of consecutive 0 or 1 means no signal change.

RZ Return to zero. Same as NRZ, but marks occupy only a fraction of the bit slot.

Manchester Also phase encoding[54] (PE). Logical 0 is a mark in the first part of the bit slot, and a space in the second one. Logical 1 is a space in the first part of the bit slot, and a mark in the second one. The average signal power is the same for both 0 and 1. The required transmission bandwidth doubles compared to the NRZ format.

Differential Manchester A differential encoding, using the presence or absence of transitions to indicate a logical value. Logical 0 is a level transition in the first part of the bit slot, logical 1 is a level transition in the second part of the bit slot.

Digital Modulation Formats — Synopsis

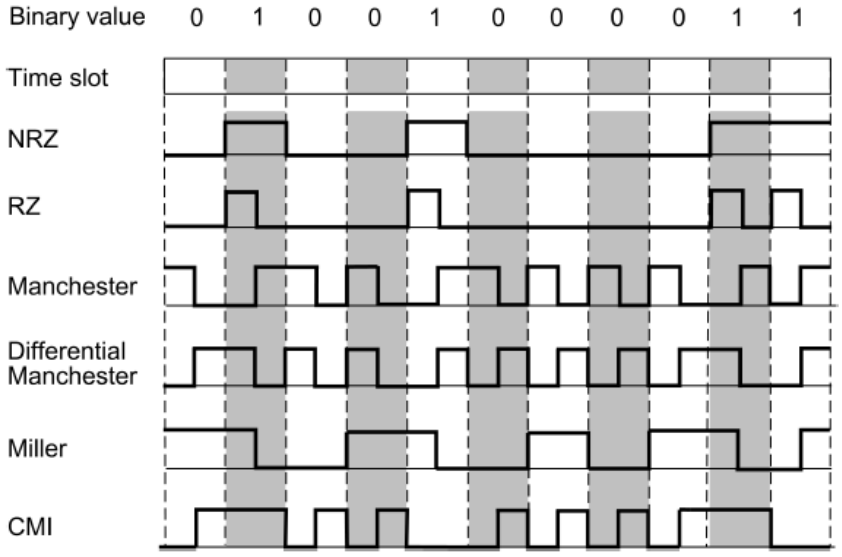

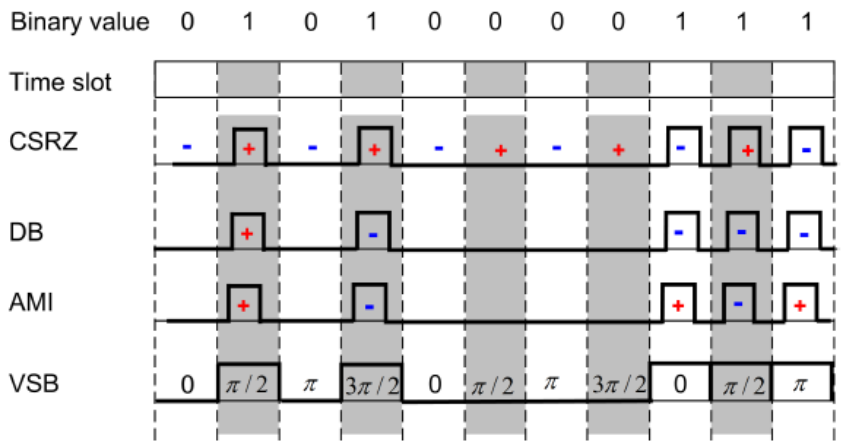

Miller Also delay modulation. Logical 0 means no signal transition, except when 0 is followed by another 0, then there is a transition at the end of the bit slot. Logical 1 is signalled by a transition at the centre of the bit slot from either level.

CMI Coded mark inversion. An NRZ line code, in which logical 0 is encoded as a $0 \rightarrow 1$ transition at the centre of the bit slot, and logical 1 remains constantly on the previous level for the entire bit slot. For a sequence of 1 the constant level is inverted for each subsequent bit slot.

Bipolar ASK and VSB formats Figure 2.12(b) displays how a bit sequence (top row) is encoded using various bipolar ASK formats (ASK with $\{0, \pi\}$-PSK). In addition, vestigial sideband (VSB) encoding shows a combination of ASK with progressive $(\pi/2)$-PSK. The reason for this additional effort is to increase the spectral efficiency C', see Eq. (2.23) on Page 20, and to reduce intersymbol interference (ISI). For example, with VSB, the signals of bit slots adjacent to a central slot interfere destructively, if by dispersion they spill over into the central bit slot.

Digital Modulation Formats — Synopsis

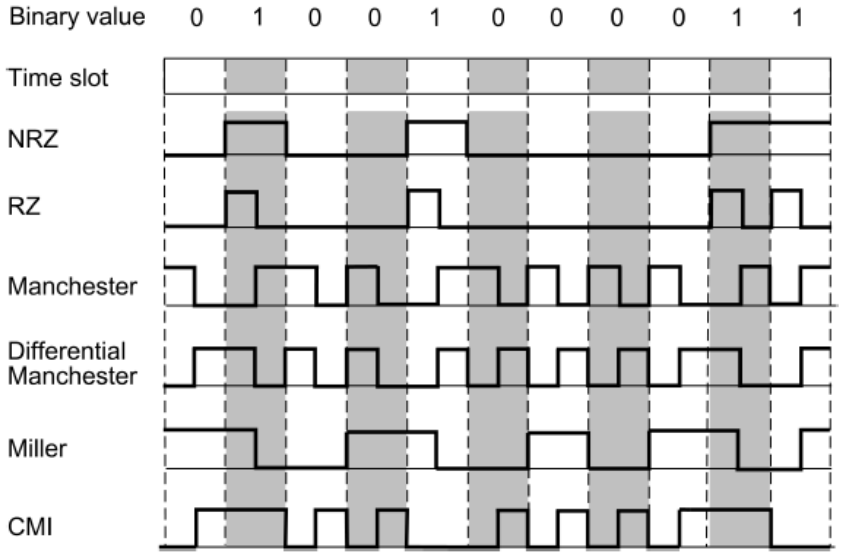

(a) Temporal signal shapes for unipolar ASK. The signal's polarity is always positive.

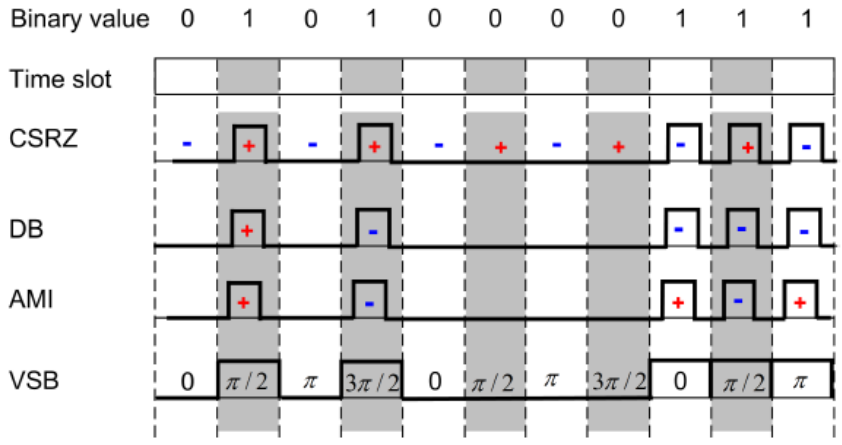

(b) Temporal signal shapes for bipolar ASK. The signal's polarity is marked by a negative (−) or a positive sign (+)

CSRZ Carrier-suppressed return to zero. This is an RZ format with additional phase modulation. If all even bit slots see a positive signal, then all odd bit slots see a negative signal, i. e., a phase shift by π separates even and odd bit slots.

DB, LP-DB Duobinary, low-pass filtered DB. Logical 0 is a space. Logical 1 is a mark without a phase shift by π if there is an even number of 0 since the last 1, and a mark with a phase shift by π if there is an odd number of 0 since the last 1. Duobinary data encoding is a form of correlative coding in partial response signalling. The modulator drive signal can be produced by adding one-bit-delayed data to the present data bit to give levels 0, 1, and 2. An identical effect can be achieved by applying a low-pass (LP) filter to the ideal binary data signal (LP-DB). The correlated three-level signal can be demodulated into a binary signal by using an optical direct detection receiver.

Digital Modulation Formats — Synopsis

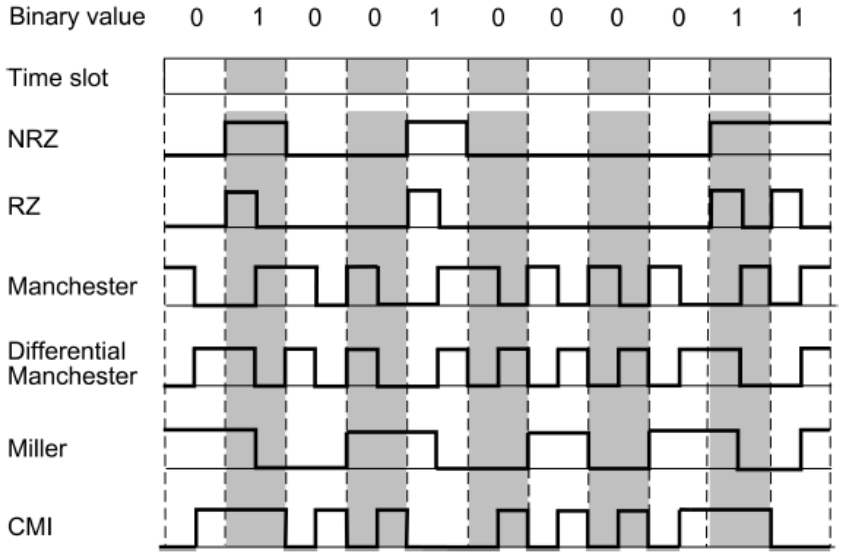

(a) Temporal signal shapes for unipolar ASK. The signal's polarity is always positive.

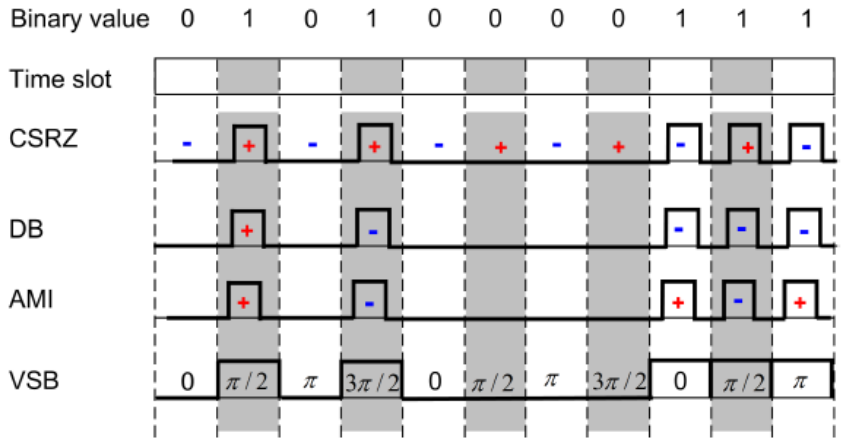

(b) Temporal signal shapes for bipolar ASK. The signal's polarity is marked by a negative (−) or a positive sign (+)

AMI Alternate mark inversion, also called modified duobinary (bipolar or decode duobinary). Logical 0 is a space. Logical 1 is a mark, where each mark is phase shifted by π compared to the previous mark (even if 0 are between consecutive marks).

VSB, AP Vestigial sideband filtering, also called $\pi/2$ alternating phase change[55]. An optical VSB signal is usually generated from an OOK-NRZ or OOK-RZ signal by an optical filter, the passband of which is detuned from the carrier, see Fig. 2.9 on Page 33. Logical 0 is a space. Logical 1 is a mark with a progressive phase shift of $\pi/2$ added for each bit slot (even when it contains a 0).

Digital Modulation Formats — (D)PSK (1)

PSK formatted data streams are generated by modulating the phase η of the carrier $\hat{a}\,\mathrm{e}^{\mathrm{j}[\omega_0 t+\eta(t)]}$, while its amplitude $\hat{a}$ and frequency f_0 are kept constant, see Fig. 2.9 on Page 34. For binary PSK formats, the phase takes two values, commonly chosen to be $\eta = 0$ and $\eta = \pi$. Because the intensity remains constant, nonlinear effects that depend on intensity are independent from the modulated data stream.

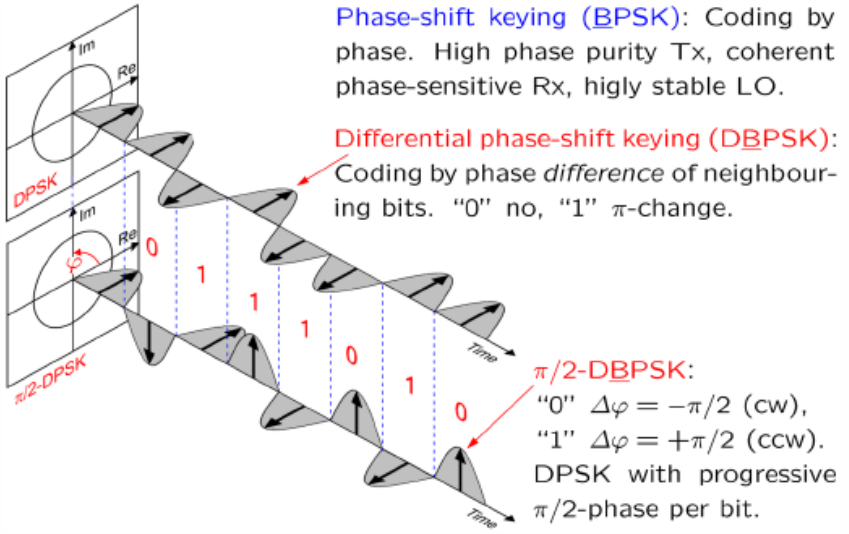

Fig. 2.14. Real part (Re) and imaginary part (Im) of a complex carrier envelope modulated with binary DPSK (DBPSK, upper graph) and binary $\pi/2$-DPSK ($\pi/2$-DBPSK, lower graph). Sinusoidally shaped RZ pulses represent the carrier envelope. The carrier time function itself is not drawn, because it oscillates very rapidly inside each pulse-shaped part of the envelope. For $\pi/2$-DPSK, logical 0 and 1 are represented by a relative phase shift of $-\pi/2$ (clockwise) and $+\pi/2$ (counter clockwise), respectively. The format $\pi/2$-DBPSK resembles minimum-shift frequency keying (MSK). The format $\pi/2$-DBPSK is identical to MSK, if the phase is not switched, but changed continuously during each time slot. [Modified from Ref. 71]

Digital Modulation Formats — (D)PSK (2)

PSK signal transmission so far is only used in backbones, where cost does not matter too much. There are mainly three reasons for this:

- PSK formats require well defined carriers with little phase noise, and phase-sensitive coherent receivers with a laser LO as discussed in Sect. 2.3.2 on Page 30. A photodetector as briefly described in Eq. (1.1) on Page 2 would only be sensitive to the intensity. Unfortunately, such an LO laser adds to cost and complexity, not to speak of the cost of the transmitting laser which must have similarly good properties. So in practice, one tries to avoid such schemes.
- In optical communications, a typical wavelength is $\lambda_0 = 1.55\,\mu\text{m}$ ($f_0 = 193.51\,\text{THz}$, see Table 2.1 on Page 21). Consider a fibre transmission span of $L = 100\,\text{km}$. Following Eq. (2.11) on Page 18, the acquired phase would be $\varphi = -\beta L \approx -k_0 n L$, where the refractive index of the fibre is about $n = 1.5$. A tiny refractive index change by only $\Delta n = 0.77 \times 10^{-11}$ (this happens easily if the temperature changes randomly by fractions of a degree) would cause a phase shift by $\Delta\varphi = -\frac{2\pi}{1.55\,\mu\text{m}} \times 0.77 \times 10^{-11} \times 100\,\text{km} = -\pi$, and thus randomly invert the meaning of space and mark with respect to the phase of the LO.
- Optical signals have a certain polarization. The mixing between the incoming signal and the LO works only if both oscillate in the same state of polarization. However, after hundreds of kilometers of transmission, the state of polarization is usually no longer known.

Digital Modulation Formats — OOK vs. PSK

Elect. field amplitude $\boldsymbol{E}$ switched on and off (on-off keying)

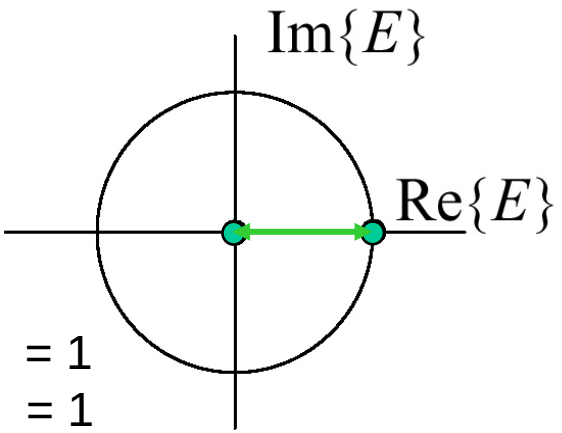

field amplit. = 1
peak power = 1
mean power = ½

OOK

random pattern ... ↑ ↑... ...010001...

Elect. field phase differ. from previous bit
$\Delta\varphi = 0$ for a logical “0”
$\Delta\varphi = \pi$ for a logical “1”

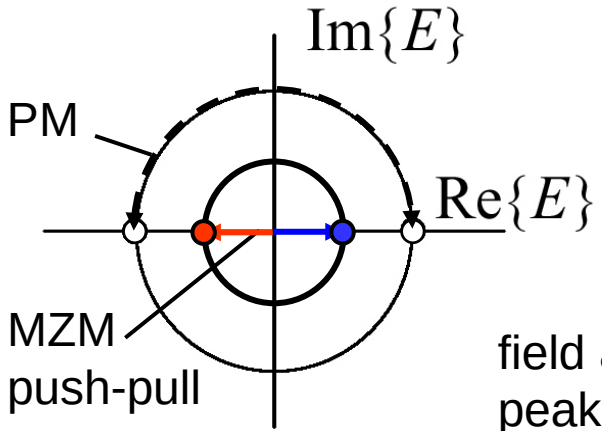

DPSK

field amplit. = ½
peak power = ¼
mean power = ¼

…↑↑↓↓↓↓↑… periodic int. pattern
...010001...

3 dB OSNR advantage wrt OOK

Ho, Keang-Po R.: Effects of Nonlinear Phase Noise to DPSK Signals (2004)

Digital Modulation Formats — DPSK

Despite these difficulties, coherent schemes are gaining ground and will be more and more deployed. However, all of these constraints can be relaxed by using a modified form of PSK, namely differential PSK (DPSK), Fig. 2.13. The scheme does not compare the phase of a transmitter laser and a receiver LO, but rather the phase difference between subsequent time slots. For high data rates, the slot width T and therefore the time difference is small, and the phase even of inexpensive transmitter lasers is stable enough during such a short time interval of, e. g., $T = 25\,\mathrm{ps}$ at a data rate of 40 Gbit/s. At present, DPSK is globally used in both long-haul backbones and medium-haul networks. Two different DPSK flavours are common:

DPSK Differential phase-shift keying[56]. Information is coded in a phase difference $\Delta\varphi = \{0, \pi\}$ between two neighbouring time slots. If η_k represents the carrier phase for the k-th time slot, the phase difference $\Delta\varphi = \eta_k - \eta_{k-1}$ is $\Delta\varphi = 0$ for encoding a logical 0, and it is $\Delta\varphi = \pi$ for a logical 1.

$\pi/2$-DPSK $\pi/2$ differential phase-shift keying[57,58]. Information is coded in a phase difference $\Delta\varphi = \pm\,\pi/2$ between subsequent time slots. The phase difference is $\Delta\varphi = -\,\pi/2$ for encoding a logical 0, and a phase difference $\Delta\varphi = +\,\pi/2$ encodes a logical 1. The procedure is identical to a progressive $\pi/2$ phase shift on top of the DPSK encoding. The unique advantage[59] of $\pi/2$-DPSK arises from its response to over-filtering, as will be shown in a later section.

For a binary NRZ DPSK signal with a symbol rate $R_s = 1/T$, the total bandwidth B_{DPSK} for signalling is essentially determined by the zero of the NRZ power spectrum at $f_0 \pm R_s$ as in Fig. 2.11(c) on Page 35,

$$B_{\mathrm{DPSK}} \approx 2R_s = \frac{2}{T}\,. \tag{2.57}$$

This is much less than would be expected from distortion-free analogue angle modulation, where Eq. (2.54b) on Page 32 would predict a bandwidth of $2\,(\eta+1)\,B = 2\,(\pi/2+1)\,R_s \approx 5\,R_s$ for an average modulation index of $\eta = \langle\,\Delta\varphi/2\rangle = \pi/2$.

Digital Modulation Formats — FSK

Frequency-shift keying (FSK) encodes data by shifting the carrier frequency f_0. Binary data are encoded in two carrier frequencies $f_0 \pm \Delta f$, which are separated by the frequency spacing ("tone" spacing) $2\Delta f$. For estimating the transmission bandwidth with Eq. (2.56b), we set $\eta = \Delta\omega/(2\pi R_s)$ according to Eq. (2.55) on Page 34 and find

$$B_{\mathrm{FSK}} \approx 2\,(\eta + 2)\,B = 2\left(\frac{\Delta f}{R_s} + 1\right) R_s = 2\,(\Delta f + R_s)\,. \tag{2.60}$$

If $\Delta f \ll R_s$ holds, we speak of narrowband FSK. The case $\Delta f \gg R_s$ is named broadband FSK. Practical implementations of, e. g., a binary FSK modulate the phase $\eta(t)$ of the optical carrier $\mathrm{e}^{\mathrm{j}[\omega_0 t + \eta(t)]}$ in a linear fashion according to $\mathrm{d}\eta(t)/\mathrm{d}t = \pm 2\pi\Delta f$, $\eta(t) = \pm\Delta\omega\, t$ with $\Delta\omega = 2\pi\Delta f$. There are two important versions:

CFSK Continuous-phase FSK. For binary CFSK, logical 0 and logical 1 are represented by carrier frequencies $f_0 - \Delta f$ and $f_0 + \Delta f$, respectively. A binary data change $0 \to 1$ is represented by switching the slope of the continuous phase change from $\mathrm{d}\eta(t)/\mathrm{d}t = -\Delta\omega$ to $\mathrm{d}\eta(t)/\mathrm{d}t = +\Delta\omega$. The data change $1 \to 0$ requires to switch the phase slope from $\mathrm{d}\eta(t)/\mathrm{d}t = +\Delta\omega$ to $\mathrm{d}\eta(t)/\mathrm{d}t = -\Delta\omega$. The "transitions" $0 \to 0$ and $1 \to 1$ leave the phase slope unchanged, and we have $\eta(t) = -\Delta\omega\, t$ and $\eta(t) = +\Delta\omega\, t$, respectively. The phase function $\eta(t)$ is continuous and consists of straight line segments. This saves bandwidth compared to a "hard" switching of independent carriers as in switched FSK.

Digital Modulation Formats — FSK and OFDM

OFDM Orthogonal frequency division multiplexing[66,67] is both, a specialized and a generalized form of CFSK. Generalized in so far, as multiple frequencies can be present at the same time, and specialized because the frequency separation is tied to the symbol duration. If the CFSK symbol shape is rectangular with a duration T, and if the participating carrier frequencies $f_\nu = \nu R_s =$ are chosen to be integer multiples ν of the symbol rate (implying a frequency line separation of $2\Delta f = 1/T$), inter-symbol interference is minimized because the symbols are orthogonal,

$$\frac{1}{T}\int_{T_0-T/2}^{T_0+T/2} \exp\left(+\mathrm{j}\,2\pi\nu\, t/T\right)\exp\left(-\mathrm{j}\,2\pi\nu'\, t/T\right)\mathrm{d}t = \delta_{\nu\nu'} \qquad \text{(arbitrary reference time } T_0\text{)}. \quad (2.58)$$

SFSK Switched FSK uses independent carriers, which are switched on and off. The phase functions then have discontinuities, which increases the required bandwidth compared to CFSK.

MSK Minimum-shift keying. If the tone spacing equals half the symbol rate, $2\Delta f = R_s/2 = 1/(2T)$, then any data transition changes the phase continuously by $|\Delta\varphi| = \Delta\omega T = \pi/2$ during the duration of a time slot T. If further the amplitudes of the two tones $f_0 \pm \Delta f$ are identical, the scheme is identical to the $\pi/2$-DPSK format as depicted in Fig. 2.13: A logical 0 is encoded by a phase change of $\Delta\varphi_0 = -\pi/2$ (the carrier frequency is switched to or remains at $f_0 - \Delta f$), and a logical 1 is encoded by a phase change of $\Delta\varphi_1 = +\pi/2$ (the carrier frequency is switched to or remains at $f_0 + \Delta f$).

FODM Similar to the relationship between CFSK and OFDM, there exists an affinity between MSK and fast orthogonal frequency division multiplexing[68] (FODM) with half the standard OFDM carrier spacing.

Digital Modulation Formats — Synopsis (1)

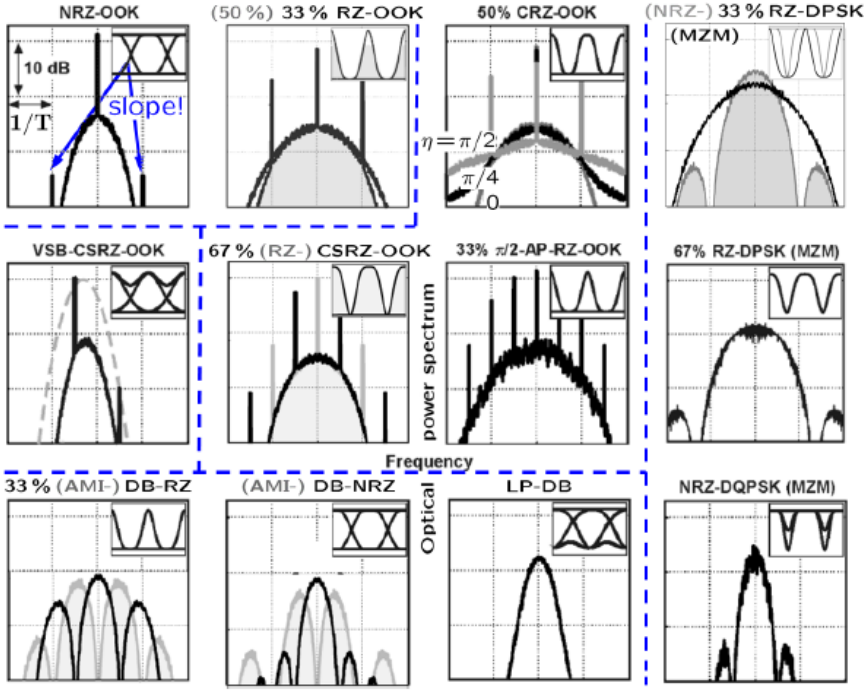

(a) Semi-logarithmic power spectra for random data encoded with various modulation formats

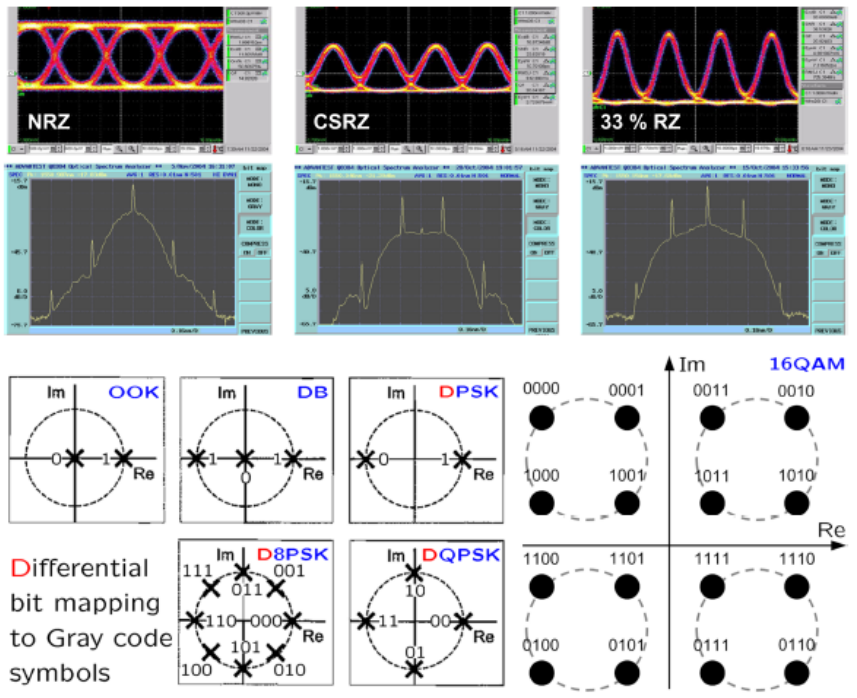

(b) [top] Eye diagrams and spectra [bottom] Constellation diagrams of binary and M-ary modulation formats

Synopsis of properties for various digital modulation formats. (a) Spectra for random binary data, grouped together by the broken blue lines (– – –). The horizontal axis represents frequency (1 div = $R_s = 1/T$, symbol time slot T), the logarithmic vertical axis gives the relative spectral power density in dB (1 div = 10 dB). Spectra in light grey are named in the subfigure texts using the same colour. Eye diagram schematics are shown in the upper right corners of the subfigures. For the NRZ spectrum, unexpected lines are to be seen at a frequency offset $\pm 1/T$ from the carrier if we compare to the spectrum in Fig. 2.11(c) at Page 35. These unexpected lines are due to the finite slopes of the actual real-world NRZ pulse, which deviates from an ideal rect-function. [Compiled from Ref. 60, 61, 62, 63, 64] (b)-[top] Measured random signals (so-called "eye diagrams") for NRZ, CSRZ and 33 % RZ formats with measured power spectra [modified from Ref. 65, 66] (b)-[bottom] Constellation diagrams for the binary formats OOK and (D)PSK, and for the M-ary formats DB, (D)QPSK, (D)8PSK, and 16QAM with mappings to so-called Gray code symbols [modified from Reference 67 and 68 (16QAM)]

Digital Modulation Formats — Synopsis (2) Gray Code

[78] Frank Gray, physicist at Bell Laboratories, ⋆ Alpine (IN) 13.9.1887, † 23.5.1969. Numerous innovations in television, both mechanical and electronic. Remembered for the invention of the Gray code (reflected binary code) in 1947. The advantage of this code: Consecutive positions of this code differ only by one bit. If a rotary position encoder reads out a number of bits in parallel (encoded in opaque and transparent ring segments with different radii), no simultaneous bit switching is required, which, when not properly done, could lead to glitches. — "In modern digital communications, Gray codes play an important role in error correction. For example, in a digital modulation scheme such as QAM where data is typically transmitted in symbols of 2 bit or more, the signal's constellation diagram is arranged so that the bit patterns conveyed by adjacent constellation points differ by only one bit. By combining this with forward error correction capable of correcting single-bit errors, it is possible for a receiver to correct any transmission errors that cause a constellation point to deviate into the area of an adjacent point. This makes the transmission system less susceptible to noise." [Cited after `http://en.wikipedia.org/wiki/Gray_code`]

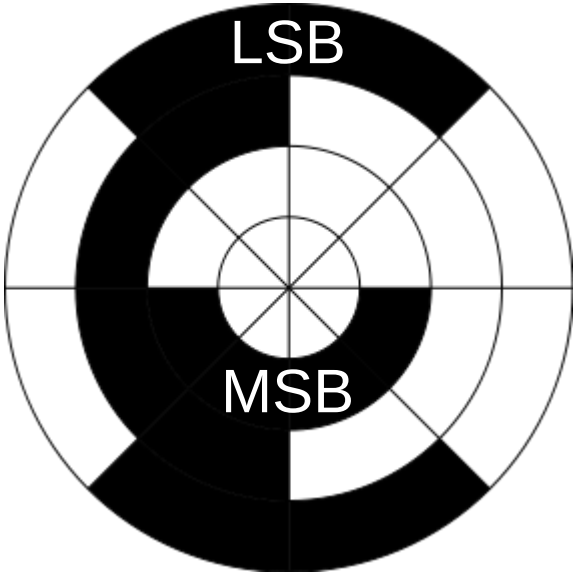

3-bit
000
001
011
010
110
111
101
100

http://en.wikipedia.org/wiki/Gray_code

Digital Modulation Formats — Synopsis (3)

40 GBd SYMBOL RATE WITH 1 bit / symbol:

OOK On-off keying. NRZ, RZ (duty cycle 33 % and 50 %), chirped RZ[78] (CRZ, duty cycle 50 %), carrier-suppressed RZ (CSRZ, duty cycle 66 %), chirped CSRZ

DB Duobinary. NRZ-DB, chirped NRZ-DB, RZ-DB (duty cycle 33 % and 50 %), CRZ-DB, CSRZ-DB, chirped CSRZ-DB

VSB Vestigial sideband filtering. Sideband and carrier (partially) suppressed

DPSK Differential binary phase shift keying (D(B)PSK), NRZ-DPSK, chirped NRZ-DPSK, RZ-DPSK (duty cycle 33 % and 50 %), CRZ-DPSK, CSRZ-DPSK, chirped CSRZ-DPSK

20 GBd SYMBOL RATE WITH 2 bit / symbol:

DQPSK Differential quaternary[79] PSK (or differential four-PSK, or differential 4QAM). (N)RZ, CSRZ (duty cycle 33 %, 50 % and 66 %)

13.3 GBd SYMBOL RATE WITH 3 bit / symbol:

D8PSK Differential octonary PSK (or differential eight-PSK)

10 GBd SYMBOL RATE WITH 4 bit / symbol:

16QAM Seno-denary quadrature amplitude modulation (or sixteen-QAM)

Pulse-Position Modulation (1)

Pulse-position modulation is a form of signalling that uses the same transmitter and receiver hardware as with OOK. In M-ary PPM (M-PPM), a number of $r = \log_2 M$ information bits is encoded by the position of an optical pulse within M equidistant time slots of a symbol with duration T, Fig. 2.15. The resulting waveforms have a low duty cycle $1/M$, and the peak power in each pulse is larger than the average power (dotted red line, ·····) by a factor of M. This makes PPM well suited for average-power limited transmitters with EDFA, but a poor choice for peak-power limited transmitters with SOA.

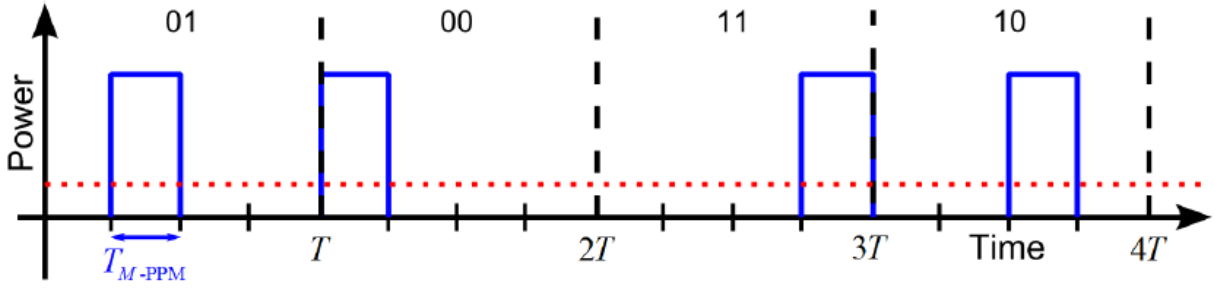

Pulse-position modulation with $M = 4$ different pulse positions inside the frame of a symbol duration T. The signal's duty cycle is $1/M$, so that the peak power in each pulse is larger than the average power (·····) by a factor of M.

the upper-frequency limit required for NRZ-OOK signalling with a symbol duration T is $1/T$. For identical bit rates $R_{b\,\text{NRZ-OOK}} = R_{b\,M\text{-PPM}} = 1/T_{\text{NRZ-OOK}}$, this leads to a larger M-PPM bandwidth $B_{M\text{-PPM}} = (M/r)\,B_{\text{NRZ-OOK}}$,

$$R_{b\,\text{NRZ-OOK}} = R_{b\,M\text{-PPM}}: \tag{2.59}$$

$$B_{\text{NRZ-OOK}} = \frac{1}{T_{\text{NRZ-OOK}}}, \quad B_{M\text{-PPM}} = \frac{1}{T_{M\text{-PPM}}} = \frac{M/\log_2 M}{T_{\text{NRZ-OOK}}} = \frac{M}{r}\,B_{\text{NRZ-OOK}}, \quad r = \log_2 M.$$

Pulse-Position Modulation (2)

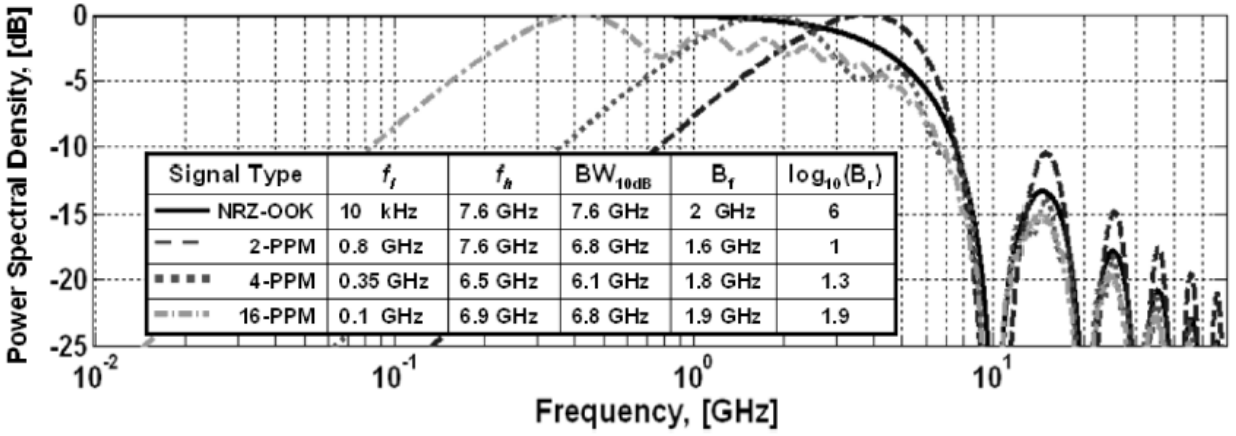

Signal Type	f_l	f_h	BW_{10dB}	B_f	$\log_{10}(B_r)$
NRZ-OOK	10 kHz	7.6 GHz	7.6 GHz	2 GHz	6
2-PPM	0.8 GHz	7.6 GHz	6.8 GHz	1.6 GHz	1
4-PPM	0.35 GHz	6.5 GHz	6.1 GHz	1.8 GHz	1.3
16-PPM	0.1 GHz	6.9 GHz	6.8 GHz	1.9 GHz	1.9

Calculated spectra for square waveforms used in OOK and 2PPM, 4PPM, and 16PPM modulation for a fixed pulse width (OOK *and* M-PPM) of $T_{M\text{-PPM}} = T_{\text{NRZ-OOK}} = 100\,\text{ps}$. Because of this choice the first spectral zero is always at $1/T_{M\text{-PPM}} = 10\,\text{GHz}$, and the bit rates for M-PPM become smaller than for NRZ-OOK, $R_{b\,M\text{-PPM}} = (r/M)\,R_{b\,\text{NRZ-OOK}}$ ($r = \log_2 M$). The M-PPM waveforms have a smaller bandwidth ratio $B_r = f_h/f_l$ of the 10 dB higher and lower limiting frequencies f_h and f_l, respectively, and a significantly smaller fractional (or relative) bandwidth $B_f = B_{10\,\text{dB}}/[(f_h + f_l)/2]$ ($B_{10\,\text{dB}} = f_h - f_l$) than the OOK waveforms. For the OOK spectrum, we set $f_l = 10\,\text{kHz}$, which is a common low-frequency specification for applicable broad-band electronics. For a constant bit rate, the M-PPM spectra are broadened by a factor of M/r, which increases the 10 dB bandwidth $B_{10\,\text{dB}}$, but does not impact B_r. [After Ref. 26 on Page 21. Fig. 9, p. 243]

If the bandwidths are kept identical by having identical pulse widths $T_{M\text{-PPM}} = T_{\text{NRZ-OOK}}$ as was assumed then the M-PPM bit rate becomes smaller, $R_{b\,M\text{-PPM}} = (r/M)\,R_{b\ \text{NRZ-OOK}}$,

$$T_{M\text{-PPM}} = T_{\text{NRZ-OOK}}:$$

$$R_{b\,\text{NRZ-OOK}} = \frac{1}{T_{\text{NRZ-OOK}}}, \quad R_{b\,M\text{-PPM}} = \frac{\log_2 M}{T_{M\text{-PPM}} M} = \frac{(\log_2 M)/M}{T_{\text{NRZ-OOK}}} = \frac{r}{M}\,R_{b\,\text{NRZ-OOK}}, \quad r = \log_2 M.$$

Pulse-Position Modulation (3)

While electrical bandwidth limitations may determine the maximum slot rate $R_{\text{slot}} = 1/T_{M\text{-PPM}}$ for a single M-PPM channel, the high-speed $10\ldots40\,\text{Gbit/s}$ electronics developed for the telecom industry make it easy to implement moderately high bit rates. For example, by transmitting 16PPM ($r = 4$) at a slot rate of $R_{\text{slot}\,16\text{PPM}} = 10\,\text{GSlot/s}$, a bit rate of $R_{b\,16\text{PPM}} = 2.5\,\text{Gbit/s}$ can be delivered with a symbol rate of $R_{s\,16\text{PPM}} = 10\,\text{GBd}\,/\,16 = 625\,\text{MBd}$.

The low duty cycle of M-PPM waveforms can also lead to impairments due to optical nonlinearities, so that the peak transmit power must be limited. Naturally, this does not apply to FSO systems, were the low duty cycle in combination with the high peak power delivered by EDFA during short signal bursts even helps in bridging longer distances. On the receive side, M-PPM requires two clocks to be recovered, a symbol and a slot clock. Clock acquisition can be challenging for large M since for a given average optical power the received electrical power at the clock frequencies becomes smaller according to $1/M^2$, which may require embedded synchronization bits.

For the same pulse width $T_{M\text{-PPM}} = T_{\text{NRZ-OOK}}$, the M-PPM waveforms compared to NRZ-OOK have a smaller bandwidth ratio B_r, and a significantly smaller fractional (or relative) bandwidth B_f. This is mainly due to the smaller 10 dB bandwidth $B_{10\,\text{dB}}$ which is defined at frequencies f_h and f_l, where the power spectrum is 10 dB down from its maximum,

$$B_r = \frac{f_h}{f_l}\,, \qquad B_f = \frac{B_{10\,\text{dB}}}{(f_h + f_l)/2}\,, \qquad B_{10\,\text{dB}} = f_h - f_l \tag{2.64}$$

For a constant bit rate, the M-PPM spectra are broadened according to Eq. (2.62) on Page 46 by a factor of M/r, which increases the 10 dB bandwidth $B_{10\,\text{dB}}$, but does not impact B_r. Assuming a pseudo-random bit sequence (PRBS) of 10 Gbit/s NRZ-OOK waveforms, B_r extends from a practical lower bound of $f_l = 10\,\text{kHz}$ up to $f_h = 10\,\text{GHz}$ (six decades!). In contrast, the spectra for M-PPM waveforms operating at the same data rate span less than two decades, reducing B_r by over 4 orders

LECTURE 8

Optical Transmitters

Light Sources

Semiconductor Laser — Counting Resonator Modes

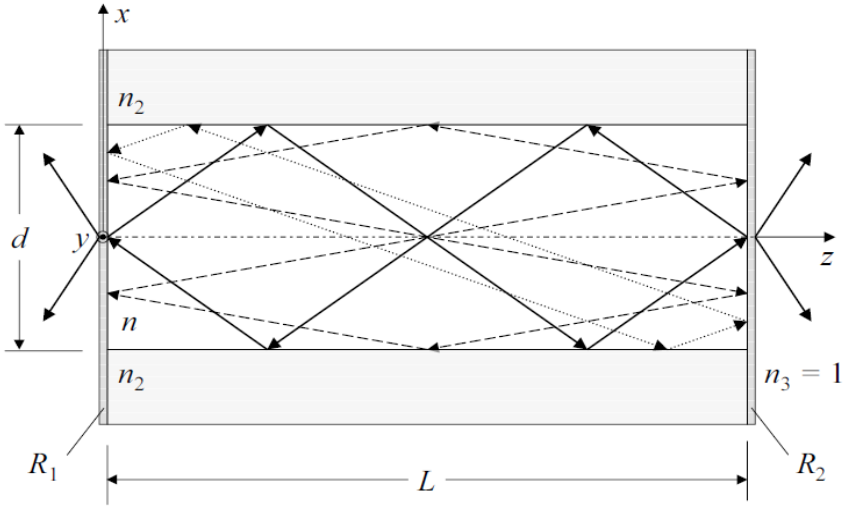

1D WG: transv. x-resonances

2D WG: transv. (x, y)-resonances

3D resonator has in addition longitudinal z-resonances.

Vol. $V = Lbd$, or configuration-space volume $V_c = L_x L_y L_z \mathrel{\widehat{=}} L^3$

Fig. 3.1. Laser resonator modes. Resonator length L, strip waveguide height d (corresponds to h in Fig. 2.7), strip waveguide height b along y-axis, active volume $V = Lbd$, mirrors with power reflection factors $R_{1,2}$

$$\text{1D}: \quad M_g^{(\text{slab})} = \frac{4}{\pi} V = 2\left(2\,\frac{h}{2}\right)\frac{f}{c}\,(2\,A_N) \qquad \left(V = \frac{h}{2}\,k_0\,A_N\right)$$

$$\text{2D}: \quad M_g^{(\text{SIF})} = \frac{1}{2} V^2 = 2\left(a^2\pi\right)\frac{f^2}{c^2}\left(\pi A_N^2\right) \qquad \left(V = a\,k_0\,A_N\right)$$

$$\text{3D}: \quad M_{\text{tot}} = 2\,V_c\,\frac{4\pi}{3}\left(\frac{fn}{c}\right)^3 \underset{n=1}{=} \frac{2}{3}\left(L^3\right)\frac{f^3}{c^3}\,(4\pi)$$

$$\text{DOS}: \quad \varrho_{\text{tot}}(f) = \frac{1}{V_c}\,\frac{\mathrm{d}M_{\text{tot}}}{\mathrm{d}f} = \frac{8\pi}{c^3}(fn)^2 n_g\,, \qquad n_g = n + f\,\frac{\mathrm{d}n}{\mathrm{d}f}$$

Free Electron as a Wave Function

Electron moving in constant potential V having momentum p. De Broglie: Described by plane-wave function, angular frequency ω, wavenumber $k = p/\hbar$ (physics notation; electrical engineering: $\psi_{\mathrm{ee}}(t,x) = \exp[\mathrm{j}(\omega t - kx)] = \psi^*(x,t)$):

$$\psi(x,t) = \exp[\mathrm{j}(kx - \omega t)]$$

Electron may be excited only with energy quanta $\hbar\omega = W$ (Einstein, photoelectric effect). Result is matter wave:

$$\psi(x,t) = \exp[(\mathrm{j}/\hbar)(p\,x - W t)]$$

Derivatives of $\psi(x,t)$ wrt x and $t \rightarrow$ differential operators for conservation quantities. Eigenvalues are momentum p and energy W:

$$\left(-\mathrm{j}\,\hbar\,\partial/\partial x\right)^2 \psi(x,t) = p^2\,\psi(x,t), \qquad \left(\mathrm{j}\,\hbar\,\partial/\partial t\right)\psi(x,t) = W\,\psi(x,t)$$

Electron energy $W = p^2/(2m_0) + V = (\hbar k)^2/(2m_0) + V$, rest mass m_0:

$$\left[\frac{1}{2m_0}\left(\frac{\hbar}{\mathrm{j}}\frac{\partial}{\partial x}\right)^2 + V\right]\psi(x,t) = -\frac{\hbar}{\mathrm{j}}\frac{\partial}{\partial t}\,\psi(x,t)$$

Schrödinger Equation for "Bound Electron" & "Two-Level Atom"

Wave function $\psi(x,t) = \psi(x)\ \mathrm{e}^{-\mathrm{j}\,\omega t}$ and dispersion relation:

$$\left[\frac{1}{2m_0}\left(\frac{\hbar}{\mathrm{j}}\frac{\partial}{\partial x}\right)^2 + V\right]\psi(x) = W\,\psi(x)\,, \qquad W = \hbar\omega = \frac{(\hbar k)^2}{2m_0} + V$$

Potential film ($\widehat{=}$ slab waveguide) with infinitely high walls. Solutions are spatial sinusoidals or superpositions of it:

$$\psi(x,t) = \mathrm{j}(1/\sqrt{2})\,\psi_2(x)\,\mathrm{e}^{-\mathrm{j}\,\omega_2 t} + (1/\sqrt{2})\,\psi_1(x)\,\mathrm{e}^{-\mathrm{j}\,\omega_1 t},$$

$$\omega_{21} = \omega_2 - \omega_1$$

Schrödinger Equation for "Two-Level Atom"

Potential film ($\widehat{=}$ slab waveguide) with infinitely high walls. Solutions are spatial sinusoidals or superpositions of it:

$$\psi(x,t) = \mathrm{j}(1/\sqrt{2})\,\psi_2(x)\,\mathrm{e}^{-\mathrm{j}\omega_2 t} + (1/\sqrt{2})\,\psi_1(x)\,\mathrm{e}^{-\mathrm{j}\omega_1 t},$$

$$\omega_{21} = \omega_2 - \omega_1$$

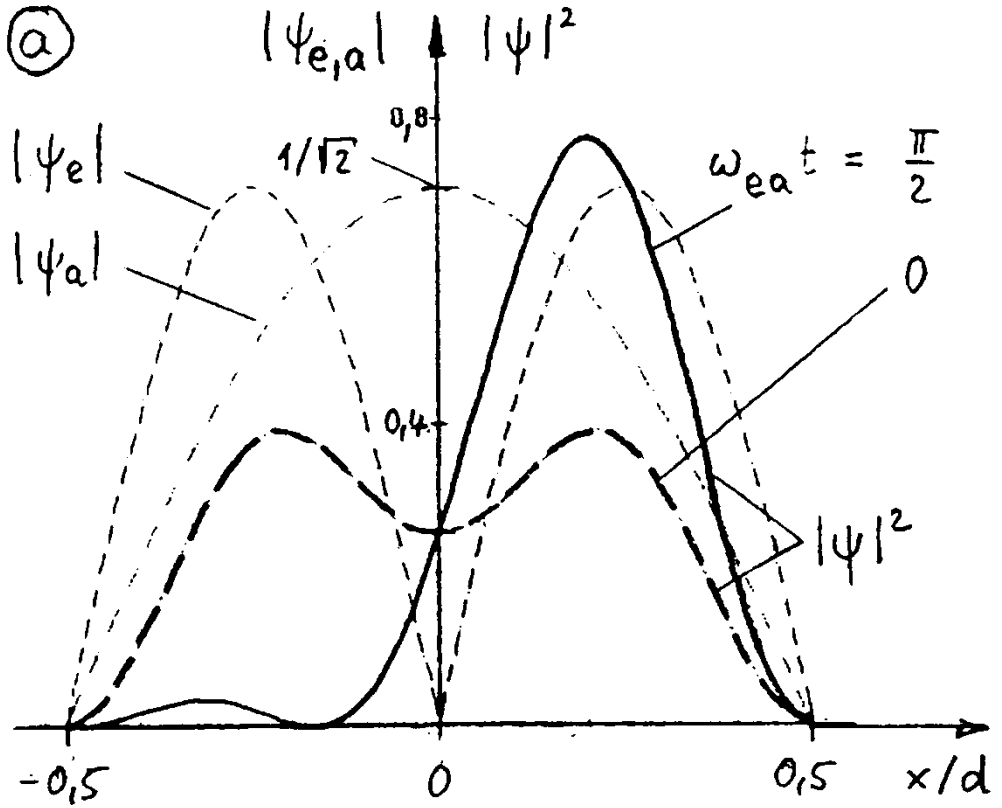

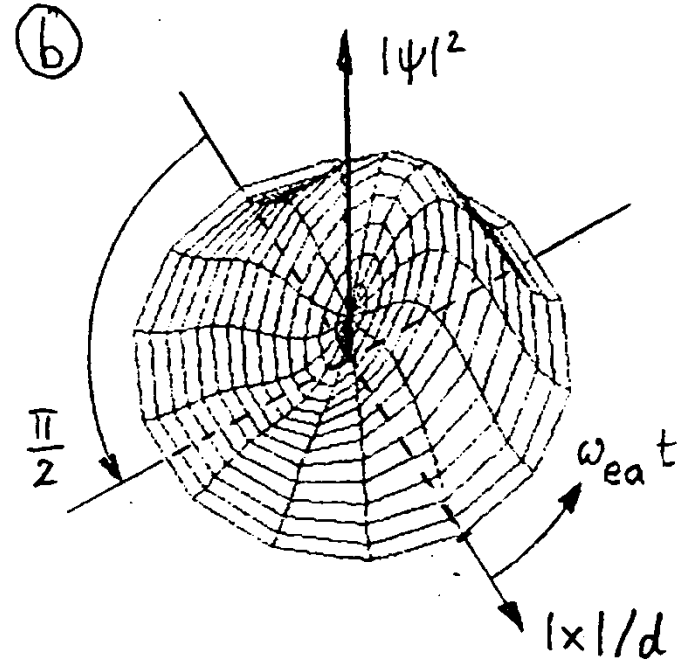

Schrödinger Equation for "Bound Electron" & "Two-Level Atom"

Wave function $\psi(x,t) = \psi(x)\ \mathrm{e}^{-\mathrm{j}\,\omega t}$ and dispersion relation:

$$\left[\frac{1}{2m_0}\left(\frac{\hbar}{\mathrm{j}}\frac{\partial}{\partial x}\right)^2 + V\right]\psi(x) = W\,\psi(x)\,, \qquad W = \hbar\omega = \frac{(\hbar k)^2}{2m_0} + V$$

Potential film ($\widehat{=}$ slab waveguide) with infinitely high walls. Solutions are spatial sinusoidals or superpositions of it:

$$\psi(x,t) = \mathrm{j}(1/\sqrt{2})\,\psi_2(x)\,\mathrm{e}^{-\mathrm{j}\,\omega_2 t} + (1/\sqrt{2})\,\psi_1(x)\,\mathrm{e}^{-\mathrm{j}\,\omega_1 t},$$

$$\omega_{21} = \omega_2 - \omega_1$$

Light-matter interaction of wave function $\psi(x,t)$ with electric field $E_0(t)$. Dipole moment $\mu = -e\,x$ leads to dipole energy $-\mu E_0(t)$:

$$\left[\frac{1}{2m_0}\left(\frac{\hbar}{\mathrm{j}}\frac{\partial}{\partial x}\right)^2 + V(x) + e\,x\,E_0(t)\right]\psi(x,t) = -\frac{\hbar}{\mathrm{j}}\frac{\partial}{\partial t}\,\psi(x,t)$$

Dipole approximation $\rightarrow$ t-dependent coefficients $c_{1,2}(t)\psi_{1,2}(x)$ $\rightarrow$ E_0-field with $\omega_0 = \omega_{21}$ $\rightarrow$ envelope with Rabi frequ. $\omega_{\mathcal{R}} = \frac{|\mu_{21}|\widehat{E}_0}{\hbar}$.

Luminescence and Laser Radiation

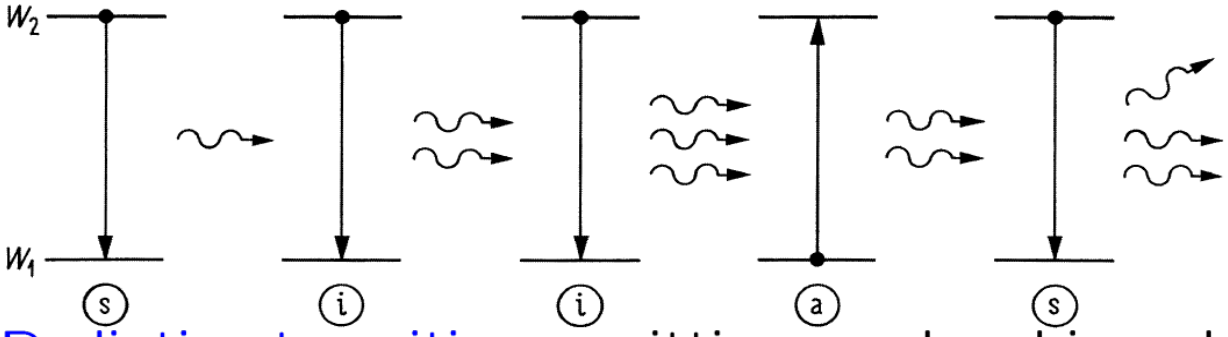

Excit. energy W_2 can be released by transition to lower-state energy W_1.

Radiative transition, emitting or absorbing photon $hf = W_2 - W_1$.

Fig. 3.2. Interaction of a two-level microsystem with electromagnetic radiation, photon energy $hf = W_2 - W_1$. (a) absorption, (s) spontaneous emission, and (i) induced (= stimulated) emission of photons

- Absorption Microsystem in ground state W_1 absorbs radiation at a frequency $f = (W_2 - W_1)/h \rightarrow$ upward transition to $W_2 \rightarrow$ induced or stimulated by an existing field.
- Spontaneous emission Excited microsystem in W_2 makes transition to ground state W_1 "spontaneously" by emitting a photon with energy $hf = W_2 - W_1$ after an average lifetime τ_{sp}.
- Induced emission $W_2 \rightarrow W_1$ induced or stimulated by radiation at $f = (W_2 - W_1)/h$. In contrast to SE: Phase coherence, same mode as stimulating radiation $\rightarrow$ amplification.

Laser Active Materials — Two-Level Systems (2)

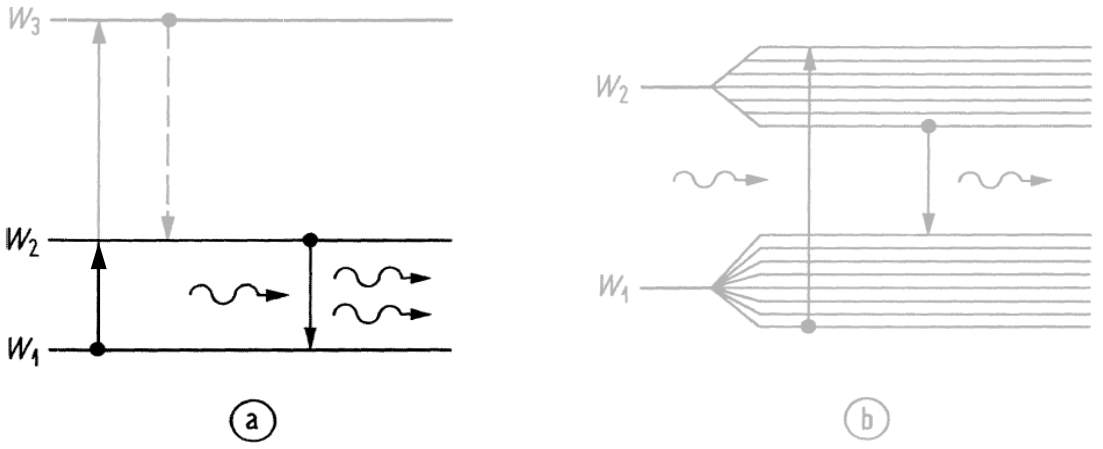

Fig. 3.3. Pump mechanism using energy levels (a) outside (three-level laser system) or (b) inside the energy level group of the laser transition (pseudo-four-level laser system)

SE reduces $N_2 \sim t$, induced emission reduces $N_2 \sim N_P t$. With elmag field of photon energy $hf \rightarrow$ dynamic equilibrium:

(induced emissions) = (induced absorptions)

For large N_P, SE is negligible $\rightarrow$ dynamic equilibrium $N_2 = N_1$ (with SE: $N_2 \leq N_1$). Medium is "transparent" in this case.

With two-level system no population inversion, no gain!

Laser Active Materials — Semiconductors

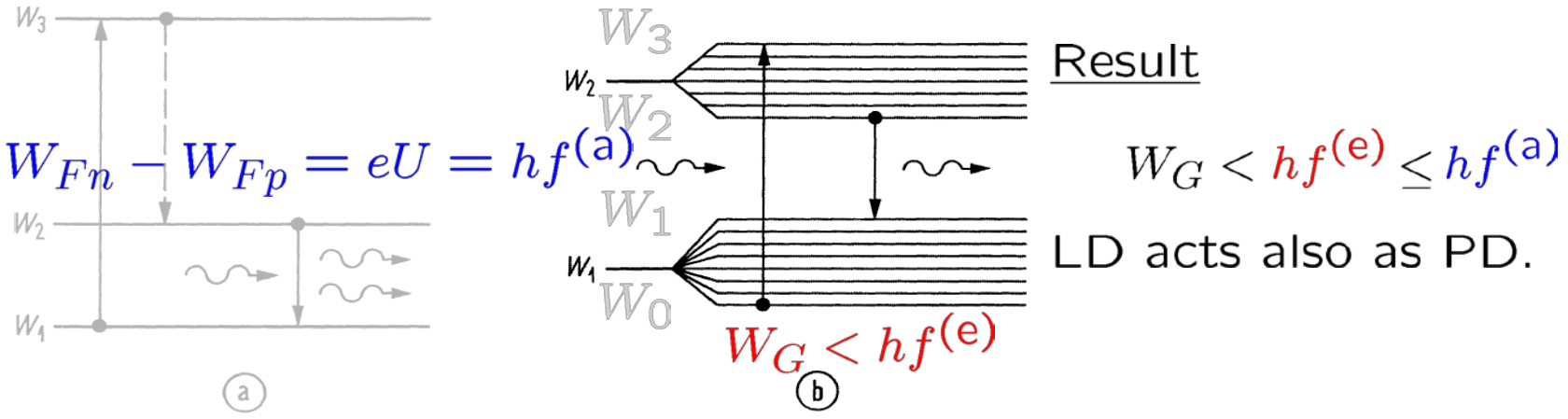

Fig. 3.3. Pump mechanism using energy levels (a) outside (three-level laser system) or (b) inside the energy level group of the laser transition (pseudo-four-level laser system)

Levels W_2 and W_1 associated with conduction and valence band states. Absorbed pump $hf^{(a)}$ ($\widehat{=} W_3 - W_0$) generates electron-hole pairs. Also with forward biased pn-diode by injecting electrons and holes for a population inversion. At $T = 0$, forward voltage U defines "pump energy" $eU = hf^{(a)} =$ (energetic difference at which electrons and holes are injected) = (difference of the quasi Fermi levels).

Band Structure of Direct and Indirect Semiconductors

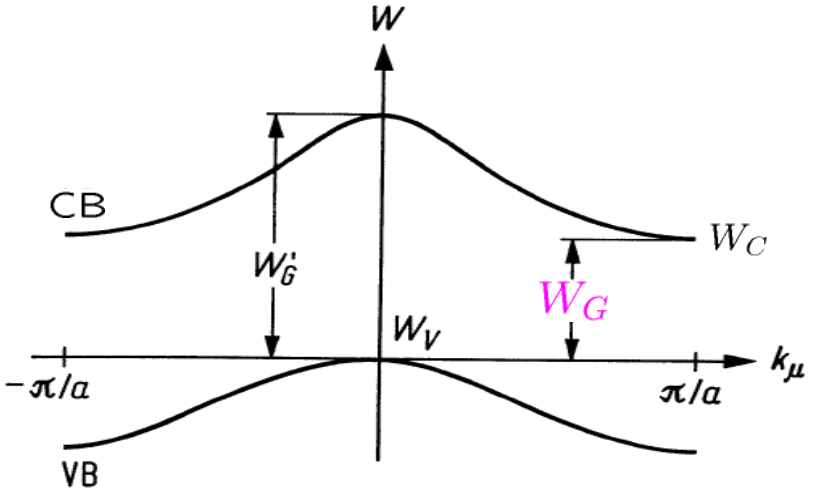

Indirect semicond. Smallest transition energy W_G for crystal momentum diff. $\Delta k_\mu = \pi/a$. Phonon required as collision partner → Radiative transition unlikely. Examples: Elemental semiconductors Si, Ge

$$W_G = \begin{cases} 0.67\,\text{eV} \mathrel{\widehat{=}} 1.85\,\mu\text{m} & \text{(Ge)} \\ 1.13\,\text{eV} \mathrel{\widehat{=}} 1.10\,\mu\text{m} & \text{(Si)} \end{cases}$$

$$W_G' = \begin{cases} 0.8\ \text{eV} \mathrel{\widehat{=}} 1.55\,\mu\text{m} & \text{(Ge)} \\ 3.4\ \text{eV} \mathrel{\widehat{=}} 0.36\,\mu\text{m} & \text{(Si)} \end{cases}$$

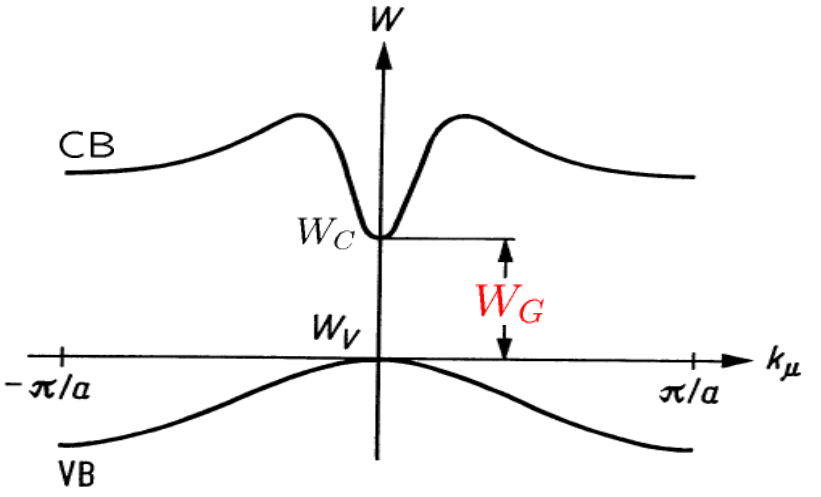

Direct semicond. Smallest transition energy W_G for crystal momentum difference $\Delta k_\mu = 0$. No collision partner required → Radiative transition likely. Examples: Compounds GaAs, InP, InGaAs

$$W_G = \begin{cases} 1.42\,\text{eV} \mathrel{\widehat{=}} 0.87\,\mu\text{m} & \text{(GaAs)} \\ 1.80\,\text{eV} \mathrel{\widehat{=}} 0.69\,\mu\text{m} & (\text{Ga}_{0.7}\text{Al}_{0.3}\text{As}) \\ 0.75\,\text{eV} \mathrel{\widehat{=}} 1.65\,\mu\text{m} & (\text{In}_{0.53}\text{Ga}_{0.47}\text{As}) \\ 1.35\,\text{eV} \mathrel{\widehat{=}} 0.92\,\mu\text{m} & \text{(InP)} \end{cases}$$

Radiative and Nonradiative Recombination

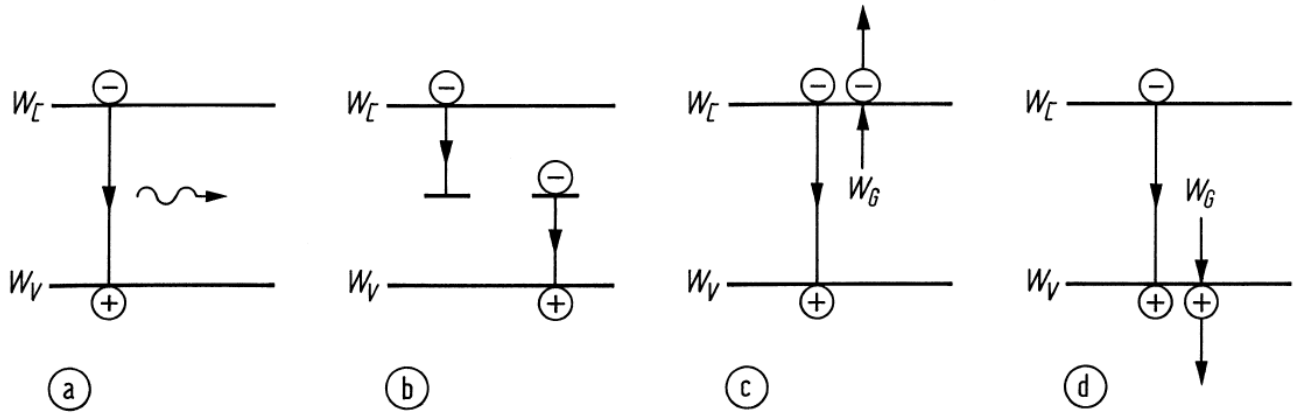

Radiative and nonradiative transitions. (a) Radiative band-band transition. (b) Nonradiative transition via localized states in the forbidden band. (c) (d) Nonradiative Auger recombinations (recombination energy excites excites an electron in the CB or in the VB)

p-Si rad. lifetime $p_p = 10^{16}\,\mathrm{cm}^{-3}$:

$$\tau_{n\,\mathrm{sp}}^{-1} = \frac{\partial\, r_{\mathrm{sp}}}{\partial n_T}$$

$$\tau_{n\,\mathrm{sp}} = 33\,\mathrm{ms}$$

Radiative recomb. (rate r_{sp}, unit $\mathrm{cm}^{-3}\,\mathrm{s}^{-1}$) of electrons and holes:

$$r_{\mathrm{sp}} = Bn_Tp, B = \begin{cases} 1 \times 10^{-10}\ldots 7\times 10^{-10}\,\mathrm{cm}^3\,\mathrm{s}^{-1} & \text{(Ga,Al)As} \\ 8.6\times 10^{-11}\,\mathrm{cm}^3\,\mathrm{s}^{-1} & \text{(In,Ga)(As,P)} \\ 3 \times 10^{-15}\,\mathrm{cm}^3\,\mathrm{s}^{-1} & \text{Si (indirect SC)} \end{cases}$$

Nonrad. recomb. (rate r_{ns}, unit $\mathrm{cm}^{-3}\,\mathrm{s}^{-1}$): Localized impurities, rate $r_{\ell S}$ (Shockley-Read-Hall, SRH). Recomb. energy transfered to e or h, rate r_{Au}, (Auger, in (In,Ga)(As,P) $\rightarrow h$, not in (Ga,Al)As):

$$r_{\mathrm{ns}} = r_{\ell S} + r_{\mathrm{Au}}, \qquad r_{\ell S} = An_T, \quad r_{\mathrm{Au}} = Cn_Tp^2$$

Filling of Electronic States — Fermi Function

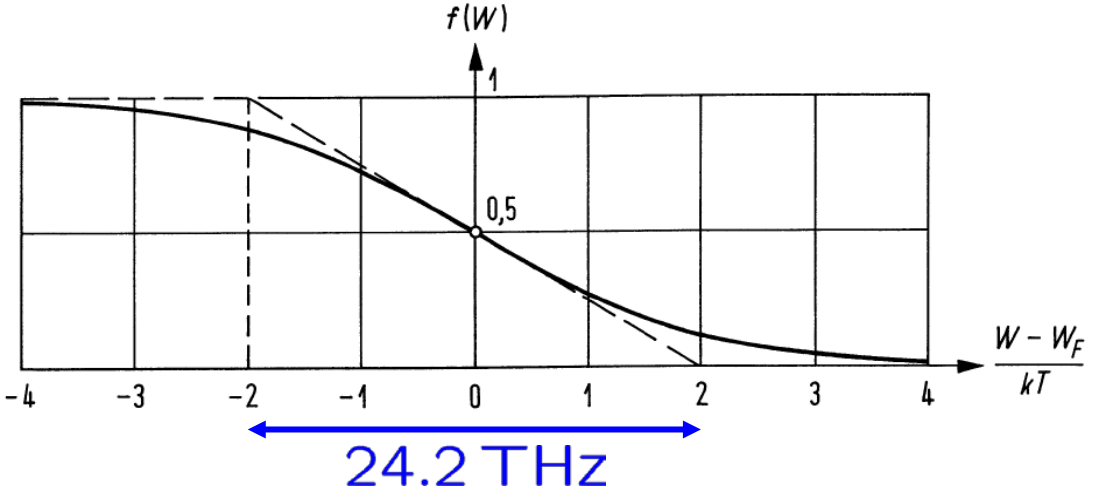

Fig. 3.8. Fermi function for band energy states ($g = 1$)

At $T = 0$ electrons fill lowest energy states. At $T > 0$ Fermi-Dirac distrib. (Fermi function):

$$f(W) = \frac{1}{1 + g \exp\left(\frac{W - W_F}{kT}\right)}$$

W_F is Fermi energy where occup. prob. $f(W) = 1/2$ at all T. Transit. "large $\rightarrow$ low": Occup. prob. $(0.88 \geq f(W) \geq 0.12)$ in region $4kT$ centred at W_F (at $T = 293\,\mathrm{K}$: $kT = 25\,\mathrm{meV}$ or $\Delta f = 2kT/h = 12.1\,\mathrm{THz}$). Boltzmann approximation:

$$f(W) \approx g \exp\left(-\frac{W - W_F}{kT}\right) \qquad \text{for } W - W_F > 3kT\,,$$

$$f(W) \approx 1 - g \exp\left(\frac{W - W_F}{kT}\right) \qquad \text{for } W - W_F < -3kT\,.$$

Density of states (parabolic bands $W_{C,V} \sim (\hbar k_\mu)^2/(2m_{n,p})$):

$$\rho_{\substack{C\\V}}(W) = \frac{1}{2\pi^2}\left(\frac{2|m_{\substack{n\\p}}|}{\hbar^2}\right)^{3/2}\sqrt{\pm(W - W_{\substack{C\\V}})}, \qquad N_{\substack{C\\V}} = 2\left(\frac{2\pi|m_{\substack{n\\p}}|kT}{h^2}\right)^{3/2}$$

Carrier concentrations in CB (n_T) and VB (p):

$$n_T = \int_{W_C}^{\infty} \rho_C(W)\, f(W)\, \mathrm{d}W, \qquad p = \int_{-\infty}^{W_V} \rho_V(W)\big[1 - f(W)\big]\, \mathrm{d}W$$

Boltzmann approximation (valid for $n_T \ll N_C$, $p \ll N_V$ only, i. e., nondegenerate doping; not true for semiconductor lasers!):

$$\left.\begin{aligned} n_T &= N_C \exp\left(-\frac{W_C - W_F}{kT}\right) \\ p &= N_V \exp\left(-\frac{W_F - W_V}{kT}\right) \end{aligned}\right\} \quad n_T p = n_i^2 = N_C N_V \exp\left(-\frac{W_G}{kT}\right)$$

Intrinsic carrier concentration n_i denotes electrons n_T (holes p) which are present pairwise in CB (VB) of pure undoped semiconductors at temperature T, independent of Fermi energy W_F.

Impurities, Doping and Carrier Concentration — Non-Equilibrium

Density of states (parabolic bands $W_{C,V} \sim (\hbar k_\mu)^2/(2m_{n,p})$):

$$\rho_{C\atop V}(W) = \frac{1}{2\pi^2}\left(\frac{2|m_{n\atop p}|}{\hbar^2}\right)^{3/2}\sqrt{\pm(W - W_{C\atop V})}\,, \qquad N_{C\atop V} = 2\left(\frac{2\pi|m_{n\atop p}|kT}{h^2}\right)^{3/2}$$

Carrier concentrations in CB (n_T) and VB (p):

$$n_T = \int_{W_C}^{\infty} \rho_C(W)\, f(W)\, \mathrm{d}W, \qquad p = \int_{-\infty}^{W_V} \rho_V(W)\big[1 - f(W)\big]\, \mathrm{d}W$$

Boltzmann approximation (valid for $n_T \ll N_C$, $p \ll N_V$ only, i. e., nondegenerate doping), quasi Fermi levels $W_{Fn,p}$:

$$\left.\begin{aligned} n_T &= N_C \exp\left(-\frac{W_C - W_{Fn}}{kT}\right) \\ p &= N_V \exp\left(-\frac{W_{Fp} - W_V}{kT}\right) \end{aligned}\right\} \qquad \begin{aligned} n_T p &= n_i^2 \exp\left(\frac{W_{Fn} - W_{Fp}}{kT}\right) \\ n_i^2 &= N_C N_V \exp\left(-\frac{W_G}{kT}\right) \end{aligned}$$

Intrinsic carrier concentration n_i denotes electrons n_T (holes p) which are present pairwise in CB (VB) of pure undoped semiconductors at temperature T, independent of Fermi energy W_F.

Quasi Fermi Levels in Non-Equilibrium

For laser threshold current $\rightarrow$ carrier concentrations n_T, p for shifting quasi Fermi levels W_{Fn}, W_{Fp} into bands. p-doped semiconductor with equilibrium concentration of n_{T0}, p_0 and $n_{T0}p_0 = n_i^2$. Carrier injection changes densities to $n_T = n_{T0} + \Delta n_T$, $p = p_0 + \Delta p$. Substitution into Fermi function:

$$W_{Fn} - W_F = kT \ln\left(1 + \frac{\Delta n_T}{n_{T0}}\right), \quad W_F - W_{Fp} = kT \ln\left(1 + \frac{\Delta p}{p_0}\right)$$

Charge neutrality $\Delta p = \Delta n_T$. Carrier injection $\rightarrow$ quasi Fermi level of minority carriers shifts first (here: W_{Fn}; change of n_T by Δn_T has largest effect because n_{T0} is small). At $\Delta n_T / n_{T0} = 1$ shift amounts to $W_{Fn} - W_F = 0.7\,kT$. Because $p_0 \gg n_{T0}$ in a p-semiconductor, quasi Fermi level for majority carriers starts shifting at much higher injection current levels when $\Delta p = \Delta n_T$ reaches the order of p_0.

Abrupt pn-Homojunction in Equilibrium (Zero Bias)

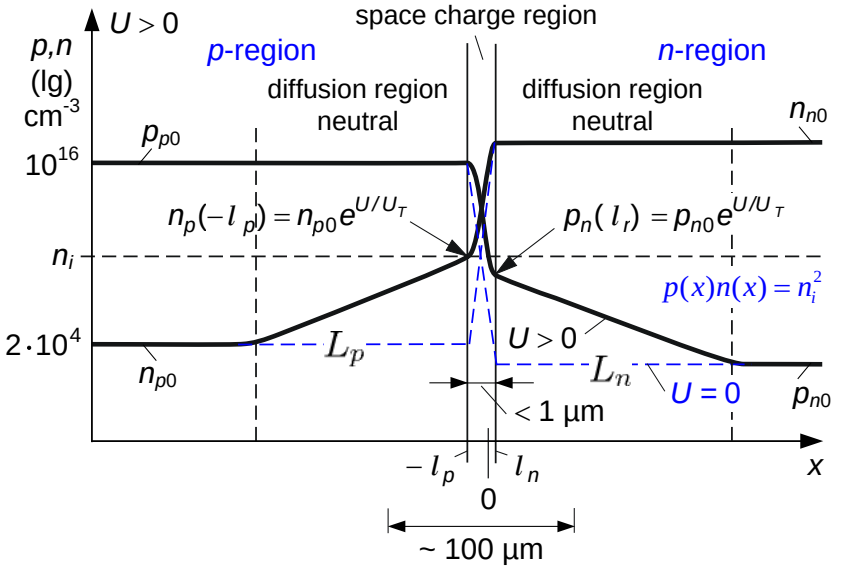

Equilibrium $U = 0$, zero current: p and n-type SC joined, majority electrons (holes) diffuse in p (n) region leaving positive (negative) donors (acceptors) in the *space charge region* → built-in potential (German: „Diffusionsspannung“):

$$U_D = U_T \ln \frac{n_D n_A}{n_i^2}, \quad U_T = \frac{kT}{e}$$

Built-in electric field draws minorities across the junction until the minority drift current compensates the majority diffusion current. For each x the mass action law holds:

$$p(x)\, n_T(x) = n_i^2$$

(Electron concentration $n_T \mathrel{\widehat{=}} n$)

Abrupt pn-Homojunction in Equilibrium (Zero Bias)

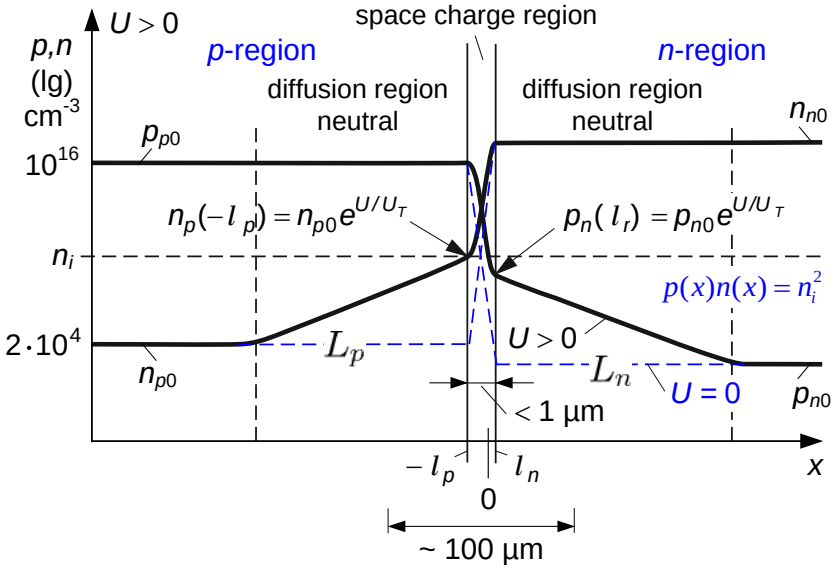

Equilibrium $U = 0$, zero current: p and n-type SC joined, majority electrons (holes) diffuse in p (n) region leaving positive (negative) donors (acceptors) in the *space charge region* → built-in potential (German: „Diffusionsspannung“):

$$U_D = U_T \ln \frac{n_D n_A}{n_i^2}, \quad U_T = \frac{kT}{e}$$

Built-in potential such that equilibrium Fermi energy is constant throughout junction:

$$eU(x) = W_{F_n}(x) - W_{F_p}(x) = 0$$

Equilibrium between carriers of conduction and valance band.

(Electron concentration $n_T \widehat{=} n$)

Abrupt pn-Homojunction in Non-Equilibrium (Non-Zero Bias)

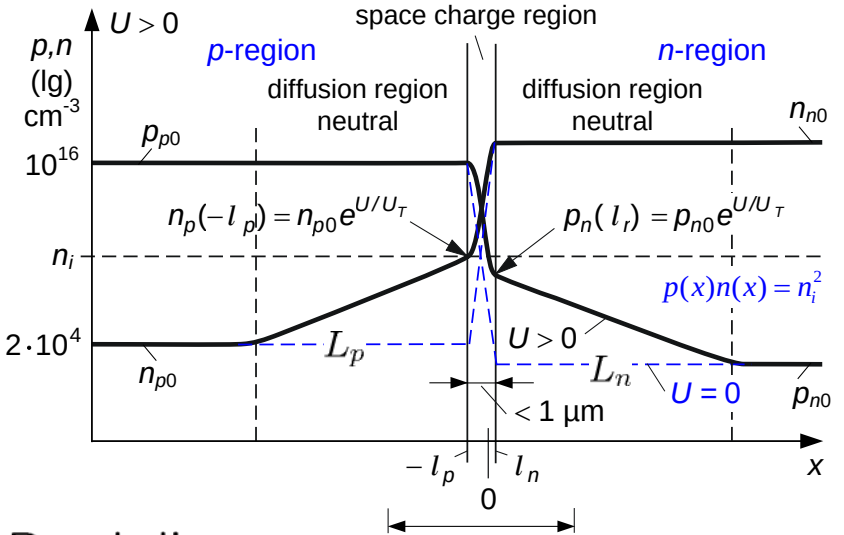

Band diagram, quasi Fermi levels $W_{Fn,p}$

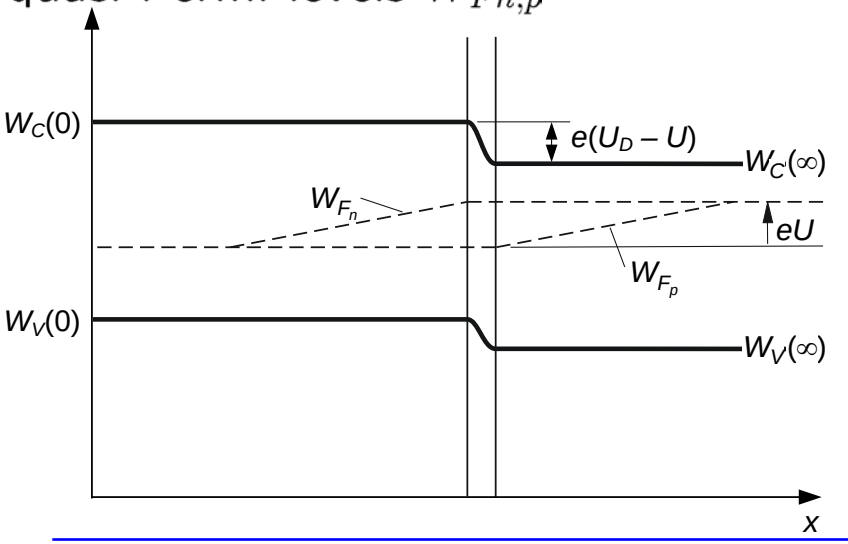

Non-equilibrium $U > 0$, forward current: Built-in potential reduced by bias U to $U_D - U$:

$$eU(x) = W_{F_n}(x) - W_{F_p}(x)$$

Increased crossing probab. for majorities → diff. current ≫ saturated minority current i_s, ext. current I:

$$I = i_s \exp\left(\frac{U}{U_T}\right) - i_s$$

Non-equilibrium $U \ll U_T$, reverse current: Built-in potential increased → diffusion current negligible wrt minority current i_s:

$$I = i_s \exp\left(\frac{-|U|}{U_T}\right) - i_s \approx -i_s$$

Abrupt pn-Homojunction in Non-Equilibrium (Non-Zero Bias)

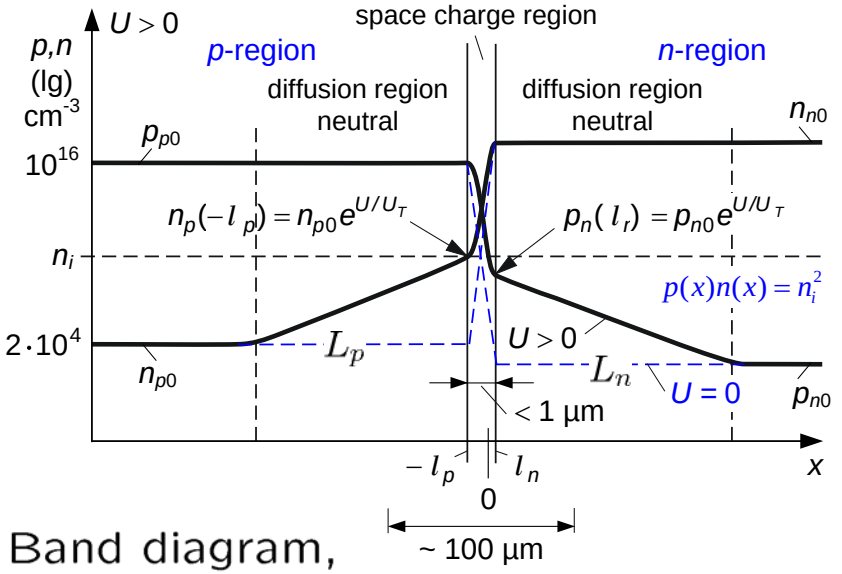

Band diagram, quasi Fermi levels $W_{Fn,p}$

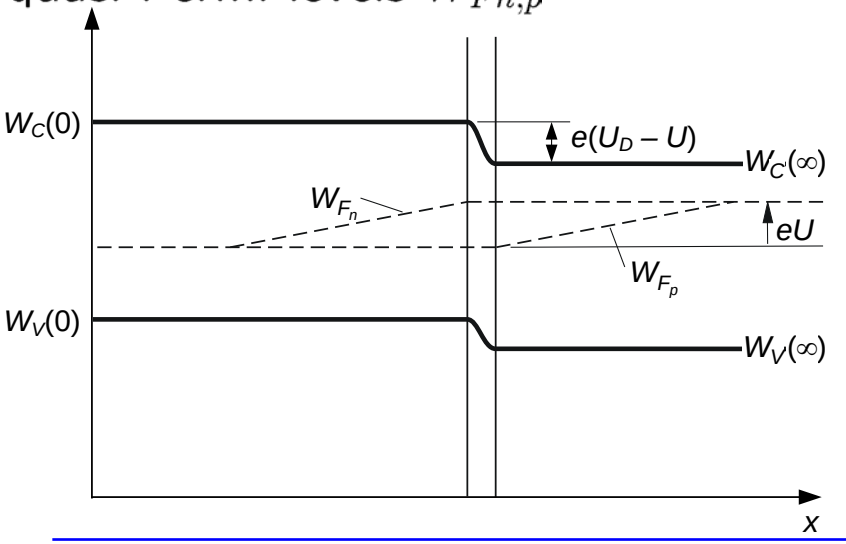

Non-equilibrium $U > 0$, forward current: Built-in potential reduced by bias U to $U_D - U$:

$$eU(x) = W_{F_n}(x) - W_{F_p}(x)$$

Increased crossing probab. for majorities → diff. current ≫ saturated minority current i_s, ext. current I:

$$I = i_s \exp\left(\frac{U}{U_T}\right) - i_s$$

Quasi Fermi levels $W_{Fn,p}$ result. Carriers inside respective bands still in equilibrium, but no equilibrium between carriers of conduction and valence bands.

Abrupt pn-Homojunction — Radiative / Nonradiative Recombinat.

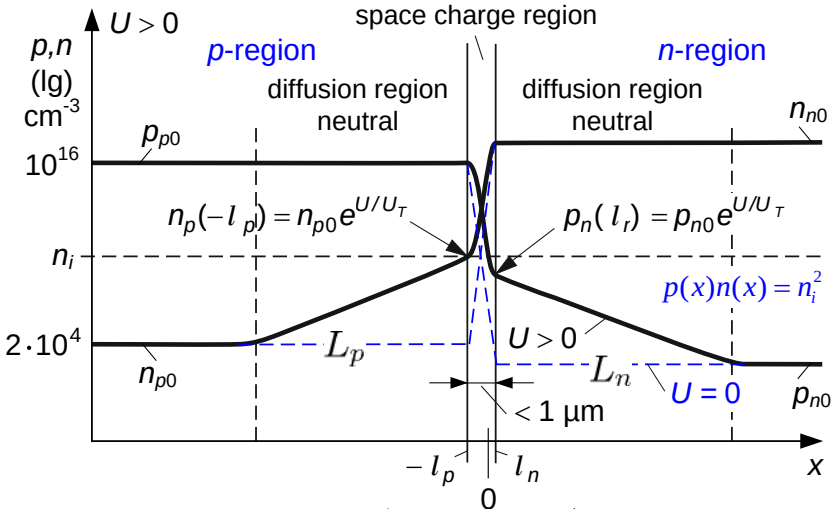

Recombination described by minorities' lifetimes $\tau_{n,p}$ in (p,n)-semiconductor (diffusion constants $D_{n,p}$, diffusion lengths $L_{n,p}$, electron n and hole concentration p):

$$\tau_{n,p} = \frac{L_{n,p}^2}{D_{n,p}}, \qquad \tau_{n\,\mathrm{sp,\,ns}}^{-1} = \frac{\partial\, r_{\mathrm{sp,\,ns}}}{\partial n_{Tp}}$$

Radiative recomb. (rate r_{sp}, unit $\mathrm{cm^{-3}\,s^{-1}}$) of electrons and holes:

$$r_{\mathrm{sp}} = B n_T p, B = \begin{cases} 1 \times 10^{-10} \ldots 7 \times 10^{-10}\,\mathrm{cm^3\,s^{-1}} & \text{(Ga,Al)As} \\ 8.6 \times 10^{-11}\,\mathrm{cm^3\,s^{-1}} & \text{(In,Ga)(As,P)} \\ 3 \times 10^{-15}\,\mathrm{cm^3\,s^{-1}} & \text{Si (indirect SC)} \end{cases}$$

Nonrad. recomb. (rate r_{ns}, unit $\mathrm{cm^{-3}\,s^{-1}}$): Localized impurities, rate $r_{\ell S}$ (Shockley-Read-Hall, SRH). Recomb. energy transfered to e or h, rate r_{Au}, (Auger, in (In,Ga)(As,P) $\rightarrow h$, not in (Ga,Al)As):

$$r_{\mathrm{ns}} = r_{\ell S} + r_{\mathrm{Au}}, \qquad r_{\ell S} = A n_T, \qquad r_{\mathrm{Au}} = C n_T p^2$$

Radiative and Nonradiative Recombination

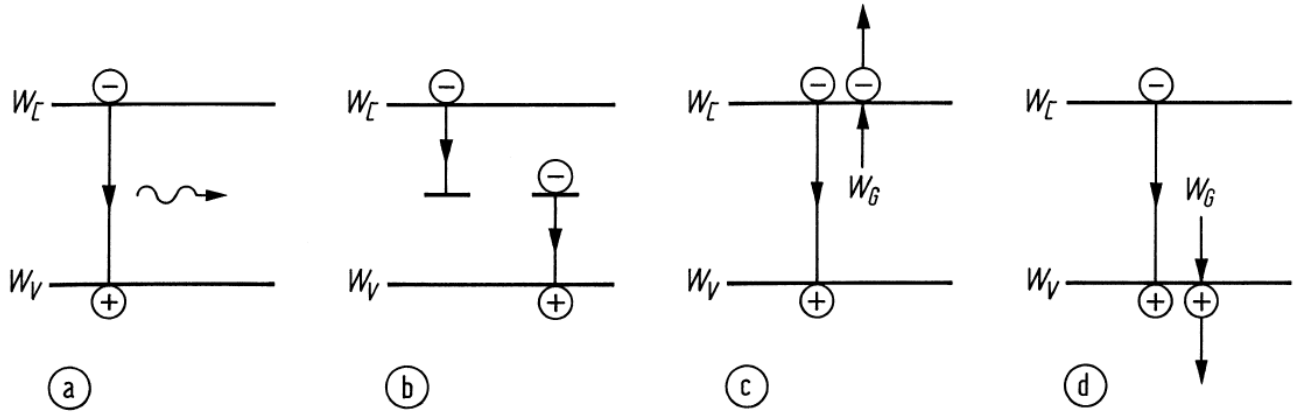

Radiative and nonradiative transitions. (a) Radiative band-band transition. (b) Nonradiative transition via localized states in the forbidden band. (c) (d) Nonradiative Auger recombinations (recombination energy excites excites an electron in the CB or in the VB)

o3e

p-Si rad. lifetime $p_p = 10^{16}\,\mathrm{cm}^{-3}$:

$$\tau_{n\,\mathrm{sp}}^{-1} = \frac{\partial\, r_{\mathrm{sp}}}{\partial n_{Tp}}$$

$$\tau_{n\,\mathrm{sp}} = 33\,\mathrm{ms}$$

Radiative recomb. (rate r_{sp}, unit $\mathrm{cm}^{-3}\,\mathrm{s}^{-1}$) of electrons and holes:

$$r_{\mathrm{sp}} = Bn_Tp,\ B = \begin{cases} 1 \times 10^{-10}\ldots 7\times 10^{-10}\,\mathrm{cm}^3\,\mathrm{s}^{-1} & \text{(Ga,Al)As} \\ 8.6\times 10^{-11}\,\mathrm{cm}^3\,\mathrm{s}^{-1} & \text{(In,Ga)(As,P)} \\ 3 \times 10^{-15}\,\mathrm{cm}^3\,\mathrm{s}^{-1} & \text{Si (indirect SC)} \end{cases}$$

Nonrad. recomb. (rate r_{ns}, unit $\mathrm{cm}^{-3}\,\mathrm{s}^{-1}$): Localized impurities, rate $r_{\ell S}$ (Shockley-Read-Hall, SRH). Recomb. energy transfered to e or h, rate r_{Au}, (Auger, in (In,Ga)(As,P) $\rightarrow h$, not in (Ga,Al)As):

$$r_{\mathrm{ns}} = r_{\ell S} + r_{\mathrm{Au}}\,, \qquad r_{\ell S} = An_T\,, \qquad r_{\mathrm{Au}} = Cn_Tp^2$$

Compound Semiconductors (1)

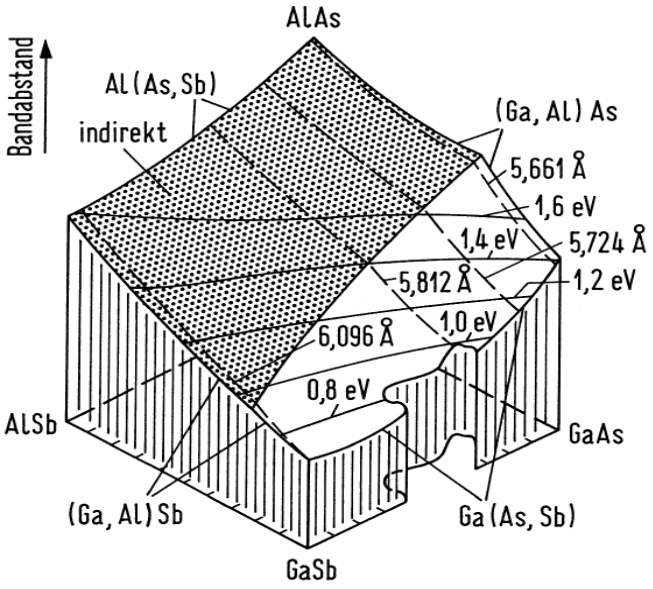

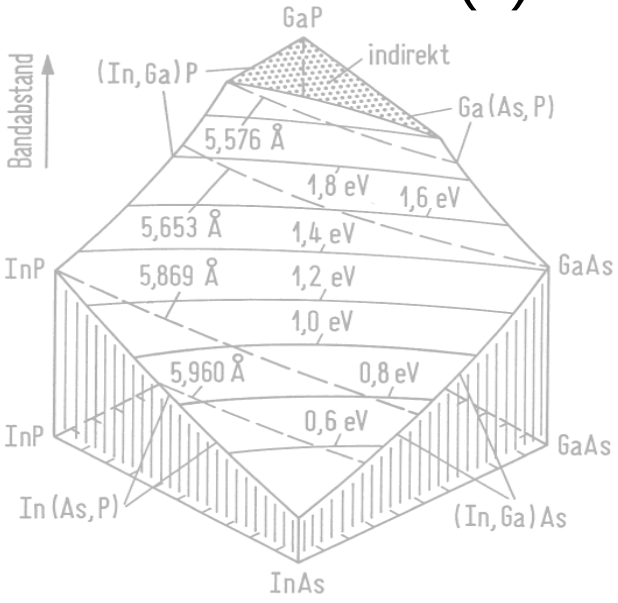

Semiconductor	W_G/ eV ($\lambda_G/\,\mu$m)	n at λ_G	a/Å
GaSb, direct	0.726 (1.708)	3.82	6.096
GaAs, direct	1.424 (0.871)	3.655	5.653
AlSb, indirect	1.58 (0.785)	3.4	6.135
AlAs, indirect	2.163 (0.573)	3.178	5.660
$(Ga_{1-x}Al_x)As$ direct: $x \leq 0.3$	$1.424 + 1.247\,x$ $1.424 \ldots 1.798$ $(0.871 \ldots 0.69)$	$3.59 - 0.71\,x +$ $+0.091\,x^2$ (at $\lambda = 0.9\,\mu$m)	$5.653 + 0.027\,x$
$(Ga_{1-x}Al_x)(As_ySb_{1-y})$ lattice-matched to GaSb direct: $x \leq 0.24$ $y = x/1.11$	$0.726 + 0.834\,x +$ $+1.134\,x^2$ $0.726 \ldots 0.991$ $(1.708 \ldots 1.25)$	?	6.096

Material system $(Ga_{1-x}Al_x)(As_ySb_{1-y})$. W_G bandgap, $\lambda_G = hc/W_G$ bandgap wavelength, n refractive index, a lattice constant

Compound Semiconductors (2)

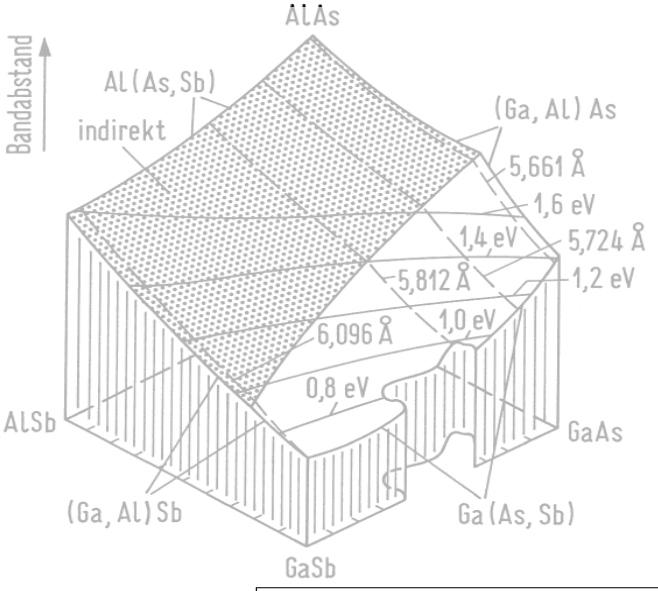

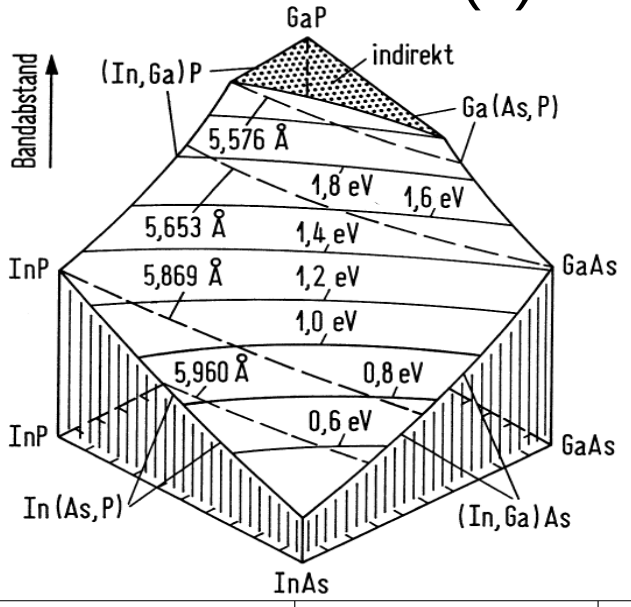

Semiconductor	W_G / eV (λ_G / μm)	n at λ_G	a / Å
InAs, direct	0.36 (3.444)	3.52	6.058
InP, direct	1.35 (0.918)	3.45	5.869
GaAs, direct	1.424 (0.871)	3.655	5.653
GaP, indirect	2.261 (0.548)	3.452	5.451
$(In_{0.49}Ga_{0.51})P$, direct lattice-matched to GaAs	1.833 (0.676)	3.451 ?	5.653
$(In_{0.53}Ga_{0.47})As$, direct lattice-matched to InP	0.75 (1.653)	3.61	5.869
$(In_{1-x}Ga_x)(As_yP_{1-y})$ lattice-matched to InP direct: $y \leq 1$ $x = y/(2.2091 - 0.06864\,y)$	$1.35 - 0.72\,y + 0.12\,y^2$ $1.35 \ldots 0.75$ $(0.918 \ldots 1.653)$	$3.45 + 0.256\,y - 0.095\,y^2$ $3.45 \ldots 3.61$	5.869

Material system $(In_{1-x}Ga_x)(As_yP_{1-y})$. W_G bandgap, $\lambda_G = hc/W_G$ bandgap wavelength, n refractive index, a lattice constant

LECTURE 9

Heterojunctions

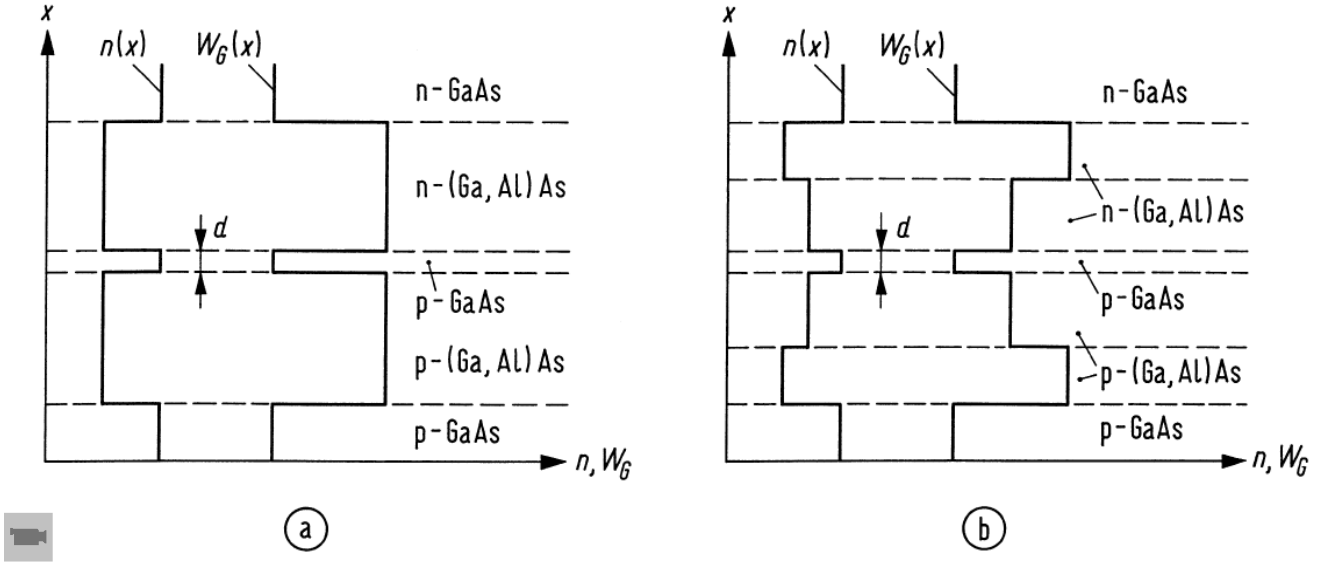

Schematic refractive index dependence n and bandgap W_G as a function of the spatial coordinate x in a (a) 3-layer heterostructure, (b) 5-layer heterostructure

"Isotype" if semiconductors have same conduction type.

"Anisotype" if conduction type differs.

Conduction type with small letters n, i, p if semiconductor has smaller bandgap than neighbour, and with capital letters N, I, P if bandgap is larger.

Fig. 3.11(a) from top: nN, Np, pP and Pp

Band Diagram for Heterostructures

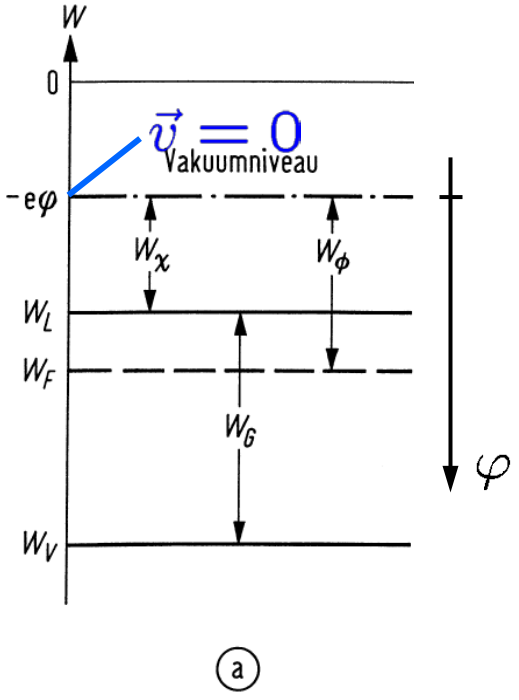

Energy scale for electrons in a semiconductor. (a) Semiconductor at potential $\varphi \neq 0$. (b) Two independent, insulated semiconductors at potential $\varphi = 0$ with different bandgaps. W_χ electron affinity, W_ϕ work function. W_L conduction band edge ($\widehat{=} W_C$, Vacuumniveau $\widehat{=}$ vacuum level)

e leaving at $\vec{v} = 0$ are at vacuum level $W = -e\varphi$. e-affinity W_χ, work function W_ϕ. $W_G = W_C - W_V$, W_χ, W_ϕ fix distances of CB edge, Fermi level, VB edge wrt vacuum level.

Band Diagram for Heterostructures

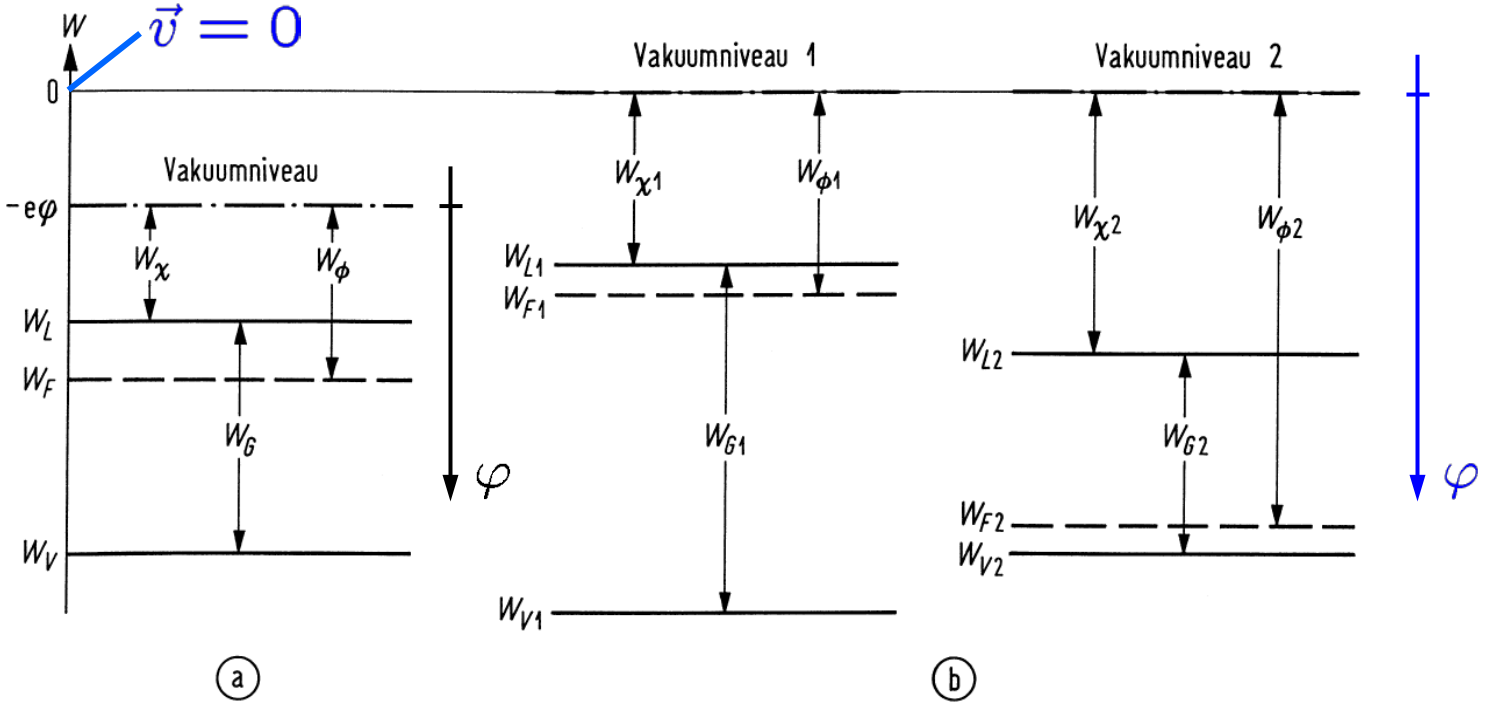

Energy scale for electrons in a semiconductor. (a) Semiconductor at potential $\varphi \neq 0$. (b) Two independent, insulated semiconductors at potential $\varphi = 0$ with different bandgaps. W_χ electron affinity, W_ϕ work function. W_L conduction band edge ($\widehat{=} W_C$, Vacuumniveau $\widehat{=}$ vacuum level)

e leaving at $\vec{v} = 0$ are at vacuum level $W = -e\varphi$. e-affinity W_χ, work function W_ϕ. $W_G = W_C - W_V$, W_χ, W_ϕ fix distances of CB edge, Fermi level, VB edge wrt vacuum level.

Band Diagram of a Left-Alone NpP-Heterojunction

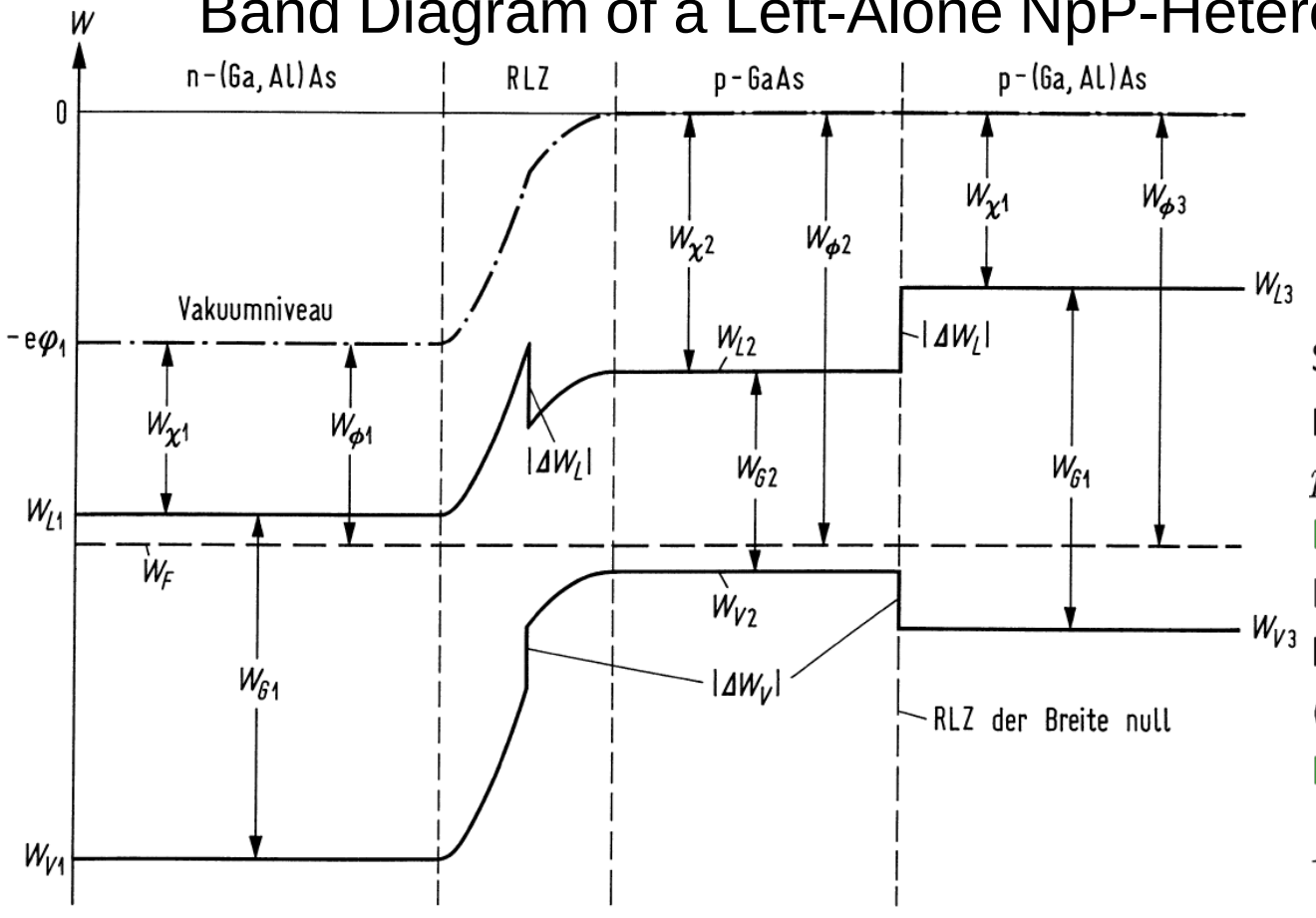

Shallow saturated impurities, $n_{T1} = n_D$, $p_2 = n_A$

Homojunction:

Diffusion voltage or built-in potential U_D (thermal voltage U_T)

Effective DOS:

$$N_B = 2\left(\frac{2\pi|m_{\text{eff}}|kT}{h^2}\right)^{\frac{3}{2}}$$

Energy-band diagram of a double-heterostructure with anisotype Np-junction and a special isotype pP-junction with diffusion voltage zero ($W_L \mathrel{\hat{=}} W_C$, Leitungsband $\mathrel{\hat{=}}$ conduction band, Vakuumniveau $\mathrel{\hat{=}}$ vacuum level, Raumladungszone RLZ der Breite null $\mathrel{\hat{=}}$ space-charge region of zero width)

$$\varphi_1 = U_D = U_T \ln \frac{n_D n_A}{n_i^2}, \qquad U_T = \frac{kT}{e}, \qquad W_G = -kT \ln \frac{n_i^2}{N_C N_V}$$

Band Diagram of a Forward-Biased NpP-Heterojunction

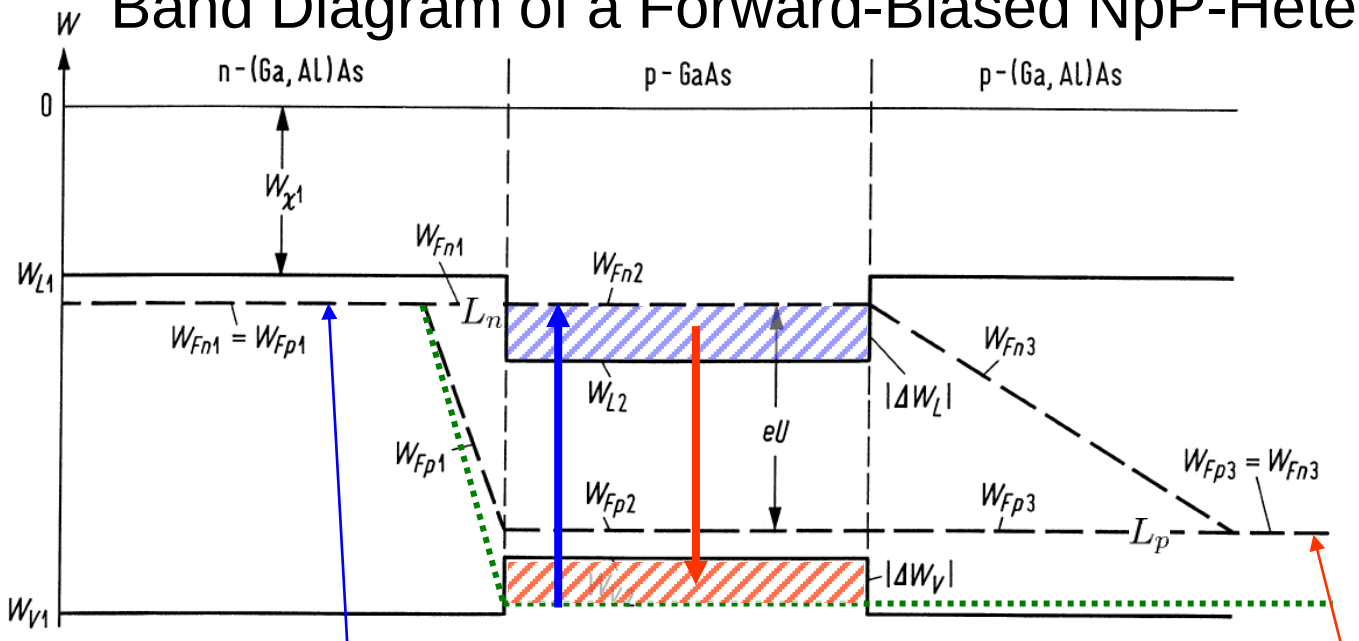

Practical for $T > 0$.

Simpler for $T = 0$:

Energy-band diagram of a NpP-heterojunction of Fig. 3.13 with a forward bias voltage. $L_p/L_n \approx 0.2$ for GaAs ($W_L \mathrel{\widehat{=}} W_C$)

Far away from junction, quasi Fermi levels of e, h unchanged. Inside thin p-GaAs layer and DZ, $W_{Fn} > W_{Fp}$ due to carrier injection. $L_n > L_p \rightarrow p$-DZ larger than n-DZ. GaAs: $L_n/L_p = 5$. e, h confined to potential well inside p-GaAs layer. Quasi Fermi level W_{Fn} moved into CB. $\rightarrow hf^{(a)} \geq W_{Fn} - W_{Fp} = eU \quad \rightarrow W_G < hf^{(e)} \leq eU$

Bulk SOA Structure for Doping Design Study at $\lambda = 1.55\,\mu m$

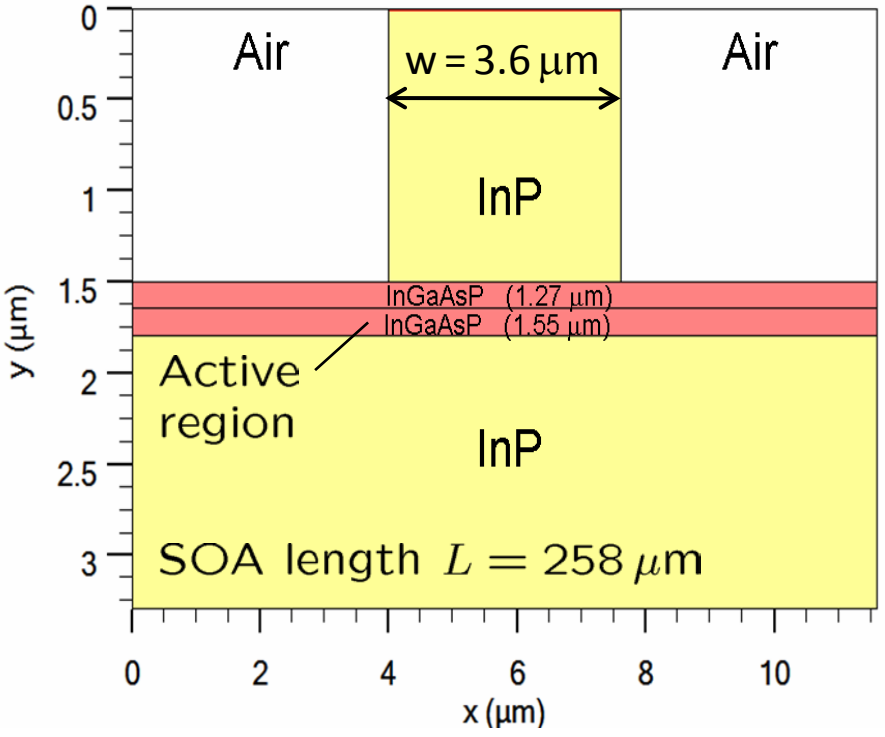

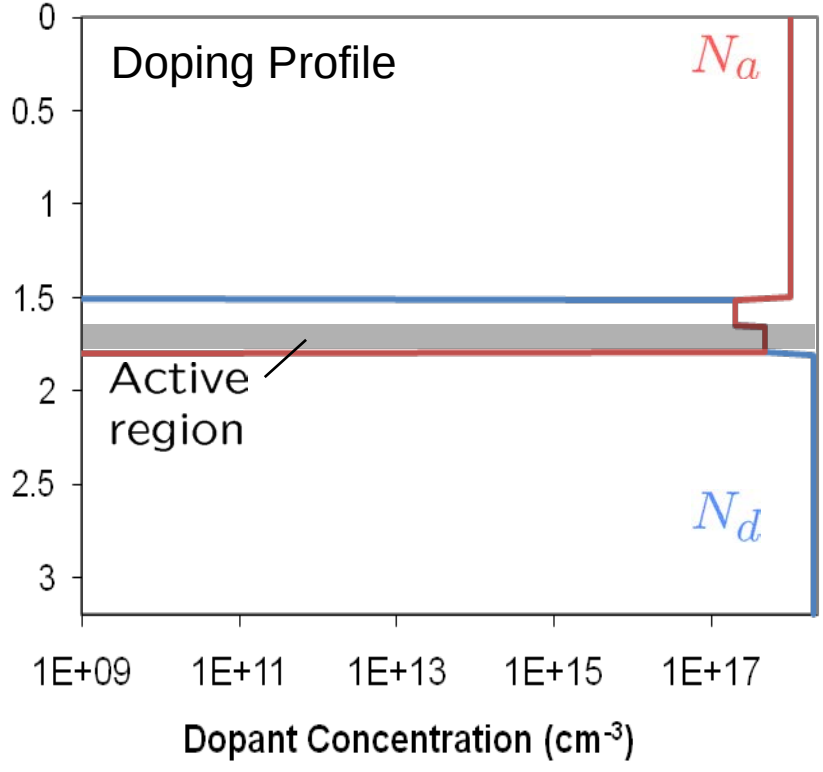

Tendencies calculated* *ab initio* with Silvaco ATLAS (modified for simulating SOA). Use of well-characterized† bulk-SOA for checking relevance of simulation results.

*Kapoor, A.; Sharma, E. K.; Freude, W.; Leuthold, J.: Investigation of the saturation characteristics of InGaAsP-InP bulk SOA. Photonics West 2010. Paper 7597-56

†Leuthold, J.: Advanced indium-phosphide waveguide Mach-Zehnder interferometer all-optical switches and wavelength converters. Konstanz: Hartung-Gorre 1999

Bulk SOA — Trends for Doping the Active Region ($\lambda = 1.55\,\mu\mathrm{m}$)

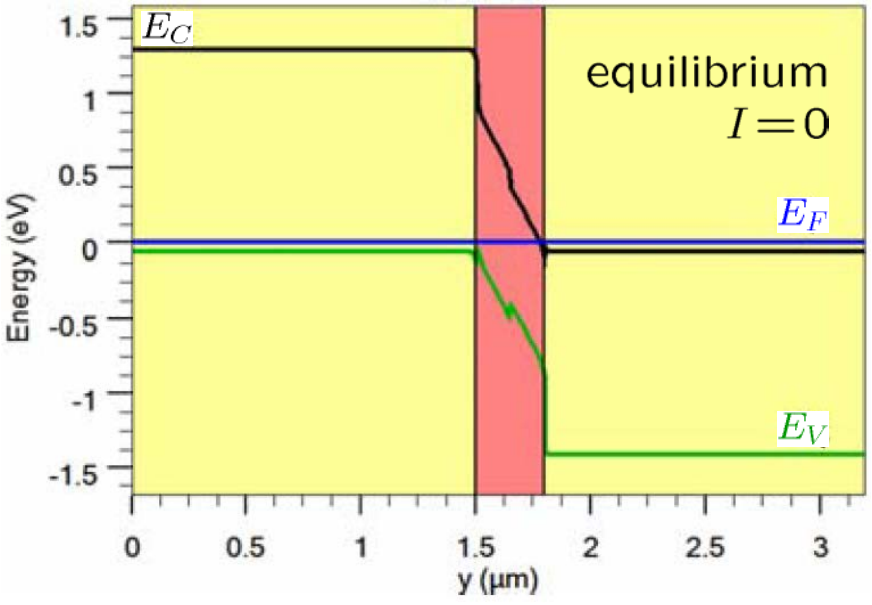

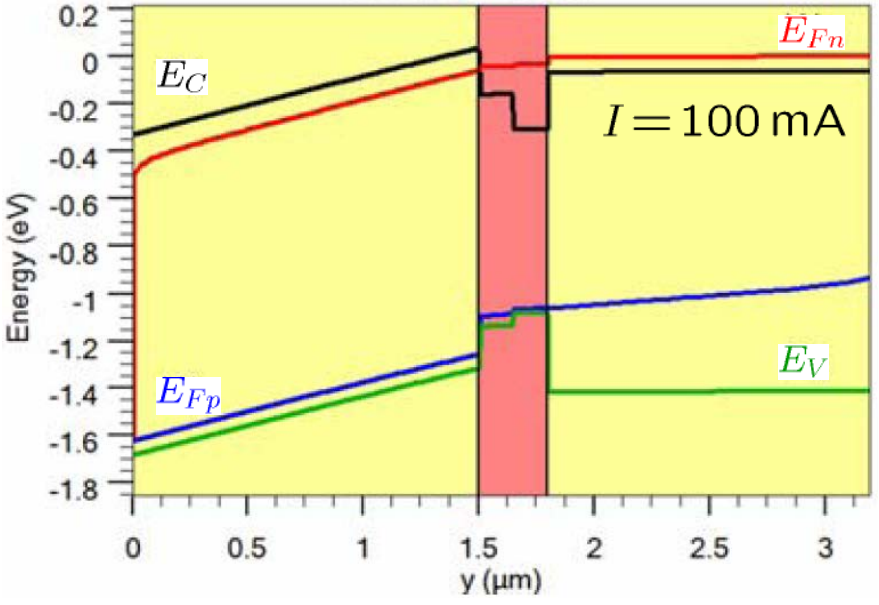

p-doping (n-doping) shifts quasi-Fermi level E_{Fp} more into (away from) the valence band $\rightarrow$ increases (decreases) small-signal gain constant g_0 and differential gain $a \rightarrow$ decreases (increases) $P_{\mathrm{sat}}^{\mathrm{in}}$:

$$P_{\mathrm{in}}^{\mathrm{sat}} = \frac{2\ln 2}{G_0 - 2}\, hf\, \frac{A/\Gamma}{a\,\tau_e}, \qquad G_0 = \mathrm{e}^{\Gamma g_0 L} \qquad P_{\mathrm{sat}}^{\mathrm{in}} \Downarrow \qquad P_{\mathrm{sat}}^{\mathrm{in}} \Uparrow$$

However, there are other influences: a & τ_e (besides Γ & L)!

Emission and Absorption in a Semiconductor. Amplification

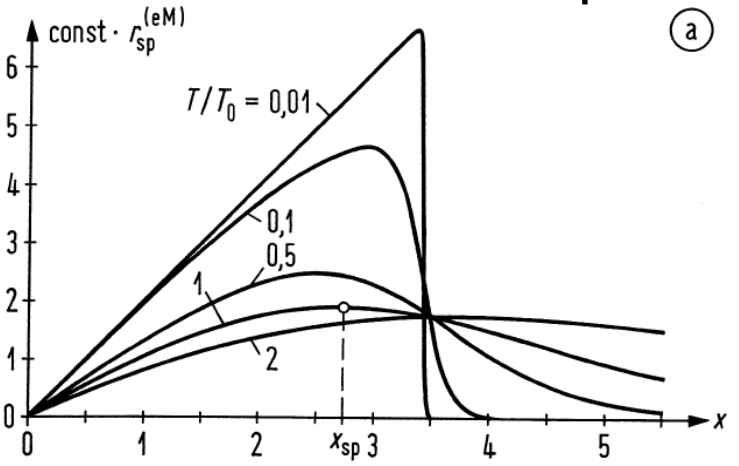

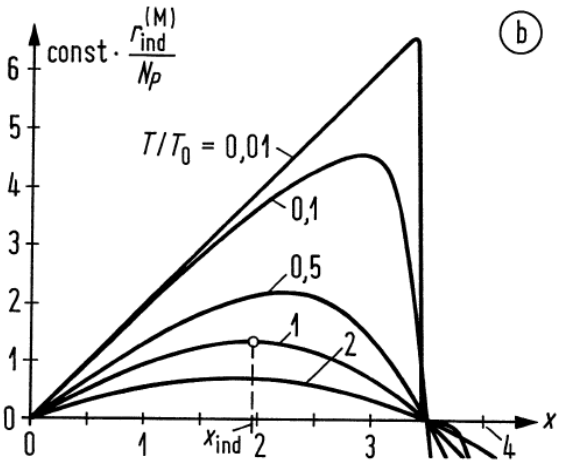

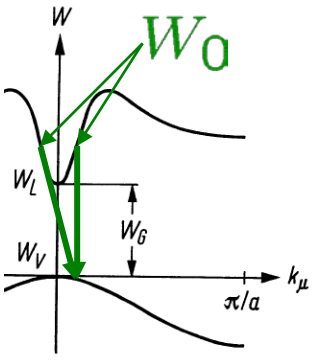

Frequency dependence of spontaneous and induced emission for various temperatures $T/T_0 = 0.01$, 0.1, 0.5, 1, 2 (T_0 reference temperature; $W_{Fn} - W_C$ and $W_V - W_{Fp}$ are kept constant to $3\,kT_0$ and $0.5\,kT_0$, respectively; $m_n/m_p = 0.14$ as in GaAs). Normalized frequency $x = (hf - W_G)/(kT_0)$. (a) Spontaneous emission and (b) induced emission per photon, Eq. (3.44). The multiplicative constant is identical in both diagrams.

$$r_{ind}^{(M)} \sim N_P\Big[f_C(W_0)[1 - f_V(W_0 - hf)] - f_V(W_0 - hf)[1 - f_C(W_0)]\Big]$$

$$r_{ind}^{(M)} = r_{ind}^{(eM)} - r_{ind}^{(aM)}$$

$$\sim N_P\Big[f_C(W_0) - f_V(W_0 - hf)\Big],$$

$$r_{sp}^{(eM)} \sim f_C(W_0)\Big[1 - f_V(W_0 - hf)\Big],$$

$$W_0 = W_C + \frac{\hbar^2 k_{\mu 0}^2}{2m_n}$$

Gain rate:

$$\left.\begin{aligned} r_{ind}^{(M)} &= \frac{1}{V}\frac{dN_P}{dt} \\ G &= \frac{1}{N_P}\frac{dN_P}{dt} \end{aligned}\right\} \quad G = \frac{r_{ind}^{(M)}}{N_P/V}$$

Emission and Absorption in a Semiconductor. Measurement

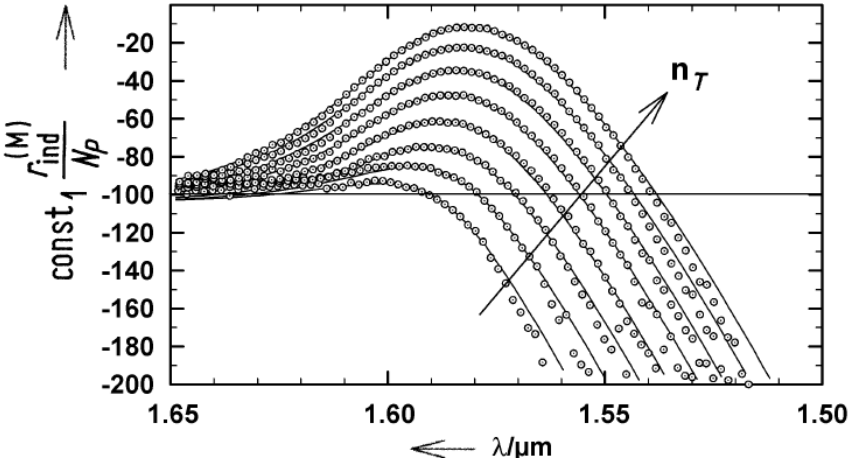

Measured wavelength dependence of induced emission per photon for various carrier densities n_T. The multiplicative constant is different

$$r_{\mathrm{ind}}^{(\mathrm{M})} = r_{\mathrm{ind}}^{(\mathrm{eM})} - r_{\mathrm{ind}}^{(\mathrm{aM})} \sim N_P\Big[f_C(W_0) - f_V(W_0 - hf)\Big],$$

$$r_{\mathrm{sp}}^{(\mathrm{eM})} \sim f_C(W_0)\Big[1 - f_V(W_0 - hf)\Big],$$

$$W_0 = W_C + \frac{\hbar^2 k_{\mu 0}^2}{2m_n}$$

Gain rate:

$$\left.\begin{aligned} r_{\mathrm{ind}}^{(\mathrm{M})} &= \frac{1}{V}\frac{\mathrm{d}N_P}{\mathrm{d}t} \\ G &= \frac{1}{N_P}\frac{\mathrm{d}N_P}{\mathrm{d}t} \end{aligned}\right\} \quad G = \frac{r_{\mathrm{ind}}^{(\mathrm{M})}}{N_P/V}$$

Radiative and Nonradiative Recombination

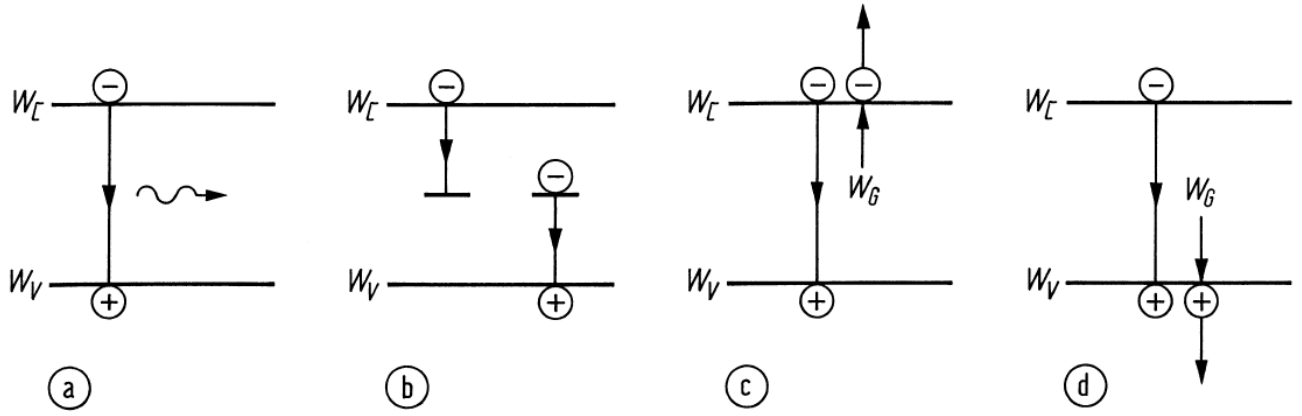

Radiative and nonradiative transitions. (a) Radiative band-band transition. (b) Nonradiative transition via localized states in the forbidden band. (c) (d) Nonradiative Auger recombinations (recombination energy excites excites an electron in the CB or in the VB)

p-Si rad. lifetime $p_p = 10^{16}\,\mathrm{cm}^{-3}$:

$$\tau_{n\,\mathrm{sp}}^{-1} = \frac{\partial\, r_{\mathrm{sp}}}{\partial n_T}$$

$$\tau_{n\,\mathrm{sp}} = 33\,\mathrm{ms}$$

Radiative recomb. (rate r_{sp}, unit $\mathrm{cm}^{-3}\,\mathrm{s}^{-1}$) of electrons and holes:

$$r_{\mathrm{sp}} = B n_T p, B = \begin{cases} 1 \times 10^{-10} \ldots 7 \times 10^{-10}\,\mathrm{cm}^3\,\mathrm{s}^{-1} & \text{(Ga,Al)As} \\ 8.6 \times 10^{-11}\,\mathrm{cm}^3\,\mathrm{s}^{-1} & \text{(In,Ga)(As,P)} \\ 3 \times 10^{-15}\,\mathrm{cm}^3\,\mathrm{s}^{-1} & \text{Si (indirect SC)} \end{cases}$$

Nonrad. recomb. (rate r_{ns}, unit $\mathrm{cm}^{-3}\,\mathrm{s}^{-1}$): Localized impurities, rate $r_{\ell\mathrm{S}}$ (Shockley-Read-Hall, SRH). Recomb. energy transfered to e or h, rate r_{Au}, (Auger, in (In,Ga)(As,P) $\rightarrow h$, not in (Ga,Al)As):

$$r_{\mathrm{ns}} = r_{\ell\mathrm{S}} + r_{\mathrm{Au}}, \qquad r_{\ell\mathrm{S}} = A n_T, \qquad r_{\mathrm{Au}} = C n_T p^2$$

Effective Carrier Recombination Lifetime. Step Response

Effective recombination rate:

$$r_{\mathrm{eff}} = r_{\mathrm{sp}} + r_{\mathrm{ns}} = r_{\mathrm{sp}} + r_{\ell \mathrm{S}} + r_{\mathrm{Au}}$$

In diode recombination zone (layer height d, cross-section area F) carrier density changes if injected carrier rate (injection current density J, elementary charge e) deviates from recombination rate:

$$\frac{\mathrm{d}n_T}{\mathrm{d}t} = \frac{J}{ed} - r_{\mathrm{eff}}(n_T)$$

Strictly speaking, $r_{\mathrm{eff}}(n_T) \to r_{\mathrm{eff}}(n_T) - r_{\mathrm{eff}}(n_{T\,\mathrm{eql}})$ for correct solution at concentration $n_{T\,\mathrm{eql}}$ for thermal equilibrium $J = 0$.
Step perturbation $J \to J_0 + J_1$. Perturbation ansatz $n_T(t) = n_{T0} + n_{T1}(t)$, series expansion $r_{\mathrm{eff}} = r_{\mathrm{eff}\,0} + (\partial r_{\mathrm{eff}}/\partial n_T) n_{T1}$ at n_{T0}:

$$n_{T1}(t) = \frac{J_1 \tau_{\mathrm{eff}}}{ed} \left(1 - \mathrm{e}^{-t/\tau_{\mathrm{eff}}}\right), \quad \text{with} \quad \tau_{\mathrm{eff}}^{-1} = \frac{\partial r_{\mathrm{eff}}}{\partial n_T}$$

LED — Generated Power, Internal and Optical Efficiency

Light-emitting diodes (LED) without end mirrors, spontaneous emission rate $r_{\mathrm{sp}}^{(\mathrm{eM})}$ dominates. Double-heterostructures common. Generated light power P:

$$P = \frac{n_T F d \cdot hf}{\tau_{\mathrm{sp}}} = \eta_{\mathrm{int}}\, hf\, \frac{I}{e}, \qquad \eta_{\mathrm{int}} = \frac{\tau_{\mathrm{eff}}}{\tau_{\mathrm{sp}}} = \frac{P/(hf)}{I/e}$$

Isotropic emission into 4π. Fraction $(1 - R_P)\,\Omega_P/(4\pi)$ (TIR solid angle Ω_P, cone semi-angle $\pi/2 - \vartheta_T$) into medium $n_1 < n_2$ (GaAs):

$$n_1 \mathrel{\widehat{=}} \text{air (silica):} \qquad \eta_{\mathrm{opt}} = \frac{\Omega_P}{4\pi}(1 - R_P) = 1.5\,\%\ (3.5\,\%)$$

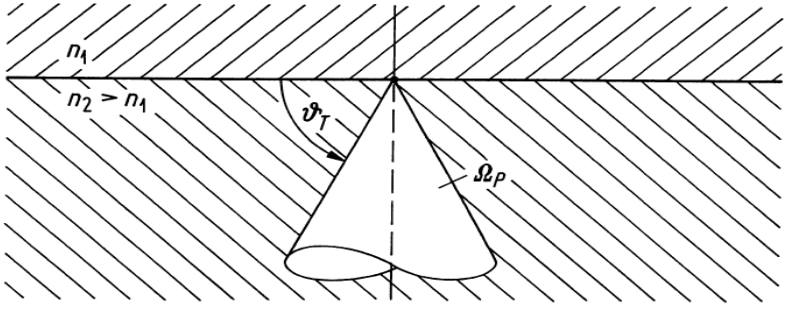

$$\begin{cases} \Omega_P = 2\pi(1 - \sin\vartheta_T) = 0.27\,\mathrm{sr}\ (0.54\,\mathrm{sr}) \\ \cos\vartheta_T = n_1/n_2 \quad = 73^\circ \quad (66^\circ) \\ R_P = \left(\dfrac{n_1 - n_2}{n_1 + n_2}\right)^2 \quad = 32\,\%\ \ (18\,\%) \end{cases}$$

Plane boundary between two media ($n_1, n_2 > n_1$ refractive indices, ϑ_T critical angle of total reflection, R_P power reflection factor). Only the fraction $(1 - R_P)$ of the radiation from the solid angle Ω_P is transmitted into the medium n_1.

LED — Device Structure. Surface and Edge Emitter, SLED

Small-area high-radiance (Ga,Al)As double-heterostructure surface-emitter LED with attached fibre (Burrus diode). Epoxydharz = epoxy resin, Anschlußdraht = bond wire, Metallkontakt = metal contact, Metallisierung = metallization

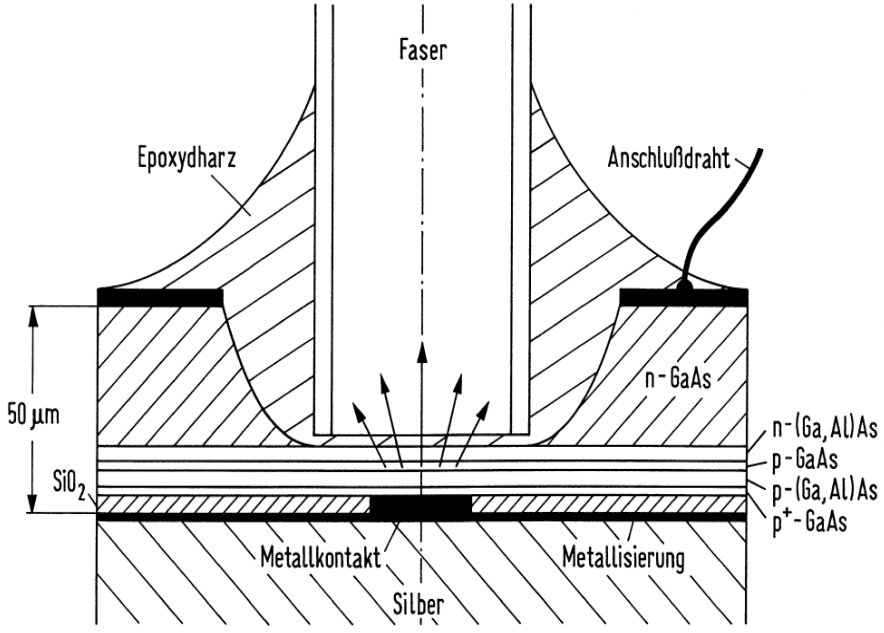

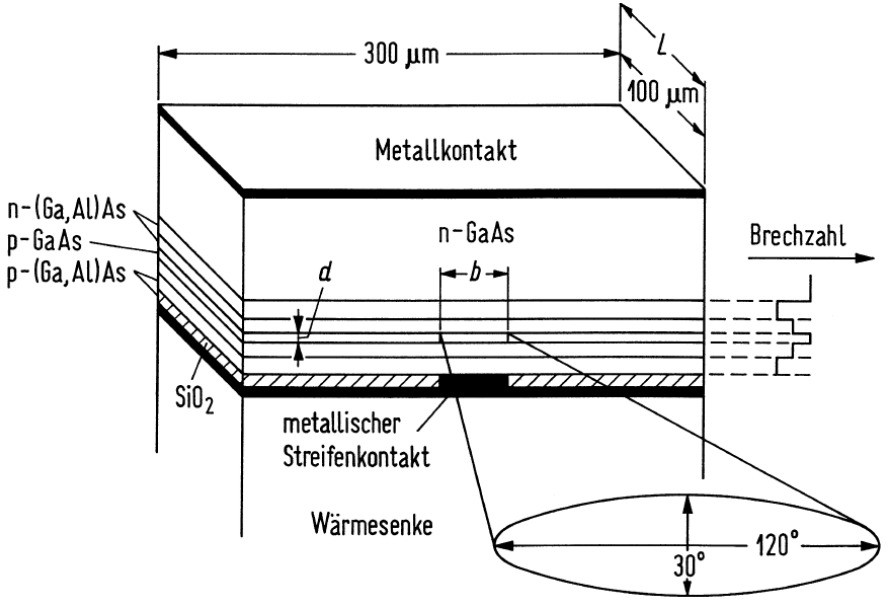

Edge-emitter double-heterostructure LED. L, b, d are length, width and thickness of the active zone. Metallkontakt= metal contact, metallischer Streifenkontakt = metallic contact strip, Wärmesenke = heat sink, Brechzahl = refractive index

LED — Power Spectrum

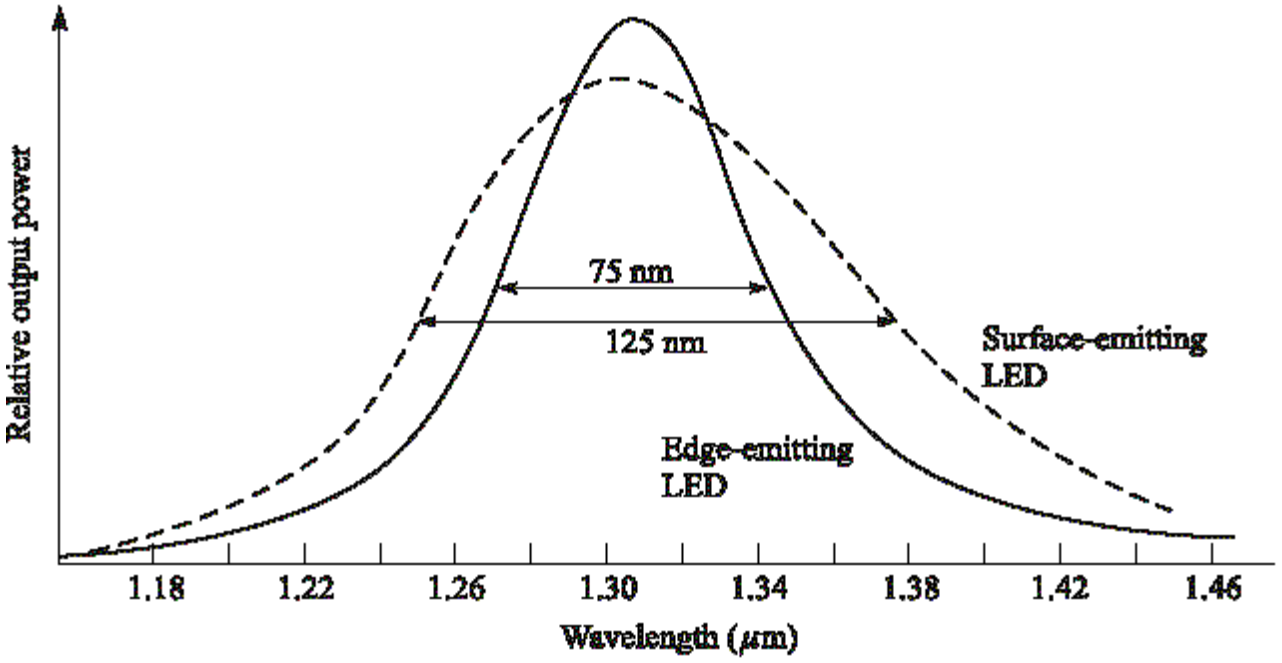

Photons emitted in spectral range $W_G \leq hf \leq (W_C + 2kT_0) - W_V$.

Total spectral emission width $h\,\Delta f_H = 2kT_0$:

$$h\,\Delta f_H = 2\,kT_0 = 50\,\text{meV}, \quad \Delta f_H = 12.1\,\text{THz} \quad \text{RT } T_0 = 293\,\text{K}$$

GaAs: $\Delta\lambda_H = 30\,\text{nm}$. (In,Ga)(As,P): $\Delta\lambda_H = 70\,\text{nm}$ at $\lambda = 1.3\,\mu\text{m}$.

Δf_{gain} also estimates amplification bandwidth of semiconductor laser devices. Corresponds to width Δf_H of lineshape $\rho(f)$.

LD — Cavity and Field Confinement

Conventional laser diode (LD) has rectangular cavity → Fabry-Perot (FP) resonator → Fabry-Perot laser diode (FP LD). Structure similar to LED edge-emitter.

Laser-active volume $V = dbL$ dimensions $d = 0.1 \ldots 0.2\,\mu$m (vertical, x-axis), $b = 2 \ldots 5\,\mu$m (lateral, y-axis), $L = 300 \ldots 1\,200\,\mu$m, (longitudinal, z-axis).

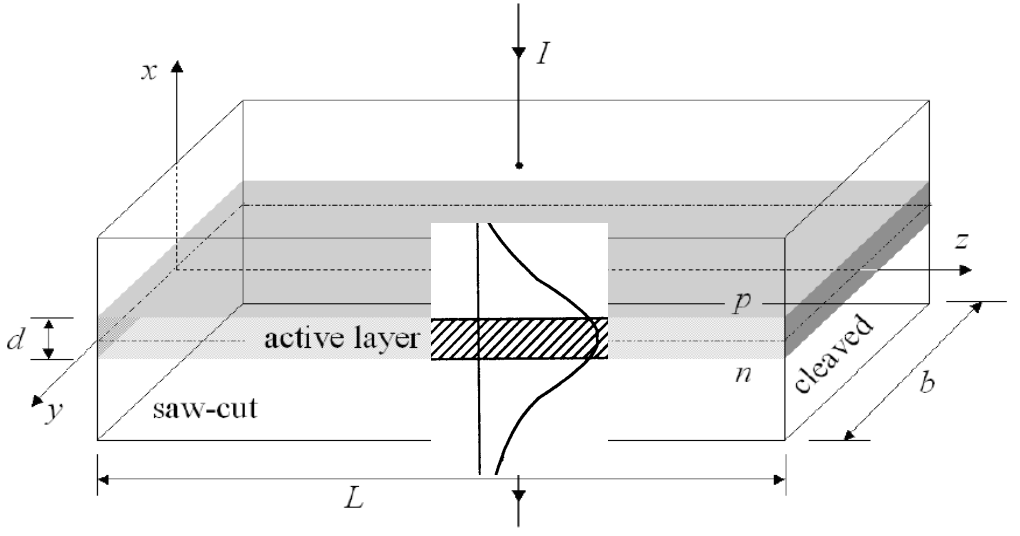

Field confinement:

$$\Gamma_{\mathrm{TE}} = \frac{\int_{-d/2}^{+d/2} |E_y(x)|^2 \,\mathrm{d}x}{\int_{-\infty}^{+\infty} |E_y(x)|^2 \,\mathrm{d}x}$$

LD: $\Gamma_{\mathrm{TE\,(TM)}} = .184\,(.145)$
SOA: .3 (.25) LD → TE
$d = .1 \rightarrow .2\,\mu$m: $\Gamma = .2 \rightarrow .6$

Forward biased semiconductor pn-homojunction acting as a laser diode. Side-walls are saw-cut, the end facets are cleaved. Typical dimensions: $d = 0.1 \ldots 0.2\,\mu$m (active layer), $b = 3 \ldots 6\,\mu$m, $L = 200 \ldots 600\,\mu$m

LD — Longitudinal Mode Spectrum

Transverse WG mechanism described by $\beta/k_0 = n_e < n$. Subscript e dropped.

Equivalent plane waves propagating along z-axis ($k_{x,y} = 0$, $k_z = k$):

$$k \times 2L = k_0 n \times 2L = \omega n \times 2L/c = m_z \times 2\pi\,, \qquad m_z = 1, 2, 3, \ldots$$

Regarding m_z as continuous:

$$\frac{\mathrm{d}(fn)}{\mathrm{d}m_z} = \frac{\mathrm{d}f}{\mathrm{d}m_z} n + f \frac{\mathrm{d}n}{\mathrm{d}f} \frac{\mathrm{d}f}{\mathrm{d}m_z} = \frac{\mathrm{d}f}{\mathrm{d}m_z} \left(n + f \frac{\mathrm{d}n}{\mathrm{d}f} \right) = \frac{c}{2L}$$

m_z discrete $\rightarrow$ $\mathrm{d}m_z \rightarrow 1$, $\mathrm{d}f \rightarrow \Delta f_z$.

Longitudinal mode spacing (free spectral range FSR, round-trip time τ_U):

$$\Delta f_z = \frac{c}{2 n_g L} = \frac{v_g}{2L} = \frac{1}{\tau_U}$$

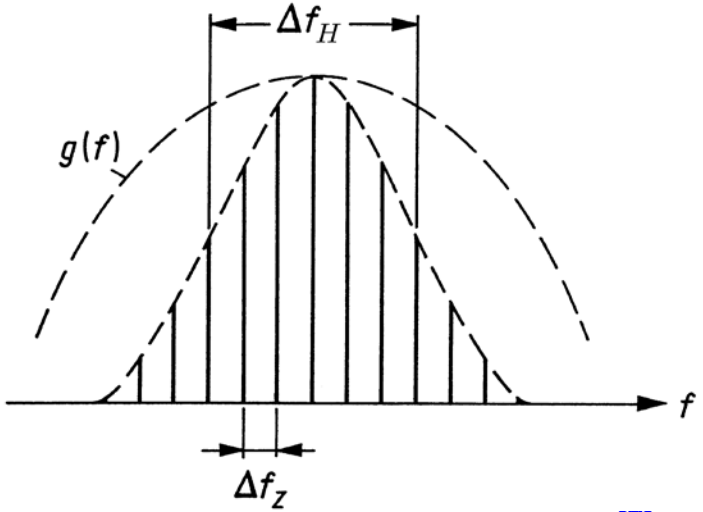

LECTURE 10

LD — Inversion Factor

$$r_{\text{ind}}^{(\text{M})} = r_{\text{ind}}^{(\text{eM})} - r_{\text{ind}}^{(\text{aM})}$$
$$\sim N_P\Big[f_C(W_0)[1 - f_V(W_0 - hf)] - f_V(W_0 - hf)[1 - f_C(W_0)]\Big]$$
$$\sim N_P\Big[f_C(W_0) - f_V(W_0 - hf)\Big],$$
$$r_{\text{sp}}^{(\text{eM})} \sim f_C(W_0)\Big[1 - f_V(W_0 - hf)\Big],$$
$$W_0 = W_C + \frac{\hbar^2 k_{\mu 0}^2}{2m_n}$$

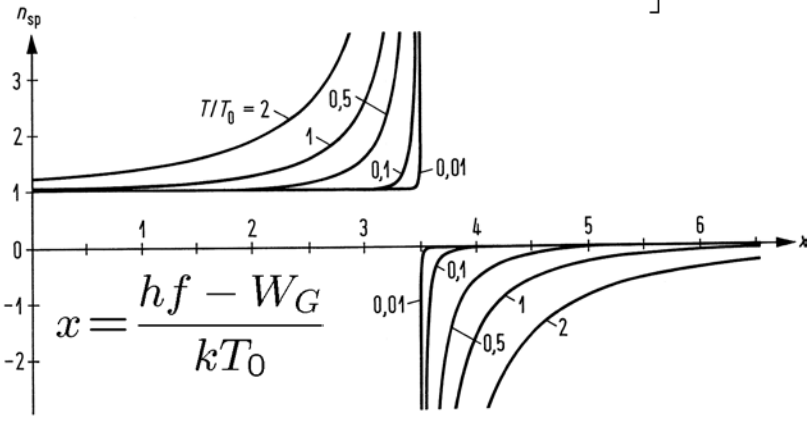

Inversion factor relates the spontaneous emission rate to the net induced emission rate per photon:

$$n_{\text{sp}} = \frac{r_{\text{sp}}^{(\text{eM})}}{r_{\text{ind}}^{(\text{M})} \Big/ N_P} = \frac{r_{\text{sp}}^{(\text{eM})}}{G/V} = \frac{f_C(W_0)\Big[1 - f_V(W_0 - hf)}{f_C(W_0) - f_V(W_0 - hf)} = \frac{N_2}{N_2 - N_1}$$

Transition probabilities are related by:

$$\frac{p_{\text{ind}}^{(\text{eM})}}{p_{\text{sp}}^{(\text{eM})}} = \frac{tN_P}{t}, \frac{p_{\text{ind}}^{(\text{eM})}}{p_{\text{ind}}^{(\text{aM})}} = \frac{tN_P}{tN_P}, \; r_{\text{sp}}^{(\text{eM})} = \frac{N_2}{V}\frac{\mathrm{d}p_{\text{sp}}^{(\text{eM})}}{\mathrm{d}t}, r_{\text{ind}}^{(\text{e,aM})} = \frac{N_{2,1}}{V}\frac{\mathrm{d}p_{\text{ind}}^{(\text{e,aM})}}{\mathrm{d}t}$$

LD — Gain and Loss

Multi-moded resonator, one mode considered. Modes replaced by plane waves with effective propagation properties, complex (effective) refractive index $\bar{n} = n - \mathrm{j}\, n_i$, real part n, imaginary part $-n_i$. Subscript e dropped as before:

$$\exp(-\mathrm{j}\,\bar{k}z), \quad \left\{ \begin{array}{l} \bar{k} = k_0 \bar{n} = k + \mathrm{j}\,\frac{1}{2}(g - \alpha_V), \\ \bar{n} = n - \mathrm{j}\, n_i, \\ k_0 = \omega/c, \end{array} \right\}, \quad g - \alpha_V = -2\, k_0 n_i$$

Modal power gain g and loss constant α_V. Corresponds to net effective gain rate ΓG due to band-band transitions and power loss time constant $1/\tau_V$ not including band-band transitions.

Localized mirror losses $\rightarrow$ power "gain" $R_1 R_2 = \exp(-\alpha_{R1} 2L) \times \exp(-\alpha_{R2} 2L) = \exp(-\alpha_R 2L)$ distributed over round-trip time τ_U. Constant gain rate per $\tau_U \rightarrow$ net N_P-increase per second:

$$G - \frac{1}{\tau_P} = \frac{1}{N_P} \frac{\mathrm{d}N_P}{\mathrm{d}t}, \quad \frac{N_P(\tau_U)}{N_P(0)} = \exp\left[\left(G - \frac{1}{\tau_P}\right)\tau_U\right], \quad \tau_U = \frac{2L}{v_g}$$

Stationary Laser Oscillation

Stationary laser oscillation with angular frequency ω_0 for $\Gamma G = 1/\tau_P \rightarrow$ modal gain compensates resonator losses. A *monochromatic* light wave makes a complete round-trip during $t = \tau = 2nL/c$ without attenuation or phase shift:

$$\exp(\mathrm{j}\,\omega_0\tau)\exp\left[\frac{1}{2}\left(\Gamma G - \frac{1}{\tau_P}\right)\tau\right] = 1\,,$$

$$\omega_0\tau = m_z \cdot 2\pi\,, \quad \tau = \frac{2nL}{c}\,, \quad m_z = 0, 1, 2, \ldots\,, \quad \Gamma G = \frac{1}{\tau_P}$$

Condition $\omega_0\tau = m_z \cdot 2\pi$ corresponds to longitudinal mode spacing $\Delta f_z \rightarrow n_g$ is effective group refractive index.

Modal gain rate $\Gamma G = \Gamma r_{\mathrm{ind}}^{(\mathrm{M})} V/N_P$. Total resonator loss rate $1/\tau_P$ from finite mirror reflectivity $R_{1,2}$ (photon loss rate $1/\tau_{R1,2}$, total loss rate $1/\tau_R$), and from background resonator losses (photon loss rate $1/\tau_V$):

$$\tau_P^{-1} = \tau_V^{-1} + \tau_R^{-1}\,, \qquad \tau_R^{-1} = \tau_{R1}^{-1} + \tau_{R2}^{-1}\,.$$

LD — Gain and Loss Distributed

Relations between gain rate and modal power gain:

$$\begin{aligned}
\exp\Big[(G-1/\tau_P)\tau_U\Big] &= \exp\Big[(G-1/\tau_V-1/\tau_R)\tau_U\Big] \\
&= R_1R_2\exp\Big[(G-1/\tau_V)\tau_U\Big] \\
&= R_1R_2\exp\Big[(G-1/\tau_V)2L/v_g\Big] \\
&= R_1R_2\exp\Big[(g-\alpha_V)2L\Big] \\
&= \exp\Big[(g-\alpha_V-\alpha_R)2L\Big] \\
&= \exp\Big[(g-\alpha_V-\alpha_{R1}-\alpha_{R2})2L\Big]
\end{aligned}$$

Comparing:

$$\begin{aligned}
G &= v_g g, \\
1/\tau_V &= v_g\alpha_V, \\
1/\tau_{R1,2} &= v_g\alpha_{R1,2} = -v_g \ln R_{1,2}/(2L), \\
1/\tau_R &= v_g\alpha_R = -v_g \ln(R_1R_2)/(2L), \\
1/\tau_P &= v_g(\alpha_V+\alpha_R) = v_g[\alpha_V - \ln(R_1R_2)/(2L)]
\end{aligned}$$

LD — Gain Model and Gain Compression

Laser oscillates near f_0 (maximum spectral gain). Larger carrier number $\rightarrow$ nonlinear gain compression $\rightarrow$ energy states near hf_0 deplete (hot carrier effects, spectral hole burning). Depleted states filled only in intraband relaxation time τ_{CB} $\rightarrow$ "bottleneck" for carrier number available near hf_0.

Nonlinear gain compression modeled with gain compression factor ε_G, differential gain G_d, transparency concentration n_t:

$$G(n_T, N_P) = \frac{G(n_T)}{1 + \varepsilon_G \frac{\Gamma N_P}{V}} = G_d \frac{n_T - n_t}{1 + \varepsilon_G \frac{\Gamma N_P}{V}}$$

Empty VB (very high and constant $p = n_A$, i. e., $f_V \approx 0$ in range of interest, complete inversion $n_{\mathrm{sp}} = 1$) $\rightarrow$ (transp. concentration) = ($n_t = 0$) $\rightarrow$ slightest n_T-concentration in CB establishes some gain. Negligible gain compression $\varepsilon_G = 0$ $\rightarrow$ linear gain dependency:

$$G(n_T) = G_d\, n_T$$

Carrier/Gain Depletion and Recovery

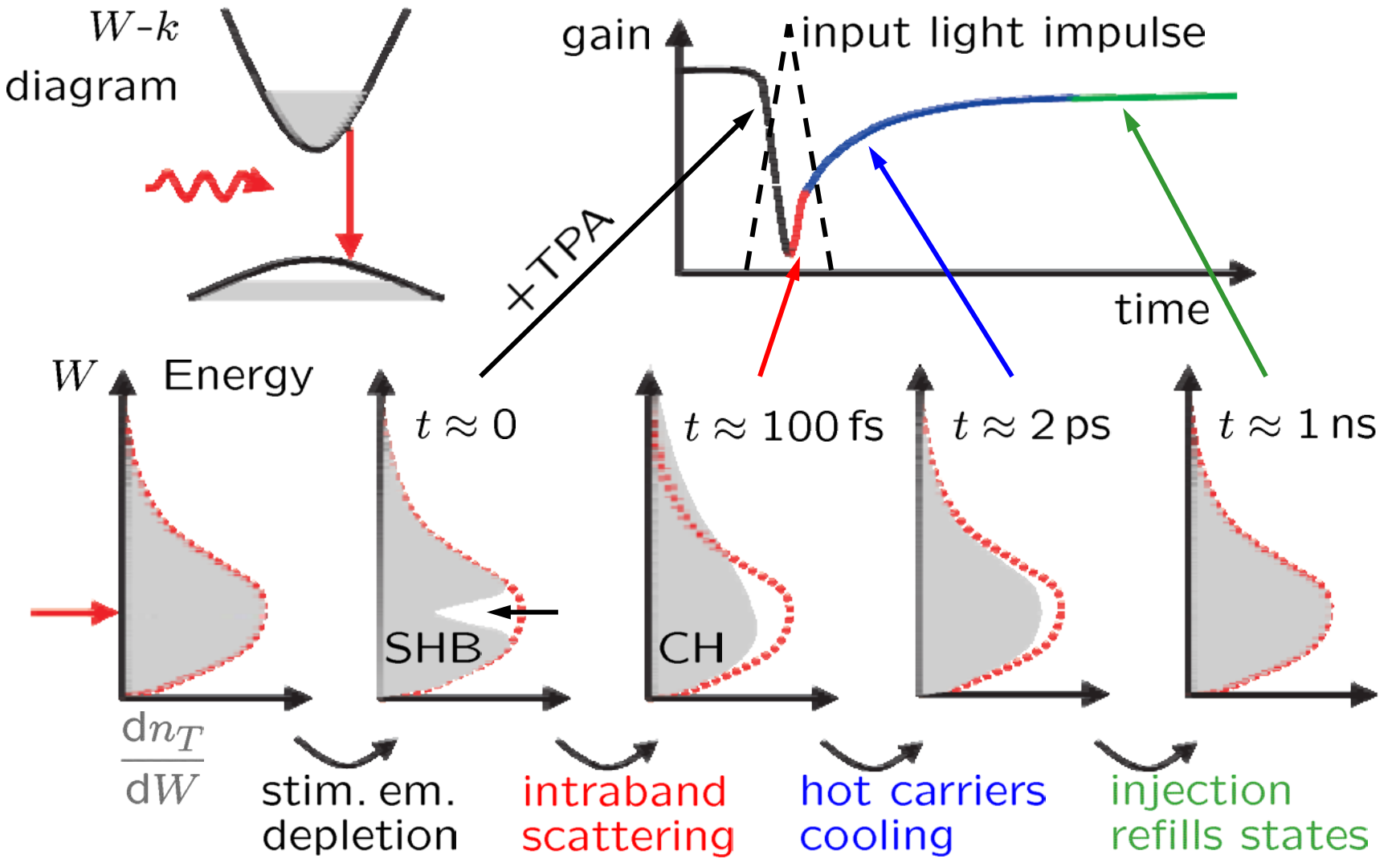

Modified from: Mørk, J. et al. IEEE LEOS Newsletter 16 (2002) 21–24. Fig. 2. — Mørk, J. et al. Optics & Photonics News July (2003) 42–48

LD — Rate Equations

Rate equations heuristically, phenomena through which N_P, $n_T V$ change in active volume V. Longitudinally and laterally single-moded laser:

$$\underbrace{\frac{\mathrm{d}N_P}{\mathrm{d}t}}_{\substack{\text{change of photon}\\ \text{number per time}}} = \underbrace{+ N_P \Gamma G(n_T, N_P)}_{\substack{\text{stim. gen.}\\ \text{photons per time}}} + \underbrace{Q \frac{n_T V}{\tau_{\text{eff}}}}_{\substack{\text{spont. gen.}\\ \text{ph. p. mode, time}}} - \underbrace{\frac{N_P}{\tau_P}}_{\substack{\text{stim. depl.}\\ \text{ph. p. time}}}$$

$$\underbrace{\frac{\mathrm{d}(n_T V)}{\mathrm{d}t}}_{\substack{\text{change of electron}\\ \text{number per time}}} = \underbrace{- N_P \Gamma G(n_T, N_P)}_{\substack{\text{stim. depl.}\\ \text{electrons per time}}} - \underbrace{\frac{n_T V}{\tau_{\text{eff}}}}_{\substack{\text{spont. depl.}\\ \text{electrons per time}}} + \underbrace{\frac{I}{e}}_{\substack{\text{inj. electr.}\\ \text{per time}}}$$

Fraction of spontaneous recombinations leading to photons in oscillating mode is spontaneous emission factor Q:

$$Q = \frac{\Gamma r_{\text{sp}}^{(\text{eM})}}{r_{\text{eff}}} = \frac{\Gamma r_{\text{sp}}}{r_{\text{eff}}} \frac{\rho(f)}{\varrho_{\text{tot}}(f) V} = \Gamma \frac{\tau_{\text{eff}}}{\tau_{\text{sp}}} \frac{\rho(f)}{\varrho_{\text{tot}}(f) V}$$

LD — Rate Equations. Threshold

$Q = 0$, $N_P G \ll n_T V/\tau_{\text{eff}} \rightarrow$ Definition of lasing threshold (subscript S) for $\mathrm{d}/\mathrm{d}t = 0$. Above threshold: Device oscillates.

$$\Gamma G(n_{TS}, 0) = \Gamma G_S = \frac{1}{\tau_P} = v_g\left(\alpha_V - \frac{\ln(R_1 R_2)}{2L}\right),$$

$$\frac{I_S}{e} = \frac{n_{TS} V}{\tau_{\text{eff}}} = r_{\text{eff}} V, \quad \frac{I_S}{e} = \left\{g = g_0\left(\frac{n_T}{n_t} - 1\right)\right\} = \frac{n_t\left(1 + \Gamma g_S/(\Gamma g_0)\right)V}{\tau_{\text{eff}}}$$

At threshold carrier concentration $n_T = n_{TS} \rightarrow$ net gain rate ΓG_S compensates loss rate $1/\tau_P$. $\Gamma G_S > G(n_T, N_P) = G(n_t, N_P) = 0$.

Only above threshold:

(photon number generated per t) $>$ (photon number annihilated)

Maximum τ_P for minimum mirror transmission losses.

Threshold current density $J_S = I_S/(bL)$ for 5-layer structure minimum for optimum height d of active layer:

$$J_S = \frac{I_S}{bL} = \frac{e n_t}{\tau_{\text{eff}}}\left[d + \frac{\Gamma\alpha_V + \alpha_R}{g_0}\frac{d}{\Gamma(d)}\right], \quad \Gamma(d) = \begin{cases} d^2 & \text{for } d \text{ small} \\ 1 & \text{for } d \text{ large} \end{cases}, \quad J_S = c_1 d + \frac{c_2}{d}$$

LD — Rate Equations. Characteristic Curves

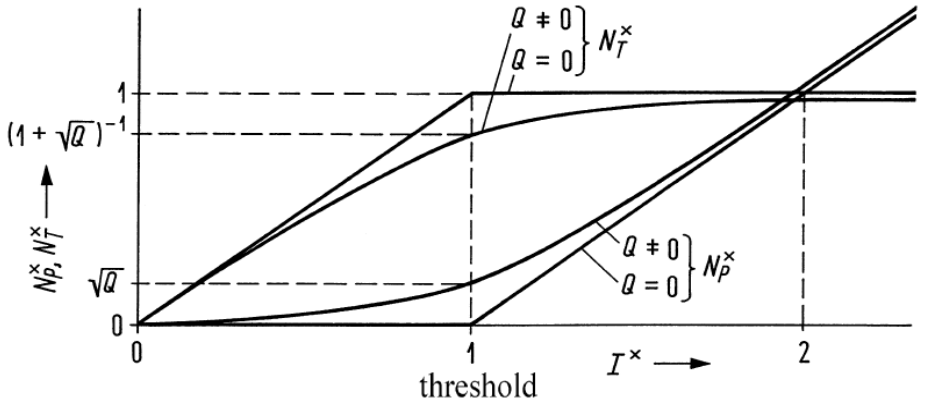

Normalized photon number $N_P^\times$ and normalized CB carrier density $N_T^\times$ as a function of the normalized injection current $I^\times$. For $Q \neq 0$ a simplified gain dependence $G^\times = N_T^\times$

DC solution:

$$I^\times \leq 1: \quad N_T^\times = I^\times, \quad N_P^\times = 0, \qquad Q = 0,$$

$$I^\times > 1: \quad N_T^\times = 1, \quad N_P^\times = I^\times - 1, \quad G^\times = 1,$$

Normalized rate equations:

$$\tau_P \frac{\mathrm{d}N_P^\times}{\mathrm{d}t} = N_P^\times (G^\times - 1) + Q N_T^\times,$$

$$\tau_{\mathrm{eff}} \frac{\mathrm{d}N_T^\times}{\mathrm{d}t} = I^\times - N_T^\times - N_P^\times G^\times$$

LD — Small-Signal Intensity Modulation

Static operation point above threshold at N_{P0}, n_{T0}, τ_P, τ_{eff}, $G_0 = G(n_{T0}, N_{P0})$, ε_G. Small perturbations $N_{P1}(t)$, $n_{T1}(t)$, $I_1(t)$:

$$N_P(t) = N_{P0} + N_{P1}(t), \quad G(t) = G_0 + \frac{\partial G_0}{\partial n_{T0}} n_{T1}(t) + \frac{\partial G_0}{\partial N_{P0}} N_{P1}(t),$$

$$n_T(t) = n_{T0} + n_{T1}(t), \qquad G_0 = G(n_{T0}, N_{P0}), \qquad I(t) = I_0 + I_1(t)$$

Elimination of $n_{T1}(\omega)$ leads to modulation transfer function:

$$\frac{N_{P1}(\omega)}{I_1(\omega)} \approx \frac{\omega_r^2}{(\mathrm{j}\,\omega)^2 + 2\gamma_r(\mathrm{j}\,\omega) + \omega_r^2}$$

Angular relaxation frequency ω_r, damping constant γ_r:

$$\omega_r^2 \tau_P \approx \frac{N_{P0}}{V} \frac{\partial \Gamma G_0}{\partial n_{T0}},$$

$$2\gamma_r \approx \frac{1}{\tau_{\text{eff}}} + \underbrace{\frac{N_{P0}}{V} \frac{\partial \Gamma G_0}{\partial n_{T0}} + \overbrace{\Gamma G_0\, \varepsilon_G \frac{\Gamma N_{P0}}{V}}^{\approx \tau_P^{-1} \varepsilon_G \Gamma N_{P0}/V}}_{= \omega_r^2 K_r}$$

LD — Small-Signal Intensity Modulation. Transfer Function

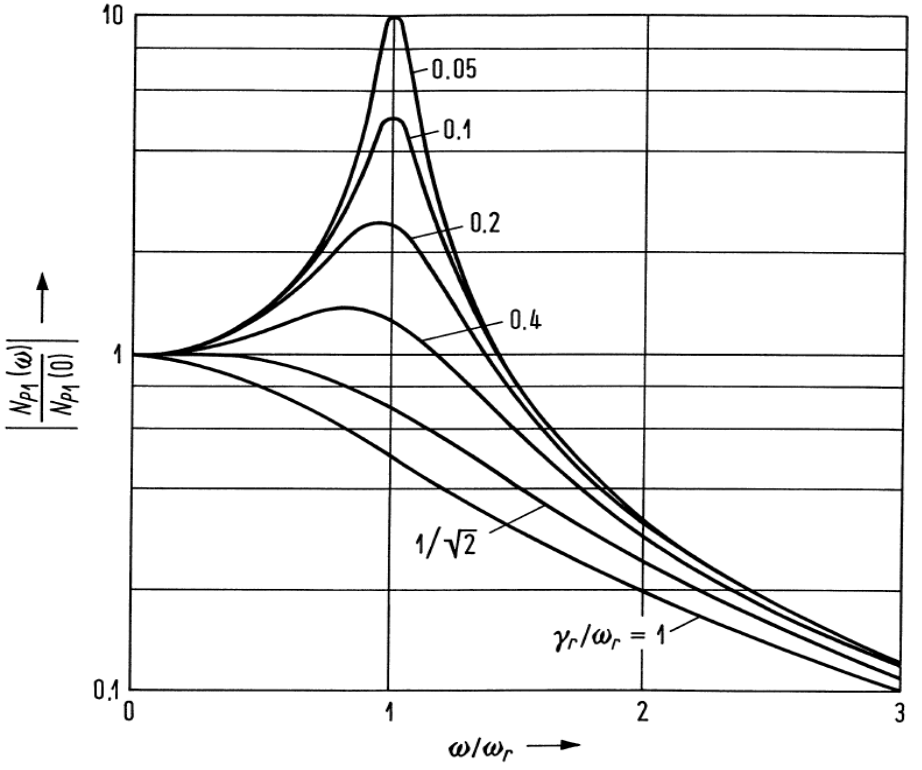

$$\left|\frac{N_{P1}(\omega)/\tau_P}{I_1/e}\right| \rightarrow \max:$$

$$\omega_R = \sqrt{\omega_r^2 - 2\gamma_r^2}$$

$$\left|\frac{N_{P1}(\omega_{3\,\mathrm{dB}})}{N_{P1}(0)}\right| = \frac{1}{\sqrt{2}},$$

$$\omega_{3\,\mathrm{dB}}^2 = (\omega_r^2 - 2\gamma_r^2) + \sqrt{(\omega_r^2 - 2\gamma_r^2)^2 + \omega_r^4}$$

Modulus of current-light modulation transfer function as a function of normalized current modulation frequency for various values of γ_r/ω_r

$$\omega_r^2 \tau_P \approx \frac{N_{P0}}{V}\frac{\partial(\Gamma G_0)}{\partial n_{T0}}; \quad \omega_{3\,\mathrm{dB}}^{\max} = \omega_r = \gamma_r\sqrt{2}, \quad \gamma_r\sqrt{2} \approx \frac{1}{2}\omega_r^2 K_r\sqrt{2},$$

$$2\gamma_r \approx \frac{1}{\tau_{\mathrm{eff}}} + \ldots \quad \omega_{3\,\mathrm{dB}}^{\max} = \frac{\sqrt{2}}{K_r}, \quad K_r = \tau_P + \frac{\varepsilon_G}{\partial G_0/\partial n_{T0}}$$

LD — Large-Signal Intensity Modulation

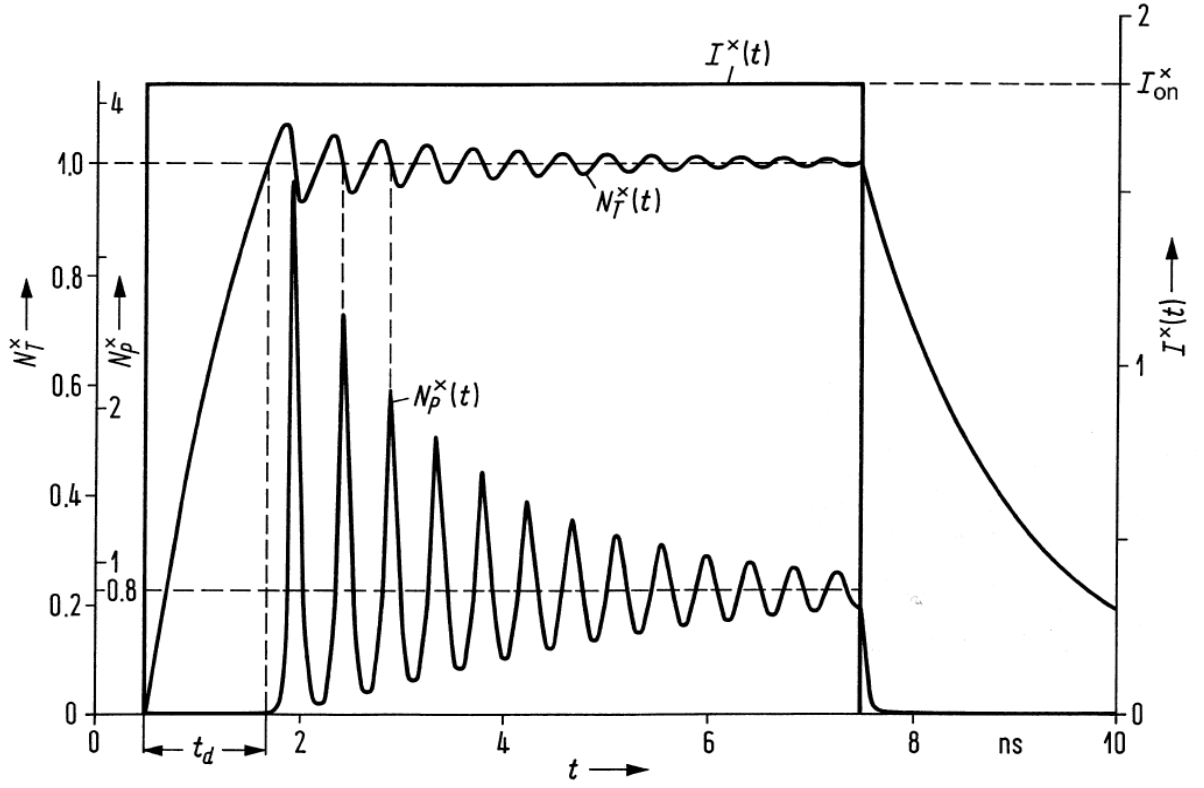

Relaxation oscillation for a current step $I^\times = 1.8$. Parameters are $\tau_P = 2.5\,\mathrm{ps}$, $\tau_{\mathrm{eff}} = 1.5\,\mathrm{ns}$, $Q = 5\times10^{-4}$

Normalized rate equations:

$$\tau_P \frac{\mathrm{d}N_P^\times}{\mathrm{d}t} = N_P^\times(G^\times - 1) + QN_T^\times\,, \qquad \tau_{\mathrm{eff}} \frac{\mathrm{d}N_T^\times}{\mathrm{d}t} = I^\times - N_T^\times - N_P^\times G^\times$$

LD and SOA — Amplitude-Phase Coupling

* LD and SOA carrier lifetimes $\tau \sim 0.1 \ldots 1\,\mathrm{ns}$ (EDFA: $\tau \sim 10\,\mathrm{ms}$)
* Transient gain variation. For Gbit / s data rates:
  - ⋆ makes WDM amplifier application difficult, but is
  - ⋆ good for nonlinear operations, i. e., signal processing.
* Fast intraband processes may be exploited, namely:
  - saturation of power gain constant $g(f) = -2k_0 n_i(f)$, and its
  - associated change of refractive index $n(f)$:
    - ◇ analytic refractive index $\underline{n}(f) = n(f) - \mathrm{j}\, n_i(f)$,
    - ◇ power gain $\mathcal{G} = \exp(gz)$, field $\propto \sqrt{\mathcal{G}} \exp\left[\mathrm{j}\,(\omega t - k_0\, n\, z)\right]$
* $g(f, N)$ and $n(f, N)$ depend on carrier concentration N, and are coupled via the Kramers-Kronig (Hilbert transform) relation:

$$n(f) = 1 - \frac{2}{\pi} \int_0^\infty f' \, \frac{-n_i(f')}{f'^2 - f^2} \, \mathrm{d}f' = 1 - \frac{c}{2\pi^2} \int_0^\infty \frac{g(f')}{f'^2 - f^2} \, \mathrm{d}f'$$

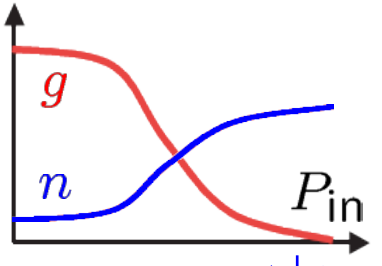

Nussenzveig, H. M.: Causality and dispersion relations. Vol. 95 in "Mathematics in science and engineering", Ed. R. Bellmann. New York: Academic Press 1972. Sect. 1.6

LECTURE 11

LD — Amplitude-Phase Coupling. Line Broadening

Dependencies of gain rate $G(f, n_T)$, modal power gain g and $-n_i$ because of emission spectrum and via quasi Fermi levels. $n(f, n_T)$ because of band filling, Coulomb interact., free-carrier absorpt.
At LD oscillation frequency $\rightarrow \Delta n < 0$ and (via Kramers-Kronig) $\Delta g > 0$ for $\Delta n_T > 0$. Line broadening factor, Henry factor, α-factor:

$$\alpha = \frac{\partial n/\partial n_T}{\partial n_i/\partial n_T} = -2k_0 \frac{\partial n/\partial n_T}{\partial(\Gamma g - \alpha_V)/\partial n_T} \approx -2k_0 \frac{\partial n/\partial n_T}{\partial(\Gamma g)/\partial n_T} > 0$$

For LD oscillator: $\alpha = 2 \ldots 8$. Correlation between amplitude and phase. Spontaneous emissions $\rightarrow$ amplitude and phase changes. Amplitude change $\rightarrow$ secondary phase change $\rightarrow$ broadening of the emission line (P_a is output (*German* Ausgang) power of resonator):

$$\Delta f_H \, P_a = \text{const} \times n_{\text{sp}}(1 + \alpha^2) h f v_g^2 (\alpha_V + \alpha_R) \alpha_R$$

LD — Amplitude-Phase Coupling. Chirp

Stationary laser oscillation, operating point (subscript 0) at $G(n_{T0}) = 1/\tau_P$, $G^{\times} = \Gamma G(n_{T0}, N_{P0})\,\tau_P = 1$. Angular optical frequency ω_0. Changing n_T differentially, $\mathrm{d}n_T \to$ gain rate $\mathrm{d}G$, and "instantaneous" (slowly varying on $(1/f_0)$-scale) optical frequency ω deviating by $\mathrm{d}\omega$. Frequency difference $\Delta\omega$ defines time derivative of optical phase, $\mathrm{d}\varphi/\,\mathrm{d}t = \Delta\omega$, $\omega n \times 2L/c = m_z \times 2\pi$:

$$\mathrm{d}(\omega n(\omega)) = \frac{\partial(\omega n)}{\partial\omega}\,\mathrm{d}\omega + \frac{\partial(\omega n)}{\partial n}\,\mathrm{d}n = \Big(\overbrace{n + \omega\frac{\partial n}{\partial\omega}}^{n_g}\Big)\,\mathrm{d}\omega + \omega\,\mathrm{d}n \stackrel{!}{=} 0\,,$$

$$\mathrm{d}\omega = -\frac{\omega}{n_g}\,\mathrm{d}n = -\frac{\omega}{n_g}\frac{\partial n}{\partial n_T}\,\mathrm{d}n_T = \frac{\alpha\omega}{2k_0 n_g}\frac{\partial(\Gamma g)}{\partial n_T}\,\mathrm{d}n_T$$

$$\approx \Delta\omega = \omega - \omega_0 = \frac{\mathrm{d}\varphi}{\mathrm{d}t} = \frac{\alpha}{2}\,v_g\frac{\partial(\Gamma g)}{\partial n_T}\Delta n_T \approx \frac{\alpha}{2}\frac{\partial(\Gamma G)}{\partial n_T}\Delta n_T$$

$$\frac{\mathrm{d}\varphi}{\mathrm{d}t} = \frac{\alpha}{2}\Big(\underbrace{\frac{\partial(\Gamma G)}{\partial n_T}\Delta n_T + \overbrace{\Gamma G(n_{T0})}^{=0}}_{\Gamma G(n_T)} - \frac{1}{\tau_P}\Big) = \frac{\alpha}{2}\Big(\Gamma G - \frac{1}{\tau_P}\Big) \approx \frac{\alpha}{2}\,\frac{1}{N_P}\,\frac{\mathrm{d}N_P}{\mathrm{d}t}$$

LD — Amplitude-Phase Coupling. Electric Field

$$\frac{\mathrm{d}\varphi}{\mathrm{d}t} = \frac{\alpha}{2}\Bigg(\underbrace{\frac{\partial(\Gamma G)}{\partial n_T}\Delta n_T + \overbrace{\Gamma G(n_{T0})}^{=0}}_{\Gamma G(n_T)} - \frac{1}{\tau_P} \Bigg) = \frac{\alpha}{2}\left(\Gamma G - \frac{1}{\tau_P}\right) \approx \frac{\alpha}{2}\,\frac{1}{N_P}\,\frac{\mathrm{d}N_P}{\mathrm{d}t}$$

Rate equations with optical phase change supplement, including spontaneous emission into oscillating mode ($Q \neq 0 \rightarrow \Gamma G < 1/\tau_P$):

$$\frac{\mathrm{d}N_P}{\mathrm{d}t} = N_P\left(\Gamma G - \frac{1}{\tau_P}\right) + Q\,\frac{n_T V}{\tau_{\mathrm{eff}}},$$

$$\frac{\mathrm{d}\varphi}{\mathrm{d}t} = \frac{\alpha}{2}\left(\Gamma G - \frac{1}{\tau_P}\right),$$

$$\underline{E}(t) \sim \sqrt{N_P(t)}\ \exp\Big\{\mathrm{j}\,[\omega_0 t + \varphi(t)]\Big\},$$

$$\frac{\mathrm{d}(n_T V)}{\mathrm{d}t} = -N_P\Gamma G - \frac{n_T V}{\tau_{\mathrm{eff}}} + \frac{I}{e}$$

LD — Device Structures with Gain and Index Guiding

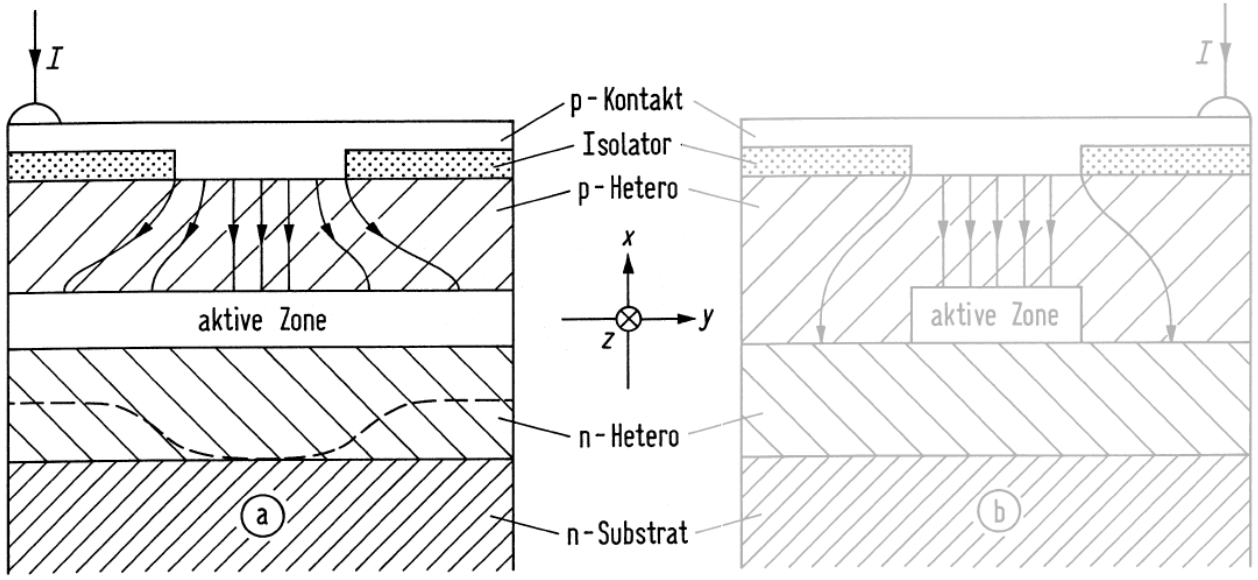

Basic laser diode structures. (a) Gain-guided laser (b) Index-guided laser. The origin of the coordinate system is located in the centre of the active zones (p-Kontakt = p-contact, Isolator = insulator, aktive Zone = active zone).

Gain guiding: Current confined $\rightarrow g - \alpha_V = -2k_0 n_i$

Effective n in high-current region lower $\rightarrow$ antiguiding

Lateral decrease of n_i dominates.

High threshold $I_S = 100\,\mathrm{mA}$

Index guiding: Strip waveguide cavity by lateral heterojunctions.

Low threshold $I_S = 10\,\mathrm{mA}$

Vertical Cavity Surface Emitting Laser — VCSEL

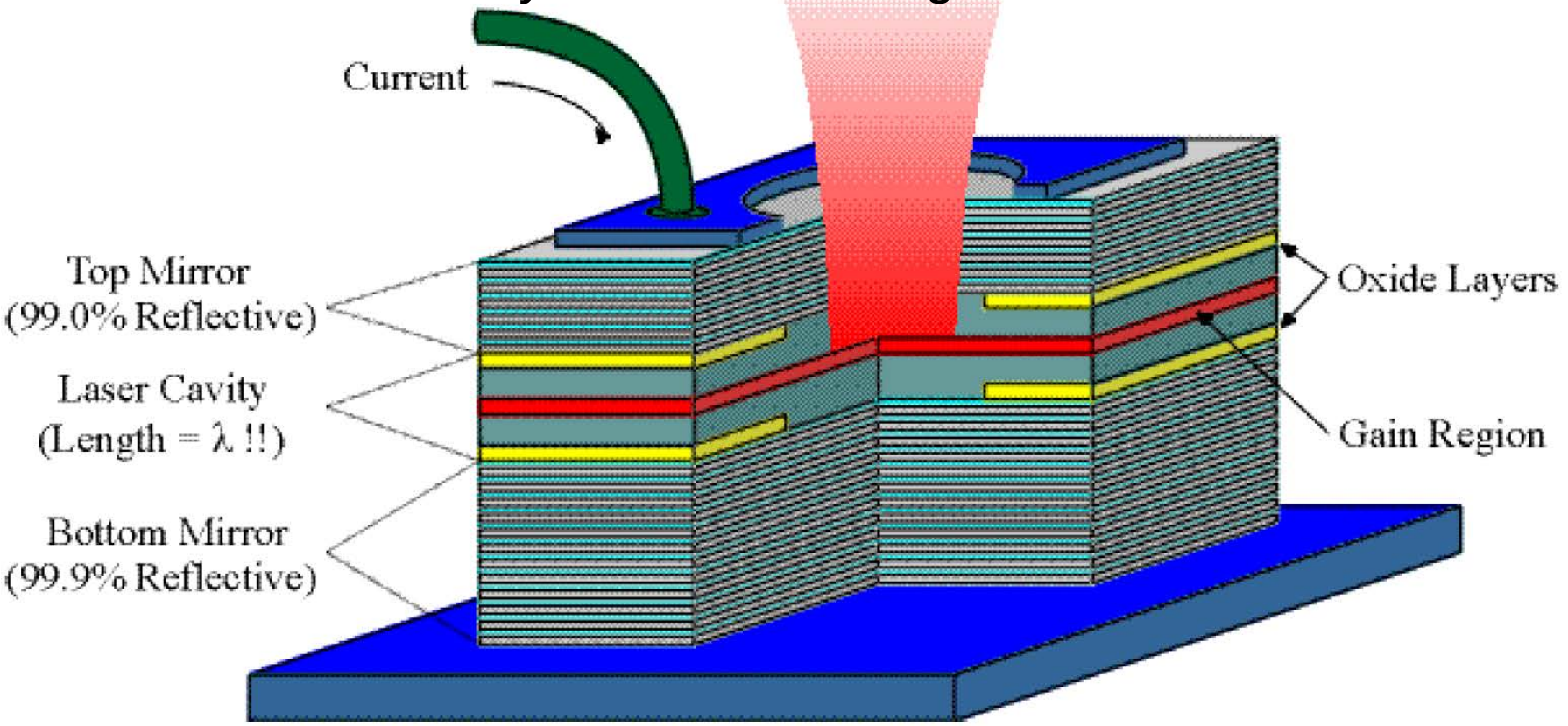

VCSEL operates in single longitudinal mode: Extremly small cavity length $L = \lambda_e/2 \approx 1\,\mu$m so that $m_z = 1$.

Mode spacing $\Delta f_z = c/(n_g\lambda_e) = c/\lambda \approx 300\,\text{THz}$ for $\lambda = 1\,\mu$m exceeds gain bandwidth $\Delta f_H \approx 12\,\text{THz}$ by far.

Vertical Cavity Surface Emitting Laser — Beam Shape and SEM

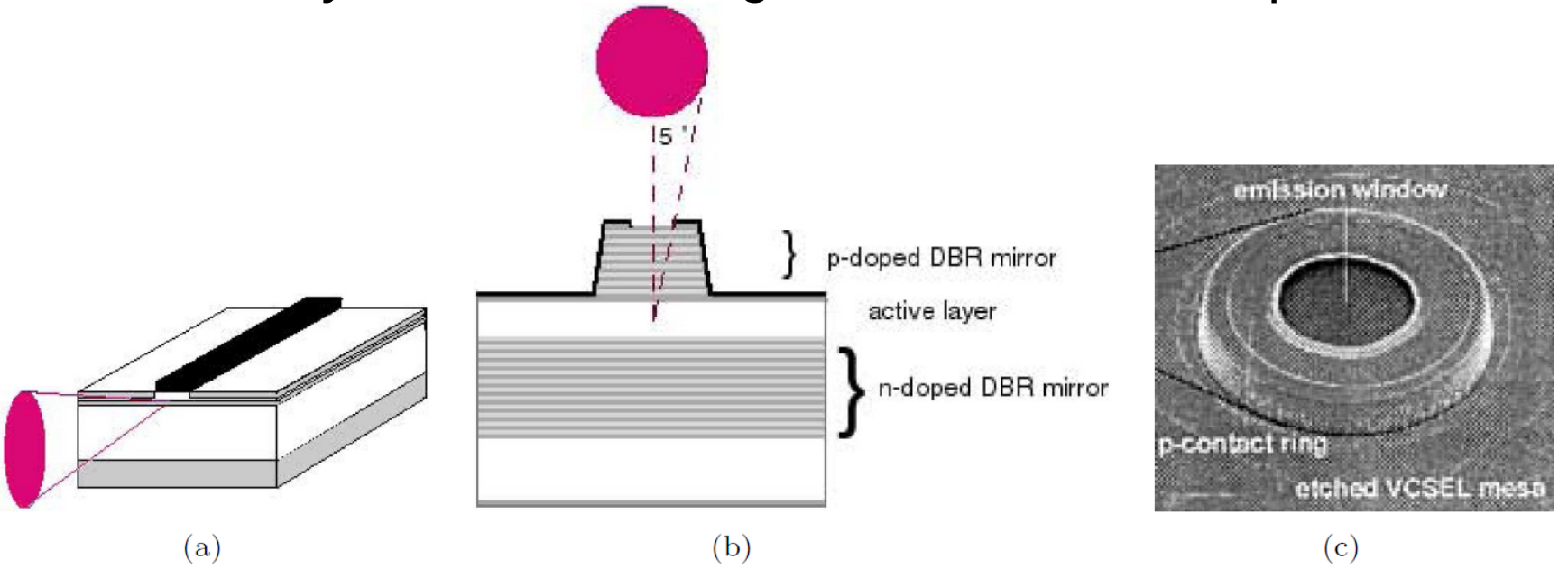

Edge-emitting and vertically-emitting laser diodes (a) edge-emitting laser diode and far-field radiation characteristic (b) VCSEL layer structure. p-doped DBR mirror: 25 layers $Al_{0.3}Ga_{0.7}As/AlAs$; active zone: 220 nm $Al_{0.3}Ga_{0.7}As$ with 3 $Al_{0.12}Ga_{0.88}As$ quantum films, height about 7 nm each; n-doped DBR mirror: 40 layers $Al_{0.3}Ga_{0.7}As/AlAs$ (c) microscopic image of VCSEL (all after reference Footnote 49 on Page 122)

Lower resonator mirror: 40 alternating layers of $Al_xGa_{1-x}As$ and AlAs, each layer $\lambda_e/4$ thick, power reflection factor $R_1 \geq 99.99\,\%$

Output top mirror: 25 $\lambda_e/4$ layers, reflectivity $R_2 = 99.9\,\%$

High resonator efficiency, small gain medium volume $\rightarrow I_{th} \sim$ mA

Modulators

Electro-Absorption Modulator (EAM) — QCS

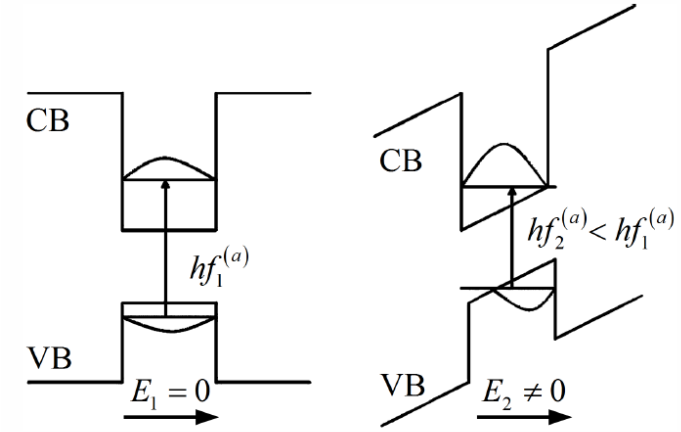

(a) Energy-band diagram of double-heterostructure quantum film with and without applied electric field $E_{1,2} \sim V_b$ (bias voltage V_b)

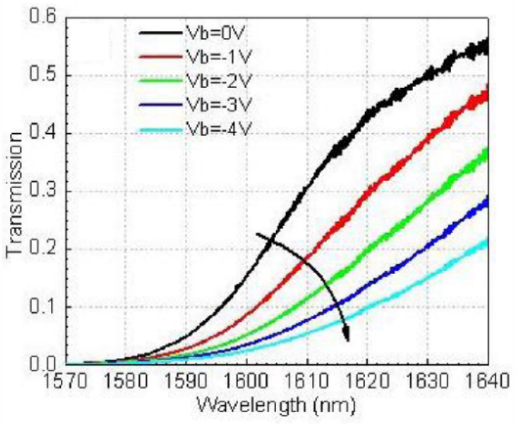

(b) Measured transmission spectra of a Ge electro-absorption modulator for various bias voltages V_b

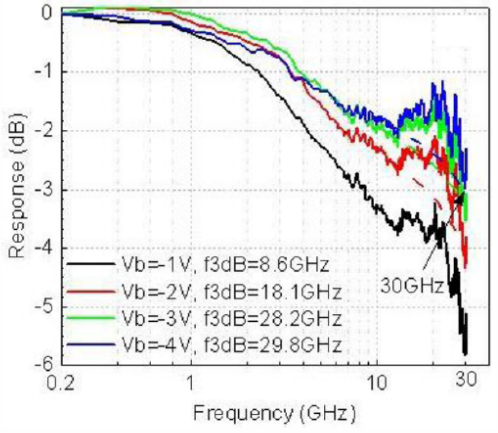

(c) Measured frequency response of a Ge electro-absorption modulator for various bias voltages V_b

Fig. 3.27. Electro-absorption modulator based on the quantum-confined Stark effect. (a) Energy-band diagrams of a quantum film with and without a bias field. The tilt of the band diagram reduces the energy difference between the (schematicall drawn) electronic wave function in the conduction band (CB) and the hole wave function in the valence band (VB) from a photon absorption energy of $hf_1^{(a)}$ to $hf_2^{(a)} < hf_1^{(a)}$. [Modified from Reference 60, Fig 4] (b) Transmission spectra of an electro-absorption modulator and its (c) frequency response for various bias voltages [after Ref. 61, Figs. 3(a) and 4(a)]

Electro-Optic Modulator

An electro-optic modulator makes use of the electro-optic effect or Pockels[62] effect, where the second-order nonlinear susceptibility $\chi^{(2)}$ enables a change of the refractive index n for an optical wave E_{opt} in proportion to a "low" radio-frequency (RF) controlling field E_{RF}, which is in proportion of a controlling voltage V,

$$n \sim E_{\mathrm{RF}} \sim V \sim \vartheta. \tag{3.120}$$

This can be also concluded from Eq. (A.10) on Page 148 and the following text. If a guided wave propagates in the Pockels medium, the optical phase ϑ is shifted according to the controlling voltage V and the length of the phase shifter region. Importantly, the Pockels effect reacts virtually instantaneously to the controlling voltage. In addition, the usual Pockels media are lossless in the wavelength region of interest. Frequently used $\chi^{(2)}$-media are lithium niobate ($LiNbO_3$), gallium arsenide (GaAs) and $\chi^{(2)}$-nonlinear organic materials[63,64].

Other options are using the plasma dispersion effect[65,66] in depleted pn-junctions, or the injection of carriers into pn-junctions. Both, depletion and injection of charge carriers in an active volume, changes the refractive index in this region. However, the plasma dispersion effect is never lossless (hence cannot realize a pure phase modulation), and it suffers from speed limitations due to the finite carrier lifetime.

Directional Coupler — Four-Port Scattering Matrix

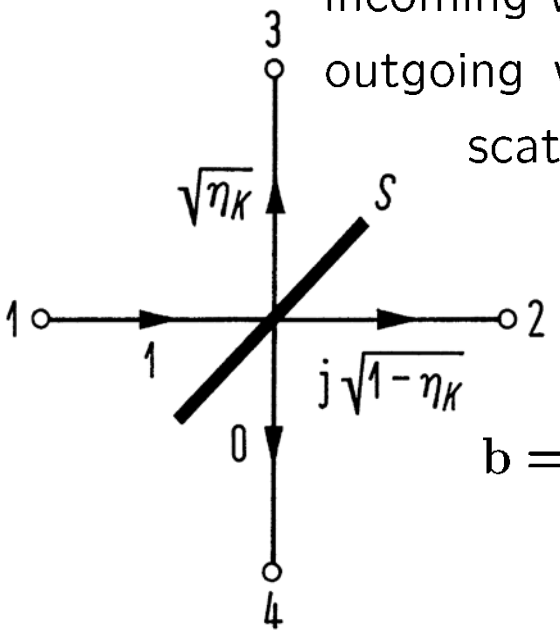

incoming wave ampl. at ith port: a_i → column matrix $\mathbf{a}$

outgoing wave ampl. at ith port: b_i → column matrix $\mathbf{b}$

scattering matrix elements: S_{mn} → square matrix $\mathbf{S}$

$$\mathbf{b} = \mathbf{S}\,\mathbf{a}$$

$$\mathbf{b} = \begin{pmatrix} b_1 \\ b_2 \\ b_3 \\ b_4 \end{pmatrix}, \quad \mathbf{S} = \begin{pmatrix} S_{11} & S_{12} & S_{13} & S_{14} \\ S_{21} & S_{22} & S_{23} & S_{24} \\ S_{31} & S_{32} & S_{33} & S_{34} \\ S_{41} & S_{42} & S_{43} & S_{44} \end{pmatrix}, \quad \mathbf{a} = \begin{pmatrix} a_1 \\ a_2 \\ a_3 \\ a_4 \end{pmatrix}$$

Lossless four-port:

$\mathbf{S}^\dagger\mathbf{S} = \mathbf{I}$ (= unity)

$\sum_{i=1}^{4} S_{i\,m}^* S_{i\,n} = \delta_{m\,n}$

$$|S_{21}|^2 + |S_{31}|^2 = 1\,,$$
$$S_{21}^* S_{31} + S_{21} S_{31}^* = 0\,,$$

Symmetrical and matched → directivity ∞:

$$\mathbf{S} = \begin{pmatrix} 0 & S_{21} & S_{31} & 0 \\ S_{21} & 0 & 0 & S_{31} \\ S_{31} & 0 & 0 & S_{21} \\ 0 & S_{31} & S_{21} & 0 \end{pmatrix}$$

$$\Re\{S_{21}^* S_{31}\} = 0 \;\rightarrow\; S_{31} = \sqrt{\eta_K},\; S_{21} = j\sqrt{1-\eta_K}$$

Mach-Zehnder Modulator (1)

Such a pure phase modulator becomes significantly more versatile when inserted into the arms of a Mach[67]-Zehnder[68] interferometer (MZI) as in Fig. 3.28(a). The transfer function of a MZI modulator (Mach-Zehnder modulator for short, MZM) can be easily calculated when taking into account that the power is split (and combined) evenly between the arms, i. e., the fields have a split (or combine) factor of $1/\sqrt{2}$.

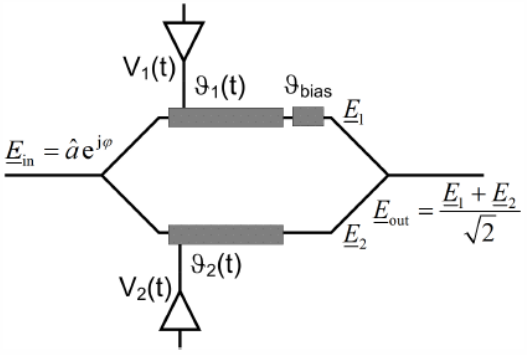

(a) Mach-Zehnder interferometer modulator with voltage-controlled modulator sections in both arms

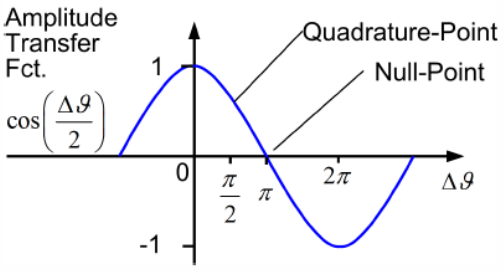

(b) Amplitude transfer function in dependence of the phase difference $\Delta\vartheta$ in both arms

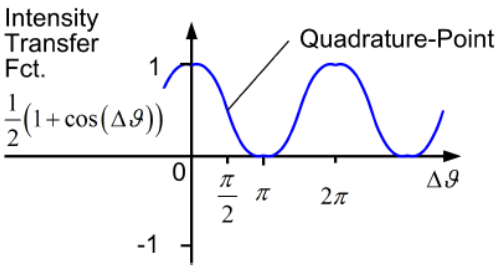

(c) Intensity transfer function in dependence of the phase difference $\Delta\vartheta$ in both arms

Fig. 3.28. Schematic and characteristics of an electro-optic modulator in form of a Mach-Zehnder interferometer (MZI) with phase modulators in both arms based on the Pockels effect. (a) Schematic of a Mach-Zehnder interferometer with input waveguide splitter, phase modulator sections $\vartheta_{1,2}(t)$, bias phase adjustment ϑ_{bias}, optical electric fields $E_{1,2}(t)$ at the outputs of both arms, and output waveguide combiner. Electrical amplifiers supply the control voltages $V_{1,2}(t)$. (b) Amplitude transfer function of an MZI push-pull modulator as a function of the phase difference $\Delta\vartheta = \vartheta_1 + \vartheta_{\text{bias}} - \vartheta_2$ in both arms. (c) Intensity transfer function of an MZI push-pull modulator as a function of the phase difference $\Delta\vartheta = \vartheta_1 + \vartheta_{\text{bisas}} - \vartheta_2$ in both arms [modified from Fig. 2.21(a) and 2.22 of Ref. † on the Preface page]

Mach-Zehnder Modulator (2)

With this information, the complex amplitude at the interferometer output reads in matrix notation (using also a column and a row matrix)

$$\underline{E}_{\text{out}} = \begin{pmatrix} 1/\sqrt{2} & 1/\sqrt{2} \end{pmatrix} \begin{pmatrix} \mathrm{e}^{\mathrm{j}(\vartheta_1+\vartheta_{\text{bias}})} & 0 \\ 0 & \mathrm{e}^{\mathrm{j}\,\vartheta_2} \end{pmatrix} \begin{pmatrix} 1/\sqrt{2} \\ 1/\sqrt{2} \end{pmatrix} \underline{E}_{\text{in}} \,. \tag{3.121}$$

From Eq. (3.121) the amplitude transfer function $\underline{T}$ follows,

$$\underline{T} = \frac{\underline{E}_{\text{out}}}{\underline{E}_{\text{in}}} = \mathrm{e}^{\mathrm{j}\left(\frac{\vartheta_1+\vartheta_2}{2}+\frac{\vartheta_{\text{bias}}}{2}\right)} \cos\left(\frac{\Delta\vartheta}{2}\right), \qquad \Delta\vartheta = \vartheta_1 - \vartheta_2 + \vartheta_{\text{bias}} \,. \tag{3.122}$$

When varying $\vartheta_{1,2}$, both, the phase and the amplitude of $\underline{T}$ change. However, if $\vartheta_1 = -\vartheta_2$ is chosen, i. e., if $V_1 = -V_2$ holds, the phase factor remains constant (but the sign of $\underline{T}$ could change). This so-called push-pull operation mode is most common. If $\vartheta_1 = \vartheta_2$ is maintained in push-push mode, we have a pure phase modulator.

In the following, we concentrate on push-pull operation, for which the field transfer characteristic is displayed in Fig. 3.28(b), (c). The bias determines the operating point. For an optimum field linearity it has to be chosen at the null-point. The quadrature-point is optimum for intensity linearity, where the intensity transfer characteristic is

$$|\underline{T}|^2 = \left|\frac{\underline{E}_{\text{out}}}{\underline{E}_{\text{in}}}\right|^2 = \cos^2\left(\frac{\Delta\vartheta}{2}\right) = \frac{1}{2}\left(1+\cos\Delta\vartheta\right), \qquad \Delta\vartheta = \vartheta_1 - \vartheta_2 + \vartheta_{\text{bias}} \,. \tag{3.123}$$

The characteristic Eq. (3.123) is displayed in Fig. 3.28(c).

Optical IQ-Modulator (1)

For optical IQ-modulation we need to realize the scheme as discussed in Sect. 2.3.2 on Page 28 ff. To this end we use two MZM nested in a MZI, Fig. 3.29. The control voltages $V_1(t)$ and $V_2(t)$ represent the in-phase and quadrature signals $I(t)$ and $Q(t)$, respectively, as specified in Eq. (2.43) on Page 28. The combiners in Fig. 2.7 are assumed to perform a *summation* (factors $1/\sqrt{2}$ are omitted), and the phase $\vartheta_{\text{bias}} = \pi/2$ *advances* the local oscillator (LO) signal $\cos(\omega_0 t)$ to be $-\sin(\omega_0 t)$.

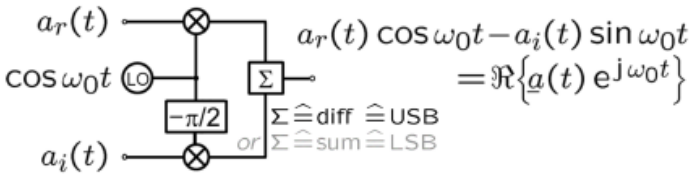

(a) IQ-modulator for encoding real and imaginary data on two orthogonal carriers (Σ ≙ subtract)

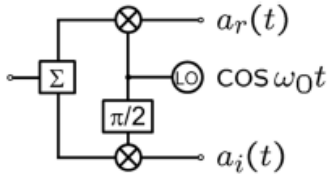

(b) IQ-demodulator for complex data (Σ ≙ split)

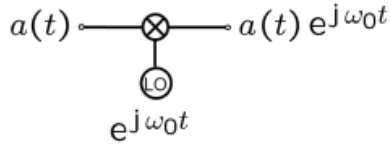

(c)Modulation of a complex carrier with complex data

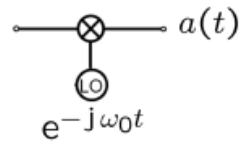

(d)Demodulation of complex data

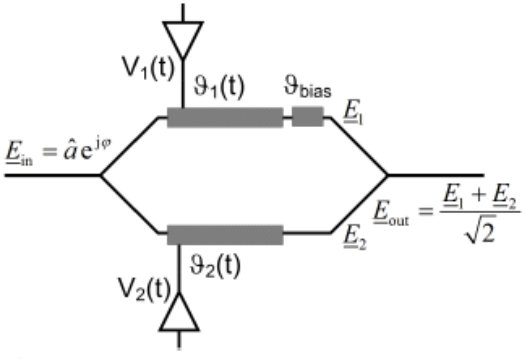

(a) Mach-Zehnder interferometer modulator with voltage-controlled modulator sections in both arms

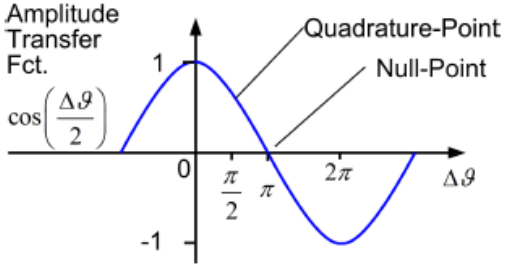

(b) Amplitude transfer function in dependence of the phase difference $\Delta\vartheta$ in both arms

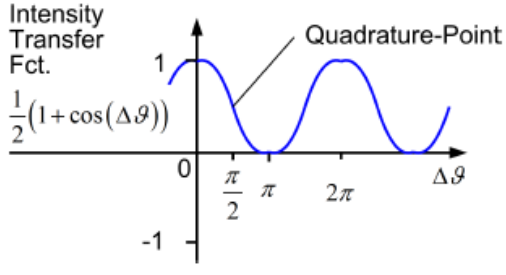

(c) Intensity transfer function in dependence of the phase difference $\Delta\vartheta$ in both arms

LECTURE 12

Optical IQ-Modulator (2)

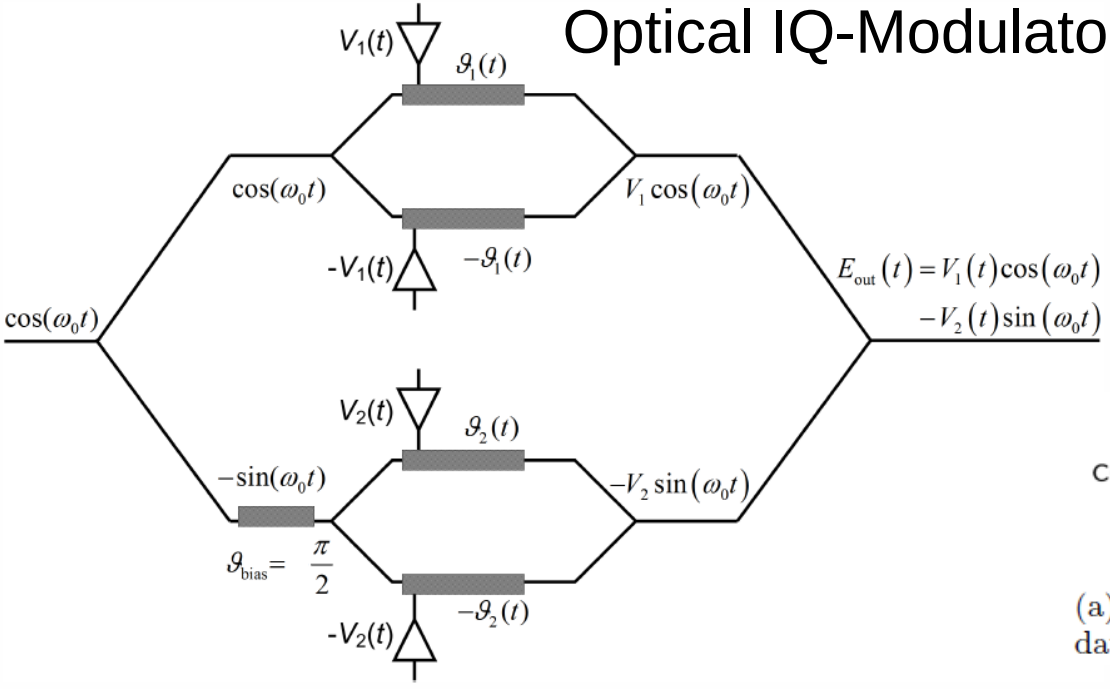

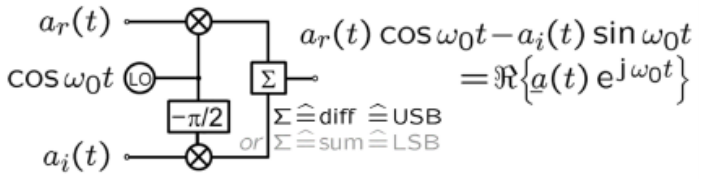

(a) IQ-modulator for encoding real and imaginary data on two orthogonal carriers ($\Sigma \widehat{=}$ subtract)

Fig. 3.29. Optical IQ-modulator with two push-pull Mach-Zehnder interferometer modulators nested in a Mach-Zehnder interferometer. The control voltages $V_1(t)$ and $V_2(t)$ represent the in-phase and quadrature signals $I(t)$ and $Q(t)$, respectively, as specified in Eq. (2.43) on Page 27. [Modified from Fig. 2.25 of Ref. † on the Preface page]

we use two MZM nested in a MZI, Fig. 3.29. The control voltages $V_1(t)$ and $V_2(t)$ represent the in-phase and quadrature signals $I(t)$ and $Q(t)$, respectively, as specified in Eq. (2.43) on Page 27. The combiners in Fig. 2.6 are assumed to perform a *summation* (factors $1/\sqrt{2}$ are omitted), and the phase $\vartheta_{\text{bias}} = \pi/2$ *advances* the local oscillator (LO) signal $\cos(\omega_0 t)$ to be $-\sin(\omega_0 t)$.

$$\underline{E}_{\text{out}} = (V_1 + \mathrm{j}\,V_2)\,\mathrm{e}^{\mathrm{j}\,\omega_0 t}, \qquad E_{\text{out}} = \Re\{\underline{E}_{\text{out}}\} = V_1\cos(\omega_0 t) - V_2\sin(\omega_0 t)\,. \tag{3.124}$$

Implementation of Selected Modulation Formats

Implementation of Modulation Formats — NRZ-OOK

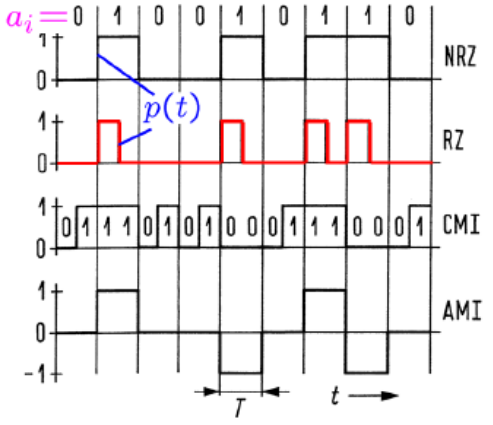

(a) Temporal signal shapes for ASK modulation formats

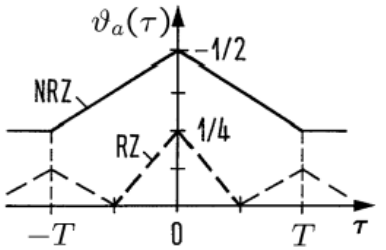

(b) Autocorrelation functions for NRZ and RZ

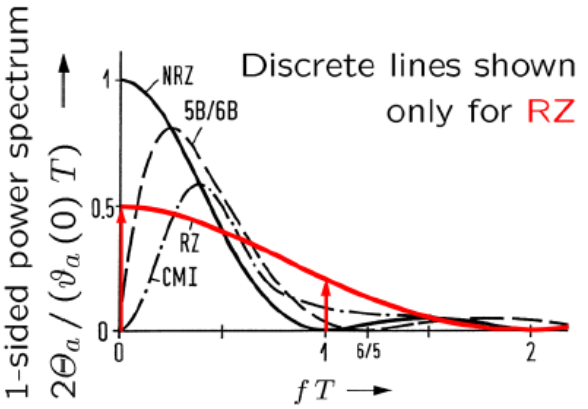

(c) Spectra for random bit sequences encoded with different modulation formats

Amplitude-shift keying (ASK) formats, autocorrelation functions of random non-return-to-zero (NRZ) and return-to-zero (RZ) data, and one-sided power spectra for some modulation formats. (a) Binary data $a_i \in \{0, 1\}$, encoded with the formats NRZ, RZ, coded mark inversion (CMI), and alternate mark inversion (AMI, a pseudo-ternary

- Directly modulating a laser diode by switching the injection current. Directly modulated lasers (DML) can be operated with data rates up 20 Gbit/s. However, significant chirp leads to distortions due to increased chromatic dispersion in the transmitting fiber.

- Externally modulating a CW laser diode with an electro-absorption modulator. This technique is good for data rates up to 40 Gbit/s. Again, a relatively small chirp associated with the absorption change limits the signal quality.

- Externally modulating a CW laser diode with a MZI modulator. This technique is used for data rates up to 40 Gbit/s. Time division multiplexing techniques enable operation up to 160 Gbit/s. If used in push-pull operation mode, there is basically no chirp.

Implementation of Modulation Formats — RZ-OOK (1)

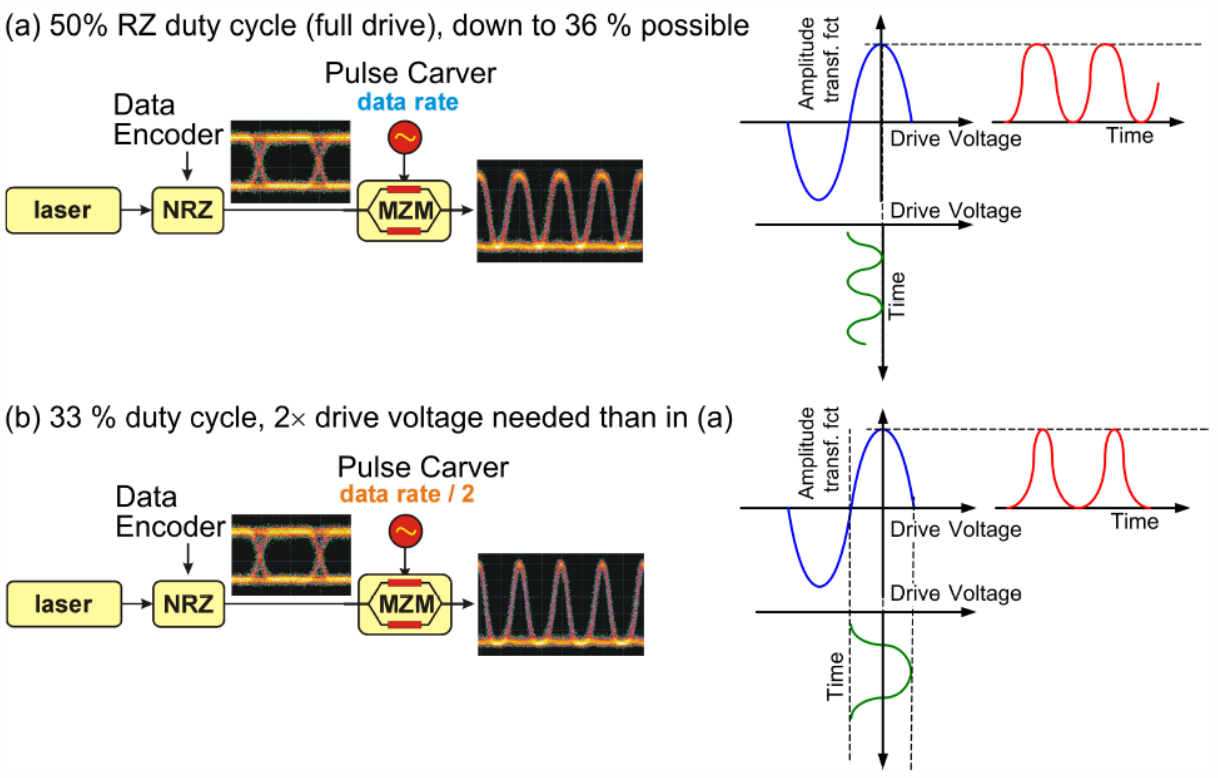

Fig. 3.30. Implementation of RZ-OOK with a pulse "carver" driven in synchronism with the data by a sinusiodal voltage. Eye diagrams of NRZ and resulting RZ data are shown as insets. (a) Pulse carver for RZ pulses with 50 % duty cycle (b) Pulse carver for RZ pulses with 33 % duty cycle. In this case, the drive voltage is twice the drive voltage for a 50 % duty cycle. [Modified from Fig. 2.32 of Ref. † on the Preface page]

Implementation of Modulation Formats — RZ-OOK (2)

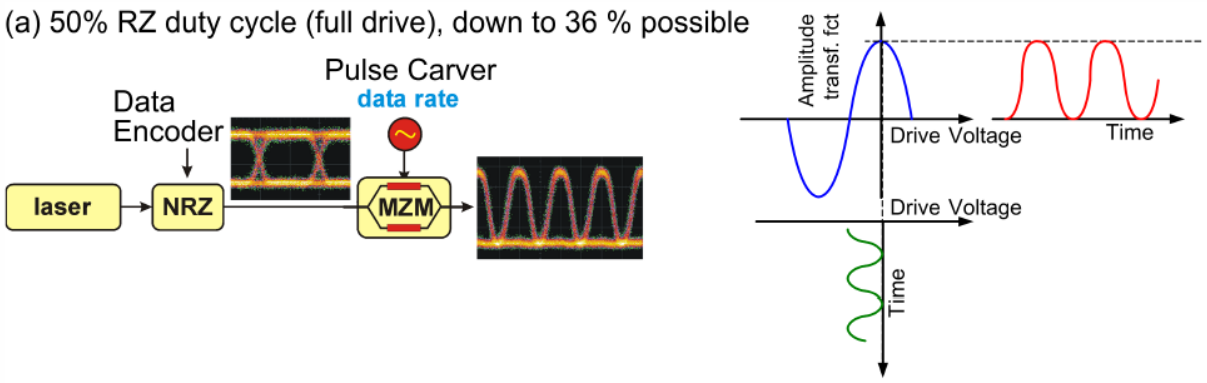

What are the advantages of using RZ-OOK over NRZ-OOK for transmission? The answer is that the RZ format has a receiver sensitivity advantage of about 1 . . . 3 dB. This is a significant improvement, since a 3 dB advantage translates in doubling the transmission distance. The reasons for this improvement are:

- For the same average power, a RZ signal has more power within the pulse centre where sampling takes place. This gives a RZ format a typical 2 dB advantage. This is due to the fact that in a RZ signal all of the energy is confined to within part of a symbol slot. As a drawback, nonlinearities due to high peak powers can lead to degradation.
- Second, RZ signals suffer less from inter-symbol interference (ISI), since leading and trailing edges of the pulse do not easily extend into neighbouring time slots.

One now might wonder if reducing the duty cycle below 33 % will bring an additional advantage (let aside fibre nonlinearities). However, narrower pulse require a larger receiver bandwidth, and this means more noise, so that a 33 % duty cycle is near optimum.

Duobinary and Alternate Mark Inversion (1)

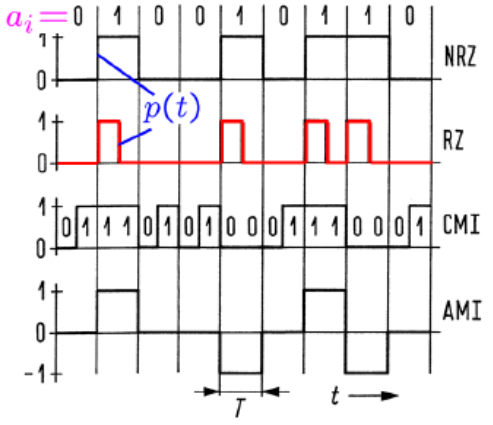

(a) Temporal signal shapes for ASK modulation formats

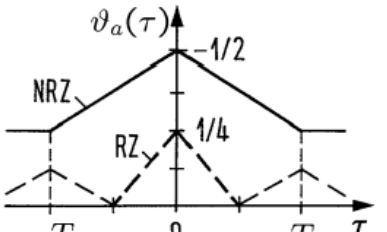

(b) Autocorrelation functions for NRZ and RZ

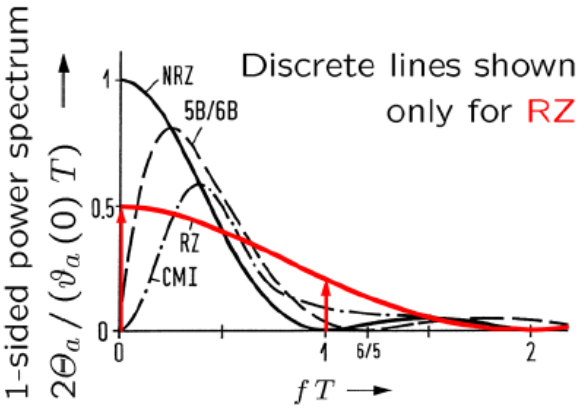

(c) Spectra for random bit sequences encoded with different modulation formats

Amplitude-shift keying (ASK) formats, autocorrelation functions of random non-return-to-zero (NRZ) and return-to-zero (RZ) data, and one-sided power spectra for some modulation formats. (a) Binary data $a_i \in \{0, 1\}$, encoded with the formats NRZ, RZ, coded mark inversion (CMI), and alternate mark inversion (AMI, a pseudo-ternary

Duobinary (DB) and alternate mark inversion (AMI) signals are bipolar binary signals. As discussed in Sect. 2.4.2 on Page 40 they employ the three-level signalling set $\{-1, 0+1\}$, where the optical phases of the individual bits additionally depend on the bit pattern: For DB signaling, a phase change occurs whenever there is an odd number of logical 0 between two successive logical 1, whereas for AMI the phase changes for each logical 1 (even for adjacent logical 1), independent of the number of logical 0 in-between. Chirp-free optical DB and AMI signals are obtained when operating the MZI in push-pull mode.

Duobinary and Alternate Mark Inversion (2)

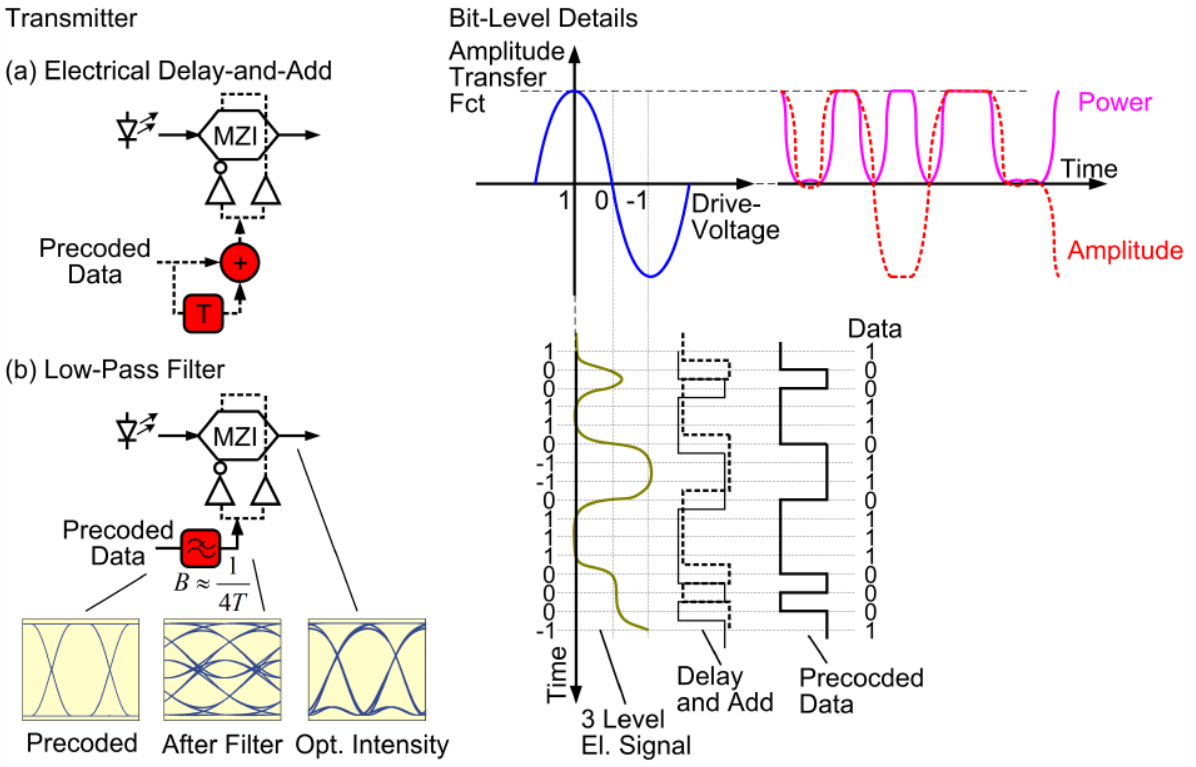

Fig. 3.31. Transmitter for duobinary signals with precoder and (a) delay-and-add circuit, or (b) low-pass filter with bandwidth $B \approx 1/(4T)$ equal to about one quarter of the symbol rate for generating three-level signals [modified from Fig. 2.49 and 2.50 of Ref. † on the Preface page]

For DB signaling, a phase change occurs whenever there is an odd number of logical 0 between two successive logical 1, whereas for AMI the phase changes for each logical 1 (even for adjacent logical 1), independent of the number of logical 0 in-between. Chirp-free optical DB and AMI signals are obtained when operating the MZI in push-pull mode.

Duobinary and Alternate Mark Inversion (3)

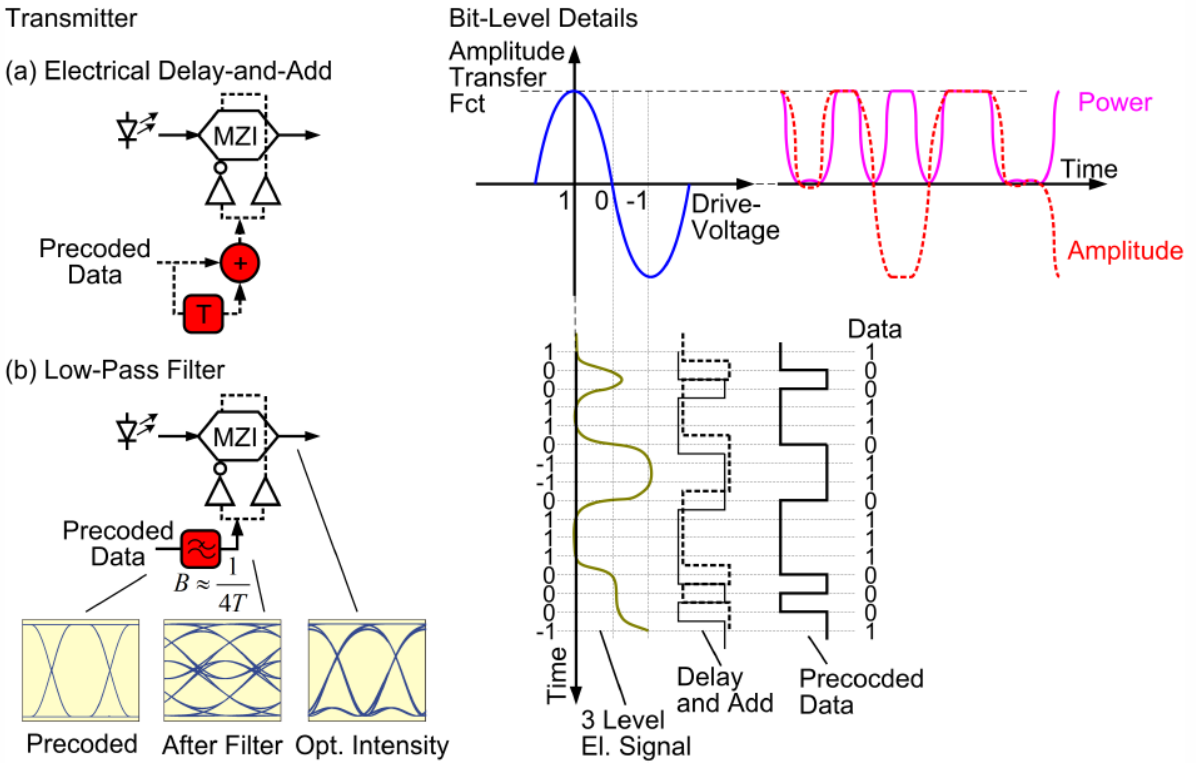

- Precoding of data by differential encoding. For each occurrence of a logical 0 there is a transition of the electrical level. Logical 1 leaves the previous electrical level unchanged.
- The thus generated precoded drive voltage is added (DB, Fig. 3.31(a)) or subtracted (AMI, not shown) from the 1 bit-delayed replica of itself. Alternatively, a low-pass filter with a bandwidth $B \approx 1/(4T)$ equal to about one quarter of the symbol rate serves the same purpose, Fig. 3.31(b).
- This three-level signal controls the MZI modulator, which is operated in push-pull and biased at $\vartheta = \pi/4$.

Polarization Mode Shift Keying (PMSK)

If two orthogonal polarizations (DP) carry independent information, the effective data rate can be doubled when compared to transmission in a single polarization (SP). If not capacity, but sensitivity is of primary importance, polarization mode shift keying (PMSK) in the form of polarization switching (PS) is of interest. Particularly the PS-QPSK format is very noise resilient[70]. Figure 3.32 shows a PS-QPSK

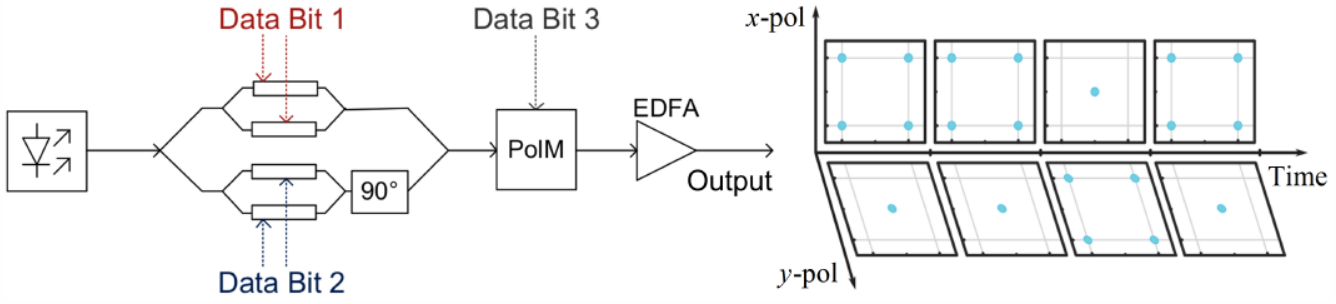

Fig. 3.32. Transmitter for polarization mode shift keying (PMSK), here polarization switching (PS). The example shows QPSK encoding (2 bit), which can appear in either of two polarizations (1 bit) named x-pol and y-pol, respectively. Thus, 3 bit are transmitted in each symbol period. The QPSK constellations illustrate the polarization switching. The central dot represents a zero electric field and indicates that no signal is transmitted in this very polarization. [Modified from Fig. 2.59 of Ref. † on the Preface page]

transmitter along with the constellation diagrams in both polarizations. A single dot in the centre indicates that this polarization has a zero field strength at this very moment. The modulation format worked well[71] for a data rate of 112 Gbit/s (symbol rate 37.3 GBd, 3 bit / symbol.

Software-Defined Transmitter

What is Software-Defined Optical Transmission?

Software-define optical transmission (SDO):

- Frowin Derr (1991): Concept of digital demodulation for optical communications

Software-defined radio (SDR):

- Joseph Mitola III (1993): Set of DSP primitives combined into transmitter, channel model, receiver, plus set of target processors for real-time hosting SDR

Transfering the SDR idea to optics: What could providers expect?

- High data rates, optimum spectral efficiency
- Universal Tx and Rx with reprogrammable DSP for optimum network utilization (applications, channel requirements, QoS) by choosing multi-carrier and multilevel modulation
- SDO promises quick time-to-market.

F. Derr, Electron. Lett., vol. 27, no. 23, pp. 2177–2179, Nov. 1991
J. Mitola III, IEEE AES Systems Magazine, vol. 8, no. 4, pp. 25–26, April 1993
C. Glingener, Proc. OFC'11, March 6–10, 2011, Los Angeles (CA), USA. Paper OThAA1

Software-Defined Optical Transmission – Advantages and Issues

Shannon's limiting channel capacity C (signal/noise power ratio S/N, channel bandwidth B):

- $C = B \log_2\left(1 + \frac{S}{N}\right) = B \times 3.32 \lg\left(1 + \frac{S}{N}\right)$
- To approach C: Multilevel (M-ary) modulation
- Then, S/N reduces (symbols more closely spaced)

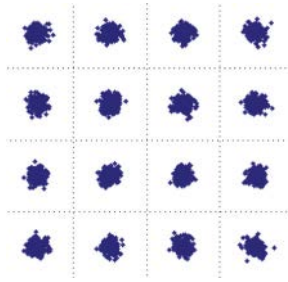

- Improvement with FEC (correcting errors by redundancy), improves S/N by coding gain γ
- Modulation formats not easily handled by hard-wired circuitry
- Electronic digital signal processing (DSP) required (FEC, M-ary, FFT, ...)

- FFT is electronic bottleneck for OFDM systems
- Optical FFT overcomes this issue

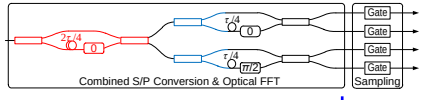

Performance of State-of-the-Art FPGA and DAC

SDOTx: Mltfmt 168 Gbit/s, OFDM 101 Gbit/s, OTDM 56 Gbit/s

- 6 bit DAC resolution, 28 GBd
- 168 Gbit/s data throughput to DAC
- Virtex-5 FPGA, 195 MHz, 17 % of chip area busy

New-generation FPGA: FFT with $N = 256$

- 6 bit input, 14 bit output resolution for $\Re$ and $\Im$ each
- 97.5×10^6 transfers / s
- Virtex-6 FPGA, 390 MHz, 24 % of chip area busy (88 410 LUT)

New-generation DAC: InP DHBT, 3 bit, 42 GBd

- 3 D-flip-flops directly drive an active combiner
- No analogue amplifiers
- Direct drive of MZM

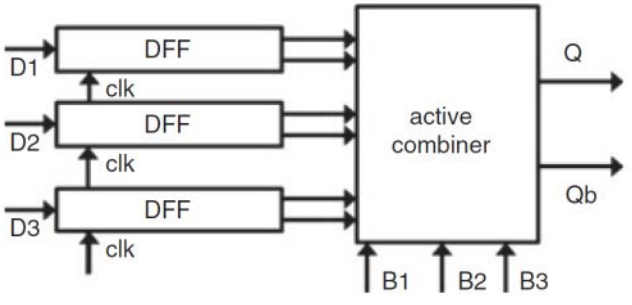

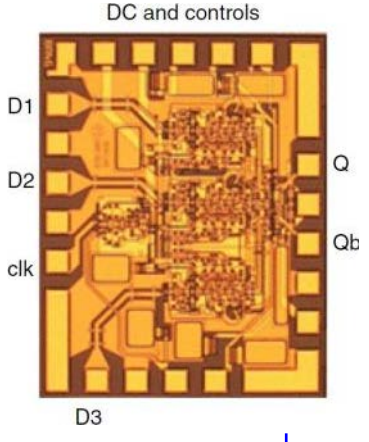

A. Konczykowska, J.-Y. Dupuy, F. Jorge, M. Riet, J. Moulu, V. Nodjiadjim, P. Berdaguer, J. Godin: 42 GBd 3-bit power-DAC for optical communications with advanced modulation formats in InP DHBT. Electron. Lett. 47 (2011) 389–390

Modulator Directly Driven By FPGA Board Without Amplifier

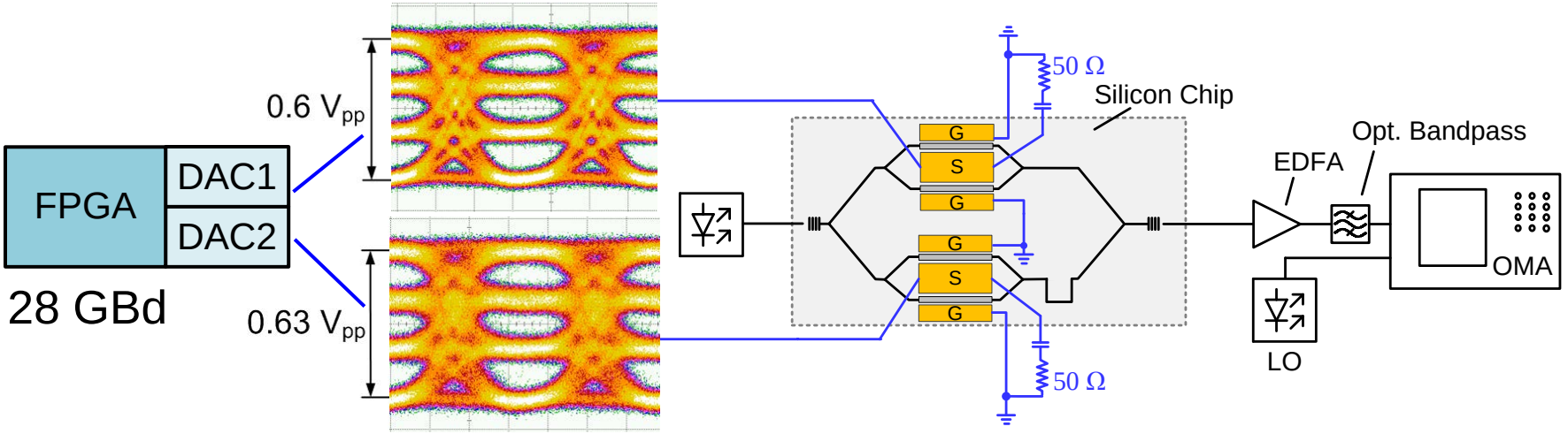

- Regular constellation, no amplitude-phase coupling
- Record-low BER for 16QAM, 28GBd in silicon, far below hard-decision FEC

16QAM, 112 Gbit/s

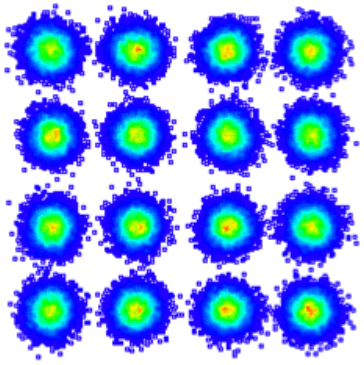

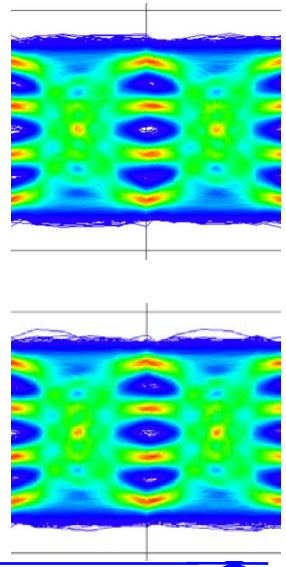

EVM = 8.7 %

BER = 5.1×10^{-5}

Lauermann, M.; Palmer, R.; Koeber, S.; Schindler, P.; Korn, D.; Wahlbrink, T.; Bolten, J.; Waldow, M.; Elder, D.; Dalton, L.; Leuthold, J.; Freude, W.; Koos, C.: '16QAM silicon-organic hybrid (SOH) modulator operating with 0.6 Vpp and 19 fJ/bit at 112 Gbit/s,' *Conf. on Lasers and Electro-Optics (CLEO'14)*, San Jose (CA), USA, June 8–13, 2014. Paper SM2G.6 (**invited**)

Modulator Driven By FPGA Board Without DAC and Amplifier

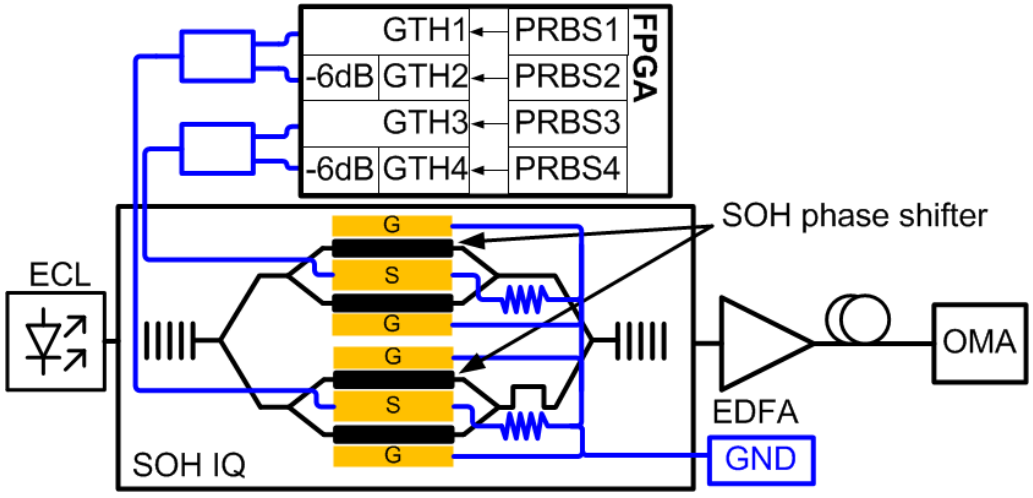

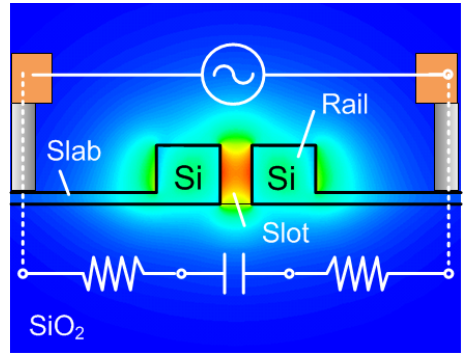

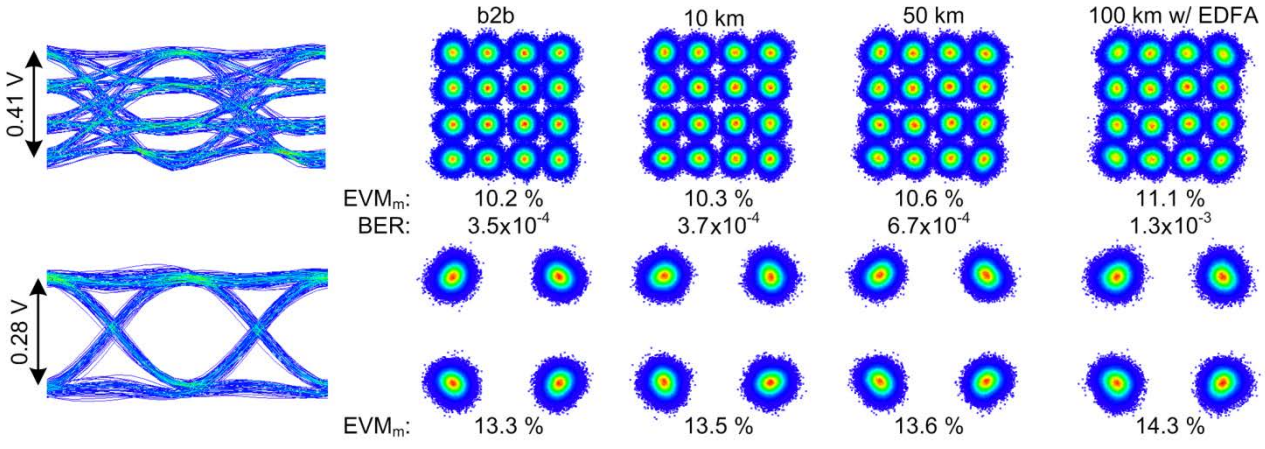

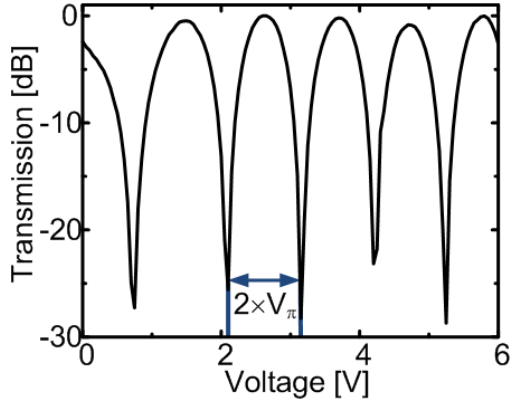

Wolf, S.; Schindler, P. C.; Ronniger, G.; Lauermann, M.; Palmer, R.; Koeber, S.; Korn, D.; Bogaerts, W.; Leuthold, J.; Freude, W.; Koos, C.: '10 GBd SOH modulator directly driven by an FPGA without electrical amplification,' 40th European Conf. Opt. Commun. (ECOC'14), Cannes, France, Sept. 21–25, 2014. **Postdeadline Paper PD.4.5**

Software-Defined Transmitter (1)

So far, each modulation format required a specific hardware setup. It would be more convenient, if the same hardware could produce a variety of modulation formats. This task is solved by a software-defined transmitter as shown in Fig. 3.33. Inside 5 ns and without loosing any data, this transmitter[72] can switch to a different modulation format. The field-programmable gate arrays (FPGA) generate two digital signal streams, which are then converted to analogue voltages by digital-to-analog converters (DAC). The resulting analogue drive voltages control the phase modulator sections of the optical IQ-modulator.

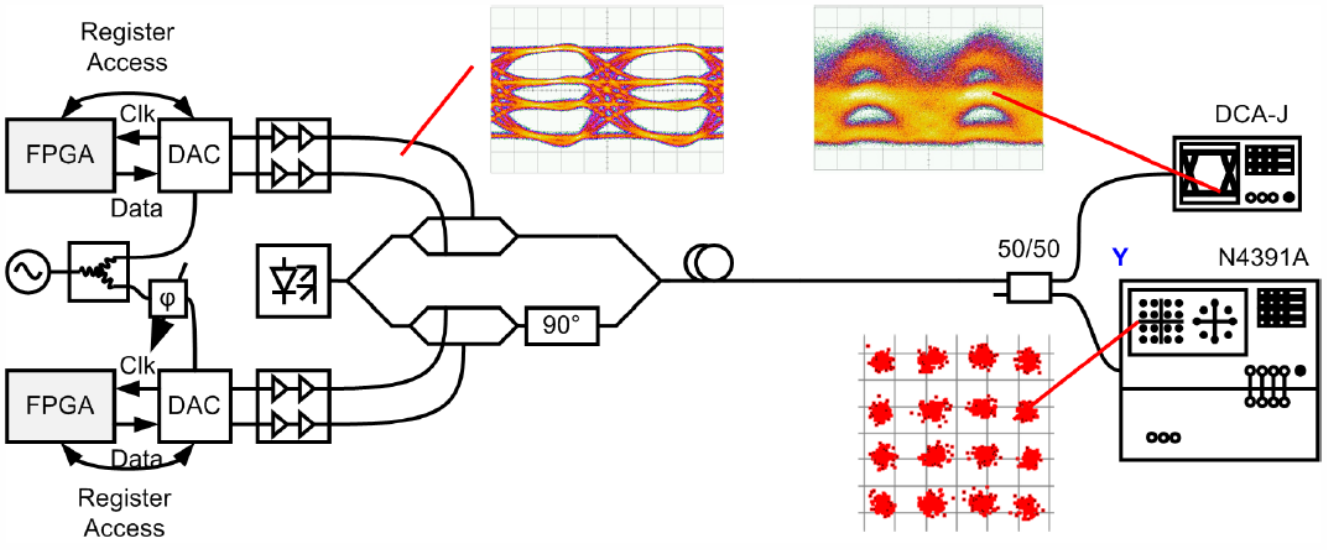

Fig. 3.33. Software-defined transmitter with field-programmable gate arrays (FPGA), digital-to-analogue converters (DAC), laser and optical IQ-modulator, and receiver (DCA, digital communications analyzer and optical modulation analyzer).

While the approach Fig. 3.33 is most versatile, it would be useful to find configurations without the DAC and their electrical drive circuitry. This would require to translate each and every binary electrical signal directly into an optical constellation. However, this puts much more complexity to the optical modulators.

Software-Defined Transmitter (2)

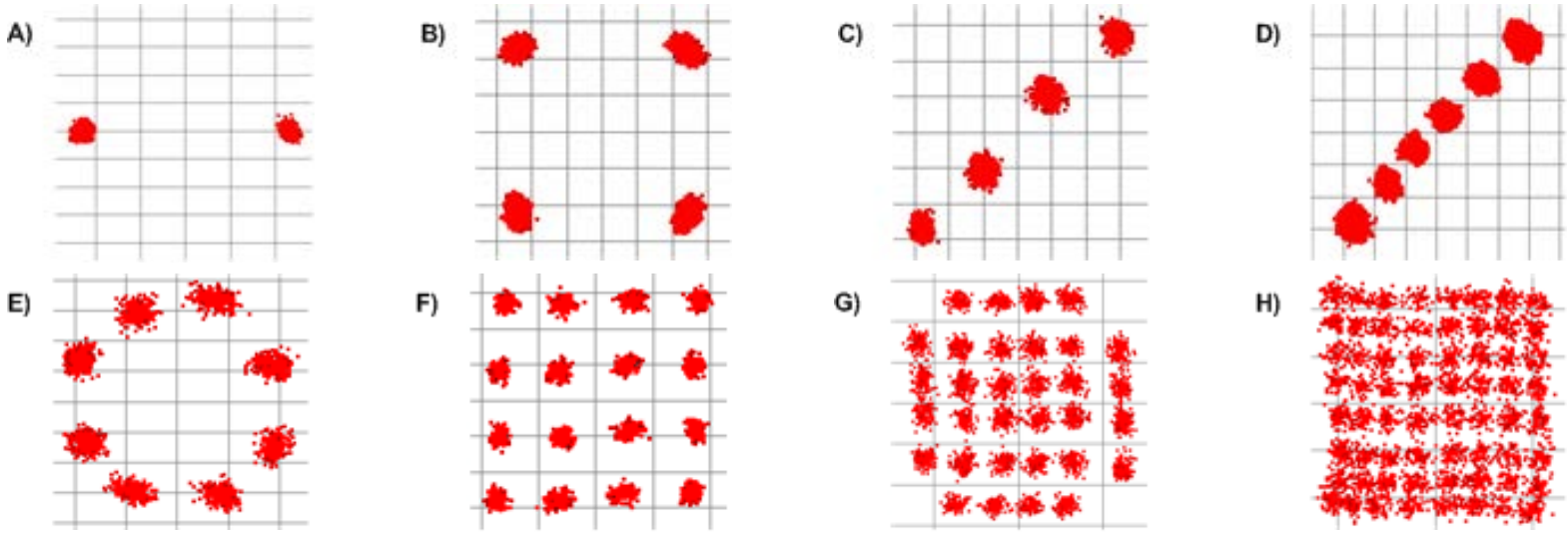

Received constellation diagrams:

A) BPSK at 28 GBd with EVM = 5.7 % (no errors)
B) QPSK at 28 GBd with EVM = 8.5 % (no errors)
C) 4PAM at 20 GBd
D) 6PAM at 20 GBd
E) 8PSK at 28 GBd with EVM = 12.5 % (no errors)
F) 16QAM at 28 GBd with EVM = 8.6 % (no errors)
G) 32QAM at 28 GBd with EVM = 9.1 %
H) 64QAM at 28 GBd with EVM = 10.1 %

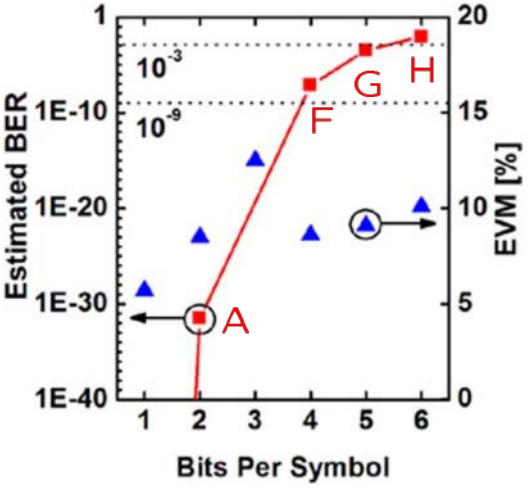

R. Schmogrow, D. Hillerkuss, M. Dreschmann, M. Huebner, M. Winter, J. Meyer, B. Nebendahl, C. Koos, J. Becker, W. Freude, J. Leuthold: Real-time software-defined multiformat transmitter generating 64QAM at 28 GBd. IEEE Photon. Technol. Lett. 22 (2010) 1601–1602

Optical Amplifiers

Laser Diode (LD) — Cavity and Longitudinal Modes

Conventional laser diode (LD) has rectangular cavity → Fabry-Perot (FP) resonator → Fabry-Perot laser diode (FP LD).

Active volume $V = dbL$ dimensions $d = 0.1 \ldots 0.2\,\mu$m (vertical, x-axis), $b = 2 \ldots 5\,\mu$m (lateral, y-axis), $L = 300 \ldots 1\,200\,\mu$m, (longitudinal, z-axis).

Longitudinal mode spacing (FSR, round-trip time τ_U, group refractive index n_g):

$$\Delta f_z = \frac{c}{2 n_g L} = \frac{v_g}{2L} = \frac{1}{\tau_U}$$

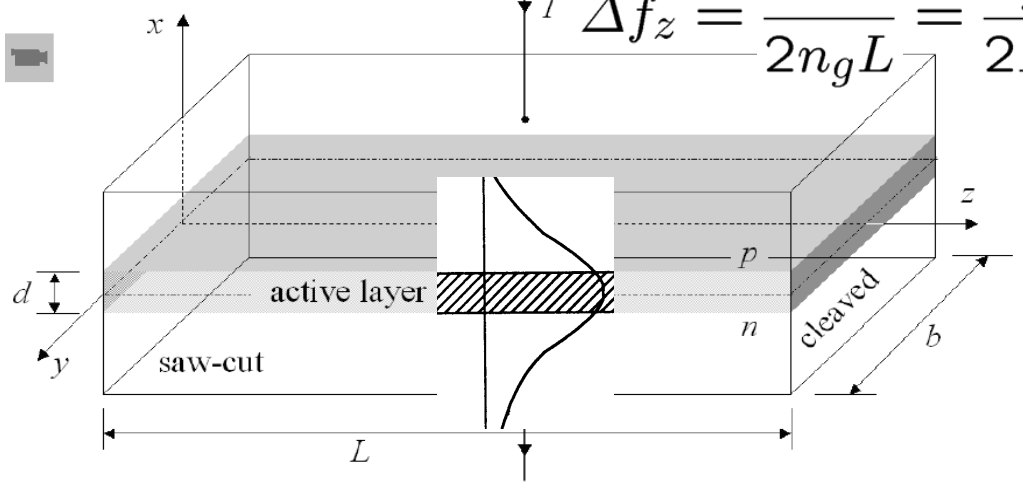

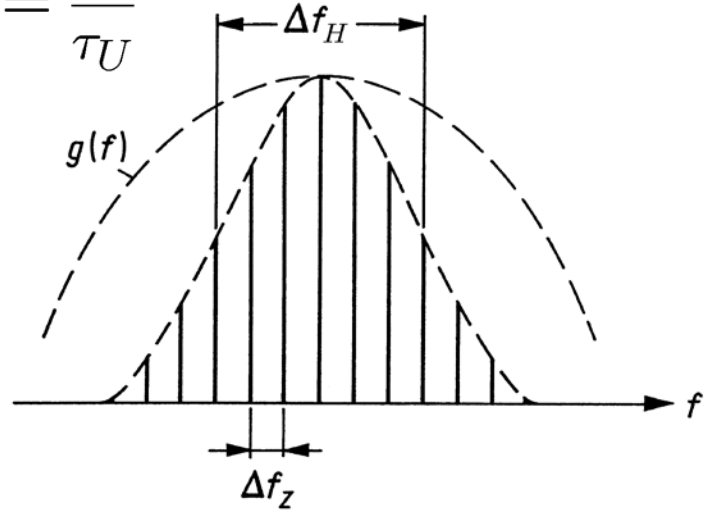

Forward biased semiconductor pn-homojunction acting as a laser diode. Side-walls are saw-cut, the end facets are cleaved. Typical dimensions: $d = 0.1 \ldots 0.2\,\mu$m (active layer), $b = 3 \ldots 6\,\mu$m, $L = 200 \ldots 600\,\mu$m

LD Mirrors Removed — Semiconductor Optical Amplifier (SOA)

Gain relations of Fabry-Perot laser:

$$\exp(-\mathrm{j}\,\bar{k}z), \qquad \left\{ \begin{array}{l} \bar{k} = k_0\bar{n} = k + \frac{1}{2}\mathrm{j}\,(g - \alpha_V), \\ \bar{n} = n - \mathrm{j}\,n_i, \\ k_0 = \omega/c, \end{array} \right\}, \qquad g - \alpha_V = -2\,k_0 n_i$$

$$G - \frac{1}{\tau_P} = \frac{1}{N_P}\frac{\mathrm{d}N_P}{\mathrm{d}t}, \qquad \frac{N_P(\tau_U)}{N_P(0)} = \exp\left[\left(G - \frac{1}{\tau_P}\right)\tau_U\right], \qquad \tau_U = \frac{2L}{v_g}$$

$$\exp\Big[(G - 1/\tau_P)\tau_U\Big] = R_1 R_2 \exp\Big[(g - \alpha_V)2L\Big]$$

SOA with distributed single-pass gain $\mathcal{G}_s$:

$$\mathcal{G}_s = \exp\left[(\Gamma g - \alpha_{Ve})\,L\right], \qquad \varphi = \beta L = k_0 n_e L$$

Residual mirror reflectivities $R_{1,2} \neq 0 \rightarrow$ FP amplification factor $\mathcal{G}$:

$$\mathcal{G} = \frac{\mathcal{G}_s(1 - R_1)(1 - R_2)}{\left(1 - \mathcal{G}_s\sqrt{R_1 R_2}\,\right)^2 + 4\mathcal{G}_s\sqrt{R_1 R_2}\,\sin^2\varphi},$$

$\varphi = \beta L$, resonances: $\varphi_z = \omega_z n_e L/c = m_z\pi\,, \qquad m_z = 1, 2, 3, \ldots$

SOA Single-Pass Gain and Ripple

FP amplification factor $\mathcal{G}$:

$$\mathcal{G} = \frac{\mathcal{G}_s(1-R_1)(1-R_2)}{(1-\mathcal{G}_s\sqrt{R_1R_2}\,)^2 + 4\mathcal{G}_s\sqrt{R_1R_2}\,\sin^2\varphi}\,;$$

$$\varphi = \beta L, \quad \text{res.: } \varphi_z = \omega_z n_e L/c = m_z\pi\,.$$

Res. & anti-res.:

$$\mathcal{G}_{\max} = \frac{\mathcal{G}_s(1-R_1)(1-R_2)}{(1-\mathcal{G}_s\sqrt{R_1R_2})^2},$$

$$\mathcal{G}_{\min} = \frac{\mathcal{G}_s(1-R_1)(1-R_2)}{(1+\mathcal{G}_s\sqrt{R_1R_2})^2}$$

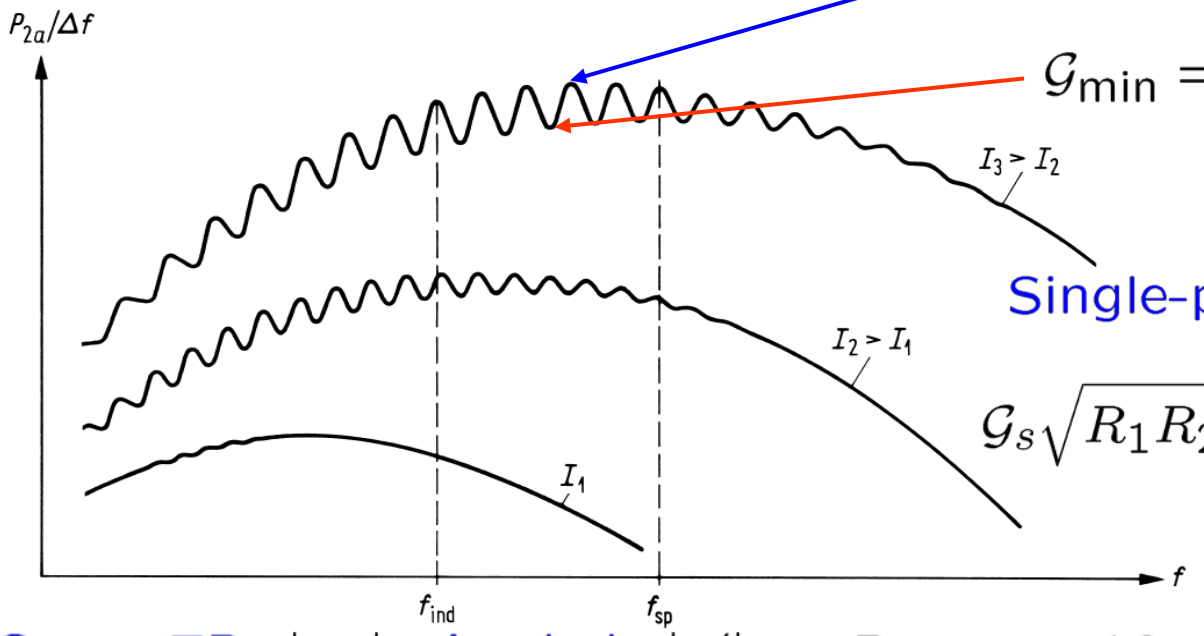

Single-pass gain from ripple:

$$\mathcal{G}_s\sqrt{R_1R_2} = \frac{\sqrt{\mathcal{G}_{\max}/\mathcal{G}_{\min}}-1}{\sqrt{\mathcal{G}_{\max}/\mathcal{G}_{\min}}+1}$$

$$\mathcal{G}_{\max}/\mathcal{G}_{\min} = 2:$$

$$\mathcal{G}_s\sqrt{R_1R_2} = 0.17$$

Conv. FP: |—|. Angled: |/| $\rightarrow R_{\text{eff}\,1,2} \approx 10^{-4}$

Near-travelling-wave amplifier. Schematic of the spectral output power density $P_{2a}/\Delta F$ of amplified spontaneous emission as transmitted through mirror R_2 for varying injection currents $I_1 < I_2 < I_3$. The frequencies of maximum gain and maximum spontaneous emission are denoted as f_{ind} and f_{sp} for an operating current $I = I_3$.

SOA Chip with Angled Facets and Lensed Fibres

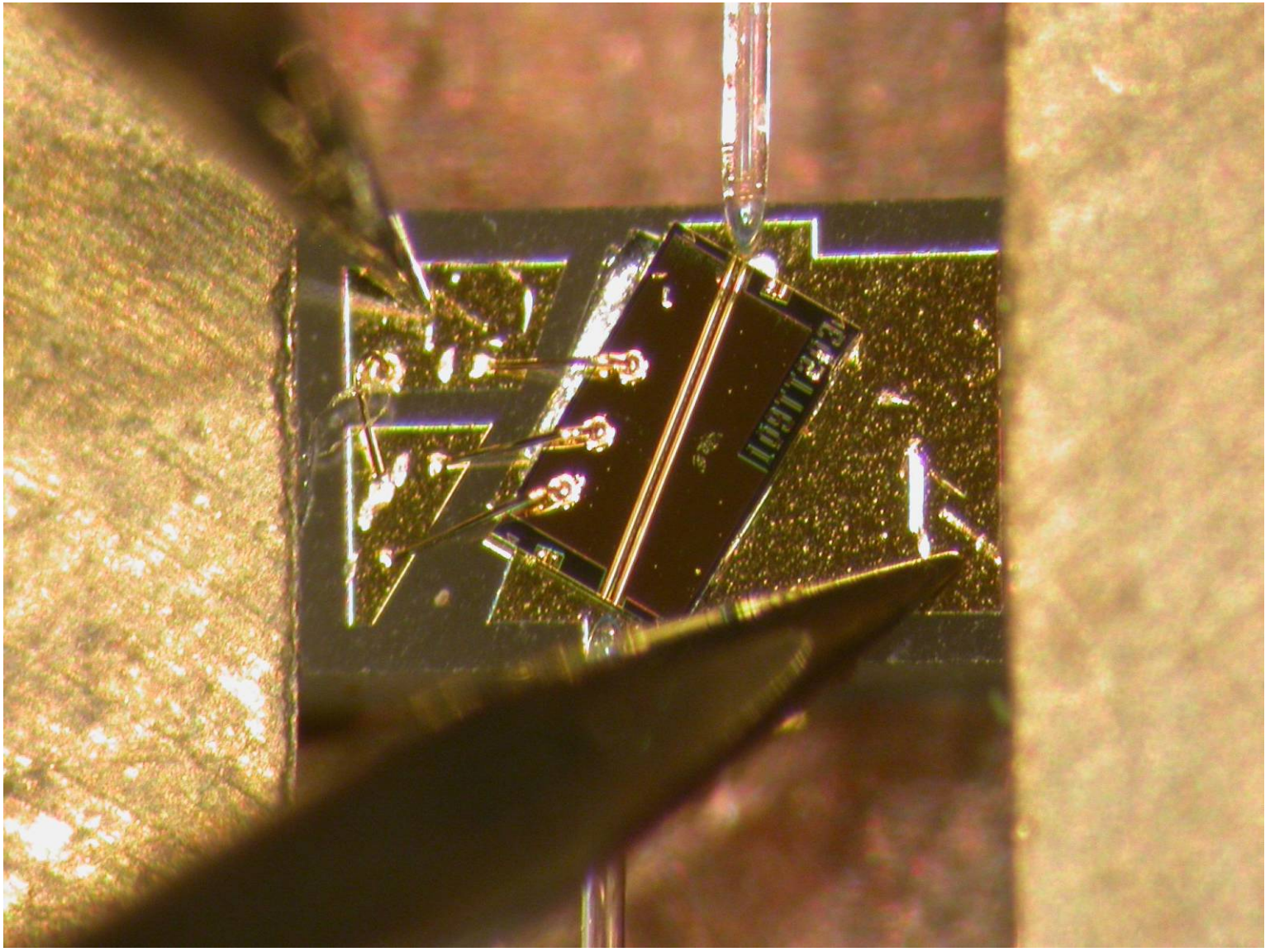

Er-Doped Optical Amplifier

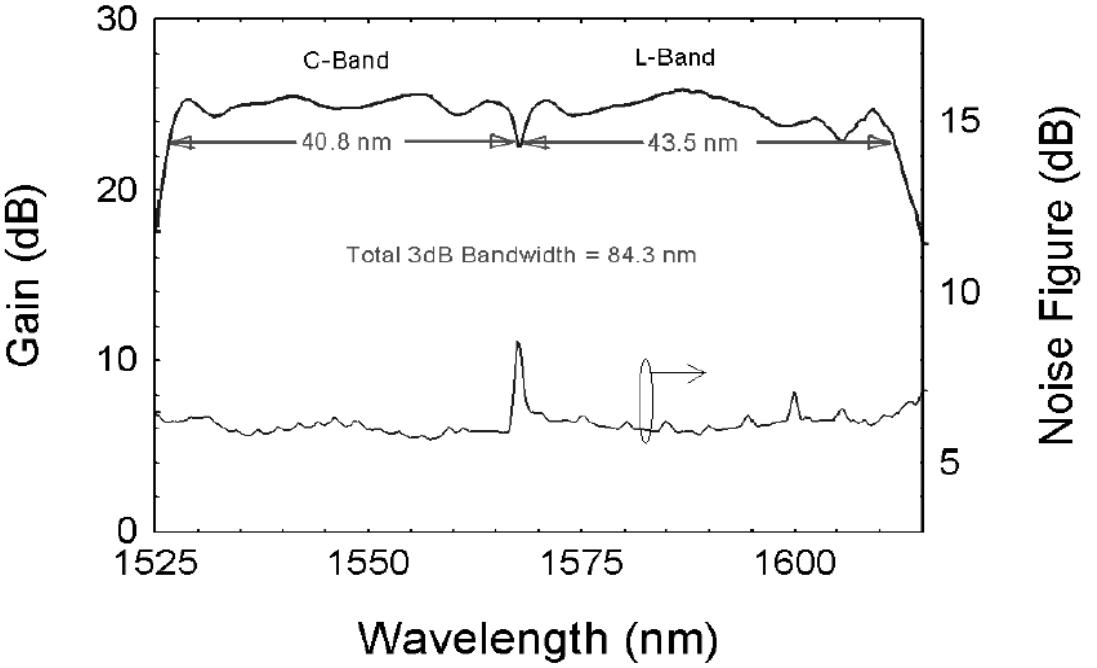

Er-doped optical ultra-broadband amplifier (ECOC'1998)

LECTURE 13

Optical Receivers

pin-Photodiode

pin-Photodiode

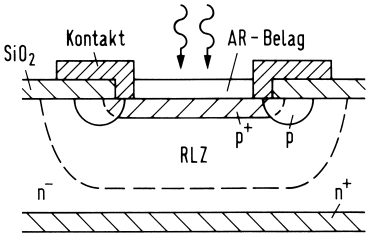

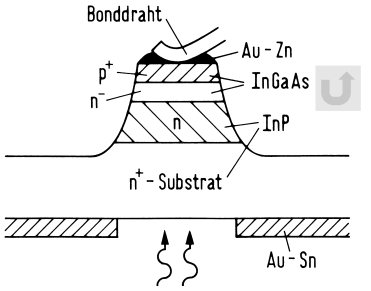

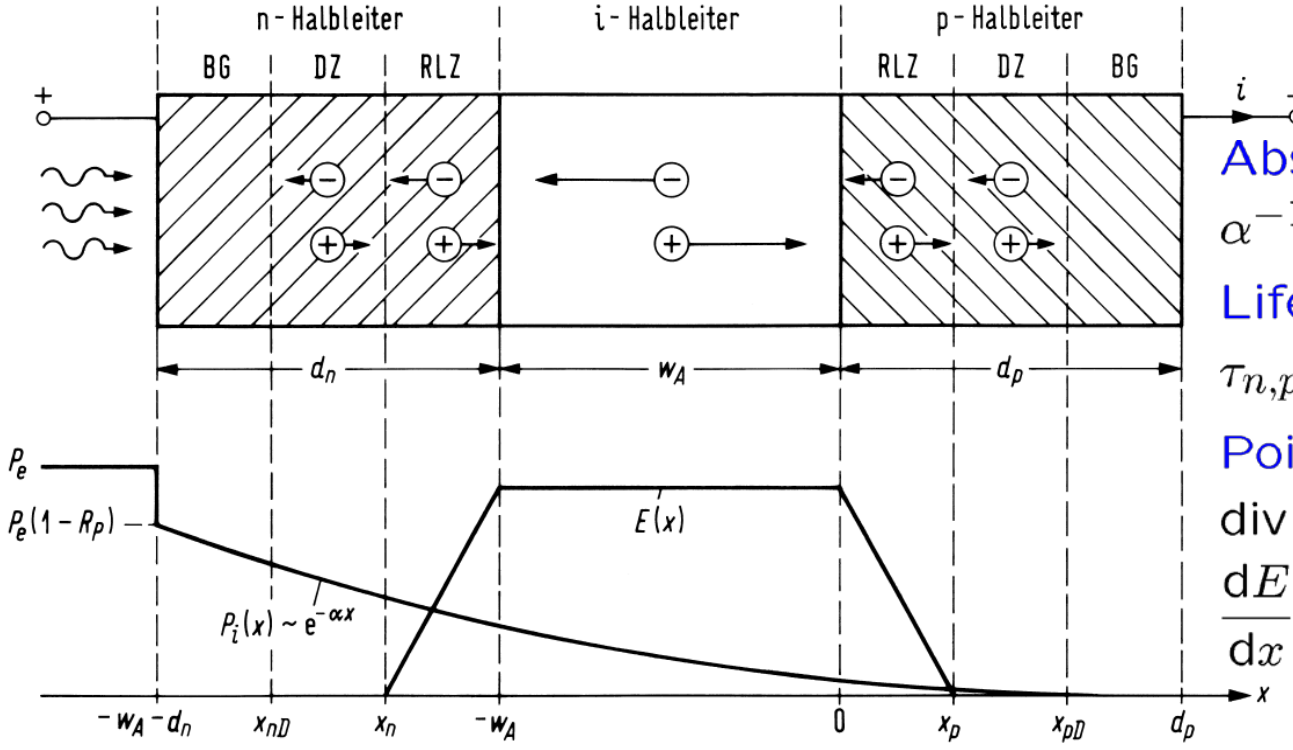

Absorption length:

$$\alpha^{-1} = 1 \ldots 10 \ldots 20\,\mu\mathrm{m}$$

Lifetime:

$$\tau_{n,p} = L_{n,p}^2 / D_{n,p}$$

Poisson equation:

$$\mathrm{div}\left(\epsilon_0 \epsilon_r \vec{E}\right) = \varrho$$

$$\frac{\mathrm{d}E}{\mathrm{d}x} = \pm \frac{e n_{D,A}}{\epsilon_0 \epsilon_r}$$

Schematic of a pin-diode. BG contact region (= *B*ahn*g*ebiet), DZ diffusion zone, RLZ space-charge (or depletion) region (= *R*aum*l*adungs*z*one). P_e light power incident from region external of semiconductor, R_P power reflection factor of the semiconductor surface, $P_i(x)$ light power inside the semiconductor, α light power attenuation constant, d_n (d_p) length of n-doped (p-doped) semiconductor, w_A length of intrinsic absorption zone, $E(x)$ x-component of electric bias field. Halbleiter = semiconductor

Sensitivity of a pin-Photodetector

We compute the sensitivity S (responsivity) of a pin-photodiode, which we describe by

- its technological structure, by
- a reduction to an easy-to-handle model, and by
- appropriate basic equations.

Continuity and transport equations are written

- in one-dimensional form, specified with
- quantum efficiency and generation rate, and finally
- solved for the DC case.

We find that for an external optical power P_e (photon energy hf_e)

- each absorbed photon generates one e-h pair (prob. η), which
- transports one elementary charge e in the external circuit, so
- the rate of generated charges i/e (photocurrent i) equals
- the photon absorption rate $\eta P_e/(hf_e)$ resulting in
- the sensitivity $S = \dfrac{\eta e}{hf_e}$ and a photocurrent $i = SP_e$.

Photodiode — Characteristic Curves and Operating Regions

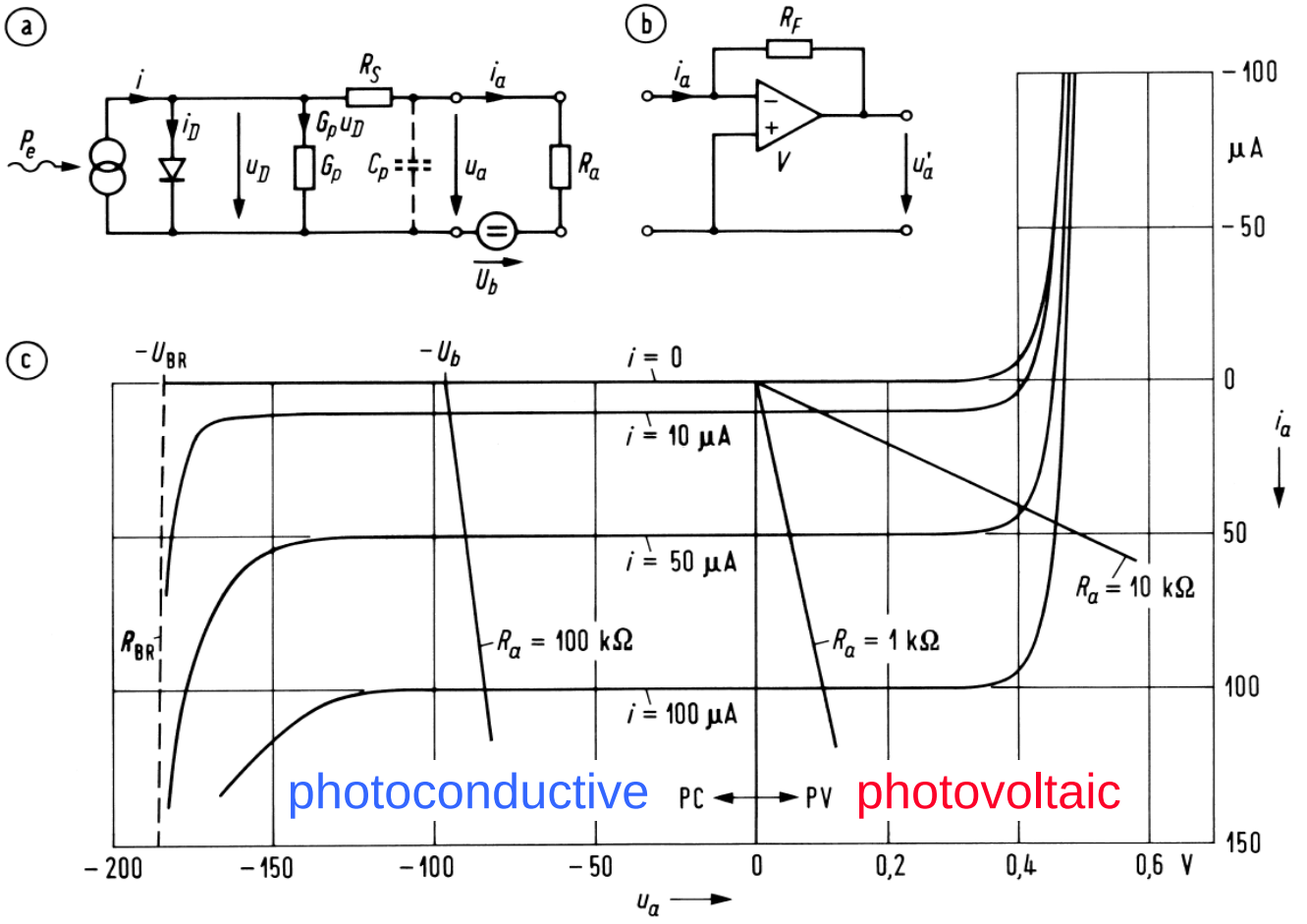

Static equivalent circuit and current-voltage characteristic of a photodiode. (a) Equivalent circuit. External incident power P_e, parasitic conductance G_p, series contact resistance R_S, parasitic capacitance C_p, load resistance R_a, bias voltage U_b. (b) Transimpedance amplifier (c) i_a-u_a characteristics for different photo currents i. Breakdown voltage U_{BR}, differential breakdown resistance R_{BR}

Absorption Zone — Quantum Efficiency

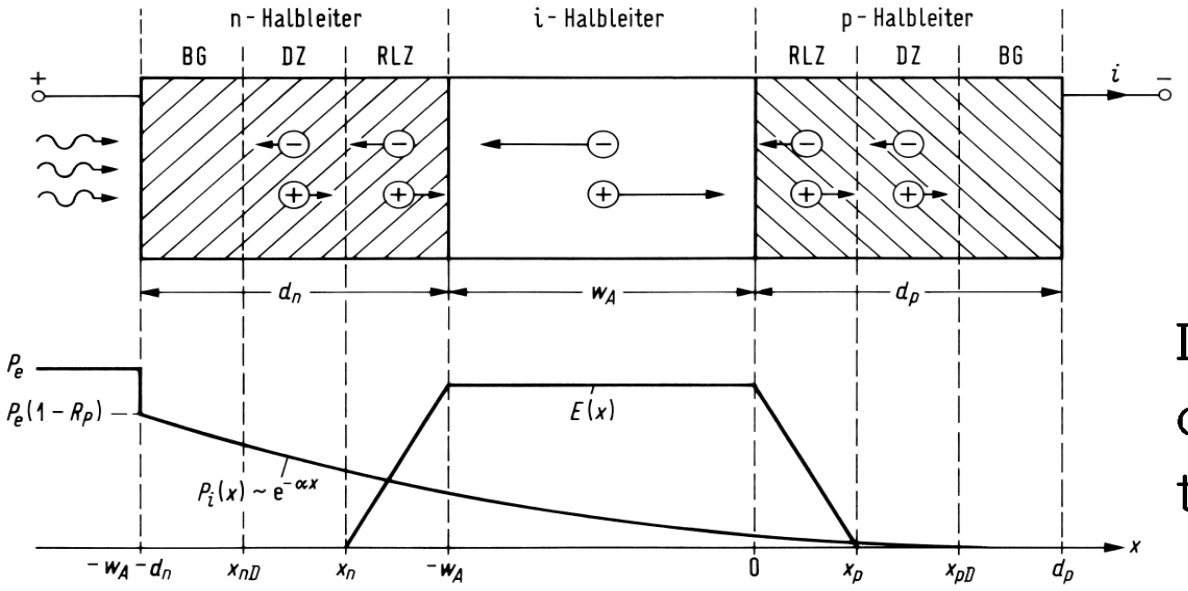

If $\alpha\, d_n \to 0$ (n-SC small comp. to abs. length), then $P_i(x,t)$ in i-region:

$$P_i(x,t) = P_e(t)\,(1-R_P)\,\mathrm{e}^{-\alpha(x+w_A)}$$

Light transit time neglected. P_e, P_i are powers averaged over a few optical periods. Fraction of power absorbed in i-zone is quantum efficiency η:

$$\eta = \frac{P_i(-w_A,t) - P_i(0,t)}{P_e(t)} = (1-R_P)\left(1-\mathrm{e}^{-\alpha w_A}\right)$$

Absorption Zone — Short-Circuit Current

Basic equations (no external magnetic field, no magnetic fields associated with flowing currents): Continuity equations (n_T, p electron and hole concentration; $\vec{J}_n$, $\vec{J}_p$ current densities of electrons and holes; g_n, g_p, r_n, r_p generation and recombination rates)

$$\partial p/\partial t + \text{div } \vec{J}_p/e = g_p - r_p\,, \qquad \vec{v}_p = \mu_p \vec{E}\,,$$
$$\partial n_T/\partial t - \text{div } \vec{J}_n/e = g_n - r_n\,, \qquad \vec{v}_n = -\mu_n \vec{E}$$

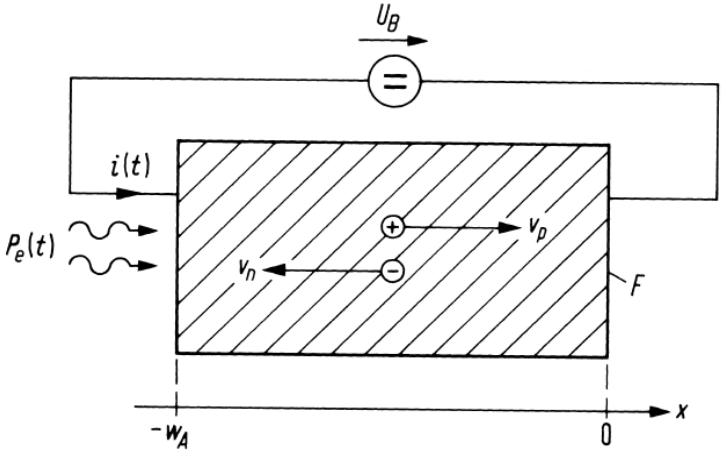

Transport equations ($\vec{v}_n$, $\vec{v}_p$ drift velocity; D_n, D_p diffusion constant; μ_n, μ_p mobility, $\vec{E}$ electric field):

$$\vec{J}_p = ep\vec{v}_p - eD_p \text{ grad } p,$$
$$\vec{J}_n = -en_T\vec{v}_n + eD_n \text{ grad } n_T$$

i-layer of a pin-photodiode (one-dimensional case, cross-section area F). Saturation drift velocities $v_n > 0$ and $v_p > 0$ for electrons and holes, incident external optical power $P_e(t)$, total conduction current $i(t)$, open-circuit voltage U_B of a battery with an internal resistance of zero

Absorption Zone — Basic 1D-Equations

Carrier transit times τ_n, τ_p (saturation drift velocity v_n, v_p):

$$w_A = v_{n,p}\,\tau_{n,p}\,, \quad v_{n,p} \sim (0.5\ldots1)\times 10^7\,\mathrm{cm/s} = (50\ldots100)\,\mu\mathrm{m/ns}$$

Recombination rates r_n, r_p neglected (carrier lifetime much larger than drift time in absorption zone $-w_A \le x \le 0$), diffusion currents neglected compared to field currents. Photogeneration dominates, $g_p = g_n = g$. Currents i instead of current densities J (cross-section area F):

$$\frac{1}{v_p}\frac{\partial i_p}{\partial t} + \frac{\partial i_p}{\partial x} = eFg\,, \qquad i_p = Fepv_p\,,$$

$$\frac{1}{v_n}\frac{\partial i_n}{\partial t} - \frac{\partial i_n}{\partial x} = eFg\,, \qquad i_n = Fenv_n\,,$$

$$\epsilon\frac{\partial E}{\partial x} = e(p-n), \qquad \frac{\partial}{\partial x}\Big(\underbrace{i_n + i_p + F\epsilon\frac{\partial E}{\partial t}}_{\text{total current } i(t),\ \text{displacement current } F\epsilon\frac{\partial E}{\partial t}}\Big) = 0$$

0 ($U_B = \text{const}$)

Absorption Zone — Generation Rate g (unit $\mathrm{cm^{-3}\,s^{-1}}$)

No (optical) harmonics by detecting $P_e \sim |E|^2$ (electric field E):

$$i \sim \left\langle |E|^2 \cos^2(\omega_e t) \right\rangle = \frac{1}{2}|E|^2 \left\langle 1 + \cos(2\omega_e t) \right\rangle^{0} = \frac{1}{2}|E|^2$$

Absorption detectors of this kind are unable to emit optical photons $2hf_e$ (let aside spont. emission by radiative recomb.)!

N_P photons, power P: $\quad N_P\, hf_e = P \times 1\,\mathrm{s}$

$$P_i(x,t) = P_e(t)\,(1-R_P)\,\mathrm{e}^{-\alpha(x+w_A)}$$

$$\left(\overline{\text{CP generation rate } g}\right) = \left(\overline{\text{photon absorption rate}/V}\right)$$

Power *gained* per ∂x:

$$\frac{\partial P_i(x,t)}{\partial x} = \frac{P_i(x+\partial x,t) - P_i(x,t)}{\partial x}$$

Power *lost* per ∂x:

$$\frac{-\partial P_i(x,t)}{\partial x} = \frac{P_i(x,t) - P_i(x+\partial x,t)}{\partial x}$$

$$= \frac{\overbrace{(\text{diff. absorbed power})/(hf_e)}^{\text{№ of absorbed photons per 1 s}}}{(\text{differential volume } F\partial x)}$$

$$g(x,t) = \frac{-\partial P_i(x,t)/(hf_e)}{F\,\partial x} = \frac{\alpha P_i(x,t)}{F h f_L}$$

Absorption Zone — External Short-Circuit Current

Quantum efficiency, power decay, and generation rate:

$$\eta = (1 - R_P)\left(1 - \mathrm{e}^{-\alpha w_A}\right)$$

$$g(x,t) = \frac{\alpha P_e(t)}{F h f_e}(1 - R_P)\,\mathrm{e}^{-\alpha(x+w_A)}$$

$$eFg(x,t) = \frac{\eta e}{h f_e}\,P_e(t)\,\frac{\alpha\,\mathrm{e}^{-\alpha(x+w_A)}}{1 - \mathrm{e}^{-\alpha w_A}}$$

A system of differential equation follows (here: 1D case):

$$\frac{1}{v_p}\frac{\partial i_p(x,t)}{\partial t} + \frac{\partial i_p(x,t)}{\partial x} = eFg(x,t), \qquad i_p(x,t) = Fep(x,t)v_p,$$

$$\frac{1}{v_n}\frac{\partial i_n(x,t)}{\partial t} - \frac{\partial i_n(x,t)}{\partial x} = eFg(x,t), \qquad i_n(x,t) = Fen(x,t)v_n,$$

$$i(t) = \frac{1}{w_A}\int_{-w_A}^{0} [\, i_n(x,t) + i_p(x,t)\,]\,\mathrm{d}x$$

External Short-Circuit Current — Static Case (DC)

Generation rate, $\partial/\partial t = 0$:

$$eFg(x) = \frac{\eta e}{h f_e} P_e \frac{\alpha \, \mathrm{e}^{-\alpha(x+w_A)}}{1 - \mathrm{e}^{-\alpha w_A}}$$

System of differential equations, $\partial/\partial t = 0$:

$$\frac{1}{v_p}\frac{\partial i_p(x,t)}{\partial t} + \frac{\partial i_p(x,t)}{\partial x} = eFg(x,t), \qquad i_p(x,t) = Fep(x,t)v_p,$$

$$\frac{1}{v_n}\frac{\partial i_n(x,t)}{\partial t} - \frac{\partial i_n(x,t)}{\partial x} = eFg(x,t), \qquad i_n(x,t) = Fen(x,t)v_n,$$

Minority current injection neglected, $i_p(-w_A) = 0$, $i_n(0) = 0$:

$$i = i_p(0) = i_n(-w_A) = \int_{-w_A}^{0} eFg(x)\,\mathrm{d}x = \frac{\eta e}{h f_e} P_e\,, \qquad i = \frac{\eta e}{h f_e} P_e = S P_e$$

Each absorbed photon generates electron-hole pair with prob. $\eta \rightarrow$ transport of one elementary charge e through external circuit.
Rate of generated charges $i/e = \eta P_e/(h f_e)$ photon absorption rate.

Direct and Indirect Semiconductors

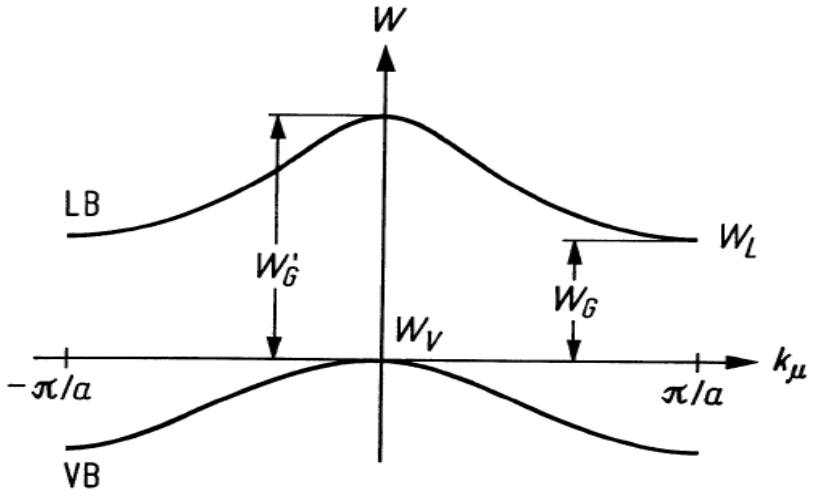

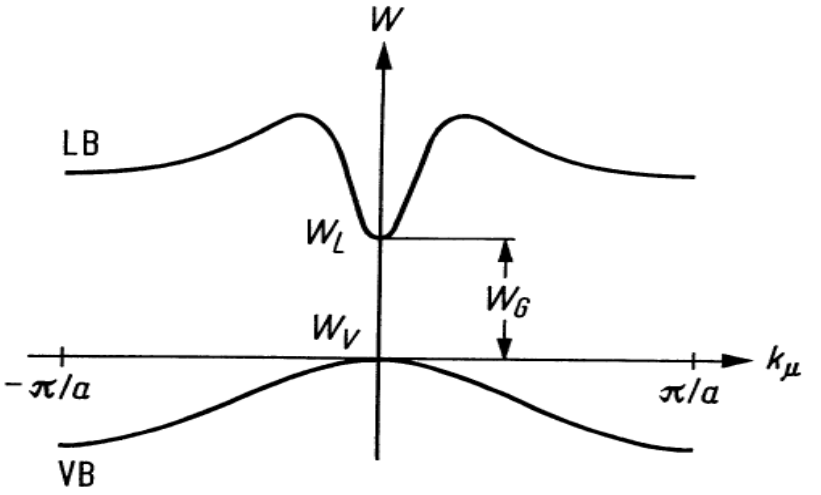

Indirect semicond. Smallest transition energy W_G for crystal momentum difference $\Delta k_\mu = \pi/a$. Phonon required for collision. Examples: Elemental semiconductors Si, Ge

$$W_G = \begin{cases} 0{,}67\,\text{eV} \mathrel{\widehat{=}} 1{,}85\,\mu\text{m} & \text{(Ge)} \\ 1{,}13\,\text{eV} \mathrel{\widehat{=}} 1{,}10\,\mu\text{m} & \text{(Si)} \end{cases}$$

$$W_G' = \begin{cases} 0{,}8\ \text{eV} \mathrel{\widehat{=}} 1{,}55\,\mu\text{m} & \text{(Ge)} \\ 3{,}4\ \text{eV} \mathrel{\widehat{=}} 0{,}36\,\mu\text{m} & \text{(Si)} \end{cases}$$

Direct semicond. Smallest transition energy W_G for crystal momentum difference $\Delta k_\mu = 0$. No collision partner required. Examples: Compounds GaAs, InP, InGaAs

$$W_G = \begin{cases} 1{,}42\,\text{eV} \mathrel{\widehat{=}} 0{,}87\,\mu\text{m} & \text{(GaAs)} \\ 1{,}80\,\text{eV} \mathrel{\widehat{=}} 0{,}69\,\mu\text{m} & \text{($Ga_{0,7}Al_{0,3}As$)} \\ 0{,}75\,\text{eV} \mathrel{\widehat{=}} 1{,}65\,\mu\text{m} & \text{($In_{0,53}Ga_{0,47}As$)} \\ 1{,}35\,\text{eV} \mathrel{\widehat{=}} 0{,}92\,\mu\text{m} & \text{(InP)} \end{cases}$$

Absorption Constants

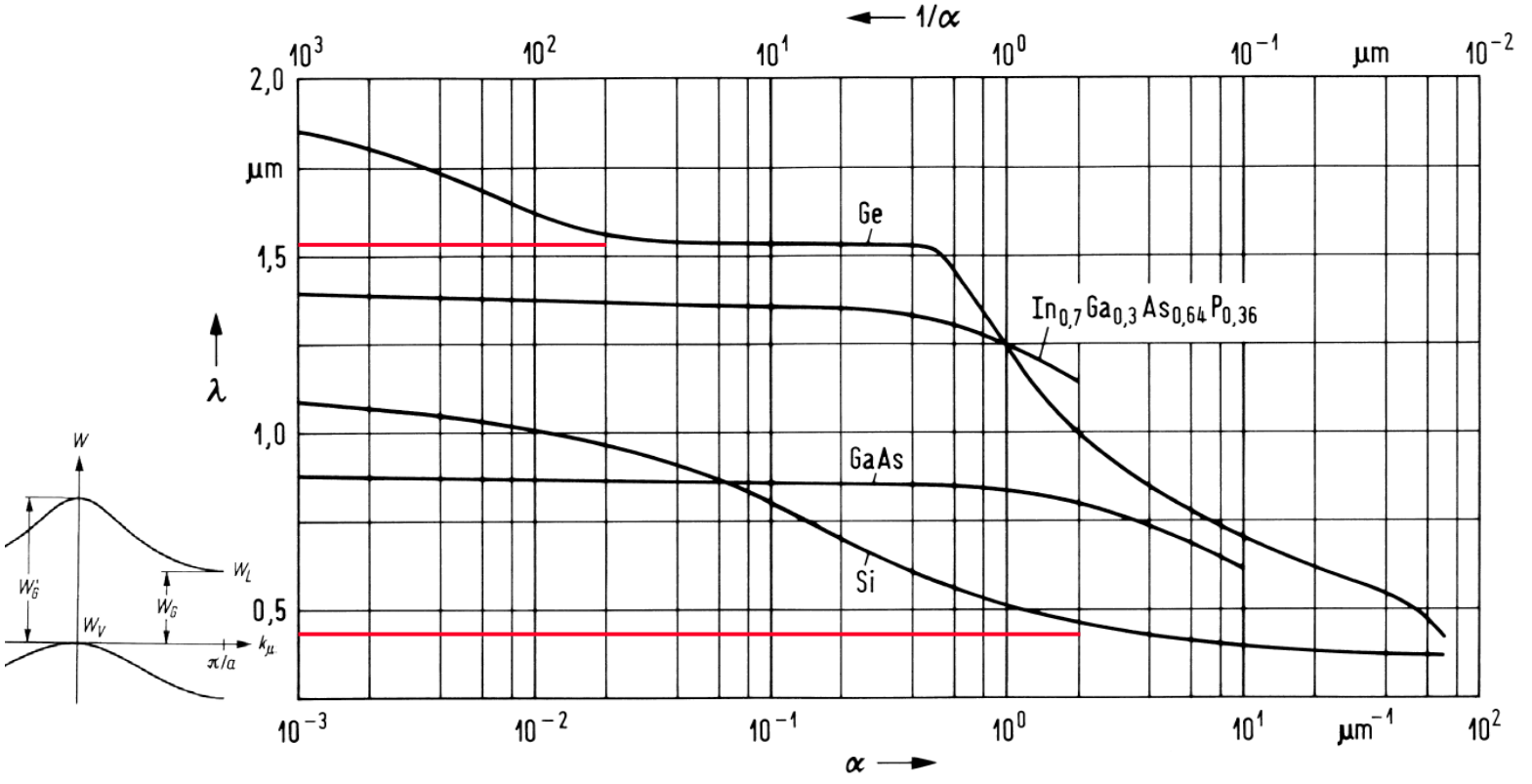

Wavelength dependence of the absorption constant α (penetration depth $1/\alpha$) for several semiconductor materials

$$W_G = \begin{cases} 0{,}67\,\text{eV} \mathrel{\widehat{=}} 1{,}85\,\mu\text{m} & \text{(Ge)} \\ 1{,}13\,\text{eV} \mathrel{\widehat{=}} 1{,}10\,\mu\text{m} & \text{(Si)} \end{cases}$$

$$W'_G = \begin{cases} 0{,}8\ \text{eV} \mathrel{\widehat{=}} 1{,}55\,\mu\text{m} & \text{(Ge)} \\ 3{,}4\ \text{eV} \mathrel{\widehat{=}} 0{,}36\,\mu\text{m} & \text{(Si)} \end{cases}$$

$$W_G = \begin{cases} 1{,}42\,\text{eV} \mathrel{\widehat{=}} 0{,}87\,\mu\text{m} & \text{(GaAs)} \\ 1{,}80\,\text{eV} \mathrel{\widehat{=}} 0{,}69\,\mu\text{m} & \text{(Ga}_{0,7}\text{Al}_{0,3}\text{As)} \\ 0{,}75\,\text{eV} \mathrel{\widehat{=}} 1{,}65\,\mu\text{m} & \text{(In}_{0,53}\text{Ga}_{0,47}\text{As)} \\ 1{,}35\,\text{eV} \mathrel{\widehat{=}} 0{,}92\,\mu\text{m} & \text{(InP)} \end{cases}$$

pin Photodiode — Dynamics

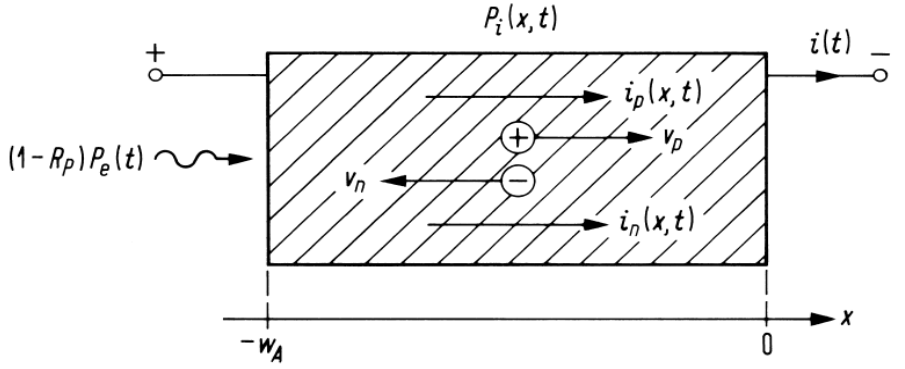

$$\eta = (1 - R_P)\left(1 - \mathrm{e}^{-\alpha w_A}\right)$$

$$eFg(x,t) = \frac{\eta e}{h f_e} P_e(t) \frac{\alpha\, \mathrm{e}^{-\alpha(x+w_A)}}{1 - \mathrm{e}^{-\alpha w_A}}$$

Absorption layer of a pin-photodiode. P_e incicent external light power, R_P power reflection coefficient, $i(t)$ external short-circuit current, P_i internal optical power; i_p, i_n convection currents of electrons and holes; v_p, v_n saturation drift velocities, w_A length of absorption region

Differential equations to be solved for ext. short-circuit current:

$$\frac{1}{v_p}\frac{\partial i_p(x,t)}{\partial t} + \frac{\partial i_p(x,t)}{\partial x} = eFg(x,t), \qquad i_p(x,t) = Fep(x,t)v_p,$$

$$\frac{1}{v_n}\frac{\partial i_n(x,t)}{\partial t} - \frac{\partial i_n(x,t)}{\partial x} = eFg(x,t), \qquad i_n(x,t) = Fen_T(x,t)v_n,$$

$$i(t) = \frac{1}{w_A}\int_{-w_A}^{0} \left[\, i_n(x,t) + i_p(x,t) \,\right] \mathrm{d}x$$

pin Photodiode — Impulse Response Strong Absorption

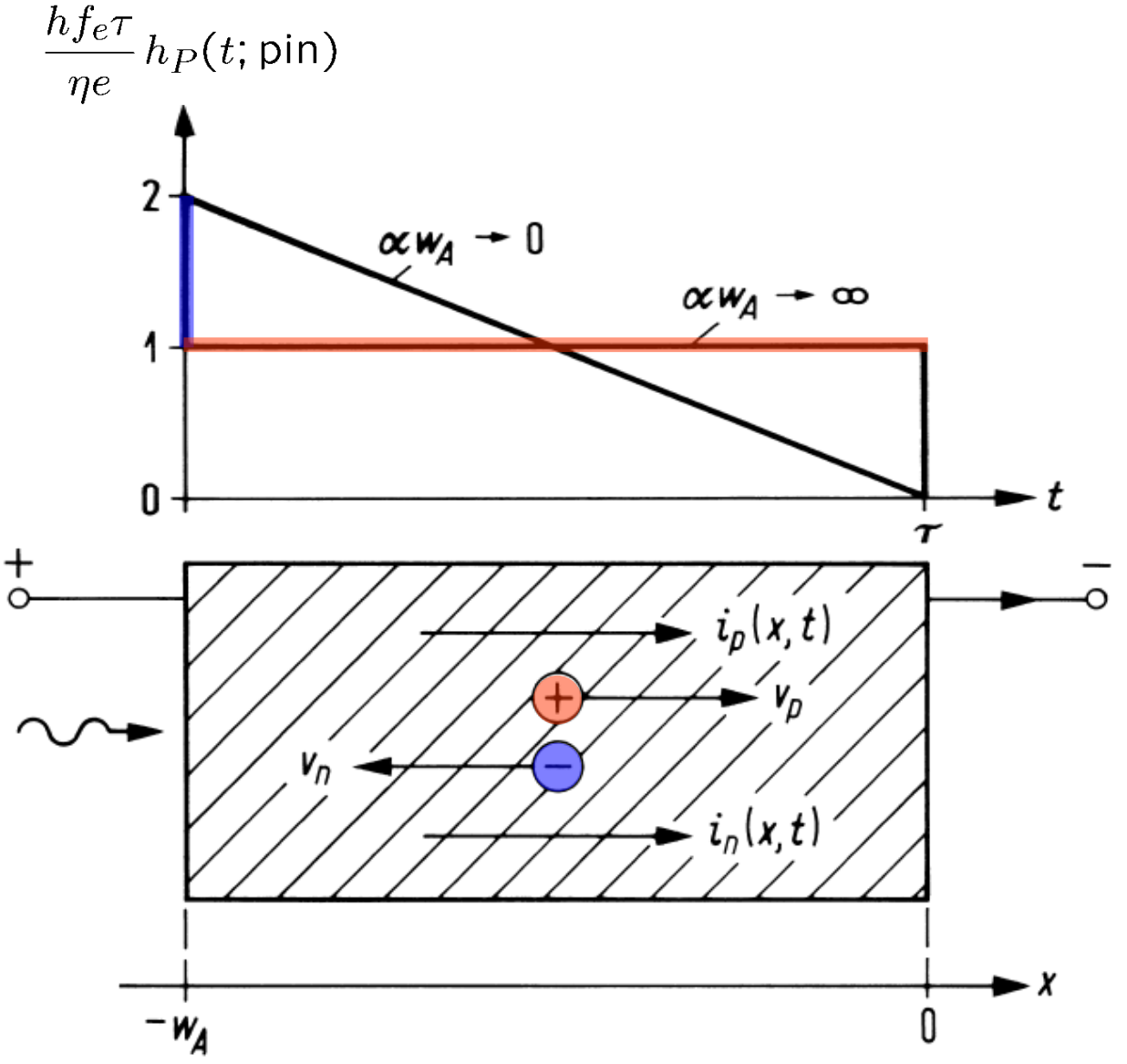

pin Photodiode — Impulse Response Weak Absorpt. ($v_n = v_p$)

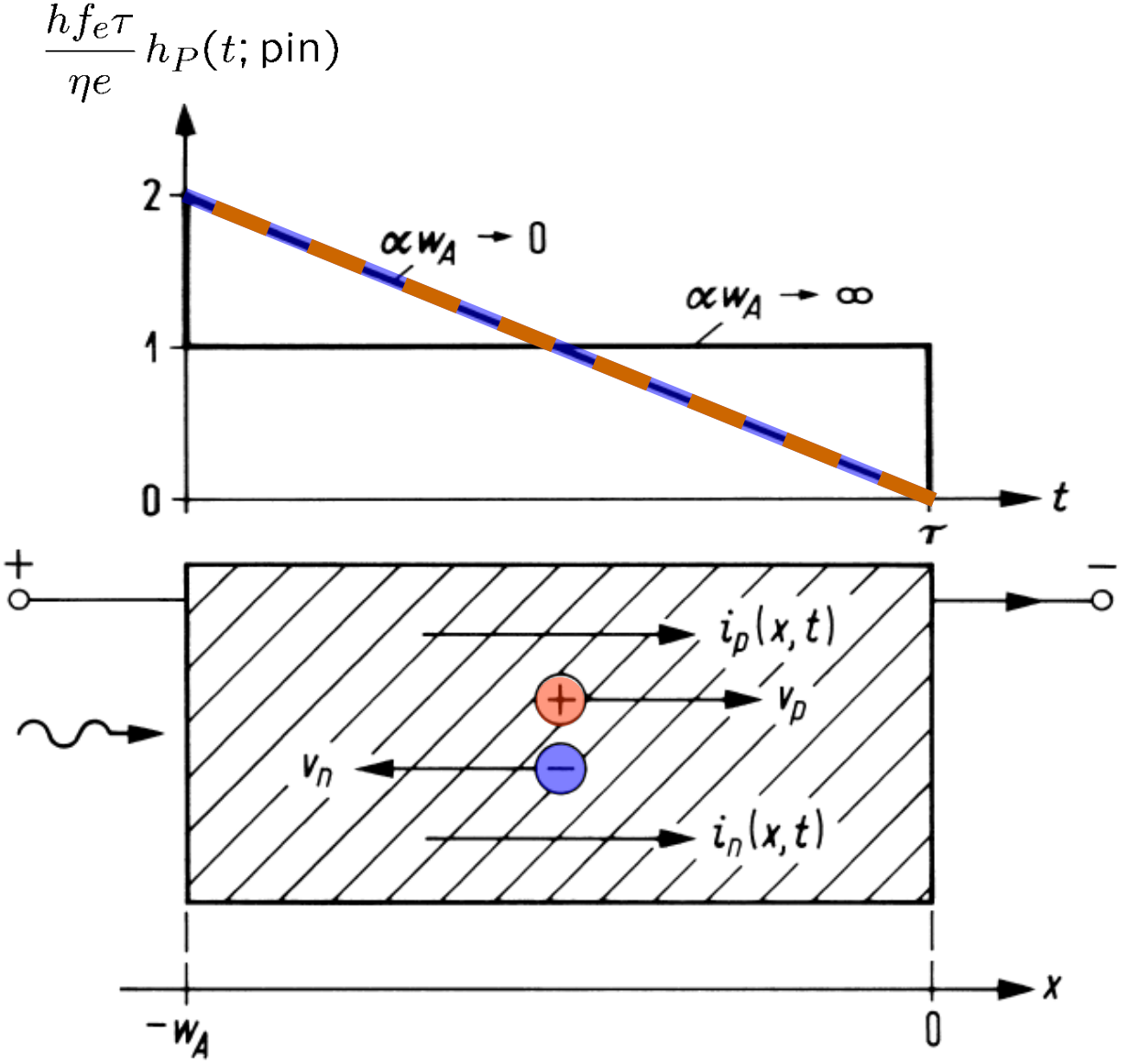

pin Photodiode — Impulse Response for Fair Absorpt. ($v_n = v_p$)

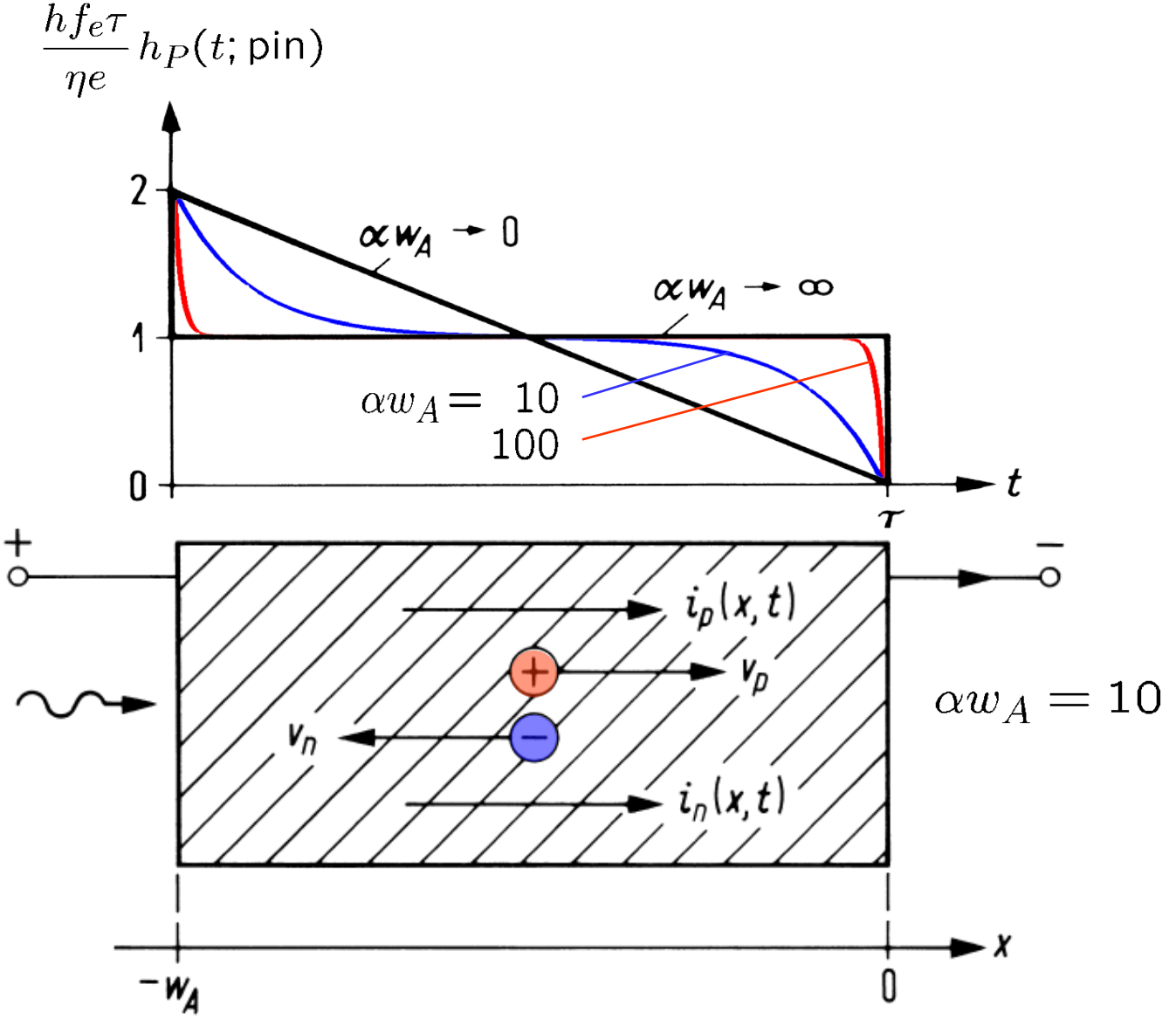

pin Photodiode — Transit Time Cutoff Frequency

Short-circuit current spectrum $I(f;\mathrm{pin})$ for light power:

$$P_e(t) = P_0 + P_1 \cos(\omega t) \quad (P_0 \geq P_1)$$

Limiting cases strong and weak absorption, for weak absorption $\tau_n = \tau_p = \tau$ holds:

$$\frac{I(f;\mathrm{pin})}{I(0;\mathrm{pin})} = \mathrm{e}^{-\mathrm{j}\omega\tau_p/2}\,\frac{\sin(\omega\tau_p/2)}{\omega\tau_p/2} \qquad \text{für } \alpha w_A \to \infty$$

$$\frac{I(f;\mathrm{pin})}{I(0;\mathrm{pin})} = \frac{1}{\mathrm{j}\omega\tau/2}\left[1 - \mathrm{e}^{-\mathrm{j}\omega\tau/2}\,\frac{\sin(\omega\tau/2)}{\omega\tau/2}\right] \qquad \text{für } \alpha w_A \to 0$$

3-dB cutoff frequency from $\left|\frac{I(f_{3\mathrm{dB}};\mathrm{pin})}{I(0;\mathrm{pin})}\right| = \frac{1}{\sqrt{2}}$:

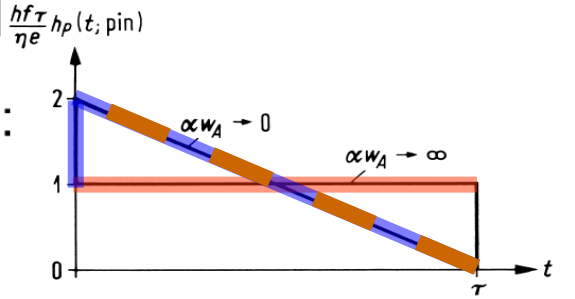

$$f_{3\mathrm{dB}} = \begin{cases} 0.44/\tau_p & \text{for } \alpha w_A \to \infty \\ 0.55/\tau & \text{für } \alpha w_A \to 0, \quad \tau_n = \tau_p = \tau \end{cases}$$

pin Photodiode — Quantum Efficiency

Quantum efficiency for weak absorption $\alpha w_A \to 0$:

$$\eta = \frac{P_i(-w_A,t) - P_i(0,t)}{P_e(t)} = (1-R_P)\left(1 - \mathrm{e}^{-\alpha w_A}\right) \underset{\alpha w_A \to 0}{=} (1-R_P)\alpha w_A$$

3-dB cutoff frequency for $\alpha w_A \to 0$:

$$f_{3\mathrm{dB}} = 0.55/\tau$$

Product of quantum efficiency and cutoff frequency:

$$\eta f_{3\mathrm{dB}} = 0.55\,(1 - R_P)\,\alpha v \qquad \text{for } \alpha w_A \to 0$$

$\eta f_{3\mathrm{dB}}$ depends for $R_P = 0$ only on material properties α, v (power attenuation constant, saturation drift velocities of carriers).
For InGaAs at $\lambda = 1.55\,\mu\mathrm{m}$ ($\alpha = 0.68\,\mu\mathrm{m}^{-1}$, $v = (v_n + v_p)/2 = 56.5\,\mu\mathrm{m/ns}$): $\eta f_{3\mathrm{dB}} = 21\,\mathrm{GHz}$; at $\lambda = 1.36\,\mu\mathrm{m}$ ($\alpha = 1.16\,\mu\mathrm{m}^{-1}$, $v = 56.5\,\mu\mathrm{m}\,/\,\mathrm{ns}$): $\eta f_{3\mathrm{dB}} = 36\,\mathrm{GHz}$.

pin Photodiode — Edge Coupling (1)

For $\alpha w_A \to 0$ better performance achieved by irradiating light $\parallel$ to pn-junction into absorption zone.

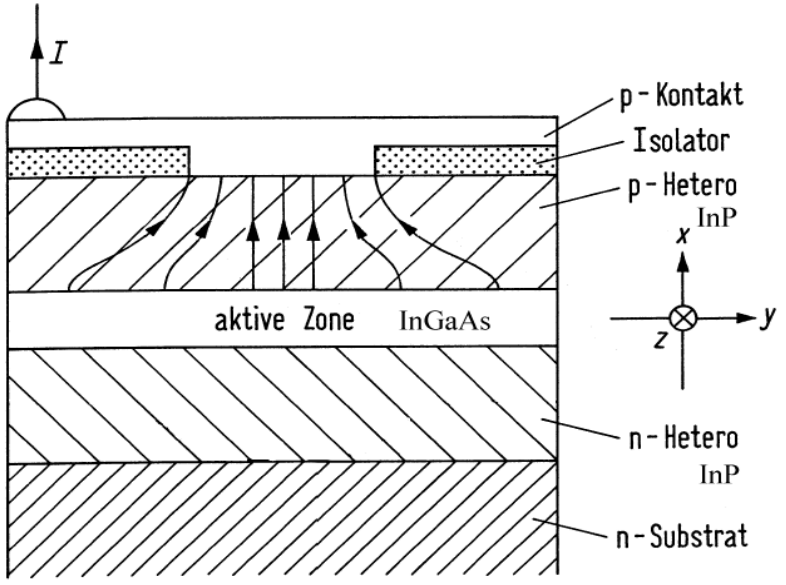

- act. InGaAs absorption zone
- n-InP/p-InP hetero layers
- reverse voltage
- InP/InGaAs/InP slab WG

Pin-diode with edge-coupling of light, w_A is the height of the active zone. x-axis: direction of current flow; z-axis: direction of light propagation (Aktive Zone = active zone, p-Kontakt = p-contact, Isolator = insulator, n-substrat = n-substrate).

For InGaAs layer with thickness $w_A = 0.2\,\mu$m: Field confinement factor $\Gamma = \frac{\text{power in core}}{\text{power in cross-section}} = 0.4$

This means difficult coupling conditions because of small WG cross-section!

pin Photodiode — Edge Coupling (2)

Eff. absorption constant $\alpha\Gamma$ for vertical fundamental mode. Length L of absorption zone in z-direction, coupling efficiency η_{coupl}. Quantum efficiency:

$$\eta = \eta_{\text{coupl}} \left(1 - \mathrm{e}^{-\alpha\Gamma L}\right)$$

Quantum efficiency ($\alpha = 0.68\,\mu\text{m}^{-1}$, $\Gamma = 0.4$, $L > 10\,\mu\text{m}$):

$$\eta \approx \eta_{\text{coupl}} \qquad \text{because} \qquad \mathrm{e}^{-\alpha\Gamma L} < 0.066$$

$\eta_{\text{coupl}} \approx 0.5$ realistic. Transit-time cutoff frequency for small w_A:

$$f_{3\text{dB}} = 0.55/\tau \quad \text{for } \alpha w_A \to 0, \quad \tau_n = \tau_p = \tau$$

$\eta \approx 0.5$ independently of $f_{3\text{dB}}$ and λ. With $w_A = 0.2\,\mu\text{m}$:

$$f_{3\text{dB}} = 124\,\text{GHz}$$

Extended Equivalent Circuit (1)

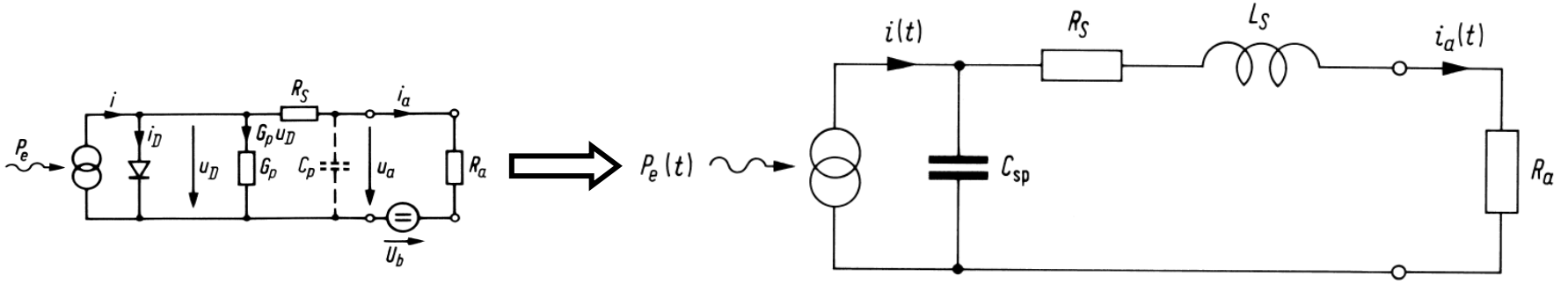

Equivalent electrical circuit of a photodiode. P_e incident external optical power, C_{sp} depletion-layer capacity, R_S series resistance, L_S series inductance, R_a load resistance

Short-circuit photo current $i(t)$ is injected into PD equivalent circuit. Fourier transform (FT $= \bar{\Psi}(f) = \mathcal{F}\{\Psi(t)\}$) and inverse FT (IFT $= \Psi(t) = \mathcal{F}^{-1}\left\{\bar{\Psi}(f)\right\}$):

$$\Psi(t) = \int_{-\infty}^{+\infty} \bar{\Psi}(f)\, \mathrm{e}^{+\mathrm{j}\,2\pi f t}\, \mathrm{d}f, \quad \bar{\Psi}(f) = \int_{-\infty}^{+\infty} \Psi(t)\, \mathrm{e}^{-\mathrm{j}\,2\pi f t}\, \mathrm{d}t$$

Functions discriminated only by argument: $\Psi(t) \neq \Psi(f = t)$, $\Psi(f) \equiv \bar{\Psi}(f)$. FT of $i(t)$, $i_a(t)$ are $I(f)$, $I_a(f)$.

Extended Equivalent Circuit (2)

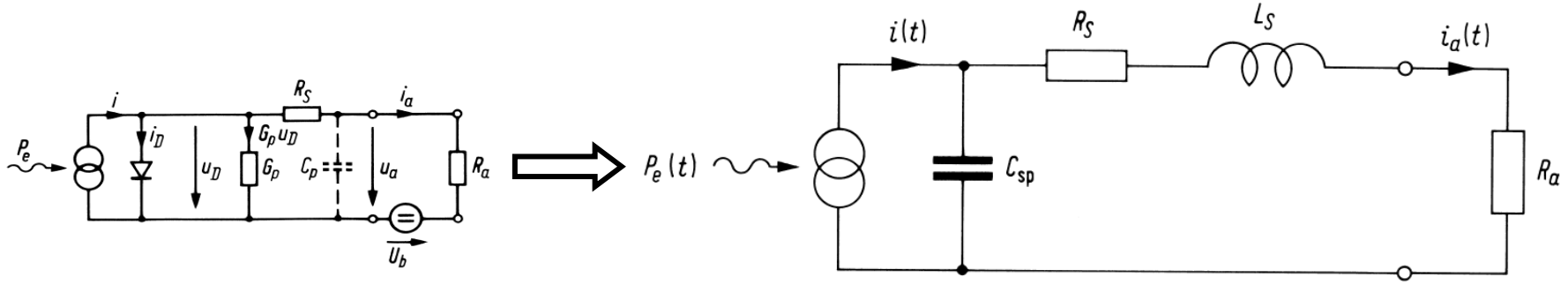

Equivalent electrical circuit of a photodiode. P_e incident external optical power, C_{sp} depletion-layer capacity, R_S series resistance, L_S series inductance, R_a load resistance

FT of $i(t)$, $i_a(t)$ are $I(f)$, $I_a(f)$ $\rightarrow$ transfer function $H_S(f)$ from photo detector to load resistor R_a:

$$H_S(f) = \frac{I_a(f)}{I(f)} = \frac{\omega_r^2}{(\mathrm{j}\,\omega)^2 + 2\gamma_r(\mathrm{j}\,\omega) + \omega_r^2},$$

$$\omega_r^2 = \frac{1}{L_S C_{\mathrm{sp}}}, \qquad 2\gamma_r = \frac{R_S + R_a}{L_S}$$

$C_{\mathrm{sp}} = 0.04 \ldots 0.2\,\mathrm{pF}$; $R_S = 10 \ldots 50\,\Omega$; $L_S = 0.15 \ldots 0.5\,\mathrm{nH}$; $R_a = 50\,\Omega$. F-diameter $7 \ldots 200\,\mu\mathrm{m}$, typically $30 \ldots 80\,\mu\mathrm{m}$.

Noise

Reasons for Noise (1)

- Photo current $i(t) \sim P(t)$ (classical instantaneous power from average over a few optical periods). Ideal sinusoidal classical signal $s\cos(\omega_S t + \varphi) \rightarrow P(t) = s^2/2 = \text{const}$, no $i(t)$-noise. Quantum theory: Ideal signal (coherent state) represented by stream of Poisson distributed statistically independent photons.
- With probability η each photon generates — independently from any other photon — an electron-hole pair. External short-circuit current behaves as stream of Poisson distributed elementary charges: Shot noise („Schrotrauschen“).
- Shot noise is interpreted as unavoidable *quantum noise*, which neither belongs to the light source nor to the photodetector alone. It only becomes relevant for a light-detector interaction.
- Classical power fluctuations $P(t) \rightarrow$ excess noise

Reasons for Noise (2)

- Basically unavoidable further noise sources: Spontaneous emission in optically amplifying media, statistical charge multiplication in an avalanche photodiode (APD), shot noise of charges when crossing a pn-junction in electronic devices (diodes, transistors), thermal noise in resistors (thermal radiation)
- Real laser light $s(t)\cos[\omega_S t + \varphi(t)]$ has — besides fundamental Poisson noise — also random amplitude (relative intensity noise, RIN) and random phase (phase noise).
- Two and multi-path interferometers convert phase noise into amplitude noise:

  Backreflections into a laser

  Modal noise in fibres

  Mode-partition noise in lasers oscillating in several modes
- Besides shot and RIN also dark current noise and noise caused by parasitic light plays a role.

Photocurrent Noise

Photocurrent Noise Statistics

Photocurrent $i(t)$ (i for short) fluctuates around expectation $\overline{i(t)}$ ($\bar{i}$ for short). Fluctuation $\delta i(t)$ (δi for short):

$$\delta i(t) = i(t) - \overline{i(t)}\,, \qquad \delta i = i - \bar{i}$$

Autocorrelation function $\vartheta_i(\tau)$ of i, related to two-sided power spectrum $\Theta_i(f)$ via Fourier transform:

$$\vartheta_i(\tau) = \overline{i(t+\tau)\,i(t)}\,, \qquad \Theta_i(f) = \int_{-\infty}^{+\infty} \vartheta_i(\tau)\,\mathrm{e}^{-\mathrm{j}\,2\pi f\tau}\,\mathrm{d}\tau$$

$\vartheta_i(\tau)$ is real $\rightarrow \Theta_i(f) = \Theta_i^*(-f)$. From definition, symmetry relation $\vartheta_i(\tau) = \vartheta_i(-\tau) \rightarrow \Theta_i(f) = \Theta_i^*(f) \rightarrow \vartheta_i(\tau) = \int_0^\infty 2\Theta_i(f)\,\mathrm{e}^{\mathrm{j}\,2\pi f\tau}\,\mathrm{d}f$ defines one-sided real spectr. $2\Theta_i(f)$. Variance $\sigma_i^2 = \vartheta_i(\tau = 0)$:

$$\sigma_i^2 = \overline{(i-\bar{i}\,)^2} = \overline{\delta i^2} = \int_{-\infty}^{+\infty} \Theta_i(f)\,\mathrm{d}f = \int_0^\infty 2\Theta_i(f)\,\mathrm{d}f$$

LECTURE 14

Photocurrent Shot Noise and Poisson Statistics

Spectral density of shot noise is $\Theta_i(f) = e\bar{i}$ (no derivation here). Differential fluctuations for observation time T inside differential bandwidth $\mathrm{d}f = 1/(2T)$ centred at f:

$$\mathrm{d}\left(\overline{\delta i^2}\right) = 2\Theta_i(f)\,\mathrm{d}f = 2e\bar{i}\,\mathrm{d}f = \overline{|i_{RD}|^2}$$

Complex phasor i_{RD} (RMS value $|i_{RD}|$) defined with same power $\overline{|i_{RD}|^2}$ as actual noise process.

Shot noise equation expresses property of underlying Poisson statistics for photons: Probability $p_N(N)$ for measuring N photons, if expectation is $\overline{N} = N_e$, and associated second central moment:

$$p_N(N) = \frac{\overline{N}^N}{N!}\,\mathrm{e}^{-\overline{N}}, \quad \overline{\delta N^2} = \overline{(N - N_e)^2} = \overline{N}\,, \qquad \overline{N} = N_e$$

pin-Photodiode Noise

Expected current $\bar{i} = S\overline{P_e}$.

Classical additional fluctuations from laser source having a total output power P_a described by relative intensity noise (RIN):

$$\mathrm{RIN} = \int_0^\infty \mathrm{RIN}(f)\,\mathrm{d}f = \frac{\overline{\delta P_a^2}}{\overline{P_a}^2}, \qquad \mathrm{d}\left(\overline{\delta P_a^2}\right) = \overline{P_a}^2\,\mathrm{RIN}(f)\,\mathrm{d}f$$

Total differential photocurrent noise fluctuation including received RIN (mean power $\overline{P_a} \sim \overline{P_e} \sim \bar{i}$) given by:

$$\mathrm{d}\left(\overline{\delta i^2}\right) = \underbrace{2e\bar{i}\,\mathrm{d}f}_{\text{shot or quantum noise}} + \underbrace{\bar{i}^2\,\mathrm{RIN}(f)\,\mathrm{d}f}_{\text{classical noise}}$$

Spectral shot noise power density for $\bar{i} = 1\,\mathrm{mA}$ measured at a resistor $R = 50\,\Omega$:

$$\frac{\mathrm{d}\left(\overline{\delta i^2}\right)R}{\mathrm{d}f} = 2e\bar{i}R \mathrel{\widehat{=}} -168\,\mathrm{dBm\,Hz^{-1}}$$

Avalanche Photodiode Noise

Avalanche photodiode (APD) amplifies the photocurrent by a current multiplication factor M (statistical average $\overline{M} = M_0$. Avalanche multiplication process contributes additional noise described by excess noise factor F_M and its approximation.):

$$F_M = \frac{\overline{M^2}}{\overline{M}^2} = \frac{\overline{M^2}}{M_0^2} = 1 + \frac{\overline{\delta M^2}}{M_0^2}, \qquad F_M = M_0^x, \quad x > 0$$

In observation time $T = 1/(2\,\mathrm{d}f)$, signal current i_S and noise current i_{RD} are

$$\bar{i} = M_0 i_{\mathrm{pr}} = M_0 \frac{\eta e}{h f_L} \overline{P_e} = i_S,$$

$$\mathrm{d}\left(\overline{\delta i^2}\right) = 2 e i_{\mathrm{pr}} M_0^2 F_M \,\mathrm{d}f + (M_0 i_{\mathrm{pr}})^2 \,\mathrm{RIN}(f)\,\mathrm{d}f = \overline{|i_{RD}|^2}.$$

For $M_0 = 1$, $F_M = 1$, the equation above reduces to the case of the pin photodiode.

Thermal Noise

Thermal Noise (1)

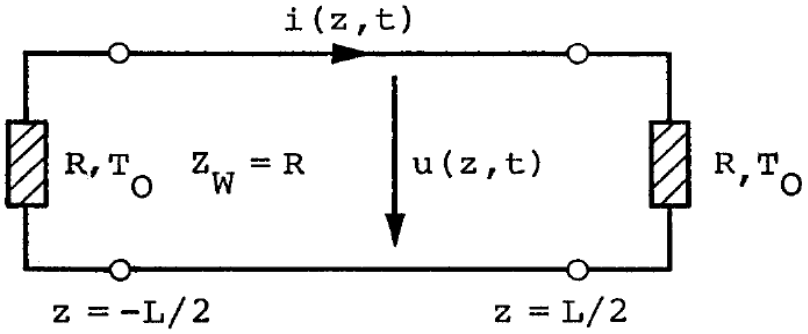

Planck's law: Single TEM mode, one polarization, $B \ll f$:

$$P_v = \bar{n} h f B = \frac{h f B}{\exp[hf/(kT_0)] - 1}$$

Wave impedance-matched lossless transmission line. Resistances R at temperature T_0 generate thermal noise.

Due to impedance matching, P_v denotes the *available* noise power of a resistor R at temperature T_0 in bandwidth B centered at frequency f. One-sided power spectrum:

$$w(f) = \frac{hf}{\exp[hf/(kT_0)] - 1}, \qquad \lim_{hf \ll kT_0} w(f) = kT_0 \quad \text{(Nyquist)}$$

Thermal Noise (2)

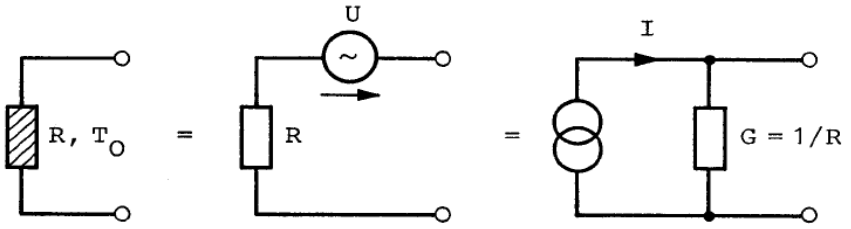

Equivalent circuit of a resistor at temperature T_0 emitting thermal noise

Planck's law: Single TEM mode, one polarization, $hf \ll kT_0$:

$$w(f) = kT_0$$

Equivalent circuit of ohmic resistance at T_0 with thermal voltage or current source and associated RMS phasors in Δf:

$$\overline{|U|^2} = w_U(f)\Delta f = 4kT_0R\Delta f, \qquad \overline{|I|^2} = w_I(f)\Delta f = 4kT_0G\Delta f$$

Equivalent shot noise and equivalent thermal noise:

$$\overline{|I|^2} = i_{\text{eff}}^2 = 2ei_{\text{eq}}\,\Delta f = 4kT_0G_{\text{eq}}\Delta f, \qquad \frac{1}{G_{\text{eq}}} = \frac{2U_T}{i_{\text{eq}}},\ U_T = \frac{kT_0}{e} = 25\,\text{mV}$$

Equivalent shot noise current:

$$\frac{i_{\text{eq}}}{\mu\text{A}} = 3.13\left(\frac{i_{\text{eff}}/\sqrt{\Delta f}}{\text{pA}/\sqrt{\text{Hz}}}\right)^2 = 50\,\frac{G_{\text{eq}}}{\text{mS}}$$

Shot noise $i_{\text{eq}} = 1\,\mu\text{A}\,(1\,\text{mA}) \mathrel{\widehat{=}}$ thermal noise $G_{\text{eq}}^{-1} = 50\,\text{k}\Omega\,(50\,\Omega)$

Thermal Noise (3)

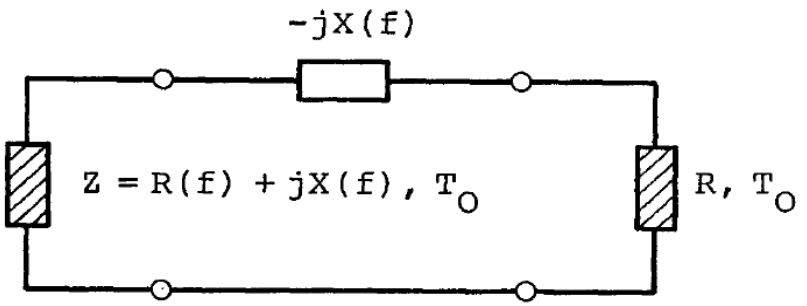

Noise in thermodynamical equilibrium. Impedance match:
(Noise pwr $\Rightarrow$) = (noise pwr $\Leftarrow$)

$$\overline{|U|^2} = 4kT_0\Re\{Z(f)\}\,\Delta f,$$
$$\overline{|I|^2} = 4kT_0\Re\{Y(f)\}\,\Delta f$$

Impedance $Z(f) = R(f) + \mathrm{j}\,X(f)$ emitting thermal noise

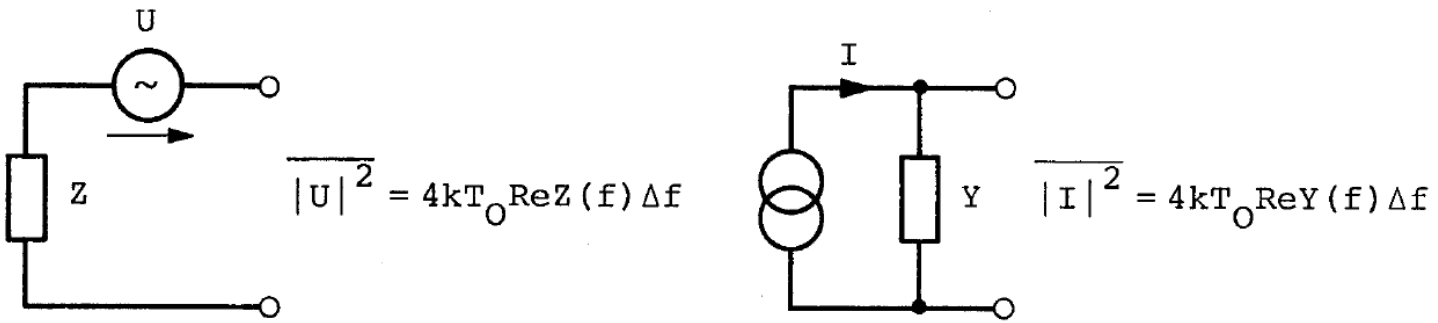

Equivalent circuit of an impedance $Z = 1/Y$ emitting thermal noise

Thermal Noise — Summary

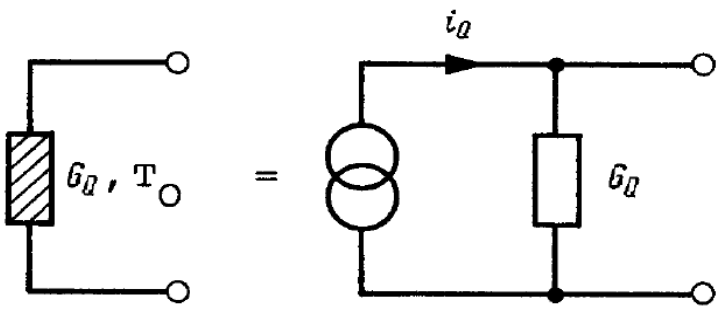

Equivalent circuit of a conductance G_Q with thermal noise

Temperature T, electrons move randomly $\rightarrow$ random current / voltage. PD load resistance at amplifier input adds noise $\rightarrow$ thermal noise, Johnson or Nyquist noise.

RMS noise phasors discussed in previous slide. Equivalent short-circuit noise phasor i_Q of conductance G_Q at temperature T_0 has an expectation $\overline{i_Q} = 0$ and a second moment:

$$\overline{|i_Q|^2} = 4kT_0G_Q\Delta f, \qquad T_0 = 293\,\mathrm{K}$$

For microwave frequencies $hf \ll kT_0$: Available noise power (absorbed by impedance-matched load in bandwidth df) and one-sided spectral density $2\Theta_T(f)$: $\quad (2e \times 1\,\mathrm{mA} \times 50\,\Omega \mathrel{\widehat{=}} -168\,\mathrm{dBm\,Hz^{-1}})$

$$P_v = kT_0\Delta f = \overline{|i_Q/2|^2}/G_Q, \quad 2\Theta_T(f) = kT_0 \mathrel{\widehat{=}} -174\,\mathrm{dBm\,Hz^{-1}}$$

Electronic Amplifier Noise

Noisy Two-Port Network — Noise Sources

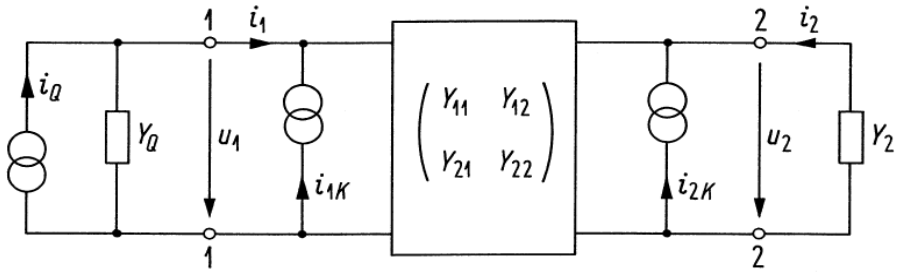

Signal source admittance $Y_Q \rightarrow$ thermal noise, current phasor i_Q ($T_0 = 293\,\mathrm{K}$):

$$\overline{|i_Q|^2} = 4kT_0G_QB,$$

$$Y_Q = G_Q + \mathrm{j}\,B_Q$$

Noisy two-port network (curent sources i_{1K}, i_{2K}) with noisy generator admittance (i_Q, Y_Q) and noise-free load admittance Y_2

Noise of two-port network known by i_{1K}, i_{2K}, $\overline{|i_{1K}|^2}$, $\overline{|i_{2K}|^2}$ and $\overline{i_{1K}i_{2K}^*}$ in B at f. Transform $i_{2K} \rightarrow$ input. Two-port noise network transparent for signal, uncorrelated noise sources i_n, u_n ($\overline{i_n u_n^*} = 0$), correlation admittance Y_c. Between terminal pairs 1-1, 2-2:

Noisy Two-Port Network — Transformation of Noise Sources

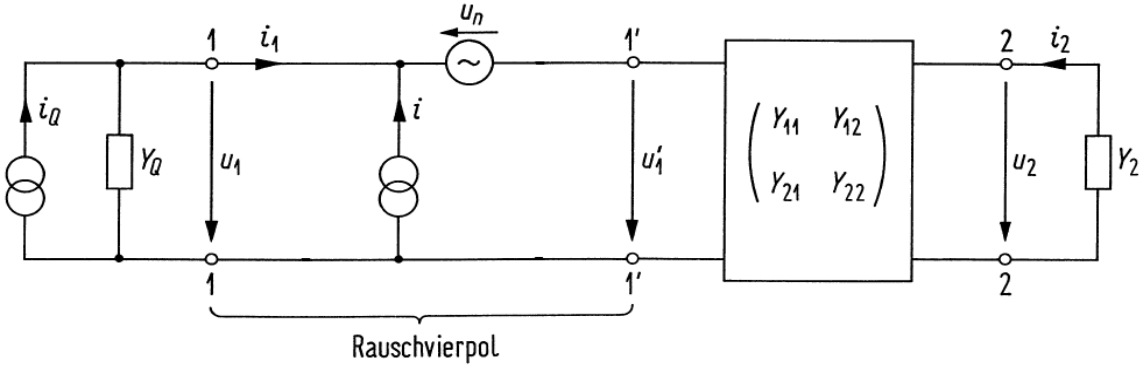

$$-i_{1K} = -i + Y_{11} u_n \,,$$
$$-i_{2K} = Y_{21} u_n \,,$$
$$i = i_{1K} - \frac{Y_{11}}{Y_{21}} i_{2K}$$

Noise properties of two-port network described by a two-port noise network („Rauschvierpol“) comprising partially correlated noise generators i, u_n ($\overline{i_n^* u_n^*} \neq 0$)

Noise of two-port network known by i_{1K}, i_{2K}, $\overline{|i_{1K}|^2}$, $\overline{|i_{2K}|^2}$ and $\overline{i_{1K} i_{2K}^*}$ in B at f. Transform $i_{2K} \rightarrow$ input. Two-port noise network transparent for signal, uncorrelated noise sources i_n, u_n ($\overline{i_n u_n^*} = 0$), correlation admittance Y_c. Between terminal pairs 1-1, 2-2:

$$\begin{pmatrix} i_1 \\ i_2 \end{pmatrix} = \begin{pmatrix} -i_{1K} \\ -i_{2K} \end{pmatrix} + \begin{pmatrix} Y_{11}\, Y_{12} \\ Y_{21}\, Y_{22} \end{pmatrix} \begin{pmatrix} u_1 \\ u_2 \end{pmatrix} = \begin{pmatrix} -i \\ 0 \end{pmatrix} + \begin{pmatrix} Y_{11}\, Y_{12} \\ Y_{21}\, Y_{22} \end{pmatrix} \begin{pmatrix} u_1 + u_n \\ u_2 \end{pmatrix}$$

Noisy Two-Port Network — Parameters of Two-Port Noise NW

$$Y_c = Y_{11} - Y_{21}\,\frac{\overline{i_{1K} i_{2K}^*}}{\overline{|i_{2K}|^2}} = G_c + \mathrm{j}\,B_c\,,$$

$$\overline{|i_{1K}|^2} = \overline{|i|^2} + |Y_{11}|^2\,\overline{|u_n|^2} - 2\Re\left\{Y_{11}^*\,\overline{i\,u_n^*}\right\}$$

$$\rightarrow\ \overline{|i_n|^2} = \overline{|i_{1K}|^2} - \left|\overline{i_{1K} i_{2K}^*}\right|^2 / \overline{|i_{2K}|^2},$$

$$\overline{|u_n|^2} = \overline{|i_{2K}|^2}/|Y_{21}|^2$$

$$-i_{1K} = -i + Y_{11} u_n\,,$$

$$-i_{2K} = Y_{21} u_n\,,$$

$$i = i_{1K} - \frac{Y_{11}}{Y_{21}}\,i_{2K}\,,$$

$$i = i_n + Y_c\,u_n\,,$$

$$\overline{i\,u_n^*} = \underbrace{\overline{i_n\,u_n^*}}_{=0} + Y_c\,\overline{|u_n|^2}$$

$$i_n = i - Y_c u_n = i_{1K} + (Y_{11} - Y_c) u_n$$

$$i_n = i_{1K} + Y_{21}\,\frac{\overline{i_{1K} i_{2K}^*}}{\overline{|i_{2K}|^2}}\,\frac{-i_{2K}}{Y_{21}}$$

Noise of two-port network known by i_{1K}, i_{2K}, $\overline{|i_{1K}|^2}$, $\overline{|i_{2K}|^2}$ and $\overline{i_{1K} i_{2K}^*}$ in B at f. Transform $i_{2K} \rightarrow$ input. Two-port noise network transparent for signal, uncorrelated noise sources i_n, u_n ($\overline{i_n u_n^*} = 0$), correlation admittance Y_c. Between terminal pairs 1-1, 2-2:

$$\begin{pmatrix} i_1 \\ i_2 \end{pmatrix} = \begin{pmatrix} -i_{1K} \\ -i_{2K} \end{pmatrix} + \begin{pmatrix} Y_{11} & Y_{12} \\ Y_{21} & Y_{22} \end{pmatrix} \begin{pmatrix} u_1 \\ u_2 \end{pmatrix} = \begin{pmatrix} -i \\ 0 \end{pmatrix} + \begin{pmatrix} Y_{11} & Y_{12} \\ Y_{21} & Y_{22} \end{pmatrix} \begin{pmatrix} u_1 + u_n \\ u_2 \end{pmatrix}$$

$$\begin{pmatrix} i_1 \\ i_2 \end{pmatrix} = \begin{pmatrix} -i_n - Y_c\,u_n + Y_{11} u_n \\ Y_{21} u_n \end{pmatrix} + \begin{pmatrix} Y_{11} & Y_{12} \\ Y_{21} & Y_{22} \end{pmatrix} \begin{pmatrix} u_1 \\ u_2 \end{pmatrix}$$

Noisy Two-Port Network — Parameter Calculation

$$Y_c = Y_{11} - Y_{21}\,\frac{\overline{i_{1K} i_{2K}^*}}{\overline{|i_{2K}|^2}} = G_c + \mathrm{j}\,B_c\,,$$

$$\overline{|i_{1K}|^2} = \overline{|i|^2} + |Y_{11}|^2\,\overline{|u_n|^2} - 2\Re\left\{Y_{11}^*\,\overline{i\,u_n^*}\right\}$$

$$\rightarrow\ \overline{|i_n|^2} = \overline{|i_{1K}|^2} - \left|\overline{i_{1K} i_{2K}^*}\right|^2 / \overline{|i_{2K}|^2},$$

$$\overline{|u_n|^2} = \overline{|i_{2K}|^2}/|Y_{21}|^2$$

$$-i_{1K} = -i + Y_{11} u_n\,,$$

$$-i_{2K} = Y_{21} u_n\,,$$

$$i = i_{1K} - \frac{Y_{11}}{Y_{21}}\,i_{2K}\,,$$

$$i = i_n + Y_c\,u_n\,,$$

$$\overline{i\,u_n^*} = \underbrace{\overline{i_n\,u_n^*}}_{=0} + Y_c\,\overline{|u_n|^2}$$

$$i_n = i - Y_c u_n = i_{1K} + (Y_{11} - Y_c) u_n$$

$$i_n = i_{1K} + Y_{21}\,\frac{\overline{i_{1K} i_{2K}^*}}{\overline{|i_{2K}|^2}}\,\frac{-i_{2K}}{Y_{21}}$$

$$Y_c = \frac{\overline{i\,u_n^*}}{\overline{|u_n|^2}} = \frac{\overline{(i_{1K} + Y_{11} u_n) u_n^*}}{\overline{|u_n|^2}} = \frac{\overline{i_{1K}\,\frac{-i_{2K}^*}{Y_{21}^*}} + Y_{11}\,\overline{|u_n|^2}}{\overline{|u_n|^2} = \overline{|i_{2K}|^2}/|Y_{21}|^2}$$

$$\overline{|i_{1K}|^2} = \overline{|i - Y_{11} u_n|^2} = \overline{|i|^2} + \overline{|Y_{11} u_n|^2} - \left[Y_{11}^*\,\overline{i\,u_n^*} + \mathrm{cc}\right]$$

$$-i_{1K} = -i_n - Y_c\,u_n + Y_{11} u_n = -i_n + \frac{Y_{11} - Y_c}{Y_{21}}\,(-i_{2K}) = -i_n - \frac{Y_{21}\,\frac{\overline{i_{1K} i_{2K}^*}}{\overline{|i_{2K}|^2}}}{Y_{21}}\,i_{2K}\,,$$

$$\overline{|i_n|^2} = \overline{\left|i_{1K} - \frac{\overline{i_{1K} i_{2K}^*}}{\overline{|i_{2K}|^2}}\,i_{2K}\right|^2} = \overline{|i_{1K}|^2} + \frac{\left|\overline{i_{1K} i_{2K}^*}\right|^2}{\overline{|i_{2K}|^2}^2}\,\overline{|i_{2K}|^2} - \left[\overline{i_{1K} i_{2K}^*}\,\frac{\overline{i_{1K}^* i_{2K}}}{\overline{|i_{2K}|^2}} + \mathrm{cc}\right]$$

Noisy Two-Port Network — Two-Port Noise Network

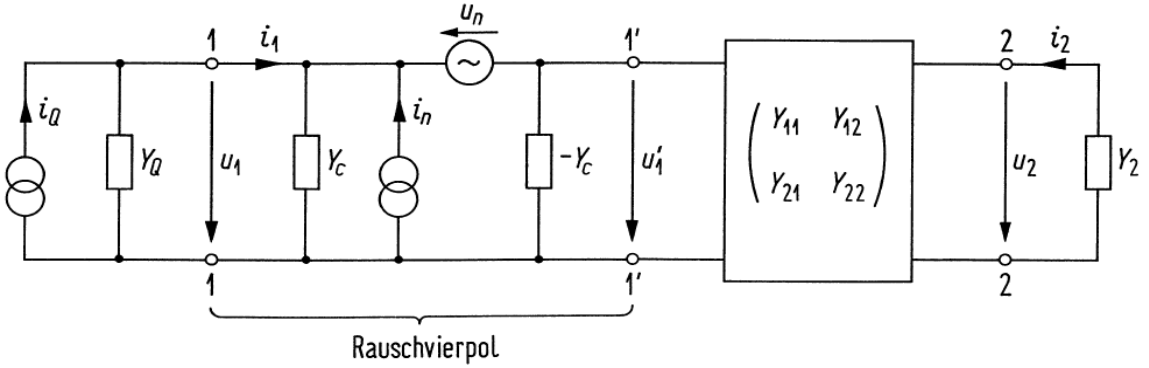

$$-i_{1K} = -i + Y_{11} u_n \,,$$
$$-i_{2K} = Y_{21} u_n \,,$$
$$i = i_{1K} - \frac{Y_{11}}{Y_{21}} i_{2K} \,,$$
$$i = i_n + Y_c u_n$$

Noise properties of two-port network described by a two-port noise network („Rauschvierpol“) comprising partially correlated noise generators i, u_n ($\overline{i_n^* u_n^*} \neq 0$)

Noise of two-port network known by i_{1K}, i_{2K}, $\overline{|i_{1K}|^2}$, $\overline{|i_{2K}|^2}$ and $\overline{i_{1K} i_{2K}^*}$ in B at f. Transform $i_{2K} \rightarrow$ input. Two-port noise network transparent for signal, uncorrelated noise sources i_n, u_n ($\overline{i_n u_n^*} = 0$), correlation admittance Y_c. Between terminal pairs 1-1, 2-2:

$$\begin{pmatrix} i_1 \\ i_2 \end{pmatrix} = \begin{pmatrix} -i_{1K} \\ -i_{2K} \end{pmatrix} + \begin{pmatrix} Y_{11} & Y_{12} \\ Y_{21} & Y_{22} \end{pmatrix} \begin{pmatrix} u_1 \\ u_2 \end{pmatrix} = \begin{pmatrix} -i \\ 0 \end{pmatrix} + \begin{pmatrix} Y_{11} & Y_{12} \\ Y_{21} & Y_{22} \end{pmatrix} \begin{pmatrix} u_1 + u_n \\ u_2 \end{pmatrix}$$

$$\begin{pmatrix} i_1 \\ i_2 \end{pmatrix} = \begin{pmatrix} -i_n - Y_c u_n + Y_{11} u_n \\ Y_{21} u_n \end{pmatrix} + \begin{pmatrix} Y_{11} & Y_{12} \\ Y_{21} & Y_{22} \end{pmatrix} \begin{pmatrix} u_1 \\ u_2 \end{pmatrix}$$

Noisy Two-Port Network — Noise Resistance and Conductance

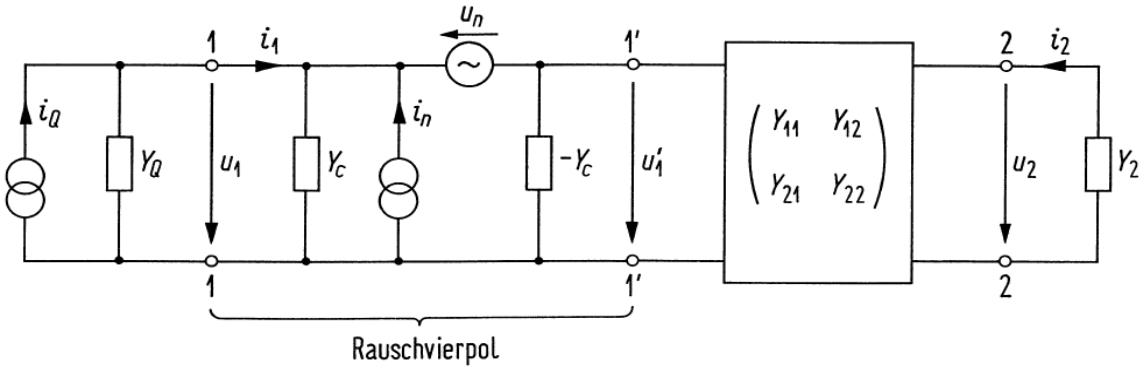

Two-port noise network („Rauschvierpol"), representing noise properties of two-port network by uncorrelated noise generators i_n, u_n ($\overline{i_n u_n^*} = 0$) together with correlation admittance Y_c

Equivalent noise resistance R_n and conductance G_n ($R_n \neq 1/G_n$):

$$\overline{|i_n|^2} := 4kT_0\,G_n B, \qquad \overline{|u_n|^2} := 4kT_0\,R_n B$$

Noise figure F: Ratio of noise power at load admittance in df for noisy and hypothetically noise-free two-port network. Computed by ratio of modulus-squared short-circuit noise currents at (physically not accessible) terminals $1' - 1'$ ($T_0 = 293\,\mathrm{K}$):

$$i_R = i_Q + i_n + u_n(Y_Q + Y_c)\,, \quad \overline{|i_Q|^2} = 4kT_0\,G_Q B\,, \quad Y_Q = G_Q + \mathrm{j}\,B_Q$$

Noisy Two-Port Network — Definitions

Transducer power gain („Übertragungsgewinn“): Ratio of power P_{S2} delivered to load admittance and available source power P_{Sv1} („verfügbare Wirkleistung“), and

Available gain („verfügbarer Gewinn“): Ratio of available power at output terminals and available power of signal source:

$$\Gamma_v(f) = \frac{P_{Sv2}}{P_{Sv1}}, \qquad \Gamma_{\ddot{u}}(f) = \frac{P_{S2}}{P_{Sv1}}$$

(Available) SNR at two-port network input (output): Ratio of (available) signal and noise power („Rauschleistung“). Input/output SNR quotient is noise figure F:

$$\mathrm{SNR}_{v1} = \frac{P_{Sv1}}{P_{Rv1}}, \quad \mathrm{SNR}_2 = \frac{P_{S2}}{P_{R2}}, \quad F = \frac{\mathrm{SNR}_{v1}}{\mathrm{SNR}_2} = \frac{P_{Sv1}}{P_{Rv1}} \frac{P_{R2}}{P_{S2}} = \frac{P_{R2}}{\Gamma_{\ddot{u}} P_{Rv1}} \geq 1$$

Noise bandwidth („Rauschbandbreite“):

$$B_R = \frac{\int_0^\infty \Gamma_{\ddot{u}}(f)\,\mathrm{d}f}{\Gamma_{\ddot{u}}(f_0)}$$

Noisy Two-Port Network — Noise Figure and Temperature

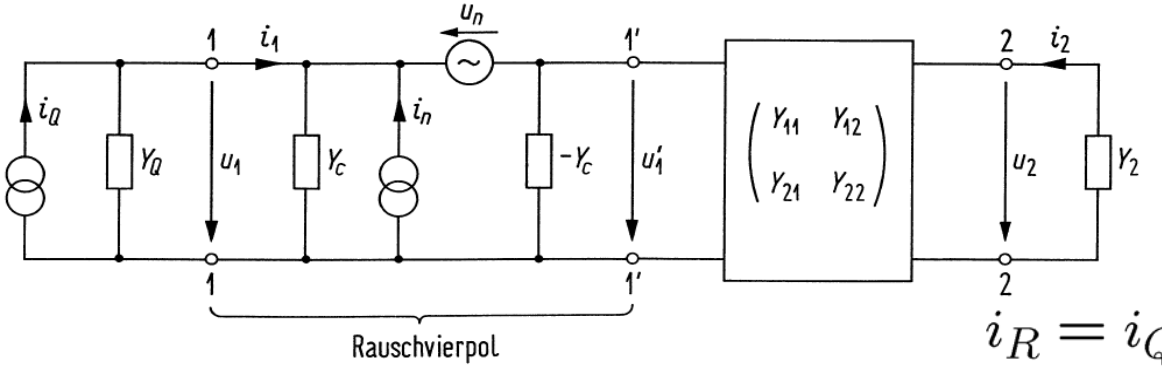

$$\overline{|i_Q|^2} = 4kT_0\,G_Q\,\mathrm{d}f,$$
$$\overline{|i_n|^2} = 4kT_0\,G_n\,\mathrm{d}f,$$
$$\overline{|u_n|^2} = 4kT_0\,R_n\,\mathrm{d}f,$$
$$i_R = i_Q + i_n + u_n(Y_Q + Y_c)$$

Two-port noise network („Rauschvierpol"), representing noise properties of two-port network by uncorrelated noise generators i_n, u_n ($\overline{i_n u_n^*} = 0$) together with correlation admittance Y_c

Noise figure F, excess NF $F_z = F - 1$, noise temperature T_R:

$$F = \frac{\mathrm{SNR}_{v1}}{\mathrm{SNR}_2} = \frac{\text{total noise power in } \mathrm{d}f \text{ at load } Y_2}{\text{noise power in } \mathrm{d}f \text{ at load } Y_2 \text{ for noise-free two-port}}$$

$$F = 1 + F_z = 1 + \frac{T_R}{T_0} = \frac{T_0 + T_R}{T_0} = \frac{\overline{|i_R|^2}}{\overline{|i_Q|^2}} = 1 + \frac{G_n + R_n|Y_Q + Y_c|^2}{G_Q}$$

Noise-free: $F = 1$ ($F_z = 0$, $T_R = 0$). Relative minimum (noise tuning: $B_Q = -B_c$). Then absolute minimum for noise matching:

$$G_{Q\mathrm{opt}} = \sqrt{G_n/R_n + G_c^2}\,, \qquad F_{z\mathrm{min}} = 2R_n(G_{Q\mathrm{opt}} + G_c)$$

Concatenation of Noisy Two-Port Networks

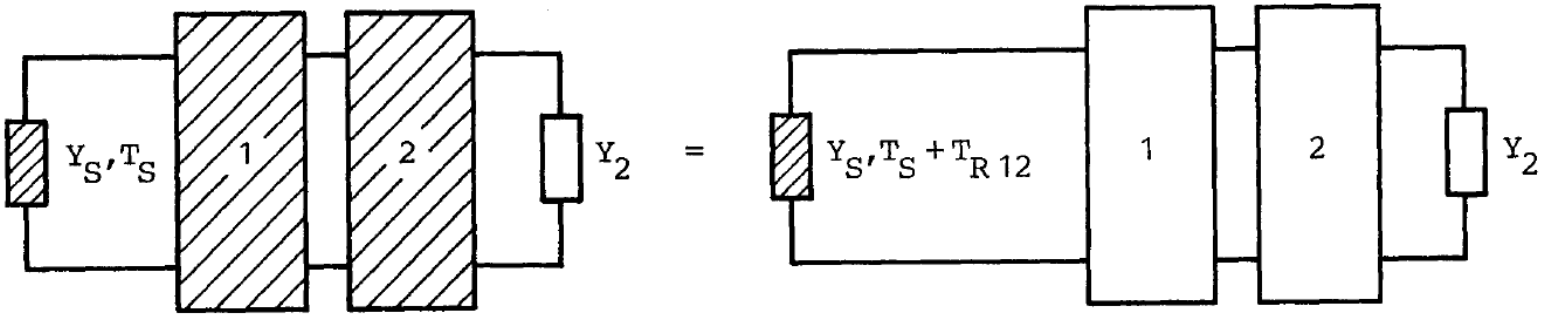

Concatenation of noisy two-port networks

Noise temperature T_{R1} for Y_S at T_S, T_{R2} defined for $Y_{\text{out}}^{(1)}$ at T_S:

$$Y_{\text{out}}^{(1)} = Y_{22}^{(1)} - \frac{Y_{12}^{(1)} Y_{21}^{(1)}}{Y_{11}^{(1)} + Y_S}, \qquad \Gamma_{\ddot{u}}(f) = \frac{P_{S2}}{P_{Sv1}}, \qquad \Gamma_v = \frac{P_{Sv2}}{P_{Sv1}}$$

Two-port (TP) network sequence $1 \rightarrow 2$:

$$F_{12} = \frac{\overbrace{k(T_S + T_{R\,1})\Gamma_{v\,1}\,\mathrm{d}f}^{\text{available total noise power from TP}_1} \times \Gamma_{\ddot{u}\,2} + \overbrace{kT_{R\,2}\Gamma_{\ddot{u}\,2}\,\mathrm{d}f}^{\text{noise power from TP}_2}}{\underbrace{kT_S\Gamma_{v\,1}\,\mathrm{d}f}_{\text{noise-free TP}_1} \times \underbrace{\Gamma_{\ddot{u}\,2}}_{\text{noise-free TP}_2}}$$

$$= 1 + \frac{T_{R\,1}}{T_S} + \frac{T_{R\,2}}{\Gamma_{v1} T_S} = 1 + \frac{T_{R\,12}}{T_S} = 1 + F_{z12}$$

Concatenation of Noisy TP NW — Friis´ Formula, Noise Measure

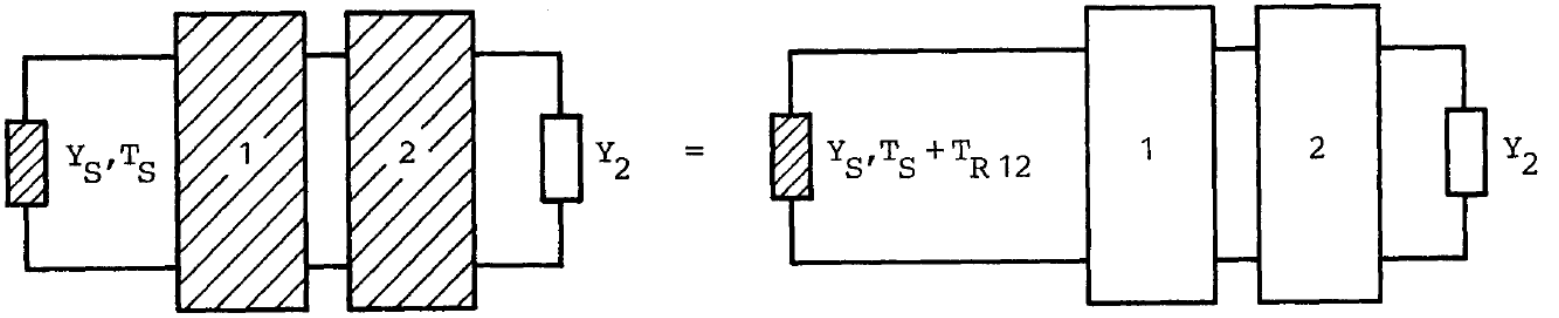

Concatenation of noisy two-port networks

Noise temperature and excess noise figure, Friis' formula:

$$T_{R12} = T_{R\,1} + \frac{T_{R\,2}}{\Gamma_{v1}}\,, \qquad F_{z12} = F_{z1} + \frac{F_{z2}}{\Gamma_{v1}}\,,$$

$$F_{z12\ldots N} = F_{z1} + \frac{F_{z2}}{\Gamma_{v1}} + \frac{F_{z3}}{\Gamma_{v1}\Gamma_{v2}} + \ldots + \frac{F_{zN}}{\Gamma_{v1}\Gamma_{v2}\cdots\Gamma_{v,N-1}}$$

Noise measure, assuming $F_{z12} < F_{z21}$ and $Y_{\text{out}}^{(1)} = Y_{\text{out}}^{(2)} = Y_S$:

$$F_{z12} = F_{z1} + \frac{F_{z2}}{\Gamma_{v\,1}} < F_{z2} + \frac{F_{z1}}{\Gamma_{v2}} = F_{z21}\,, \qquad \frac{F_{z1}}{1 - 1/\Gamma_{v1}} < \frac{F_{z2}}{1 - 1/\Gamma_{v2}}$$

$$M_i = \frac{F_{zi}}{1 - 1/\Gamma_{v\,i}}$$

Low-noise TP chain, if $M_1 < M_2$

Harald T. Friis

In 1942, Harald T. Friis, working in Bell Labs in Holmdel NJ, developed the theory of "noise figure" that allows engineers to calculate the signal-to-noise ratio at the output of a complex receiver chain, and thus has a powerful equation named after him.

Harald Friis was born in Naestved Denmark, in 1893. He graduated 1916 in Electrical Engineering from the Polytechnic Institute (founded 1829 by H.C. Oersted, the discoverer of electromagnetics). In 1919 he received a fellowship which enabled him to come to the United States where he studied radio engineering at Columbia University. In 1920, Friis joined a research group at the Western Electric Company and apparently got stuck in the U.S.A. He eventually became a U.S. citizen, which later did not prevent him from being awarded the Valdemar Poulsen Medal of the Danish Academy of Sciences.

He held 31 U. S. patents submitted over five decades of research. In 1971 he published a book on his life titled "Seventy Five Years in an Exciting World". This gem not only contains some great history, but also strange glimpses of Harald Friis' life, such as drinking *near-beer* instead of milk as a child, apprenticing as a blacksmith, being bitten by bedbugs in a New York hotel, and naming his favorite pipe tobacco.

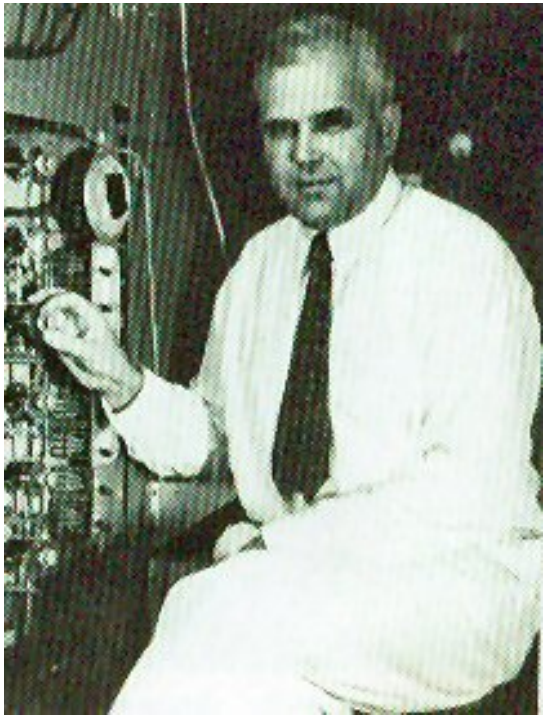

Near-beer is a malt beverage which does not contain enough alcohol to be considered a true beer. The concept of near-beer arose during the Prohibition in the United States, when alcohol was not permitted, but people still had a taste for it.

Near-beer is not the same thing as small beer, a low-alcohol beer which has been brewed for centuries.

http://www.microwaves101.com/encyclopedia/halloffame2.cfm#friis

LECTURE 15

Optical Amplifier Noise

Optical Amplifier — Amplified Spontaneous Emission (ASE)

OA single-pass gain $\mathcal{G}_s$ → signal output power $\mathcal{G}_s P_e$, $P_e = \frac{1}{2}A^2$, perturbed by narrowband noise with optical bandwidth B_O

Quantum noise (amplified spontaneous emission, ASE) is limitation in transmission systems.

ASE in 1 polarization $P_{\mathrm{ASE},x}$ (e. g., linearly polarized in x-dir.), ideal amplifier with minimum input noise spectral density $w_O = hf_e$ (*one* transverse mode, *one* polarization, inversion factor n_{sp}):

$$P_{\mathrm{ASE},x} = (\mathcal{G}_s - 1)\, n_{\mathrm{sp}} w_O B_O = \mathcal{G}_s P_{r\,\mathrm{eq},x}$$

$$P_{r\,\mathrm{eq},x} = \frac{\mathcal{G}_s - 1}{\mathcal{G}_s}\, n_{\mathrm{sp}} P_{r\,\mathrm{qu},x}$$

$$P_{r\,\mathrm{qu},x} = w_O B_O$$

Minimum-uncertainty quantum fluctuations $w_O B_O$, this power cannot be extracted. For transparent "amplifier" $\mathcal{G}_s = 1$: $P_{\mathrm{ASE},x} = 0$.

Gain and inversion factor are linked: If $\mathcal{G}_s$ is small (but $\mathcal{G}_s > 1$), the inversion factor n_{sp} becomes large!

Direct Receiver

Noisy Two-Port Network — Transimpedance Amplifier

$$Y_F = G_F + \mathrm{j}\,B_F \qquad \overline{|i_F|^2} = 4kT_0G_F\,\mathrm{d}f$$

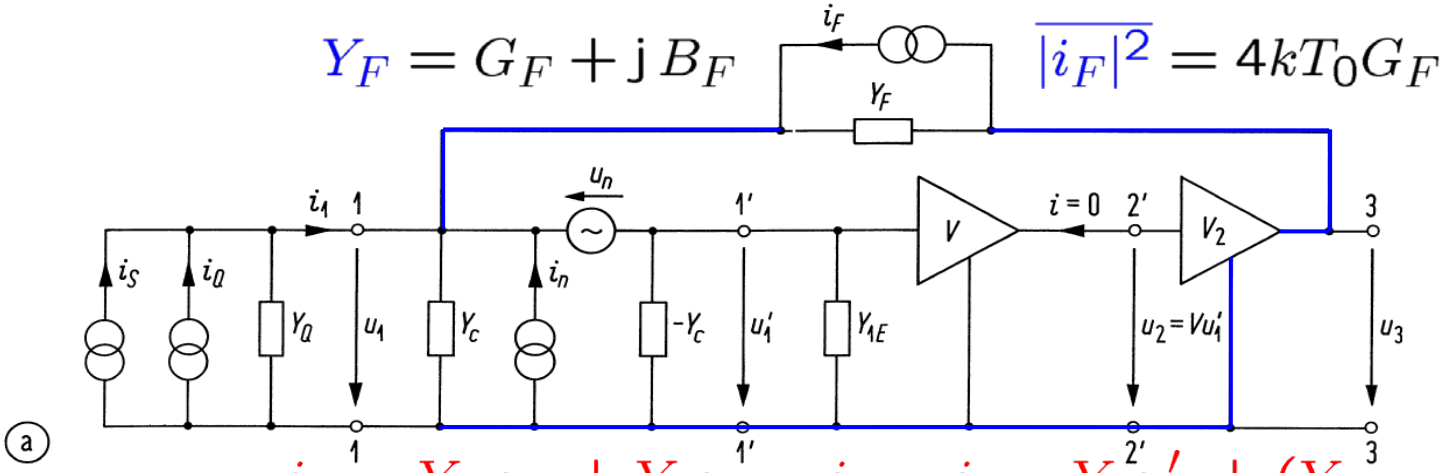

a

$$i_1 = Y_F\,u_1 + Y_c\,u_1 - i_F - i_n - Y_c\,u_1' + (Y_{1E} - VV_2Y_F)u_1'$$

Noisy negative-feedback amplifier. (a) detailed equivalent circuit ($V < 0$, $V_2 > 0$, $V' = VV_2 < 0$)

$$Y_Q' = Y_Q + Y_F, \quad Y_{1E}' = Y_{1E} + |V'|Y_F, \quad V' = VV_2 < 0\,,$$

$$i_R' = i_R + i_F = i_Q + i_n + u_n(Y_Q' + Y_c) + i_F$$

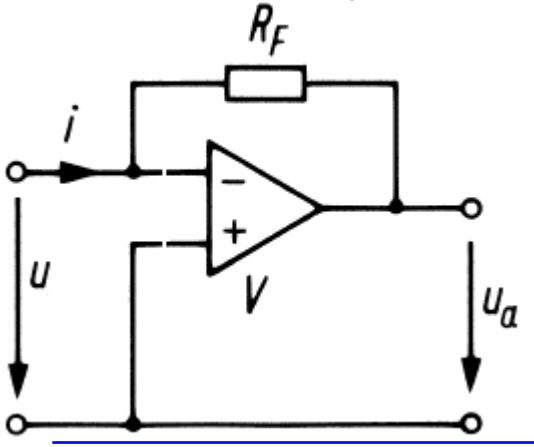

Assuming no current flows into "∓" pins:

$$u_a = -Vu$$

$$u = u_a + iR_F$$

$$u_a = -\frac{V}{V+1}R_Fi = \{V \to \infty\} = -R_Fi$$

Physical Representation of pin-PD Transimpedance Receiver

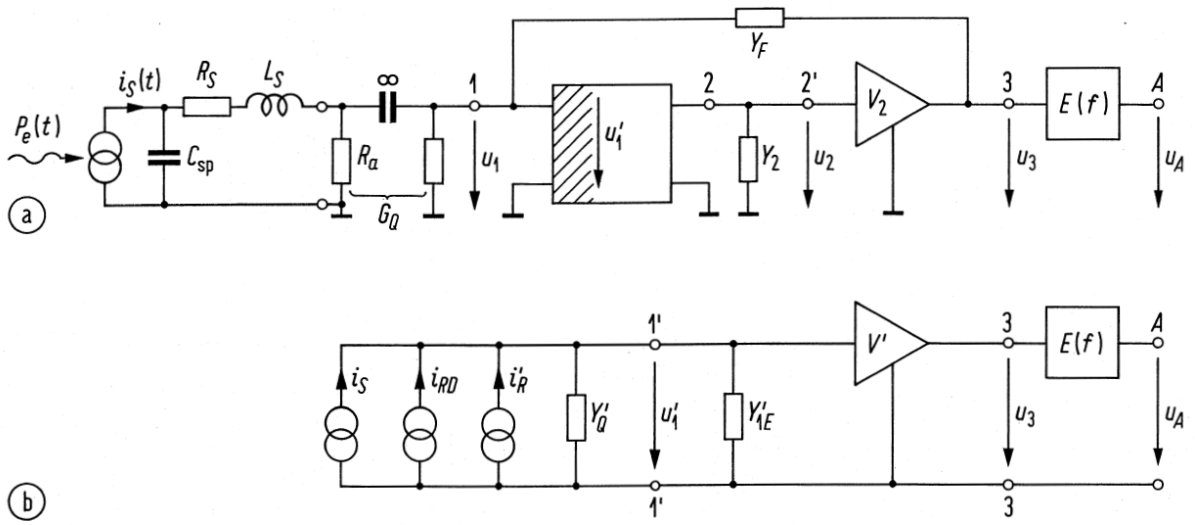

Optical direct receiver circuit with transimpedance amplifier (TIA) and equalizer (pulse shaping) network having a transfer function $u_A / u_3 = E(f)$. The quantities $i_S = SP_e$ and i_{RD} stand for the phasors of the pin photodetector signal and noise currents, Eq. (5.49) on Page 118. The phasors i_R' and Y_Q' represent the noise current of the TIA and its source admittance, Eq. (5.72) on Page 125. The voltage u_A at output A drives a data-recovery section (not drawn) consisting of a decision circuit and a clock-recovery circuit. (a) Circuit schematic with feedback admittance Y_F connecting terminals 3 and 1 of the TIA. (b) Simplified equivalent circuit, see also Fig. 5.17 on Page 125.

Direct Reception Limit

Pin Photodiode Receiver — Summary

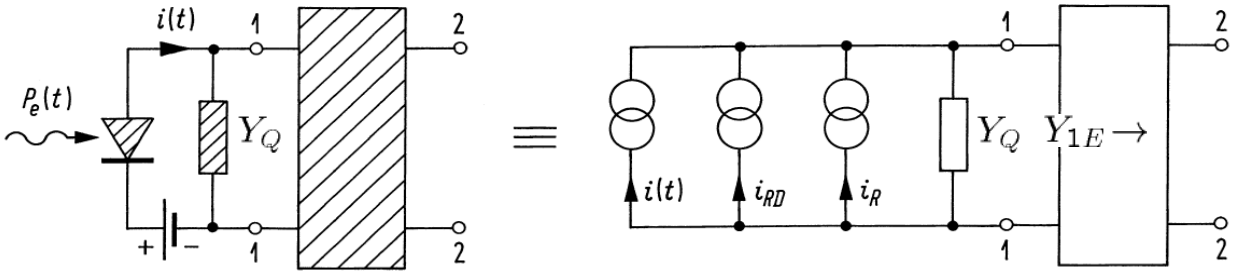

$$\overline{|i_Q|^2} = 4kT_0\,G_Q\,\mathrm{d}f,$$
$$\overline{|i_n|^2} = 4kT_0\,G_n\,\mathrm{d}f,$$
$$\overline{|u_n|^2} = 4kT_0\,R_n\,\mathrm{d}f,$$
$$i_R = i_Q + i_n + u_n(Y_Q + Y_c)$$

$$\overline{|i_R|^2} = F\,\overline{|i_Q|^2} = 4kFT_0\,G_Q\,\mathrm{d}f = 4k(1+F_z)T_0\,G_Q\,\mathrm{d}f = 4k(T_0+T_R)G_Q\,\mathrm{d}f$$

Noise figure F, excess NF F_z, noise temperature T_R:

$$F = \frac{\mathrm{SNR}_{v1}}{\mathrm{SNR}_2} = \frac{\text{total noise power in } \mathrm{d}f \text{ at load } Y_2}{\text{noise power in } \mathrm{d}f \text{ at load } Y_2 \text{ for noise-free two-port}}$$

$$F = 1 + F_z = 1 + \frac{T_R}{T_0} = \frac{T_0 + T_R}{T_0} = \frac{\overline{|i_R|^2}}{\overline{|i_Q|^2}}$$

For transimpedance receiver, replace:

$$Y_Q \rightarrow Y'_Q = Y_Q + Y_F, \qquad Y'_{1E} = Y_{1E} + |V'|Y_F$$
$$\overline{|i_R|^2} \rightarrow \overline{|i'_R|^2} = \overline{|i_R|^2} + \overline{|i_F|^2} = F'\overline{|i_Q|^2}, \qquad \overline{|i_F|^2} = 4kT_0G_F\,\mathrm{d}f$$

Photodiode Receiver

Signal current i_S, PD noise current i_{RD}, TIA noise current i'_R:

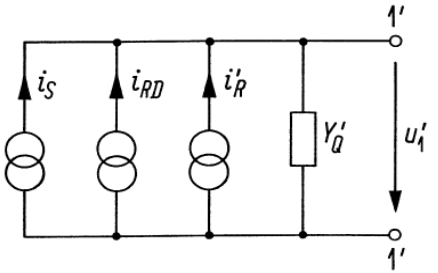

Optical receiver input

$$i_S = \frac{\eta e}{h f_e} P_e\,,$$

$$\overline{|i_{RD}|^2} = 2e i_S\,\mathrm{d}f + i_S^2\,\mathrm{RIN}(f)\,\mathrm{d}f,$$

$$\overline{|i'_R|^2} = F'\,\overline{|i_Q|^2} = 4kF'T_0G_Q\,\mathrm{d}f$$

Signal-to-noise power ratio (SNR) (good: $\mathrm{RIN}(f) \approx c_{P_e} \frac{\mathrm{RIN}(B/2)}{P_e^3}$):

$$\gamma = \frac{i_S^2}{\overline{|i_{RD}|^2} + \overline{|i'_R|^2}} = \frac{i_S}{\left[2e + \frac{4kF'T_0G_Q}{i_S} + i_S\,\mathrm{RIN}(f)\right]\mathrm{d}f}$$

Ideal quantum-noise limited receiver with pin-PD and *large* P_e (signal power $P_e = N_e\,h f_e\,2B$):

$$\gamma_{\text{dir qu}} = \frac{\eta P_e}{2h f_e B} = \eta N_e \quad \text{for direct reception, } i_S = SP_e,\ S = \frac{\eta e}{h f_e}$$

Signal Quality Metric for RZ-OOK Reception

Eye Diagram

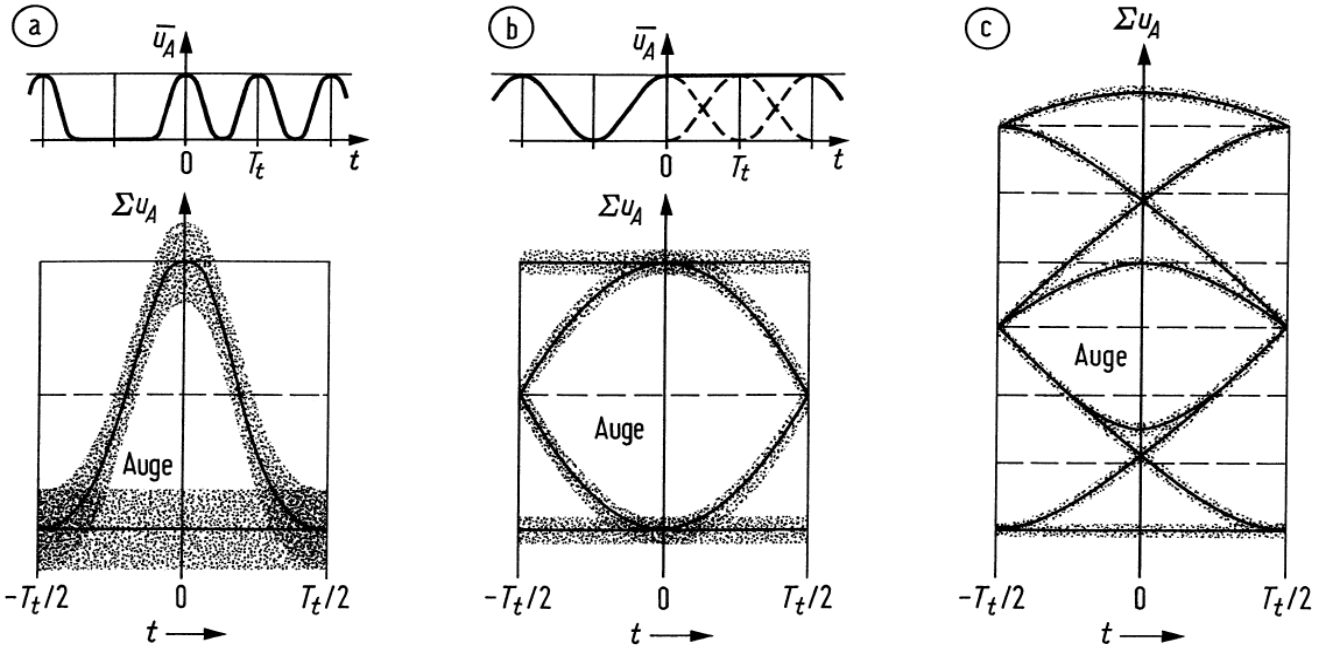

Eye diagrams for RZ (return to zero) pulses, sampling time $t = 0$; solid lines: without noise. (a) large noise, no impulse overlap (b) optimum case: small noise, impulse overlap, but no intersymbol interference at sampling time (c) low noise, strong impulse overlap, strong intersymbol interference at sampling time. Auge = eye

Detection Errors by Noise (1)

Voltage at decision circuit ($u(t) \equiv u_A(t)$):

$$u(t) = u_{R0}(t) \qquad \text{(0-bit received)},$$
$$u(t) = u_{R1}(t) + u_1 h_A(t) \qquad \text{(1-bit received)}.$$

Gaussian noise voltages with expectation zero $u_{R0}(t)$, $u_{R1}(t)$. Equalizer produces impulse $h_A(t)$, normalized such that $h_A(0) = 1$ at sampling time $t = 0$. Expectation u_1 at sampling time.

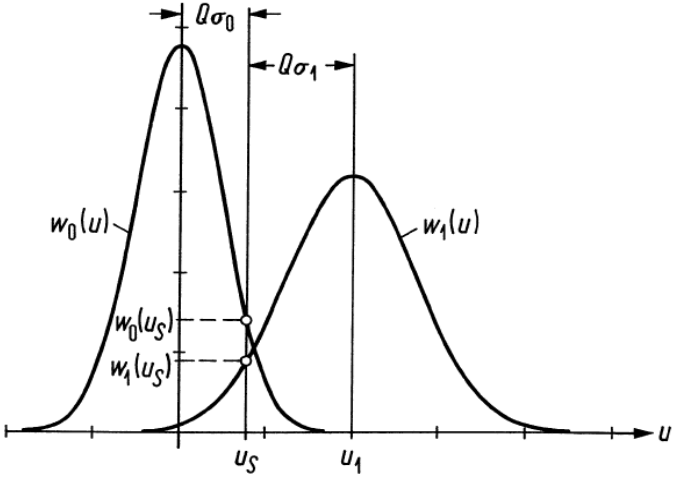

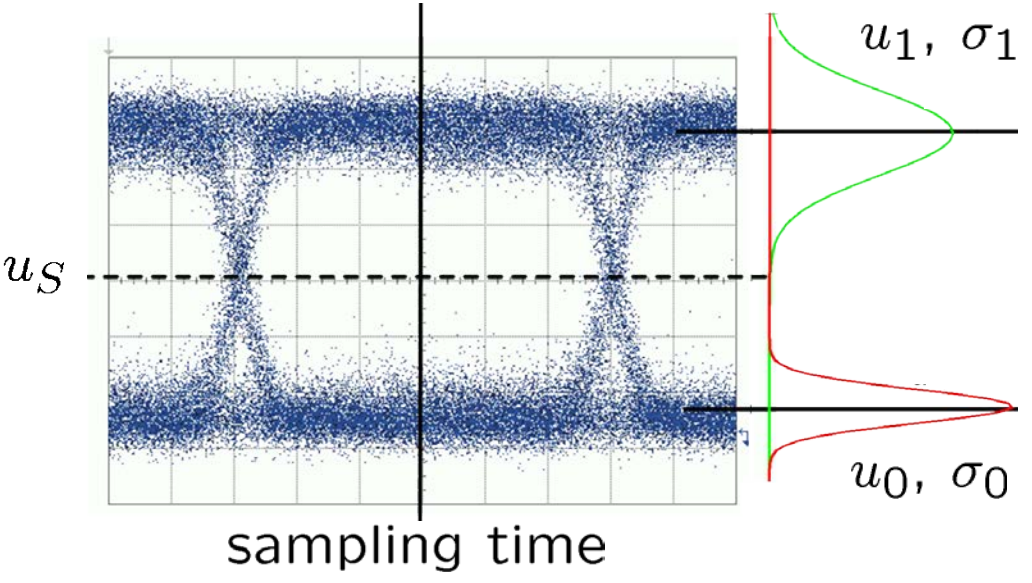

Probability densities $w_0(u)$, $w_1(u)$ of the sampled input voltage of the decision circuit for the receive symbols zero, one. σ_0, σ_1 standard deviations, u_1 expectation of voltage for a received one, u_S specific choice of decision threshold fixed by the bit error parameter Q

Detection Errors by Noise (2)

Probability density functions (pdf) for decision circuit voltages at sampling time $w_0(u)$, $w_1(u)$ (0 and 1 received, respectively):

$$w_0(u) = \frac{1}{\sqrt{2\pi\sigma_0^2}} \exp\left(-\frac{u^2}{2\sigma_0^2}\right), \qquad \overline{u} = 0, \quad \overline{(u-\overline{u})^2} = \overline{u_{R0}^2} = \sigma_0^2,$$

$$w_1(u) = \frac{1}{\sqrt{2\pi\sigma_1^2}} \exp\left[-\frac{(u-u_1)^2}{2\sigma_1^2}\right], \quad \overline{u} = u_1, \quad \overline{(u-\overline{u})^2} = \overline{u_{R1}^2} = \sigma_1^2.$$

$\sigma_1^2 > \sigma_0^2$, because logical 1 transmitted with higher power $\rightarrow$ larger PD shot noise. Usually, $1 < \sigma_1^2/\sigma_0^2 \leq 2$.

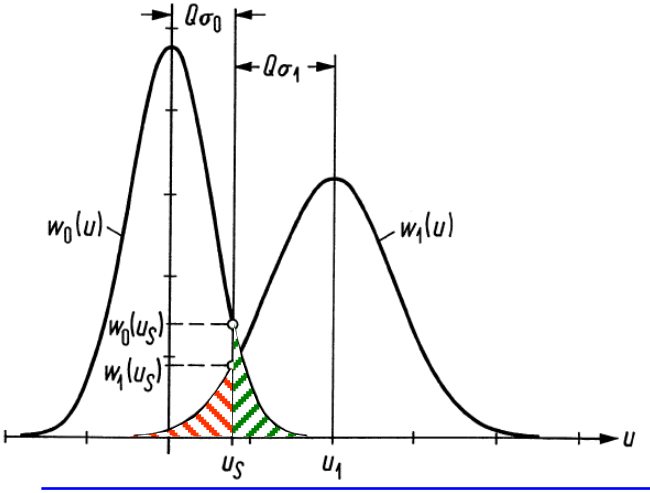

Zero: $u < u_S$. One: $u > u_S$. Prob. that 1 wrong: $p(1\text{d}|0\text{r})$; 0 wrong: $p(0\text{d}|1\text{r})$. Receiving prob. $p(0\text{r})$, $p(1\text{r})$. Bit error probability (BER, bit error ratio):

$$\text{BER} = p(1\text{r})p(0\text{d}|1\text{r}) + p(0\text{r})p(1\text{d}|0\text{r}),$$
$$p(0\text{r}) + p(1\text{r}) = 1$$

Detection Errors by Noise (3)

Minimum bit error probability:

$$\mathrm{BER} = p(1\mathrm{r}) \int_{-\infty}^{u_S} w_1(u)\,\mathrm{d}u + p(0\mathrm{r}) \int_{u_S}^{\infty} w_0(u)\,\mathrm{d}u\,,$$

$$\frac{\partial\,\mathrm{BER}}{\partial u_S} = p(1\mathrm{r}) w_1(u_S) - p(0\mathrm{r}) w_0(u_S) \stackrel{!}{=} 0\,,$$

$$\rightarrow p(1\mathrm{r}) w_1(u_S) = p(0\mathrm{r}) w_0(u_S)$$

Optimum threshold (note: $u_S - u_1 = \pm\sqrt{(u_S - u_0)^2}$):

$$p(1\mathrm{r})\,\frac{1}{\sqrt{2\pi\sigma_1^2}}\exp\left(-\frac{(u_S-u_1)^2}{2\sigma_1^2}\right) = p(0\mathrm{r})\,\frac{1}{\sqrt{2\pi\sigma_0^2}}\exp\left(-\frac{(u_S-u_0)^2}{2\sigma_0^2}\right)$$

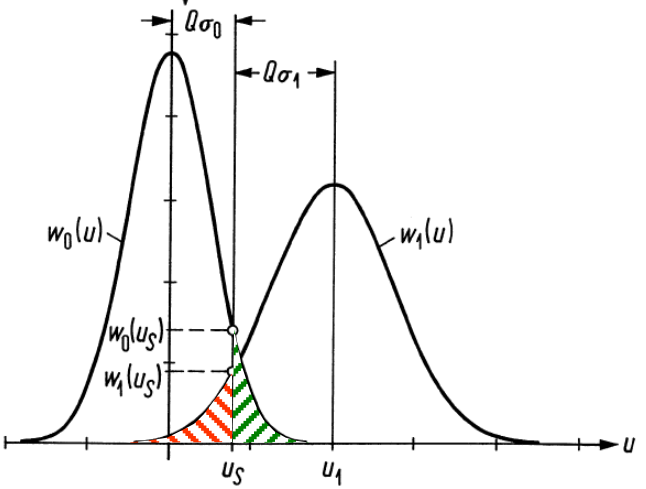

Threshold $u_S = \frac{\sigma_0 u_1 + \sigma_1 u_0}{\sigma_0 + \sigma_1}$, if $\frac{p(1\mathrm{r})}{\sigma_1} = \frac{p(0\mathrm{r})}{\sigma_0}$.

In practice:

$$1 < \sigma_1/\sigma_0 \leq \sqrt{2}\,, \qquad \sigma_1 \approx \sigma_0$$

$$p(1\mathrm{r}) = \frac{\sigma_1}{\sigma_0} p(0\mathrm{r}) \gtrapprox p(0\mathrm{r}),$$

$$p(1\mathrm{r}) \approx p(0\mathrm{r}) \approx 1/2$$

BER and Signal Quality Factor Q

$$\mathrm{erf}(z)=\frac{2}{\sqrt{\pi}}\int_0^z \exp(-t^2)\,\mathrm{d}t, \qquad \mathrm{erfc}(z)=\frac{2}{\sqrt{\pi}}\int_z^\infty \exp(-t^2)\,\mathrm{d}t,$$
$$\mathrm{erf}(\infty)=1, \qquad \mathrm{erfc}(\pm z)=1\mp\mathrm{erf}(z).$$

Optimum threshold for $p(1r)=\frac{\sigma_1}{\sigma_0}p(0r)\approx w(0r)\approx 1/2$:

$$Q=\frac{u_1-u_0}{\sigma_0+\sigma_1}=\frac{u_1-u_S}{\sigma_1}=\frac{u_S-u_0}{\sigma_0} \qquad \text{(here: } u_0=0\text{)},$$
$$p(1\mathrm{r}|0\mathrm{d})=p(0\mathrm{r}|1\mathrm{d})=\tfrac{1}{2}\,\mathrm{erfc}(Q/\sqrt{2}),$$
$$\sigma_0 w_0(u_S)=\sigma_1 w_1(u_S)=\exp(-Q^2/2)/\sqrt{2\pi},$$

Minimum BER$=p(1\mathrm{r})\int_{-\infty}^{u_S} w_1(u)\,\mathrm{d}u+p(0\mathrm{r})\int_{u_S}^{\infty} w_0(u)\,\mathrm{d}u$:

$$\mathrm{BER}=\frac{1}{2}\,\mathrm{erfc}\left(\frac{Q}{\sqrt{2}}\right) \qquad \gamma=\frac{P_S}{P_R}=Q^2$$

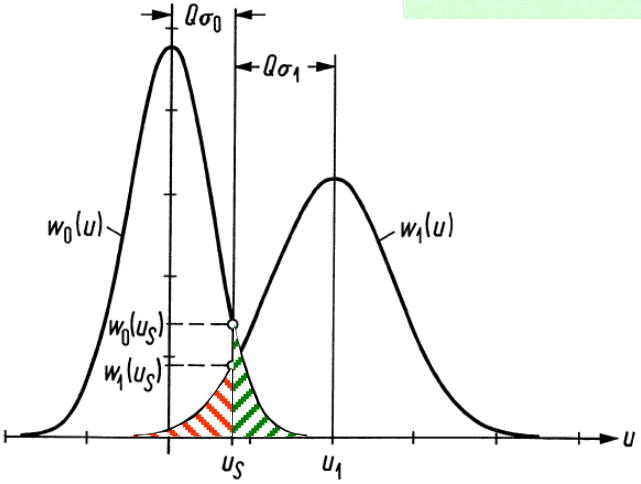

Signal quality factor Q for BER $=10^{-9}$, 10^{-11}, 10^{-13}, 10^{-15} amounts to $Q=6$, 6.7, 7.3, 7.9.

BER $=10^{-9}\rightarrow Q=6\rightarrow\gamma=36\mathrel{\widehat{=}}$ 15.6 dB. Connection el. SNR $\gamma\leftrightarrow Q$:

Bit-Error Parameter (Signal Quality Factor) and SNR

Connection between SNR γ at decision circuit (mean and RMS value measured) and bit error parameter Q?

No intersymbol interference, bit rate f_t, clock period $T_t = 1/f_t$, el. signal bandwidth $B = f_t/2$. Average el. power at decision circuit:

$$P = \frac{1}{2}\left\{\frac{1}{T_t}\int_{-T_t/2}^{+T_t/2} \overline{[u_1 h_A(t) + \underbrace{u_{R1}(t)}_{\overline{u_{R1}}=0}]^2}\,\mathrm{d}t + \frac{1}{T_t}\int_{-T_t/2}^{+T_t/2} \overline{u_{R0}^2(t)}\,\mathrm{d}t\right\}$$

$$= \frac{u_1^2}{2} I(h_A) + \frac{1}{2}(\sigma_0^2 + \sigma_1^2), \qquad I(h_A) = \frac{1}{T_t}\int_{-T_t/2}^{+T_t/2} h_A^2(t)\,\mathrm{d}t \approx \tfrac{1}{2}$$

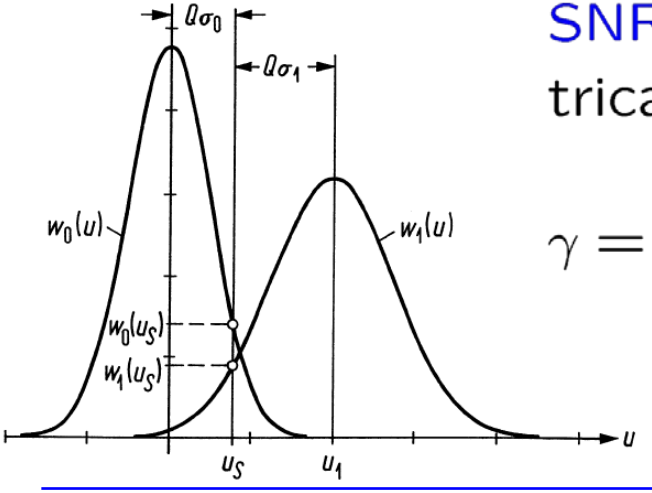

SNR follows, with $u_1 = (\sigma_0 + \sigma_1)Q$ and electrical signal power P_S to noise power P_R:

$$\gamma = \frac{P_S}{P_R} = \frac{u_1^2 I(h_A)/2}{(\sigma_0^2 + \sigma_1^2)/2} = Q^2 \frac{(\sigma_0 + \sigma_1)^2 I(h_A)}{\sigma_0^2 + \sigma_1^2}$$

$$= (0.97 \ldots 1) \times Q^2, \;\rightarrow\; \gamma = \frac{P_S}{P_R} = Q^2$$

BER and Power Penalty (1)

Compensation of additional noise (noise power P_{Rz}) by an increase of signal power $P_S \to P_{S+}$ possible?

$$\gamma = Q^2 = \frac{P_S}{P_R} = \frac{P_{S+}}{P_R + P_{Rz}},\ \gamma_+ = Q_+^2 = \frac{P_{S+}}{P_R},\ \mathrm{BER}_+ = \frac{1}{2}\,\mathrm{erfc}\left(\frac{Q_+}{\sqrt{2}}\right)$$

γ_+, Q_+, BER_+ for P_{S+} without additional noise.

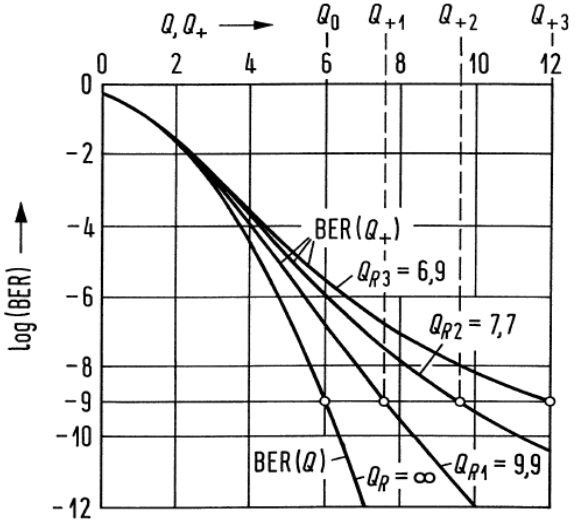

Additive noise: Compensation by increase of opt. input power P_{opt} always possible. El. signal $P_S \sim (P_{\mathrm{opt}})^2$. Power penalty:

$$p_B = 10\ \mathrm{lg}\left(\frac{P_{\mathrm{opt}+}}{P_{\mathrm{opt}}}\right) = 5\ \mathrm{lg}\left(\frac{P_{S+}}{P_S}\right)$$
$$= 10\ \mathrm{lg}\left(\frac{Q_+}{Q}\right) = 5\ \mathrm{lg}\left(1 + \frac{P_{Rz}}{P_R}\right)$$

Bit error probability as a function of the bit error parameters Q (denoted as $\mathrm{BER}(Q)$) and Q_+ (denoted as $\mathrm{BER}(Q_+)$) for various values of the residual bit error parameter Q_R

BER and Power Penalty (2)

Multiplicative noise: Noise power $P_{Rz} = \frac{1}{\gamma_R} P_S = \frac{1}{Q_R^2} P_S$ compensatable by increased signal power $P_S \to P_{S+}$?

$$\gamma = Q^2 = \frac{P_S}{P_R} = \frac{P_{S+}}{P_R + P_{Rz}} = \frac{P_{S+}}{P_R + P_{S+}/Q_R^2} = \frac{Q_+^2 Q_R^2}{Q_+^2 + Q_R^2} \overset{P_{S+}\to\infty}{=} Q_R^2$$

γ_+, Q_+, BER_+ for P_{S+} without additional noise.

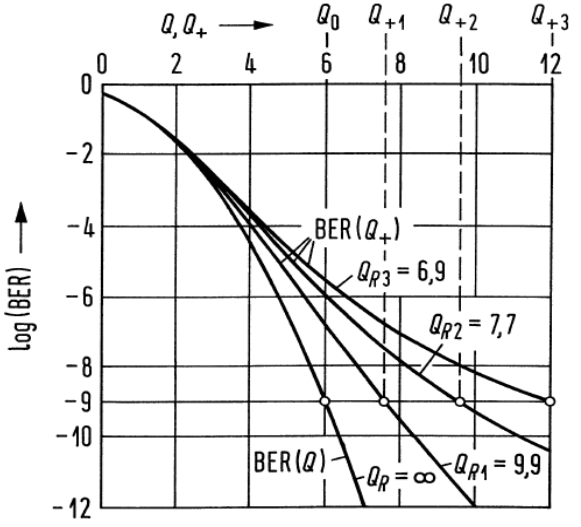

Compensation with increased opt. input power P_{opt} not complete possible. El. signal $P_S \sim (P_{\mathrm{opt}})^2$. Power penalty, floor BER:

$$p_B = 10 \lg \left(\frac{P_{\mathrm{opt}+}}{P_{\mathrm{opt}}} = \frac{Q_+}{Q} \right) = 5 \lg \left(\frac{Q_R^2}{Q_R^2 - Q^2} \right),$$

$$\mathrm{BER}_R = \frac{1}{2} \operatorname{erfc} \left(\frac{Q_R}{\sqrt{2}} \right)$$

Bit error probability as a function of the bit error parameters Q (denoted as $\mathrm{BER}(Q)$) and Q_+ (denoted as $\mathrm{BER}(Q_+)$) for various values of the residual bit error parameter Q_R

WDM System Simulations: BER for NRZ-OOK and RZ-DPSK

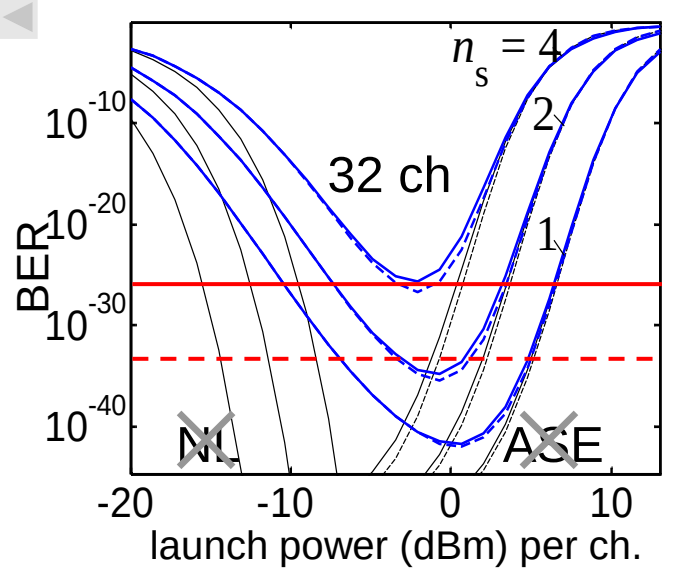

n_s spans
including (——),
neglecting (- - -)
3rd order disp.,
self-steepening,
Raman effect.
Asympt. (— , ·····)
without ASE and
nonlin. noise

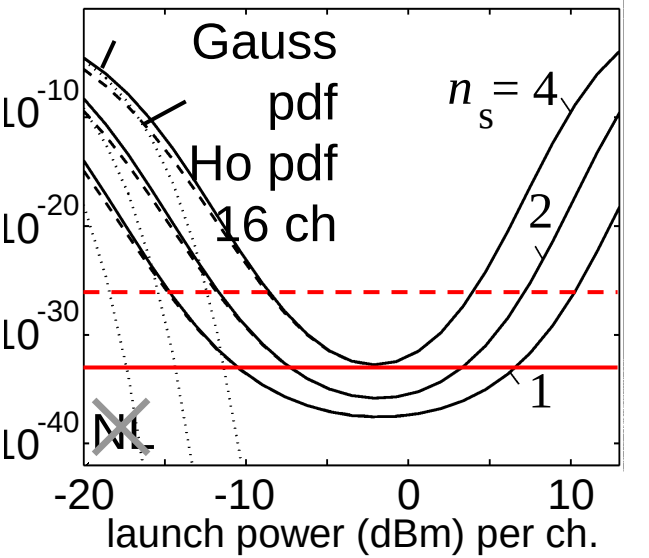

40 Gbit/s

100 GHz ch grid

1024 bit PRBS / ch

0.45 mW / ch

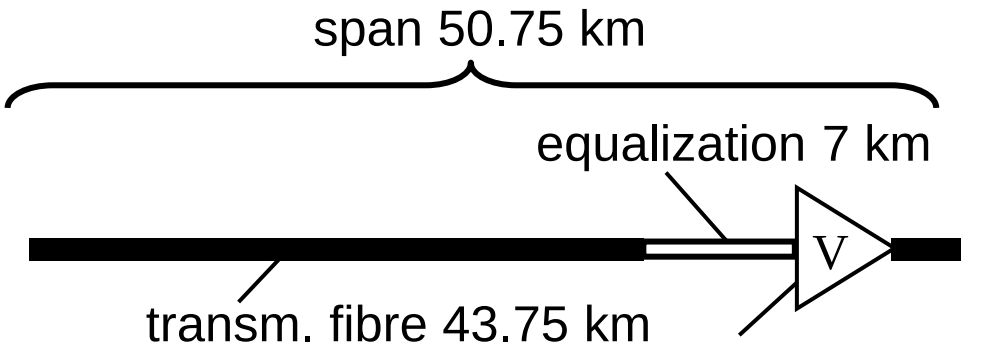

Kremp, T.; Freude, W.: 'DWDM transmission optimization in nonlinear optical fibres with a fast split-step wavelet collocation method', Proc. 7th Intern. Conf. on Optoelectronics, Fiber Optics & Photonics (Photonics 2004), Kochi, India, November 9–11, 2004 (invited)

Limiting Sensitivity for Direct Detection (1)

No electron. noise. PD $\eta = 1$. Zero: $\overline{N_{e\,0}} = 0$. One: $\overline{N_e} \neq 0$. Prob. $p(1\mathrm{d}|0\mathrm{r}) = 0$ that 0 wrongly detected as 1. Threshold $u_S \to u_S = 0$. Only logical 1 perturbed, $p(0\mathrm{d}|1\mathrm{r}) \neq 0$. Poisson probability of photons:

$$p_{N_e}(N_e) = \frac{\overline{N_e}^{N_e}}{N_e!}\,\mathrm{e}^{-\overline{N_e}}, \quad \overline{\delta N_e^2} = \overline{N_e}, \quad (\overline{N_e} \text{ arbitrary})$$

$p_{N_S}(N_e = 0)$ is probability that logical 1 with $\overline{N_e} > 0$ wrongly detected as logical 0:

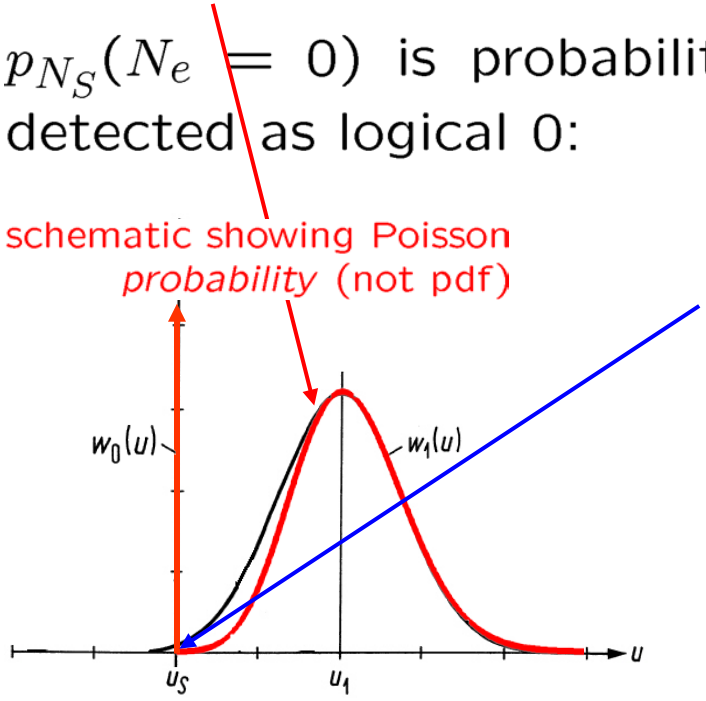

$$p_{N_e}(0) = \frac{\overline{N_e}^{0}}{0!}\,\mathrm{e}^{-\overline{N_e}} = \mathrm{e}^{-\overline{N_e}} > 0$$

Poisson probability is discrete, therefore probability density function:

$$w_{N_e}(N_e) = \sum_{N_e'=0}^{\infty} p_{N_e}(N_e)\,\delta(N_e - N_e')$$

Limiting Sensitivity for Direct Detection (2)

Prob. One: $p(1\mathrm{r}) = 1/2$. Because of Poisson statistics, prob. that One $\rightarrow$ Zero: $p(0\mathrm{d}|1\mathrm{r}) = p_{N_e 1}(0) = \mathrm{e}^{-\overline{N_e}}$. BER:

$$\mathrm{BER} = \overbrace{p(1\mathrm{r})}^{1/2}\overbrace{p(0\mathrm{d}|1\mathrm{r})}^{\exp(-\overline{N_e})} + \overbrace{p(0\mathrm{r})}^{1/2}\overbrace{p(1\mathrm{d}|0\mathrm{r})}^{0}, \qquad p(0\mathrm{r}) + p(1\mathrm{r}) = 1\,,$$

$$\rightarrow \quad \boxed{\mathrm{BER} = \frac{1}{2}\,\mathrm{e}^{-\overline{N_e}}}$$

For bit error probability $\mathrm{BER} = 10^{-9}$ therefore:

$$\overline{N_e} = -\ln\left(2 \times 10^{-9}\right) = 20 \quad \rightarrow \quad \boxed{\overline{N_e} = 20 \quad \text{for} \quad \mathrm{BER} = 10^{-9}}$$

schematic showing Poisson *probability* (not pdf)

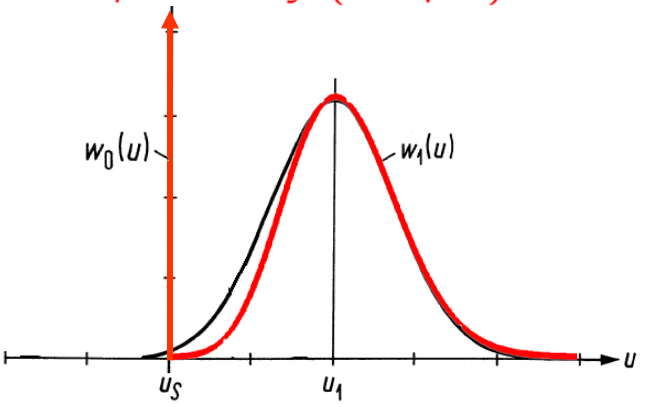

Photons for One ($w(1\mathrm{r}) = 1/2$). On average:

$$\overline{N_{e\,\mathrm{bit}}} = \overbrace{\overline{N_e}}^{20}\overbrace{p(1\mathrm{r})}^{1/2} + \overbrace{\overline{N_{e\,0}}}^{0}\overbrace{p(0\mathrm{r})}^{1/2}$$

$$\overline{N_{e\,\mathrm{bit}}} = 10 \quad \text{for} \quad \mathrm{BER} = 10^{-9}$$

Realized: $N_{e\,\mathrm{bit}} = 4\,000$ (pin-PD), $N_{e\,\mathrm{bit}} = 150$ (APD), 152 (pin & OA)

Measured Sensitivities for Direct Detection

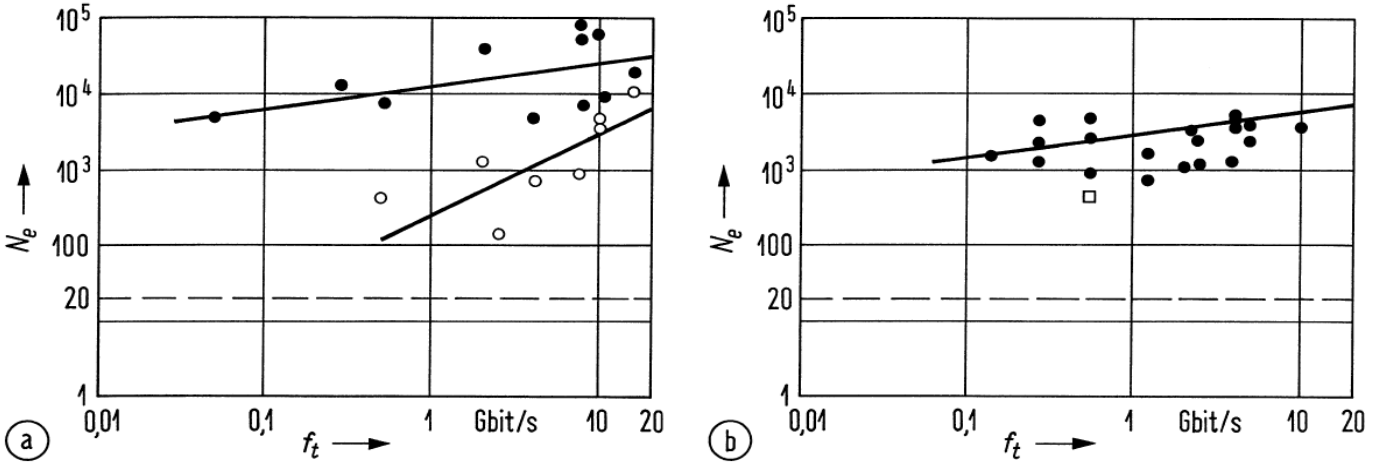

Measured minimum received photon numbers N_e for a 1 bit (η not known, BER $= 10^{-9}$). Quantum limit $N_e = 20$, $\eta = 1$ (– – –). (a) pin-photodiode $\lambda = 1.3$; $1.55\,\mu$m (•), pin-photodiode with optical amplifier (○) (b) avalanche photodiode (APD) $\lambda = 1.55\,\mu$m (•), $\lambda = 0.85\,\mu$m (□)

Coherent Receiver

Coherent Receiver (1)

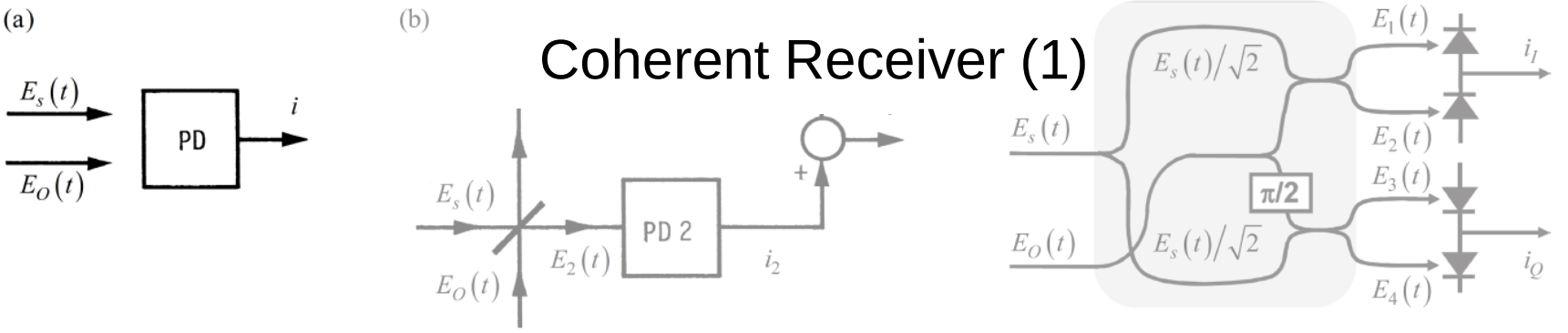

Fig. 5.24. Heterodyne receiver for mixing the superposition of an optical signal field $E_s(t) = \hat{E}_s(t)\cos(\omega_s t + \varphi_s)$ and a copolarized optical local oscillator (LO) field $E_O(t) = \hat{E}_O \cos(\omega_O t + \varphi_O)$ on a photodedetctor (PD), resulting in a photocurrent $i_Z(t)\cos(\omega_Z t - \varphi_O)$ at the intermediate frequency (IF) $f_Z = f_s - f_O = \omega_Z/(2\pi)$. (a) Unbalanced receiver with one PD. (b) Balanced receiver with beam splitter and two photodetectors PD 1 and PD 2. The output IF current $i(t) = i_2(t) - i_1(t)$ represents the difference of the individual photocurrents. [Modified from Ref. 29. Folie 2] (c) Optical hybrid (shaded box) with 2×2 directional couplers (instead of the beam splitter in Subfigure (b)) and a $\pi/2$ phase shifter for the LO. The circuit is equivalent to the schematic of an IQ-demodulator in Fig. 2.6(b) on Page 28. [After Ref. 30 Fig. 2.6]

Photomixing A photodetector as in Sect. 5.1 on Page 109 ff. delivers electrons at a rate $i(t)/e$ that is determined by the received photon rate $P_e(t)/(hf_O)$, Eq. (5.119). Assume for the moment that $\hat{E}_s = \hat{E}_O = \hat{E}_e$ and $\varphi_s = \varphi_O = 0$ hold. The envelope of the superimposed (beating) fields is periodic with half the difference frequency f_Z,

$$E_e(t) = \hat{E}_e\left[\cos(\omega_s t) + \cos(\omega_O t)\right] = 2\hat{E}_e \cos\left(\frac{\omega_s - \omega_O}{2}t\right)\cos\left(\frac{\omega_O + \omega_s}{2}t\right). \tag{5.114}$$

The rate of arriving photons with energy $(\omega_O + \omega_s)/2 \approx \omega_O$ depends on the power $P_e(t)$ which results when averaging $\cos^2[(\omega_O + \omega_s)/2]$ over an optical cycle of about $1/f_O$,

$$P_e(t) = \overline{E_e^2(t)} = \left(2\hat{E}_e\right)^2 \cos^2\left(\frac{\omega_s - \omega_O}{2}t\right) \times \frac{1}{2} = \hat{E}_e^2\left(1 + \cos\omega_Z t\right), \qquad \omega_Z = 2\pi f_Z = \omega_s - \omega_O\,. \tag{5.115}$$

Photomixing

Photomixing A photodetector as in Sect. 5.1 on Page 109 ff. delivers electrons at a rate $i(t)/e$ that is determined by the received photon rate $P_e(t)/(hf_O)$, Eq. (5.119). Assume for the moment that $\hat{E}_s = \hat{E}_O = \hat{E}_e$ and $\varphi_s = \varphi_O = 0$ hold. The envelope of the superimposed (beating) fields is periodic with half the difference frequency f_Z,

$$E_e(t) = \hat{E}_e\left[\cos(\omega_s t) + \cos(\omega_O t)\right] = 2\hat{E}_e \cos\left(\frac{\omega_s - \omega_O}{2}t\right)\cos\left(\frac{\omega_O + \omega_s}{2}t\right). \tag{5.114}$$

The rate of arriving photons with energy $(\omega_O + \omega_s)/2 \approx \omega_O$ depends on the power $P_e(t)$ which results when averaging $\cos^2[(\omega_O + \omega_s)/2]$ over an optical cycle of about $1/f_O$,

$$P_e(t) = \overline{E_e^2(t)} = \left(2\hat{E}_e\right)^2 \cos^2\left(\frac{\omega_s - \omega_O}{2}t\right) \times \frac{1}{2} = \hat{E}_e^2\left(1 + \cos\omega_Z t\right), \qquad \omega_Z = 2\pi f_Z = \omega_s - \omega_O\,. \tag{5.115}$$

This scheme is named heterodyne reception. Obviously, the received photon rate $P_e(t)/(hf_O) \sim \cos\omega_Z t$ varies with the intermediate frequency f_Z, and therefore the current rate $i(t)/e \sim \cos\omega_Z t$ reproduces this periodicity. It would be the wrong idea with this type of photodetector to blindly calculate the square in Eq. (5.115), (5.114), and then worry about the sum frequency $\omega_s + \omega_O$ in the product term $2\hat{E}_s\hat{E}_O\cos(\omega_s t)\cos(\omega_O t)$ — this type of photodetector *cannot emit*, e. g., green light at $\lambda = 0.53\,\mu$m when fed with infrared light having wavelengths of $\lambda_{s,O} = 1.06\,\mu$m.

$$N_P \sim \overline{\left(\hat{E}_e \cos\omega_s t + \hat{E}_e \cos\omega_O t\right)^2}$$

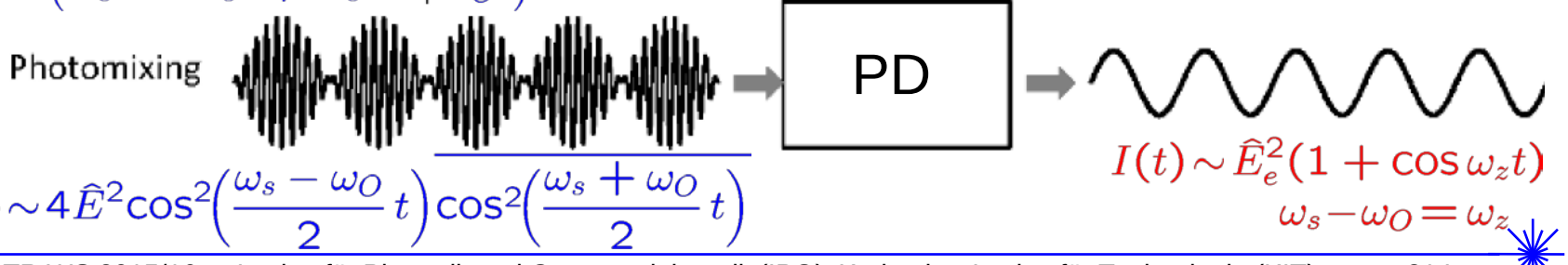

Beam Splitter, Optical Hybrid and IQ-Demodulator

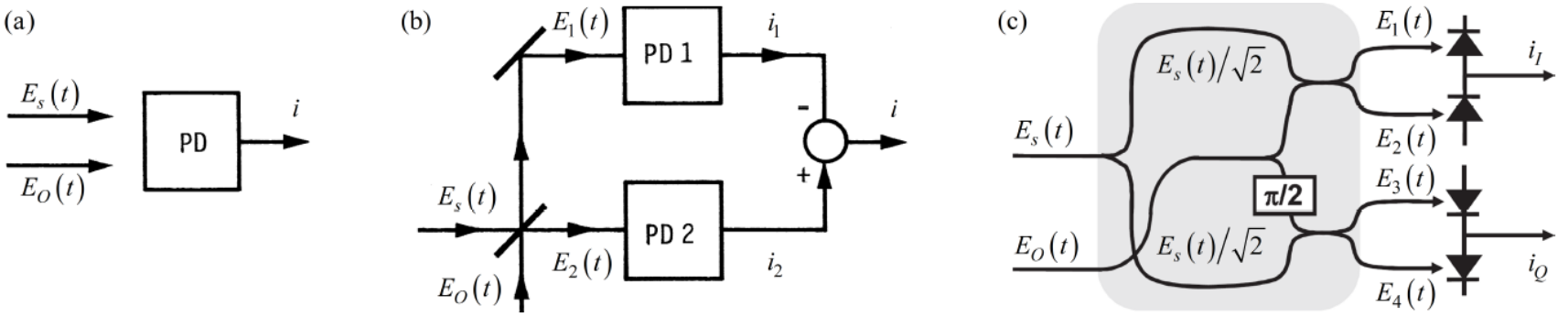

Beam splitter and optical hybrid If a beam splitter is lossless, its scattering matrix is unitary. With a proper choice of the reference planes, the fields at the output of a symmetric, matched beam splitter as in Fig. 5.24(b) are

$$E_1(t) = \frac{1}{\sqrt{2}}\left[E_s(t) - E_O(t)\right], \qquad E_2(t) = \frac{1}{\sqrt{2}}\left[E_s(t) + E_O(t)\right].$$

Such a four-port is mostly used in form of an optical 2×2 directional coupler realized in fibre or in integrated technology.

Figure 5.24(c) displays the schematic of an IQ-demodulator as in Fig. 2.6(b) on Page 28. Optical 2×2 directional couplers are the basic building blocks. Such a circuit (without the photodiode mixers) is called an optical hybrid.

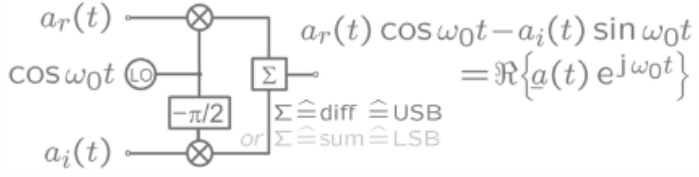

(a) IQ-modulator for encoding real and imaginary data on two orthogonal carriers (Σ ≙ subtract)

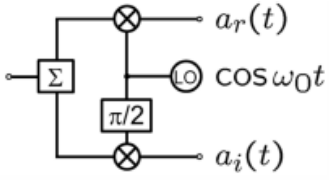

(b) IQ-demodulator for complex data (Σ ≙ split)

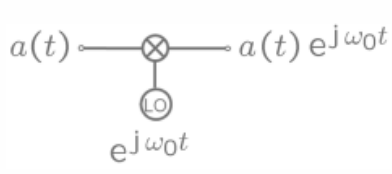

(c)Modulation of a complex carrier with complex data

(d)Demodulation of complex data

LECTURE 16

Relative Intensity Noise and Phase Noise

Relative intensity noise and phase noise Both setups Fig. 5.24(a) and (b) have the same limiting sensitivity as long as the LO behaves ideally, i. e., if only the shot (quantum) noise of an (in the classical sense ideally stable) oscillator has to be taken into account. In practice, a laser oscillator with an average output power $\overline{P_O}$ exhibits also classical amplitude noise, so-called relative intensity noise (RIN) with a one-sided power spectrum $\mathrm{RIN}\,(f)$, which describes power fluctuations due to amplified spontaneous emission (ASE),

$$\mathrm{RIN}_{P_O} = \int_{-\infty}^{+\infty} \mathrm{RIN}\,(f, \overline{P_O})\,\mathrm{d}f = \frac{\overline{\left(P_O - \overline{P_O}\right)^2}}{\overline{P_O}^2} = \frac{\overline{\delta P_O^2}}{\overline{P_O}^2}\,, \qquad \mathrm{RIN}\,(f, \overline{P_O}) = c_{P_O}\frac{\mathrm{RIN}\,(f)}{\overline{P_O}^3}\,.$$

Combining the informations on $\sigma_{\varphi_i}^2$ and Δf_H, we can establish a relation for the phase noise variance in terms of observation time τ (again, $\tau = T$ could be chosen to be the symbol duration) and various laser parameters,

$$\sigma_{\varphi_i}^2 = 2\pi\Delta f_H \tau, \qquad \Delta f_H = \mathrm{const} \times n_{\mathrm{sp}}(1+\alpha^2)\frac{h f_O}{P_O \tau_P^2}\,. \tag{5.118}$$

The linewidth Δf_H of the "hot" (oscillating) laser is in proportion to the square of the linewidth $1/\tau_P$ of the "cold" resonator (no oscillation), so a narrow resonator bandwidth decreases Δf_H greatly. The quantities n_{sp} and α are the inversion factor Eq. (3.41) on Page 70 ($n_{\mathrm{sp}} = 1$ for ideally full inversion) and the line broadening factor (Henry factor for amplitude-phase coupling) Eq. (3.113) on Page 90, respectively. From Eq. (5.118) it can be concluded that phase noise influences are minimum for high symbol rates (small $\tau = T$), optimum inversion ($n_{\mathrm{sp}} = 1$), small α-factor, large optical power P_O, and a small "cold" resonator bandwidth.

Coherent Receiver (2)

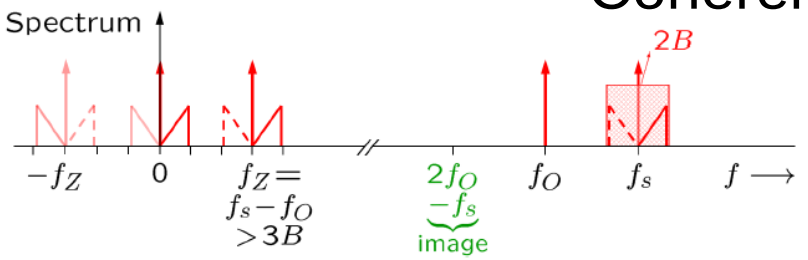

Fig. 5.25. Heterodyne spectra (also homodyne spectra for $f_O = f_s$). A real signal with bandwidth B is modulated on an optical carrier with frequency f_s. Upper and lower optical sidebands are correlated, see Eq. (2.36) on Page 26. This optical signal together with a local oscillator (LO) at frequency f_O illuminates a photodiode and is down-converted to a current at an intermediate-frequency $f_Z = f_s - f_O$. For the IF, the condition $f_Z > B$ must be fulfilled, otherwise the IF-USB at negative frequencies overlaps with the IF-LSB for positive frequencies, and this would lead to distortions. For direct detection of the IF signal, the IF should be chosen according to $f_Z > 3B$. This avoids that in the case of direct IF detection the baseband signal is perturbed by mixing products of the IF sidebands, which would fall into a frequency range $0 \le f \le 2B$.

$$P_e(t) = \left[\hat{E}_s \cos(\omega_s t + \varphi_s) + \hat{E}_O \cos(\omega_O t + \varphi_O)\right]^2, \qquad i = SP_e, \qquad S = \frac{\eta e}{h f_O}, \tag{5.119}$$

$$P_s(t) = \tfrac{1}{2}\hat{E}_s^2, \qquad P_O = \tfrac{1}{2}\hat{E}_O^2, \qquad P_O \gg P_s.$$

When performing the squaring operation in Eq. (5.119), we respect the physical restrictions of the detection process as formulated in Eq. (5.115). The resulting photocurrent (usually amplified with a transimpedance amplifier, Page 130 ff.) comprises an IF component with amplitude i_Z,

$$i(t) = SP_e(t) \approx SP_O + i_Z \cos(\omega_Z t + \varphi_s - \varphi_O), \quad i_Z = S\hat{E}_s\hat{E}_O, \quad P_s \ll P_O. \tag{5.120}$$

Remarkably, the signal amplitude $\hat{E}_s$ in the IF current amplitude i_Z is multiplied by the (large) LO field strength $\hat{E}_O$. By a proper evaluation of the IF current, we can retrieve both, amplitude $\hat{E}_s$ and phase information φ_s of the signal, provided that amplitude $\hat{E}_O$ and phase φ_O of the LO are sufficiently stable.

Heterodyne Reception Limit

For calculating the SNR in the IF range, we first have to average the squared electrical IF signal over an intermediate frequency cycle, which results in the average electrical signal power $P_S = i_Z^2/2$. The electrical noise power P_R is determined by the shot noise $\overline{|i_{RD}|^2} = 2eSP_O \times 2B$ caused by the strong LO, and by electrical noise $\overline{|i'_R|^2}$ from the amplifier. Analogous to we find the IF SNR

$$\gamma = \frac{P_S}{P_R}, \quad \gamma_{\text{IF-het}} = \frac{i_Z^2/2}{\overline{|i_{RD}|^2} + \overline{|i'_R|^2}} = \frac{\frac{1}{2}S^2\hat{E}_s^2\,2P_O}{(2eSP_O + 4kF'T_0G_Q)\,2B} = \frac{\eta P_s}{2hf_OB}\,\frac{1}{1 + 4kF'T_0G_Q/(2eSP_O)}.$$

If the LO power is chosen large enough, we actually realize shot (quantum) noise limited reception, even with small received optical signal powers P_s,

$$\gamma_{\text{IF-het qu}} = \frac{\eta P_s}{2hf_OB} = \gamma_{\text{dir qu}} \quad (\text{quantum noise limited, } \frac{4kF'T_0G_Q}{2eSP_O} \ll 1).$$

This SNR is identical as for direct reception , $\text{SNR}_{\text{IF-het qu}} = \text{SNR}_{\text{dir qu}}$, albeit both SNR are not really comparable — we relate the IF-band SNR of heterodyne reception to the baseband SNR of direct reception.
shot-noise limited BB SNR doubles as compared to the IF-band SNR,

$$\gamma_{\text{BB-het qu}} = \frac{\eta P_s}{hf_OB} = 2\gamma_{\text{dir qu}} \quad (\text{quantum noise limited, } \frac{4kF'T_0G_Q}{2eSP_O} \ll 1). \tag{5.117}$$

Compared to the quantum noise limited SNR for direct reception, the baseband SNR for heterodyne reception is twice as large. It corresponds to two times the mean number ηN_s of received signal photons per symbol duration $T_s = 1/(2B)$,

$$\gamma_{\text{BB-het qu}} = 2\eta N_s\,.$$

Balanced Heterodyne Reception (1)

Amplitude noise Looking at the RIN influence only, the SNR relation has to be modified, where the shot noise term $\overline{|i_{RD}|^2}$ would be replaced with the help

$$\overline{|i_{RD}|^2} \quad \longrightarrow \quad 2eS\overline{P_O}\,2B + \left(S\overline{P_O}\right)^2 \int_{f_Z-B}^{f_Z+B} \mathrm{RIN}\left(f, \overline{P_O}\right) \approx 2eS\overline{P_O}\,2B + \left(S\overline{P_O}\right)^2 \frac{c_{P_O}}{\overline{P_O}^3}\,\mathrm{RIN}\left(f_Z\right)\,2B.$$

The resulting IF SNR including the influence of RIN then becomes

$$\begin{aligned}\gamma_{\text{IF-het}} &= \frac{\frac{1}{2}S^2\hat{E}_s^2\,2\overline{P_O}}{\left(2eS\overline{P_O} + \left(S\overline{P_O}\right)^2 \frac{c_{P_O}}{\overline{P_O}^3}\,\mathrm{RIN}\left(f_Z\right) + 4kF'T_0G_Q\right)2B} \\ &= \frac{\eta P_s}{2hf_OB}\,\frac{1}{1+\eta c_{P_O}\,\mathrm{RIN}\left(f_Z\right)/\left(2hf_O\overline{P_O}^2\right) + 4kF'T_0G_Q/\left(2eS\overline{P_O}\right)}.\end{aligned}$$

Phase noise If the actual LO phase fluctuates, the constant phase has to be replaced by a random phase $\varphi_O \to \varphi_O(t)$. The IF current is inevitably influenced, and a measurement of the signal phase φ_s becomes inaccurate to a certain degree. The only countermeasure is to reduce the LO phase noise variance $\sigma^2_{\varphi_i}$.

Balanced Heterodyne Reception (2)

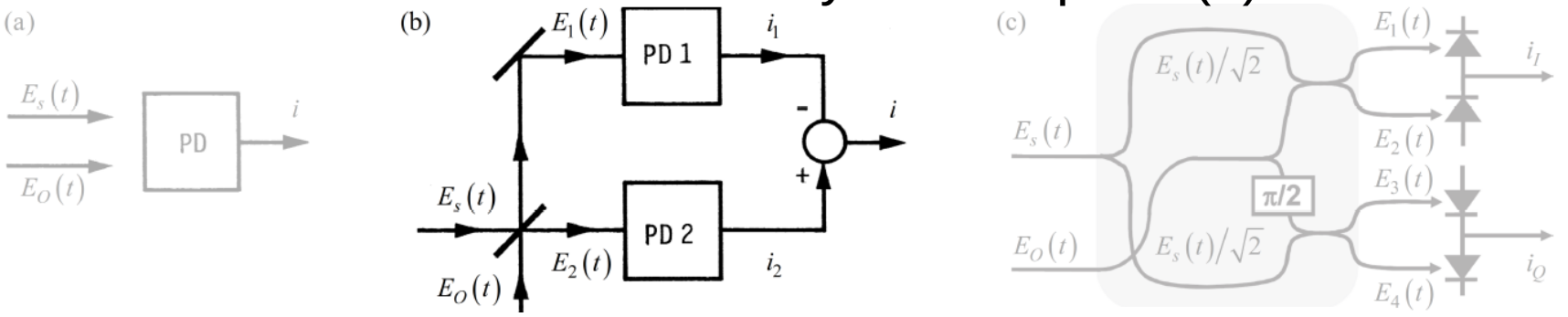

$$i_{1,2}(t) = SE_{1,2}^2(t) \approx \frac{1}{2}SP_O(t) \mp \frac{1}{2}i_Z(t)\cos\left[\omega_Z t + \varphi_s - \varphi_O(t)\right], \quad i_Z(t) = S\hat{E}_s\hat{E}_O(t), \quad P_s \ll P_O$$

$$i(t) = i_2(t) - i_1(t) = i_Z(t)\cos\left[\omega_Z t + \varphi_s - \varphi_O(t)\right].$$

The balanced heterodyne receiver eliminates the DC term $S\overline{P_O(t)}$ and thus also the LO RIN, which is detected in both photodetectors alike and therefore correlated. Still, even with a balanced receiver, the IF current amplitude $i_Z(t)$ is slightly perturbed by the fluctuating $\hat{E}_O(t)$, but much less than through the LO RIN using an unbalanced receiver.

The LO phase noise $\varphi_O(t)$, however, directly influences the photocurrent phase even for a balanced receiver. Thus the LO quality $\sigma_{\varphi_i}^2$, i.e., the linewidth Δf_H and the obervation time τ in terms of the symbol duration T determine the reception quality for phase sensitive modulation formats.

Quantum noise limited sensitivity The shot (quantum) noise limited sensitivity for both, balanced and unbalanced heterodyne receivers is identical

Homodyne Reception and Reception Limit

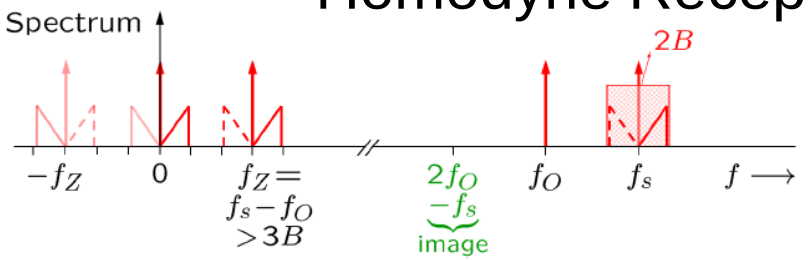

Fig. 5.25. Heterodyne spectra (also homodyne spectra for $f_O = f_s$).

$$i = SP_e(t) = SP_O + i_Z \cos(\varphi_s - \varphi_O), \quad i_Z = S\hat{E}_s\hat{E}_O, \quad f_Z = 0, \quad P_s(t) \ll P_O.$$

The signal-dependent part $i_Z \cos(\varphi_s - \varphi_O)$ of the photocurrent i is maximum if $\varphi_s - \varphi_O = 0$ is chosen, i. e., we receive only the in-phase component with respect to the LO phase, and the quadrature component $\sin(\varphi_s - \varphi_O)$ cannot be detected. This renders homodyne detection more sensitive than heterodyne reception, if we are interested in the signal amplitude $\hat{E}_s$ only. However, when employing an optical hybrid

The limiting sensitivity for homodyne reception is derived in analogy to the heterodyne case, only that we have to observe $f_O = f_s$ which leads to an IF frequency $f_Z = 0$. Further, the optical band is directly transferred to the baseband, see Fig. 5.25 on Page 136. The relevant receiver bandwidth corresponds to the signal bandwidth B, but the average electrical signal power is $P_S = i_Z^2$ (not $P_S = i_Z^2/2$ as before). Compared to $\gamma_{\text{BB-het qu}}$, the SNR doubles,

$$\gamma_{\text{hom qu}} = \frac{\eta P_s}{\frac{1}{2}hf_OB} = 2\gamma_{\text{BB-het qu}} = 4\gamma_{\text{dir qu}} \quad \text{(quantum noise limited, } \frac{4kF'T_0G_Q}{2eSP_O} \ll 1\text{)}.$$

Compared to the quantum noise limited SNR for direct reception, Eq. (5.75) on Page 126, the SNR for homodyne reception is four times as large. It corresponds to four times the mean number ηN_s of received signal photons with energy $hf_s \approx hf_O$ per symbol duration $T_s = 1/(2B)$,

$$\gamma_{\text{hom qu}} = 4\eta N_s.$$

Intradyne Reception (1)

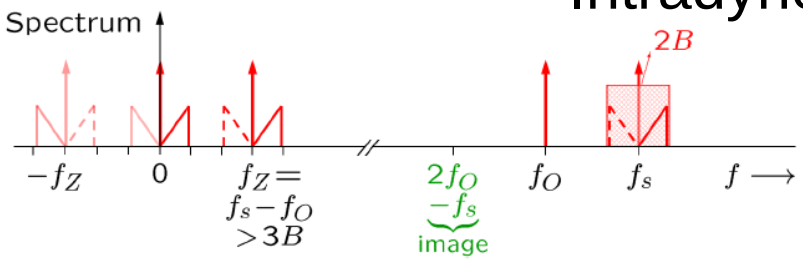

Fig. 5.25. Heterodyne spectra (also homodyne spectra for $f_O = f_s$).

COHERENT OPTICAL TRANSMISSION SYSTEMS (IF = INTERMEDIATE FREQUENCY; B = BANDWIDTH OF BASEBAND SIGNAL)

system	IF spectrum	IF
homodyne	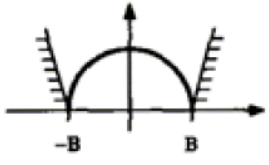	IF = 0 Optical PLL
intradyne	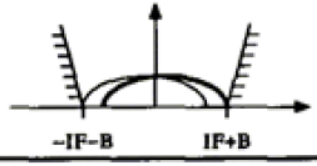	IF < B
heterodyne	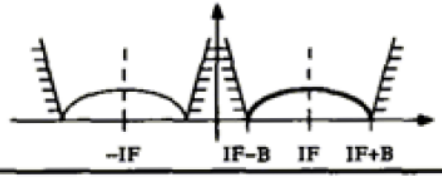	IF > B

Sidebands overlap, therefore IQ-demodulation

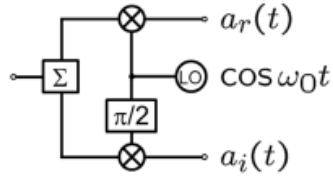

Fig. 5.26. Intradyne IF spectra (IF $\widehat{=}$ f_Z) compared to heterodyne and homodyne spectra for a baseband spectral width B. [After Ref. 38 Table I]

Intradyne Reception (2)

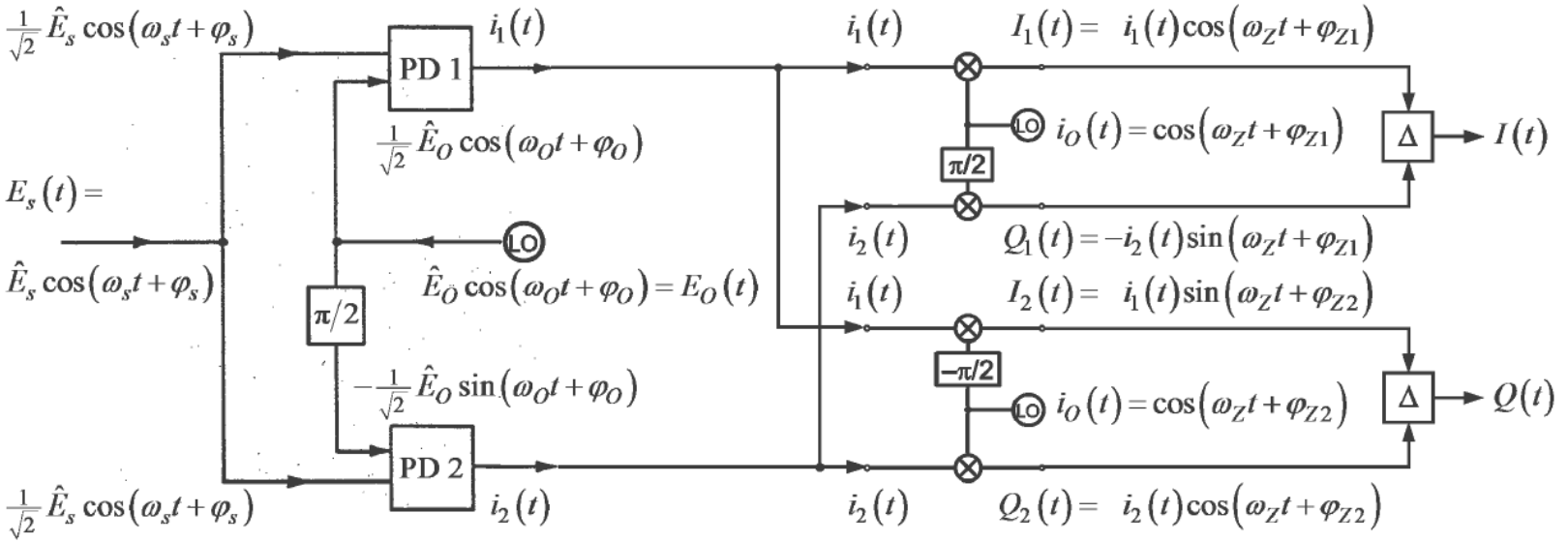

$$E_s(t)=\hat{E}_s\cos(\omega_s+\varphi_s)=\hat{E}_{s,r}\cos\omega_s t-\hat{E}_{s,i}\sin\omega_s t=\Re\left\{\left(\hat{E}_{s,r}+\mathrm{j}\,\hat{E}_{s,i}\right)\mathrm{e}^{\mathrm{j}\omega_s t}\right\},$$

$$\hat{E}_{s,r}=\hat{E}_s\cos\varphi_s,\qquad \hat{E}_{s,i}=\hat{E}_s\sin\varphi_s\,.$$

$$i_1(t)=\tfrac{1}{2}S\hat{E}_O\left[\hat{E}_{s,r}\cos(\omega_Z t-\varphi_O)-\hat{E}_{s,i}\sin(\omega_Z t-\varphi_O)\right]$$
$$i_2(t)=\tfrac{1}{2}S\hat{E}_O\left[\hat{E}_{s,i}\cos(\omega_Z t-\varphi_O)+\hat{E}_{s,r}\sin(\omega_Z t-\varphi_O)\right]$$

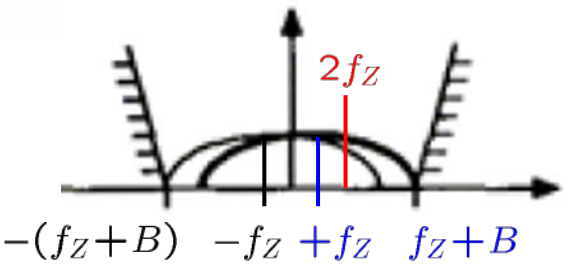

$$I_1(t)=\ i_1(t)\cos(\omega_Z t+\varphi_{Z1})$$
$$=\ \tfrac{1}{4}i_Z\cos(\varphi_s-\varphi_O-\varphi_{Z1})+\tfrac{1}{4}i_Z\cos(2\omega_Z t+\varphi_s-\varphi_O+\varphi_{Z1})$$
$$Q_1(t)=-i_2(t)\sin(\omega_Z t+\varphi_{Z1})$$
$$=-\tfrac{1}{4}i_Z\cos(\varphi_s-\varphi_O-\varphi_{Z1})+\tfrac{1}{4}i_Z\cos(2\omega_Z t+\varphi_s-\varphi_O+\varphi_{Z1})$$

Coherent Reception — Synopsis

Coherent Optical Receiver Concepts

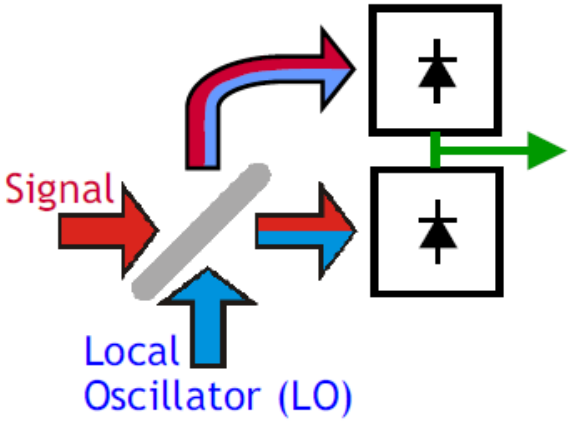

- *Beat term* from direct detection of signal plus LO:
  $|E_{Sig}(t) + E_{LO}|^2$: $\pm E_{Sig}(t)\, E_{LO} \cos(2\pi f_{IF} t + \phi_{Sig}(t))$
- Beating requires *polarization alignment* of signal and LO
- Balanced detection desirable (common mode rejection); no fundamental sensitivity gain as for DPSK w/ delay demod.
- Second signal quadrature $\sin(2\pi f_{IF} t)$ is accessible using a LO with a 90-degree phase shift → '90-deg hybrid'

- Heterodyning: Signal and LO at different optical frequencies (f_{IF} > Signal bandwidth)
- Homodyning: Signal and LO at the same optical frequency and phase-locked
- Intradyning: Signal and LO roughly at the same optical frequency (can use digital phase locking if both signal quadratures are detected)

	Heterodyne	Homodyne	Intradyne
Front-end bandwidth	~ **5* Symbol rate**	Symbol rate	~Symbol rate
Phase/frequency locking	Frequency locking	**Analog optical PLL**	**Digital electronic PLL** (free-running LO)
Spectral sketch	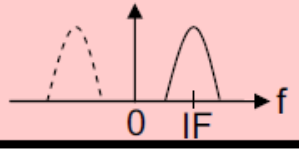	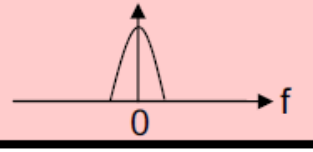	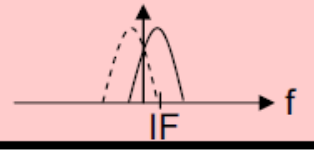

Heterodyne Reception in a WDM System

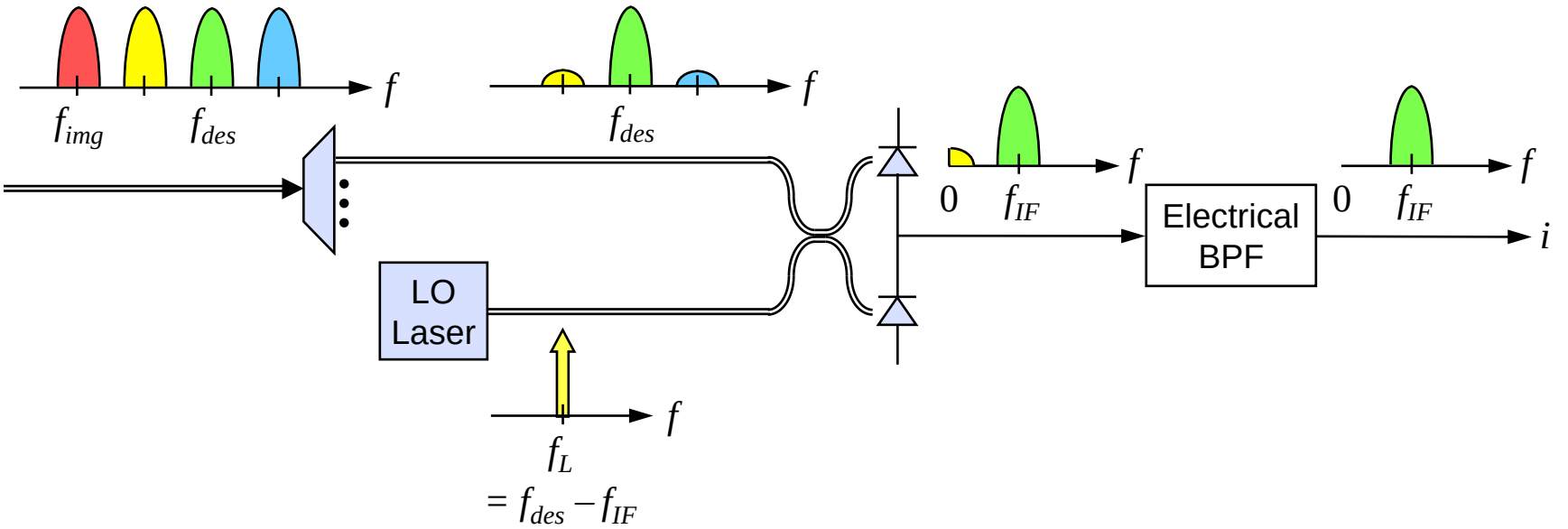

Heterodyne with narrowband filtering

- Bandwidth $\sim 2R_s$ is required at f_{IF}
- Only $f_{des} = f_L + f_{IF}$ is down-converted to f_{IF}
  → no noise penalty, no potential interference
- Both I and Q can be recovered from one signal at f_{IF}

Source of figure cannot be recovered any more

Homodyne Reception in a WDM System

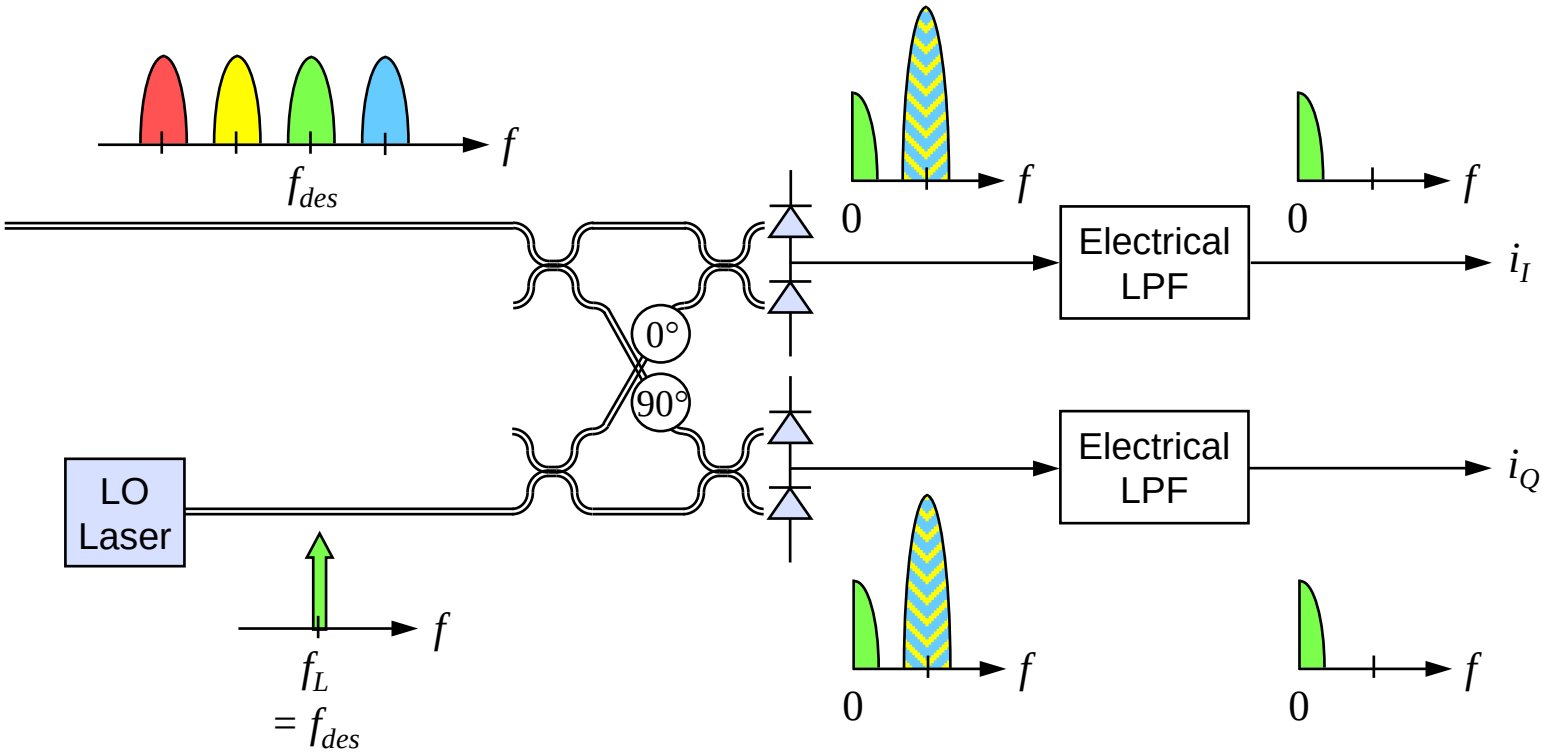

Homodyne without (or with) narrowband filtering

- Bandwidth $\sim R_s$ is required at $f = 0$
- Only $f_{des} = f_L$ is down-converted to $f = 0$

→ no noise penalty, no potential interference

- Recovering both I and Q requires two balanced receivers

Source of figure cannot be recovered any more

IQ Receiver Schematic

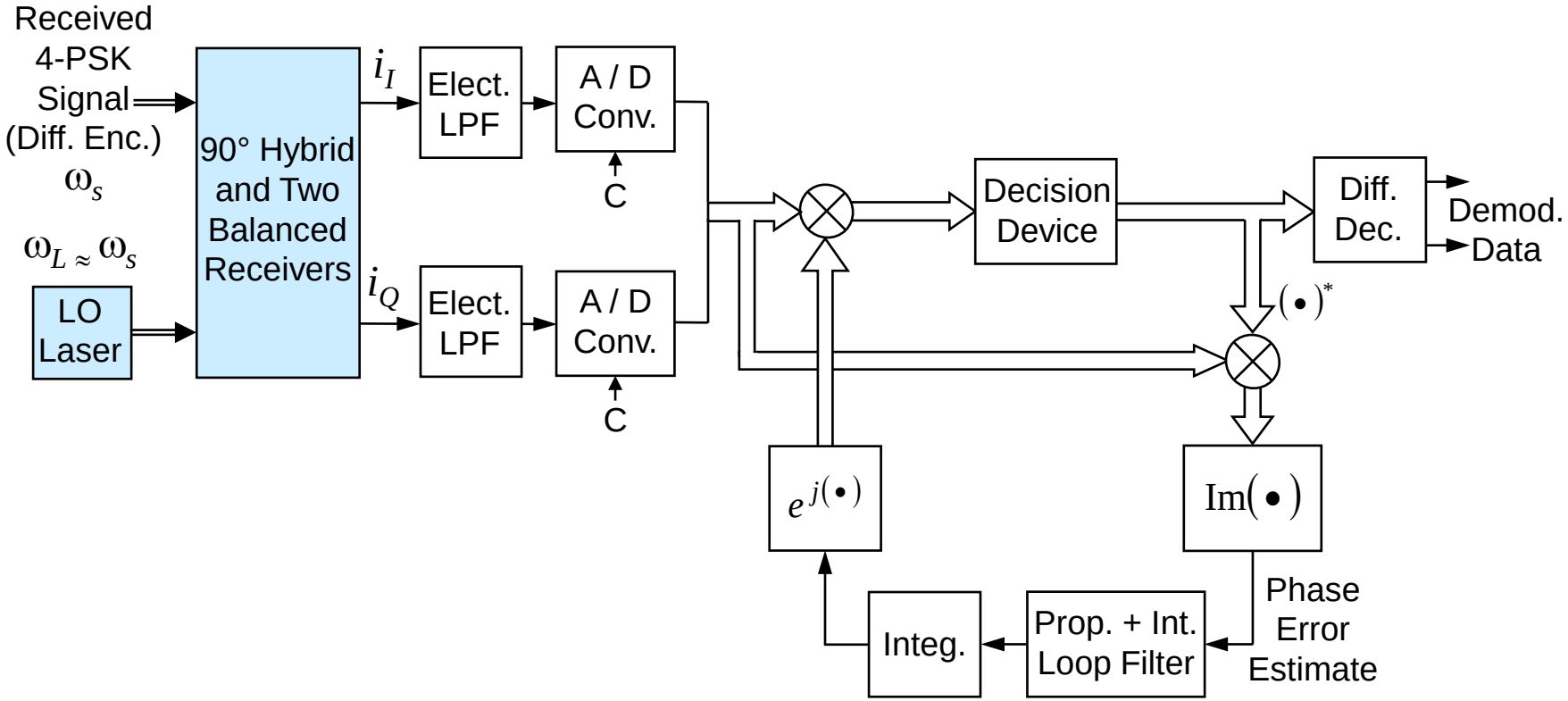

- Homodyne decision-directed PLL shown is applicable to 4-PSK.
- Optimized performance is very similar to analog PLL.
- Challenges:
  - Analog-digital converters
  - Propagation delay inside loop

R. Noé, 2003; M. G. Taylor; 2004, Ly-Gagnon et al., 2005

Signal Quality Metric for QAM Reception

Definition of Error Vector Magnitude

Error Vector Magnitude (EVM) is performance metric for M-ary signals, as is the signal quality factor Q for (binary) OOK signals.

EVM: Effective deviation of I complex electric fields $E_{\mathrm{r},i}$ of an actually received symbol (what has been arrived?) from the transmitted value $E_{\mathrm{t},i}$ (what was meant to arrive?).

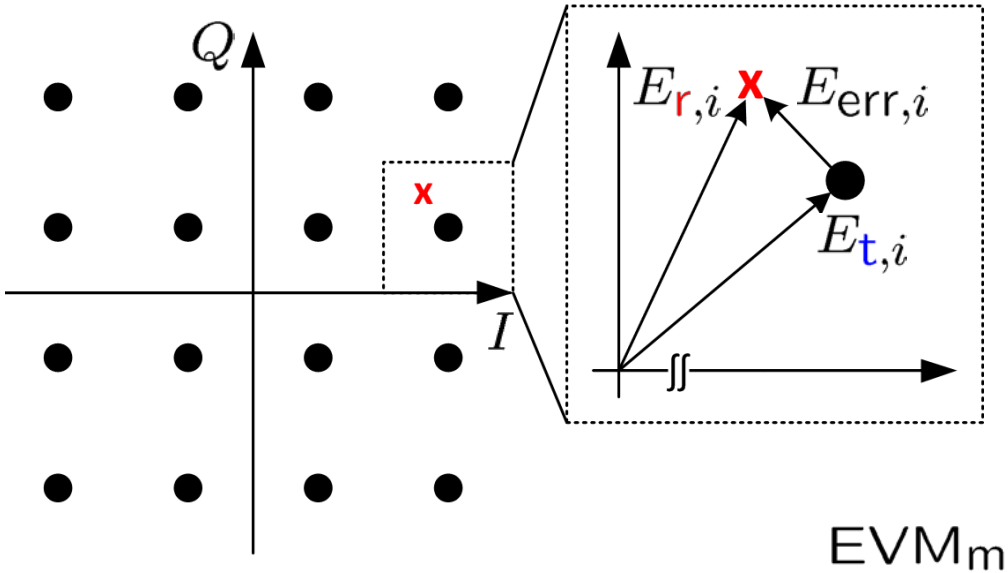

$|E_{\mathrm{t,m}}|$ is the maximal field magnitude in the constellation diagram.

The I symbols sent are randomly chosen from the symbol set.

$$\mathrm{EVM_m} = \sqrt{\frac{1}{I}\sum_{i=1}^{I} |E_{\mathrm{err},i}|^2 \Big/ |E_{\mathrm{t,m}}|^2}$$

$$E_{\mathrm{err},i} = E_{\mathrm{r},i} - E_{\mathrm{t},i}\,, \qquad i = 1, 2, \ldots, I$$

BER, Error Vector Magnitude EVM and SNR

Error vector magnitude ($\mathrm{EVM_m}$):

$$\mathrm{EVM_m} = \sqrt{\frac{1}{I}\sum_{i=1}^{I} |E_{\mathrm{err},i}|^2 \Big/ |E_{\mathrm{t,m}}|^2} = \frac{1}{k}\,\mathrm{EVM_a}$$

$$E_{\mathrm{err},i} = E_{\mathrm{r},i} - E_{\mathrm{t},i}\,, \quad i = 1, 2, \ldots, I$$

Additive white Gaussian noise (AWGN) in channel → relation between EVM and BER (*square* constellations only!):

$$\mathrm{BER} \approx \frac{1 - \frac{1}{L}}{\log_2 L}\,\mathrm{erfc}\left(\sqrt{\frac{3\log_2 L}{L^2-1}\,\frac{1}{(k\,\mathrm{EVM_m})^2 \log_2 M}}\right)$$

$$k^2 = \frac{|E_{\mathrm{t,m}}|^2}{|E_{\mathrm{t,a}}|^2 = \frac{1}{M}\sum_{i=1}^{M} |E_{\mathrm{t},i}|^2}$$

L : N° levels in each orthog. const. dim.
M : N° constellation points
$\log_2 M$: N° bits for each QAM symbol

	BPSK	QPSK	8PSK	16QAM	32QAM	64QAM
k	1	1	1	$\sqrt{9/5}$	$\sqrt{17/10}$	$\sqrt{7/3}$

Complementary error function: $\mathrm{erfc}(z) = \frac{2}{\sqrt{\pi}} \int_z^\infty \exp(-t^2)\,\mathrm{d}t$

Shafik, R.; Rahman, S.; Islam, A. R.: On the extended relationships among EVM, BER and SNR as performance metrics. Proc. 4th Intern. Conf. Electrical and Computer Engineering (ICECE), pages 408–411, December 2006.

Arslan, H.; Mahmoud, H.A.: **Error vector magnitude to SNR conversion** for nondata-aided receivers, Trans. Wireless Comm., vol. 8, no.5, pp.2694-2704, May 2009

Signal Quality Metric for QAM Reception — EVM, BER and SNR

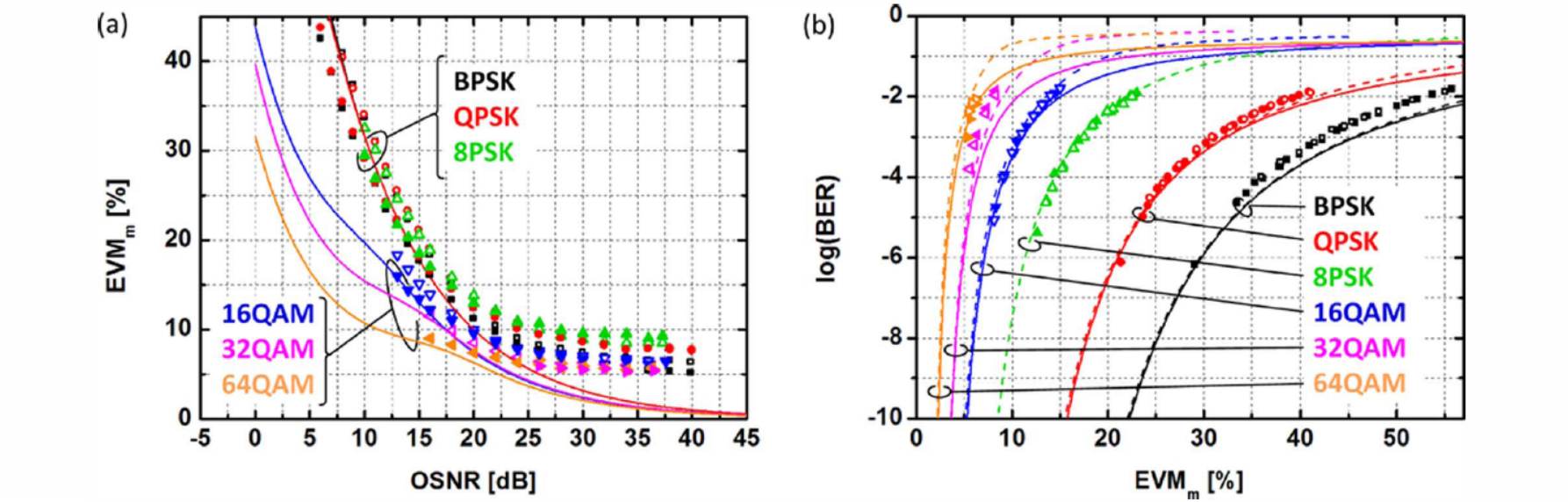

Interdependencies of OSNR, EVM_m, and BER. Filled symbols represent measurements for a symbol rate of 20 GBd, open symbols for 25 GBd. (a) Measured (symbols) and calculated [8] EVM_m (solid lines) as a function of OSNR. For high OSNR levels, the measured plots have an error floor due to the electronic noise of the transmitter and receiver. The different error floors for Q/8PSK and xQAM stem from different factors k. The error floor for BPSK is lower because of transmitter specific properties. (b) Measured (symbols), simulated (dashed lines), and calculated [7] BER (solid lines) as a function of EVM_m.

M-ary Signals, Constellation Diagrams, EVM_m and BER

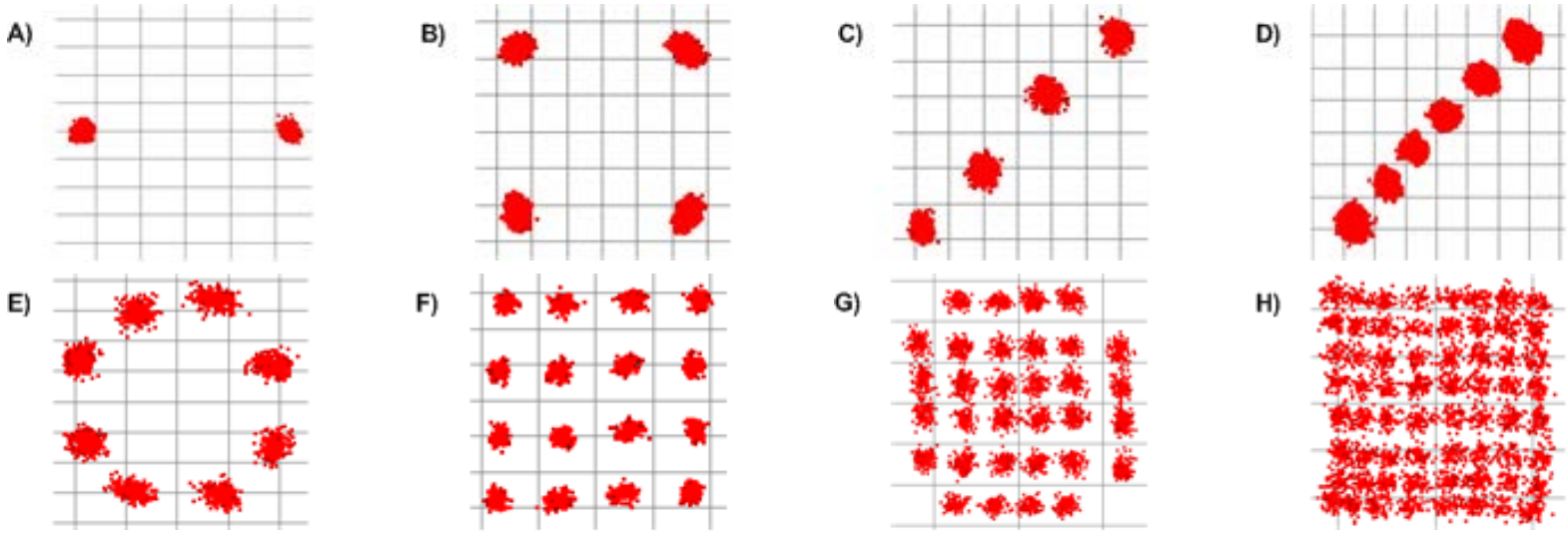

Received constellation diagrams:

A) BPSK at 28 GBd with EVM = 5.7 % (no errors)
B) QPSK at 28 GBd with EVM = 8.5 % (no errors)
C) 4PAM at 20 GBd
D) 6PAM at 20 GBd
E) 8PSK at 28 GBd with EVM = 12.5 % (no errors)
F) 16QAM at 28 GBd with EVM = 8.6 % (no errors)
G) 32QAM at 28 GBd with EVM = 9.1 %
H) 64QAM at 28 GBd with EVM = 10.1 %

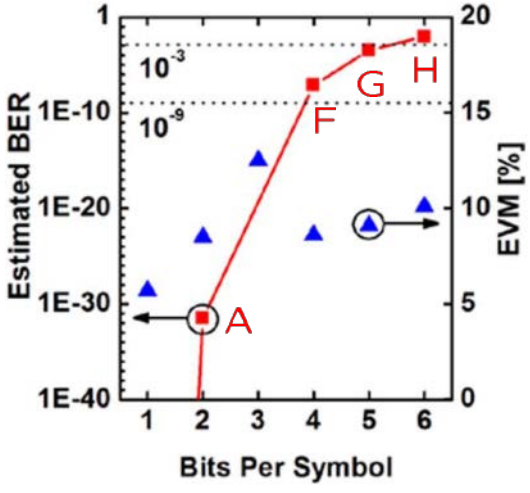

R. Schmogrow, D. Hillerkuss, M. Dreschmann, M. Huebner, M. Winter, J. Meyer, B. Nebendahl, C. Koos, J. Becker, W. Freude, J. Leuthold: Real-time software-defined multiformat transmitter generating 64QAM at 28 GBd. IEEE Photon. Technol. Lett. 22 (2010) 1601–1602

Self-Coherent Receiver

Self-Coherent Receiver — RZ-DPSK Reception

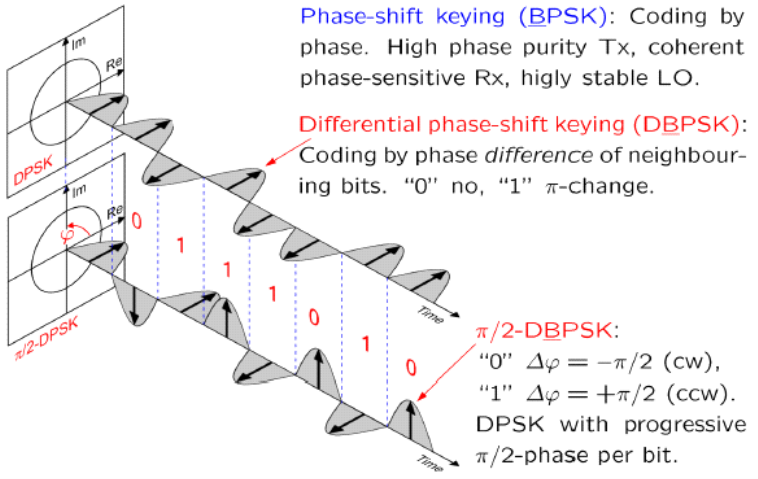

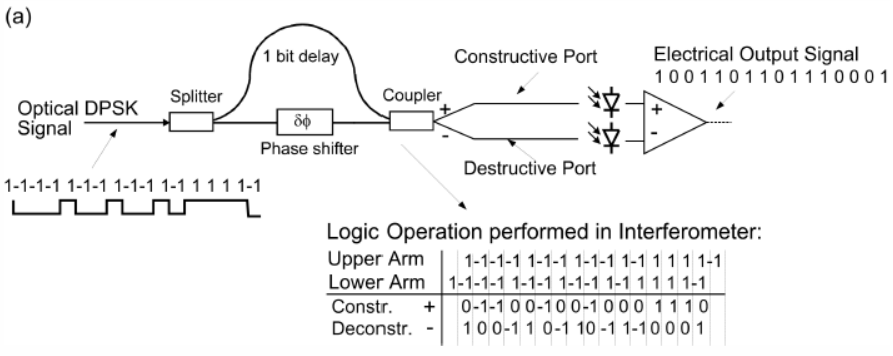

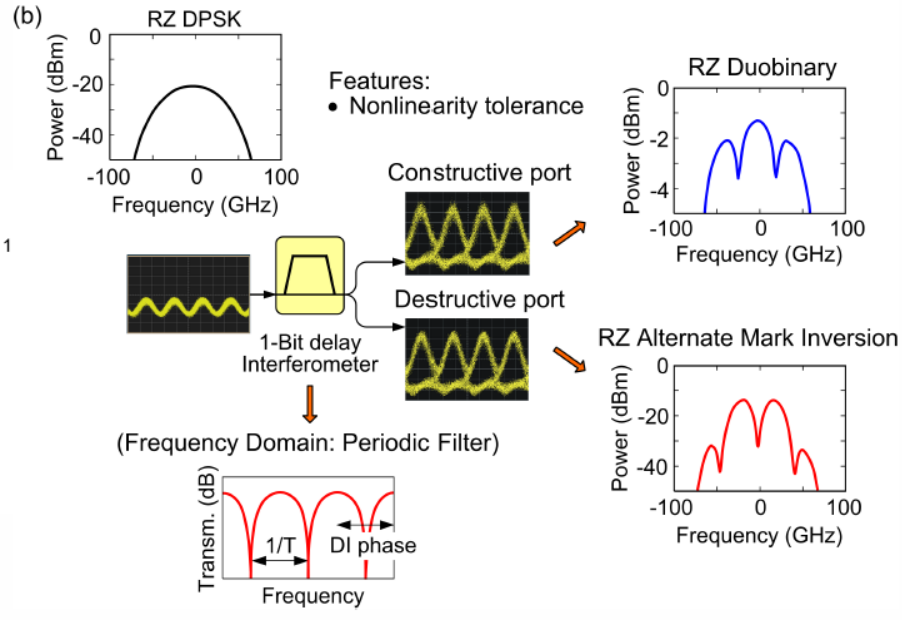

Self-coherent receiver setup (a) Interferometer with 1-symbol delay in one arm, balanced direct photoreceiver, and differential electrical amplifier (b) Input and output spectra of a 1-symbol delay interferometer. Its transfer function is periodic. With an RZ-DPSK input spectrum, the spectra at the constructive and destructive output ports belong to an RZ-DB and an RZ-AMI modulation format, respectively. [After Fig. 2.57 of Ref. † on the Preface page]

RZ-DPSK Demodulation With 1-bit Delay Discriminator

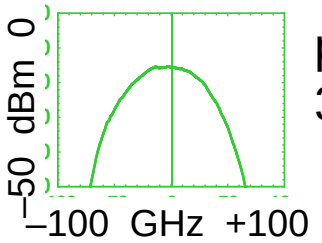

power spectrum of
33-% RZ-DPSK

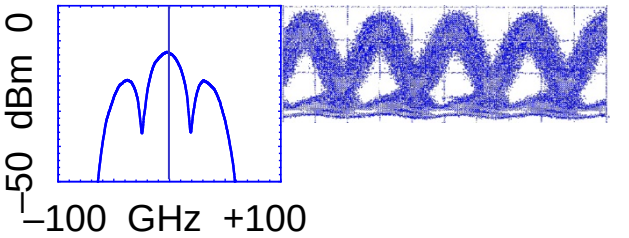

111111 = Σ – Δ

↑↓↓↑↓↑↑ = DPSK

010001 ... ↑↓↓↑↓↑↑ ...

111111

010001 = Σ

Optical filter

... ↑↓↓↑↓↑↑ ...

... ↑↓↓↑↓↑↑ ...

101110 = Δ

Asymmetric Mach-Zehnder

1 bit delay

010001

101110

Balanced photodetector

↑ positive *E*

↓ negative *E*

„1“ pos. voltage

„1“ neg. voltage

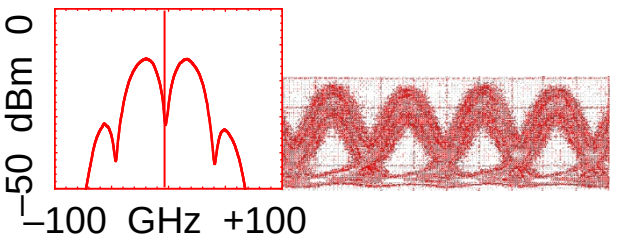

Bosco, G.; Poggiolini, P.: On the Q factor inaccuracy in the performance analysis of optical direct-detection DPSK systems. PTL 16 (2004) 665–667

Zhu, B.; Nelson, L. E.; Stulz, S.; Gnauck, A. H.; Doerr, C.; Leuthold, J.; Grüner-Nielsen, L.; Pedersen, M. O.; Kim, J; Lingle, Jr., R. L.: High spectral density long-haul 40-G b/s transmission using CSRZ-DPSK format. JLT 22 (2004) 208–214

Self-Coherent Reception

No LO, similar to DPSK receiver

$s(t) = r(t)\,\mathrm{e}^{\mathrm{j}\,\phi(t)}$

Orthogonal phase offsets in both ODI

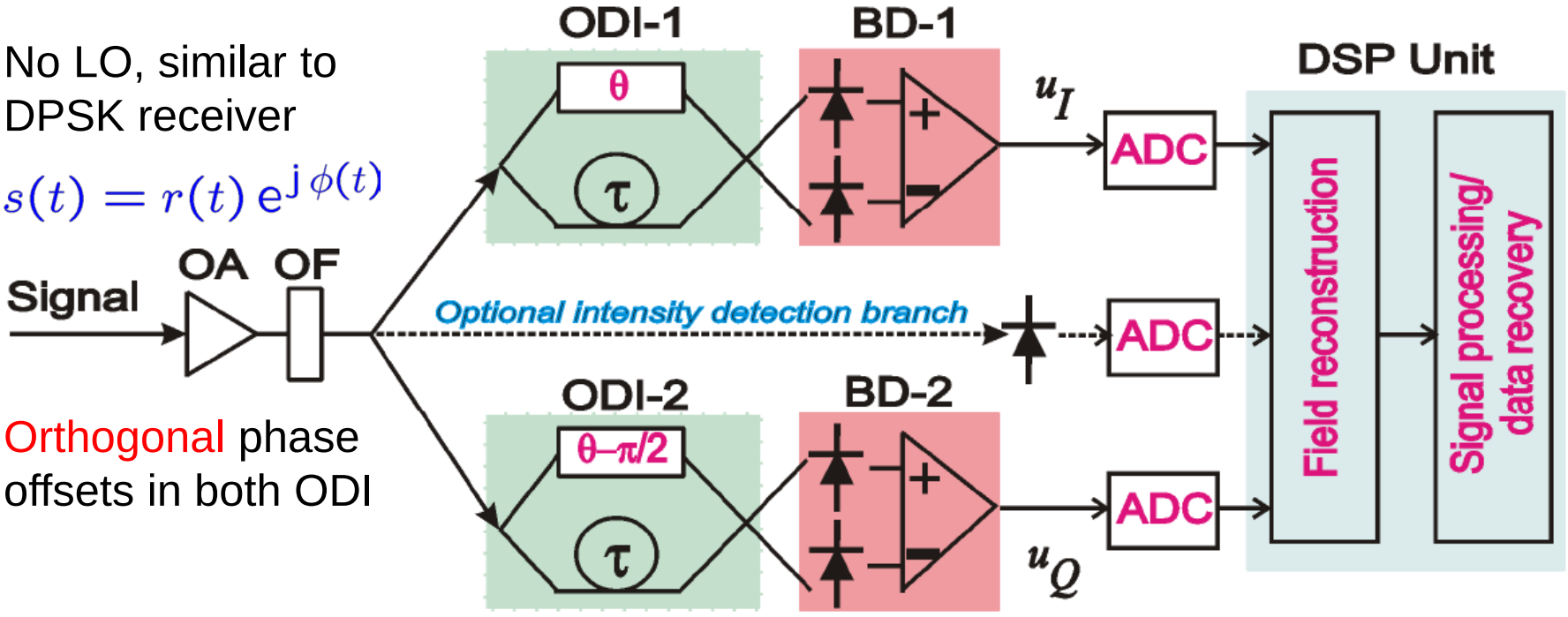

Fig 1. Schematic DSCD architecture based on orthogonal differential direct-detection followed by ADC and DSP. OA: optical pre-amplifier; OF: optical filter; ODI: optical delay interferometer; BD: balanced detector; ADC: analog-to-digital converter.

$$u_I(t) = \left|s(t)\,\mathrm{e}^{\mathrm{j}\,\theta} + s(t-\tau)\right|^2 - \left|s(t)\,\mathrm{e}^{\mathrm{j}\,\theta} - s(t-\tau)\right|^2 = \Re\left\{s(t)s^*(t-\tau)\,\mathrm{e}^{\mathrm{j}\,\theta}\right\}$$

$$u_Q(t) = \left|s(t)\,\mathrm{e}^{\mathrm{j}(\theta-\frac{\pi}{2})} + s(t-\tau)\right|^2 - \left|s(t)\,\mathrm{e}^{\mathrm{j}(\theta-\frac{\pi}{2})} - s(t-\tau)\right|^2 = \Im\left\{s(t)s^*(t-\tau)\,\mathrm{e}^{\mathrm{j}\,\theta}\right\}$$

$$u(t) = u_I(t) + \mathrm{j}\,u_Q(t) = s(t)s^*(t-\tau)\exp(\mathrm{j}\,\theta) \qquad \text{(factor 4 omitted)}$$

Xiang Liu, S. Chandrasekhar, and Andreas Leven: Digital self-coherent detection. Opt. Expr. 16 (2008) 792-803

Self-Coherent Reception — Signal Field Reconstruction

Optical input: $s(t) = r(t)\,\mathrm{e}^{\mathrm{j}\,\phi(t)}$

Electrical output:

$$u_I(t) = \Re\left\{ s(t)s^*(t-\tau)\,\mathrm{e}^{\mathrm{j}\,\theta} \right\}$$

$$u_Q(t) = \Im\left\{ s(t)s^*(t-\tau)\,\mathrm{e}^{\mathrm{j}\,\theta} \right\}$$

$$u(t) = u_I(t) + \mathrm{j}\,u_Q(t) = s(t)s^*(t-\tau)\,\mathrm{e}^{\mathrm{j}\,\theta}$$

$$= \underbrace{r(t)r(t-\tau)}_{|u(t)|}\,\mathrm{e}^{\mathrm{j}[\phi(t)-\phi(t-\tau)]}\,\mathrm{e}^{\mathrm{j}\,\theta}$$

Digital field reconstruction:

Phase difference: $\mathrm{e}^{\mathrm{j}(\phi(t)-\phi(t-\tau))} = \dfrac{u(t)}{|u(t)|}\,\mathrm{e}^{-\mathrm{j}\,\theta}$

Optical input: $s(t_0+n\tau) = r(t_0+n\tau)\,\mathrm{e}^{\mathrm{j}\,\phi(t_0)}$

Phase history example:

$$\times \prod_{m=1}^{n} \mathrm{e}^{\mathrm{j}(\phi(t_0+m\tau)-\phi(t_0+(m-1)\tau)}$$

$$\phi(t_0+3\tau) = \phi(t_0) + \Big[\phi(t_0+\tau) - \phi(t_0)\Big] + \Big[\phi(t_0+2\tau) - \phi(t_0+\tau)\Big] + \Big[\phi(t_0+3\tau) - \phi(t_0+2\tau)\Big]$$

Xiang Liu, S. Chandrasekhar, and Andreas Leven: Digital self-coherent detection. Opt. Expr. 16 (2008) 792-803

Pre-Amplifier Receiver

Photodetection of Signal and Noise

Super-broadband Er-doped fibre amplifier (EDFA)

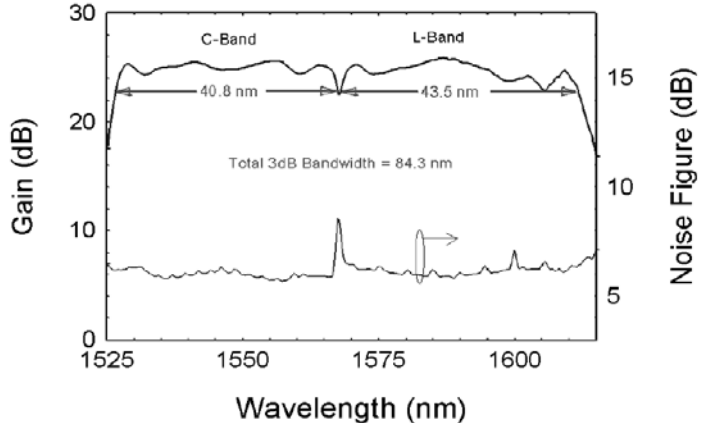

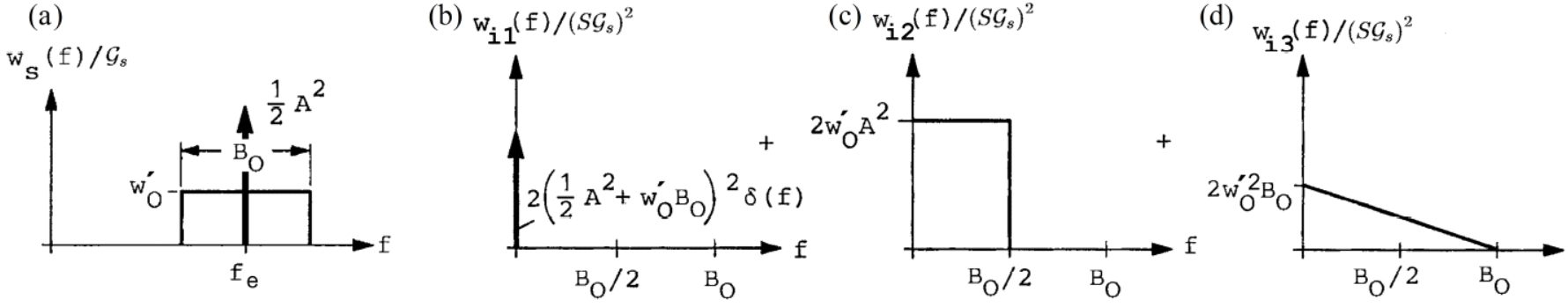

Signal and co-polarized noise at the output of an optical amplifier with single-pass optical power gain $\mathcal{G}_s \gg 1$. (a) One-sided output power spectrum $w_s(f)$ of a sinusoidal optical signal with an input amplitude $A = \sqrt{2P_e}$ and a frequency f_e, superimposed with ASE noise of spectral density $(\mathcal{G}_s - 1)\, w'_O$ ($w'_O = n_{\mathrm{sp}} w_O$, inversion factor n_{sp}, $w_O = h f_e$). The amplifier bandwidth is narrow, $B_O \ll f_e$. Signal and narrowband noise are received with a photodetector. The optical input signal power P_e leads to a photocurrent $i = S\mathcal{G}_s P_e$ where $S = \eta e/(h f_e)$ is the sensitivity. (b) One-sided direct current (DC) power spectrum with photocurrents $i_S = S\mathcal{G}_s A^2/2$ and $i_R = S\,(\mathcal{G}_s - 1)\, w'_O B$. The total DC power is $(i_S + i_R)^2$. The integral over half a Dirac function is $\int_0^\infty \delta(f)\,\mathrm{d}f = \frac{1}{2}$. (c) Carrier-noise interference (d) Noise-noise interference. — Partial detector spectra w_{i1}, w_{i2} and w_{i3} are uncorrelated and may be added. Therefore the total power equals the sum of the partial powers.

Bose-Einstein Distribution for Thermal Photons

The Bose-Einstein distribution for the probability that in thermal equilibrium a number of N_P photons is measured in a total of m modes reads

$$p_{N_P}(N_P) = \frac{(N_P+m-1)!}{N_P!(m-1)!}\,\frac{1}{(1+\overline{N_P}/m)^m(1+m/\overline{N_P})^{N_P}}\,, \qquad \overline{\delta N_P^2} = \overline{(N_P-\overline{N_P})^2} = \underbrace{\overline{N_P}}_{\substack{\text{Particle}\\ \text{aspect:}\\ \text{Poisson}}} + \underbrace{\frac{\overline{N_P}^2}{m}}_{\substack{\text{Wave aspect:}\\ \text{Exponential for } m=1}}.$$

If only one transverse mode is regarded (e. g., in a single-mode fibre), then m corresponds to the number of longitudinal modes $m = M_L = B_O\tau$ as calculated in Eq. (3.4) on Page 48. The observation time $\tau = 1/B$ is determined by the signal bandwidth, and usually the condition $B \ll B_O$ is fulfilled so that $m \gg 1$ holds. For moderate powers (moderate average numbers of photons $\overline{N_P}$, excluding the explosion of a fusion bomb), the condition $\overline{N_P}/m \ll 1$ is met, so that ASE noise (and also LED radiation) approximates a Poisson distribution very well.

Number of longitudinal modes, in observation time $\Delta\tau$ for process bandwidth Δf (sampling theorem, 2 measurements per $\Delta\tau$ for *one* complex Fourier coefficient of *one* longitudinal mode):

$$M_L \approx \Delta\tau\,\Delta f, \qquad \text{LED } (\Delta\tau = 25\,\text{ms},\ \Delta f = 10\,\text{THz})$$

$$M_{L,\text{LED}} \approx 2\times 10^{11}$$

Number of transverse modes, radiated from area ΔF in solid angle $\Delta\Omega$ at wavelength λ (spatial sampling theorem):

$$M_T \approx \Delta F\,\Delta\Omega/\lambda^2, \quad \text{LED } (a = 50\,\mu\text{m},\ \Delta\Omega = 2\pi,\ \lambda = 1\,\mu\text{m})$$

$$M_{T,\text{LED}} \approx 5\times 10^4$$

Bose-Einstein Distribution for Thermal Photons

The Bose-Einstein distribution for the probability that in thermal equilibrium a number of N_P photons is measured in a total of m modes reads

$$p_{N_P}(N_P) = \frac{(N_P+m-1)!}{N_P!(m-1)!}\,\frac{1}{(1+\overline{N_P}/m)^m(1+m/\overline{N_P})^{N_P}}\,, \qquad \overline{\delta N_P^2} = \overline{(N_P-\overline{N_P})^2} = \underbrace{\overline{N_P}}_{\substack{\text{Particle}\\ \text{aspect:}\\ \text{Poisson}}} + \underbrace{\frac{\overline{N_P}^2}{m}}_{\substack{\text{Wave aspect:}\\ \text{Exponential for } m=1}}.$$

If only one transverse mode is regarded (e. g., in a single-mode fibre), then m corresponds to the number of longitudinal modes $m = M_L = B_O\tau$ as calculated in Eq. (3.4) on Page 48. The observation time $\tau = 1/B$ is determined by the signal bandwidth, and usually the condition $B \ll B_O$ is fulfilled so that $m \gg 1$ holds. For moderate powers (moderate average numbers of photons $\overline{N_P}$, excluding the explosion of a fusion bomb), the condition $\overline{N_P}/m \ll 1$ is met, so that ASE noise (and also LED radiation) approximates a Poisson distribution very well.

Number of modes in 2 pol.: $m = M_{\mathsf{LED}} = M = 2M_LM_T = 2\times10^{16}$

Number of phot. per mode $N_{P,\mathsf{LED}}^{(M)}$ ($P = 1\,\mathsf{mW}$, $f = \frac{c}{\lambda} = 300\,\mathsf{THz}$):

$$N_{P,\mathsf{LED}}^{(M)} = \frac{N_{P,\mathsf{LED}}}{M} = \underbrace{\frac{P\Delta\tau}{hf}}_{\overline{N_P}=1.3\times10^{14}}\frac{1}{M} = \frac{P}{h}\,\frac{f/c^2}{2\,\Delta f\,\Delta F\Delta\Omega} = 0.005 \ll 1$$

Bose-Einstein variance well approximated by Poisson variance:

$$\overline{\delta N_P^2} = 1.3\times10^{14} + \frac{1.7\times10^{28}}{2\times10^{16}}$$
$$= 1.3\times10^{14} + 0.85\times10^{12} = 1.3085\times10^{14} \approx 1.3\times10^{14}$$

OA Noise in 1 Polarization, Electr. BW B, "LED" Noise ≈ Poisson

Quadratic rectification of noise and signal, converted to $f=0$:

$$\overline{|i_{RD,1\,\mathrm{OA}}|^2} \overset{\mathcal{G}_s \gg 1}{\approx} 2e\left[S\mathcal{G}_s\left(P_e + w'_O B_O\right)\right] B$$

Mixing of polarized signal f_S and same-polarization noise SB:

$$\overline{|i_{RD,2\,\mathrm{OA}}|^2} \overset{\mathcal{G}_s \gg 1}{\approx} 4(S\mathcal{G}_s)^2 P_e w'_O B$$

Mixing of same-polarized noise SB ($\int_0^B (B_O - f)\,\mathrm{d}f = B_O B - B^2/2$):

$$\overline{|i_{RD,3\,\mathrm{OA}}|^2} \overset{\mathcal{G}_s \gg 1}{\approx} 2(S\mathcal{G}_s)^2 w'^2_O\,(B_O - B/2)\,B$$

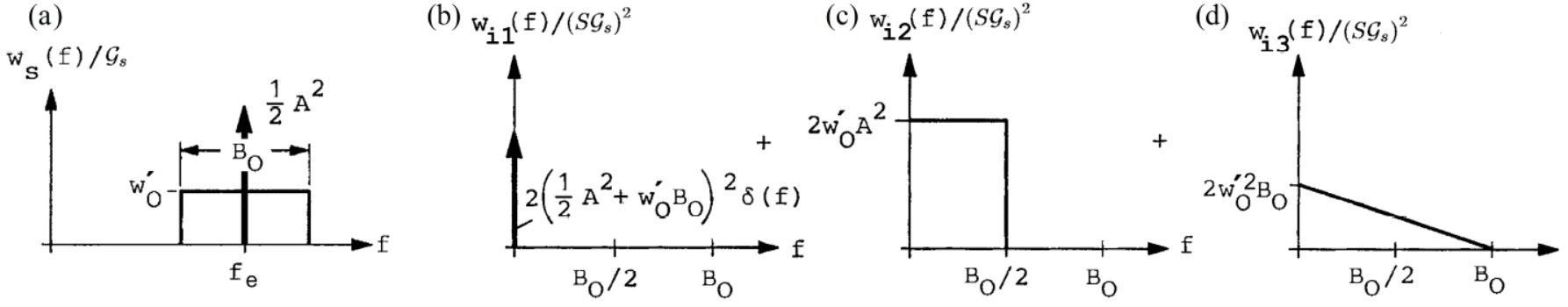

Direct Pre-Amplifier Receiver — Limiting Sensitivity

At optical amplifier output: Signal photocurrent $i'_S = S\mathcal{G}_s P_e$, optical bandwidth $B_O = 2B$ by filter $\rightarrow$ dominant noise from mixing between both lower/upper noise SB and polarized coherent carrier.

PD noise current fluctuation ($\overline{|i_{RD,2\,\mathrm{OA}}|^2} \approx 4(S\mathcal{G}_s)^2 P_e w'_O B$):

$$\overline{|i_{RD,2\,\mathrm{OA}}|^2} = (4S\mathcal{G}_s P_e) S(\mathcal{G}_s - 1) w'_O B$$

Polarized ASE optical noise power: $P_{\mathrm{ASE},x} = (\mathcal{G}_s - 1)\, w'_O\, B_O$. Spectral noise power density $w'_O = n_{\mathrm{sp}} w_O > w_O$ at OA output larger than quantum noise $w_O = h f_e$ (incomplete inversion $n_{\mathrm{sp}} = \frac{N_2}{N_2 - N_1} > 1$).

Independent of $\eta \rightarrow$ SNR (signal-to-noise power ratio) $\gamma_{\mathrm{dir\,OA}}$ (usually $\mathcal{G}_s \gg 1$, for ideal OA $w'_O = w_O$):

$$\gamma_{\mathrm{dir\,OA}} = \frac{\overbrace{(S\mathcal{G}_s P_e)^2}^{i'^2_S}}{\underbrace{4\,(S\mathcal{G}_s P_e)\,S\,(\mathcal{G}_s - 1)\,w'_O B}_{\overline{|i_{RD,2\,\mathrm{OA}}|^2}}} = \frac{1}{2}\,\frac{P_e}{2w'_O B}\,\frac{1}{1 - 1/\mathcal{G}_s} \approx \frac{1}{2n_{\mathrm{sp}}}\,\frac{P_e}{2hf_e B}$$

Coherent Pre-Amplifier Receiver

Coherent Pre-Amplifier Receiver — Heterodyne Reception

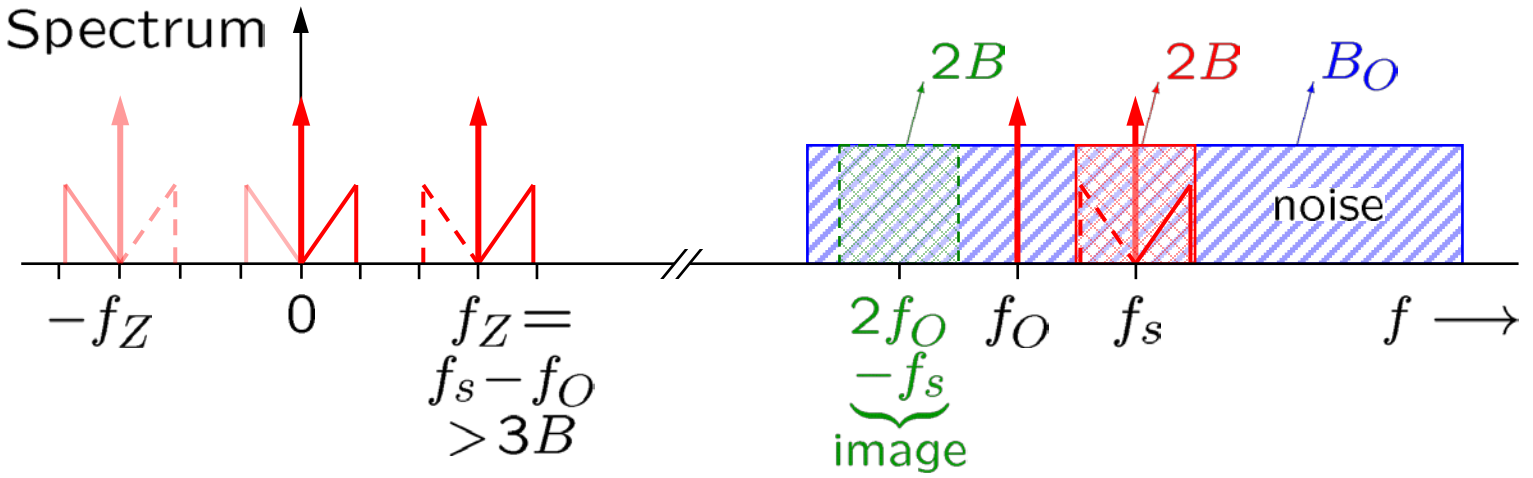

Optical carrier at f_s, signal sideband width B

Local oscillator at f_O, here $f_O \leq f_s$ ($f_O \geq f_S$ possible as well)

Mixing leads to IF $f_Z = |f_s - f_O| > 3B$ (sideband mixing to $0 \leq f \leq 2B$)

RF detection leads to baseband $0 < f < B$

Noise in bandwidth B_O around f_s, f_O

Image frequencies at $f_s - f_Z = 2f_O - f_s$ also converted to IF range!

Limit spectrum to signal band $f_s - B \leq f_s + B$ for better IF SNR!

Heterodyne Pre-Amplifier Receiver — Limiting Sensitivity

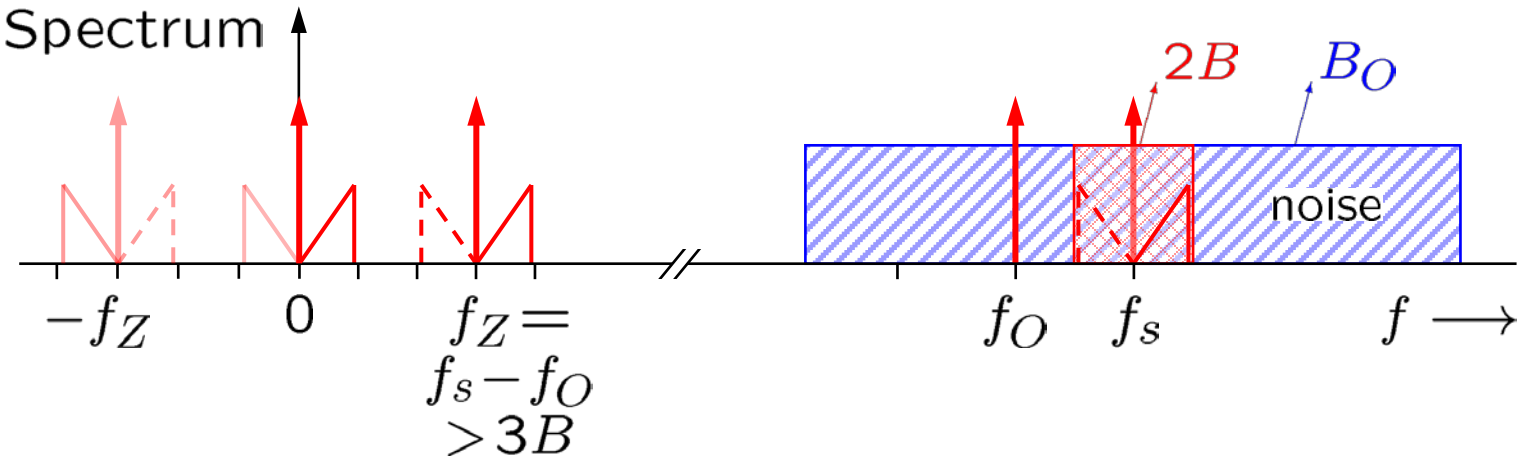

$$f_Z = f_s - f_O > 3B \text{ and } \mathcal{G}_s \gg 1,\ B_O = 2B$$

$$\gamma_{\text{IF-het OA qu}} = \frac{1}{2n_{\text{sp}}} \frac{P_s}{2hf_O B} = \gamma_{\text{dir OA}} = \frac{1}{2n_{\text{sp}}} \gamma_{\text{dir qu 1}}$$

$$\gamma_{\text{BB-het OA qu}} = \frac{1}{2n_{\text{sp}}} \frac{P_s}{hf_O B} = \frac{1}{2n_{\text{sp}}} 2\gamma_{\text{dir qu 1}}$$

Homodyne Pre-Amplifier Receiver — Limiting Sensitivity

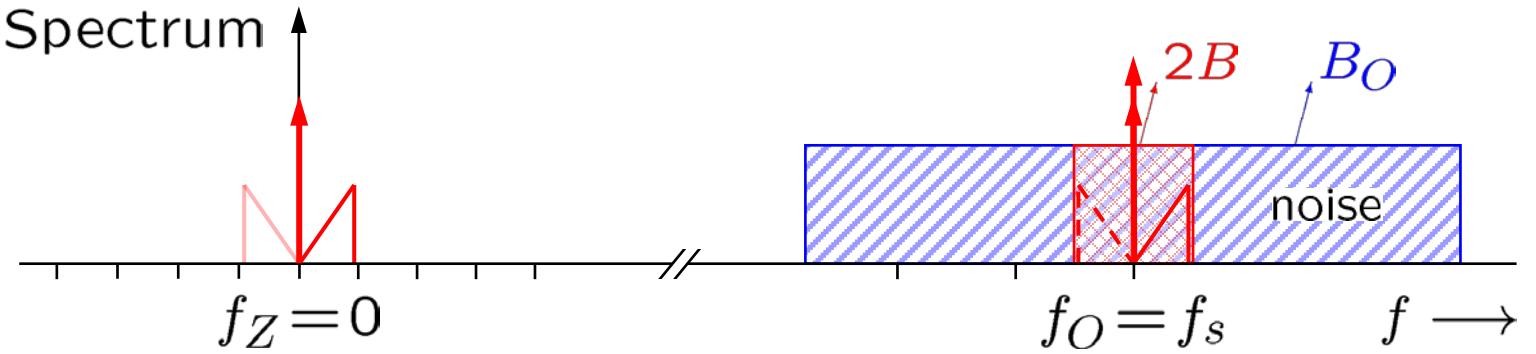

$$\mathcal{G}_s \gg 1,\ B_O = 2B,\ P_O \gg \max\left(\mathcal{G}_s P_s, n_{\mathrm{sp}} \mathcal{G}_s h f_O\, 2B\right)$$

$$\gamma_{\mathrm{hom\,OA}} =$$

$$= \frac{1}{2n_{\mathrm{sp}}} \frac{P_s}{\frac{1}{2} h f_O B}$$

$$\times \frac{1}{\underbrace{\frac{1}{2}\frac{1}{\eta n_{\mathrm{sp}} \mathcal{G}_s}\left(1 + \frac{\mathcal{G}_s P_s}{P_O} + \frac{n_{\mathrm{sp}} \mathcal{G}_s h f_O B_O}{P_O}\right)}_{\overline{|i_{RD,1\,\mathrm{OA}}|^2}} + \underbrace{\left(1 + \frac{\mathcal{G}_s P_s}{P_O}\right)}_{\overline{|i_{RD,2\,\mathrm{OA}}|^2}} + \underbrace{\frac{1}{2}\frac{n_{\mathrm{sp}} \mathcal{G}_s h f_O}{P_O}\left(B_O - \frac{B}{2}\right)}_{\overline{|i_{RD,3\,\mathrm{OA}}|^2}} + \underbrace{\frac{k F' T_0}{\mathcal{G}_s P_O}\frac{h f_O}{(\eta e)^2}}_{\overline{|i'_R|^2}}}$$

Homodyne Pre-Amplifier Receiver — Limiting Sensitivity

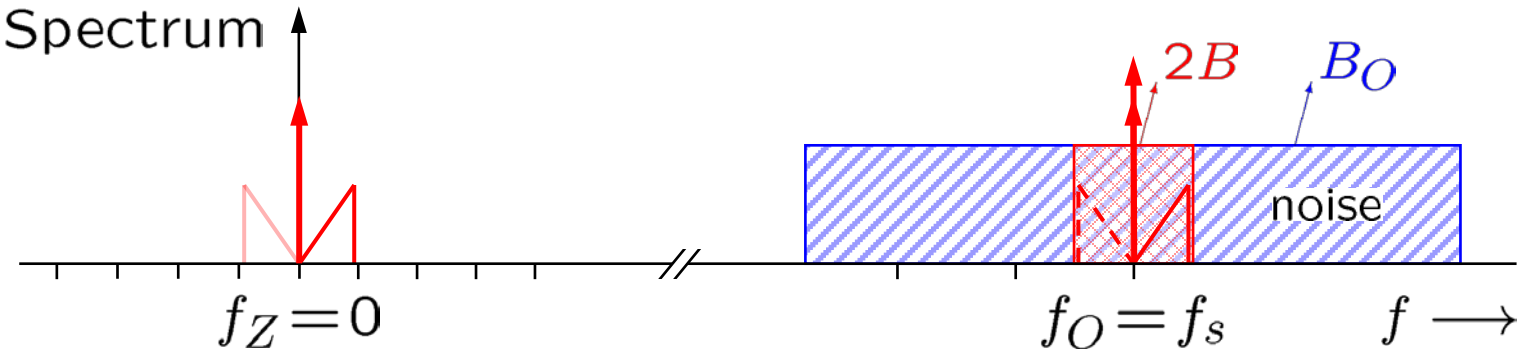

$$\mathcal{G}_s \gg 1,\ B_O = 2B,\ P_O \gg \max\left(\mathcal{G}_s P_s, n_{\mathrm{sp}} \mathcal{G}_s h f_O\, 2B\right)$$

$$\gamma_{\mathrm{hom\ OA}} = \frac{1}{2n_{\mathrm{sp}}} \frac{P_s}{\frac{1}{2} h f_O B} \frac{1}{1 + \frac{\mathcal{G}_s P_s}{P_O}}$$

$$\gamma_{\mathrm{hom\ OA\ qu}} = \frac{1}{2n_{\mathrm{sp}}} \frac{P_s}{\frac{1}{2} h f_O B} = \frac{1}{2n_{\mathrm{sp}}} 4\gamma_{\mathrm{dir\ qu\ 1}}$$

$$\gamma_{\mathrm{hom\ OA\ qu}} = 2\gamma_{\mathrm{BB\text{-}het\ OA\ qu}} = 4\gamma_{\mathrm{dir\ OA\ qu}}$$

6.1 Transmission impairments

There are numerous influences, which impair a fibre-optic transmission. A few were mentioned already and displayed in Fig. 1.6 on Page 6. Most important is attenuation of light guided in a glass fibre. This can be compensated with (noisy) optical amplifiers. Next is dispersion as described in Sect. 2.2 on Page 17 ff., which can be equalized with dispersion compensating fibres. Modern coherent receivers in combination with digital signal processing can even mitigate impairments due to nonlinearities in the fibre. Inter-symbol interference as explained in Fig. 1.5(b) on Page 5 can be avoided by proper signal shaping at the transmitter, or by equalization at the receiver as in Fig. 5.19 on Page 129.

In the following two section we discuss the noise figure of optical amplifiers and of links with concatenated amplifiers, and finally give a few results on signal shaping.

Noise Figure of Optical Amplifiers

Direct Reception Limit With Full and Matched OA Bandwidth

The optical signal bandwidth is usually much smaller than the optical amplifier bandwidth, $2B \ll B_O$, and without limiting the amplifier bandwidth B_O, we find for the SNR of a pre-amplifier receiver a much smaller value than for shot-noise limited reception (Eq. (5.81 on Page 132) without an optical amplifier,

$$\gamma_{\text{dir OA}} \approx \frac{\overbrace{\left(S\mathcal{G}_s P_e\right)^2}^{i_S^2}}{\underbrace{4\left(S\mathcal{G}_s P_e\right) S\mathcal{G}_s w'_O B}_{\overline{|i_{RD,2}|^2}} + \underbrace{2\left(S\mathcal{G}_s\right)^2 w'^2_O B_O B}_{\overline{|i_{RD,3}|^2}}} = \frac{\gamma^{(1)}_{\text{dir qu}}}{2n_{\text{sp}}} \frac{1}{1+\frac{n_{\text{sp}}}{2\gamma^{(1)}_{\text{dir qu}}}\frac{B_O}{2B}}, \quad 2B \ll B_O, \tag{5.151a}$$

$$\gamma_{\text{dir OA}} \ll \frac{1}{2n_{\text{sp}}}\gamma^{(1)}_{\text{dir qu}}, \quad \gamma^{(1)}_{\text{dir qu}} = \gamma_{\text{dir qu}}\big|_{\eta=1} = \frac{P_e}{2hf_eB}, \quad w'_O = n_{\text{sp}} w_O, \quad w_O = hf_e. \tag{5.151b}$$

It is remarkable that with a pre-amplifier receiver the photodetector's quantum efficiency η does not influence the SNR. Even for a large OA bandwidth, the SNR could be better than without an optical pre-amplifier, as long as electronic amplifier noise $\overline{|i'_R|^2}$ in Eq. (5.80) on Page 132 does not yet dominate, i. e., if with $\gamma_{\text{dir OA}} \ll \gamma^{(1)}_{\text{dir qu}}/(2n_{\text{sp}})$ we still have $\overline{|i_{RD,3}|^2} \approx \overline{|i'_R|^2}$.

If an optical filter reduces the OA bandwidth $B_O = 2B$ to the optical signal bandwidth $2B$, the SNR improves greatly. We find the SNR from Eq. (5.151b),

$$\gamma_{\text{dir OA qu}} = \frac{1}{2n_{\text{sp}}}\gamma^{(1)}_{\text{dir qu}} \frac{1}{1+\frac{n_{\text{sp}}}{2\gamma^{(1)}_{\text{dir qu}}}} \underset{\gamma^{(1)}_{\text{dir qu}} \gg 1}{=} \frac{1}{2n_{\text{sp}}}\gamma^{(1)}_{\text{dir qu}} = \frac{1}{2n_{\text{sp}}}\frac{P_e}{2hf_eB}, \quad 2B = B_O. \tag{5.151c}$$

With an ideal, fully inverted pre-amplifier ($n_{\text{sp}} = 1$) a direct receiver has — even for small received optical powers P_e — an SNR, which is as high as half the theoretical quantum limit Eq. (5.81) on Page 132.

Noise Figure of Optical Amplifiers (1)

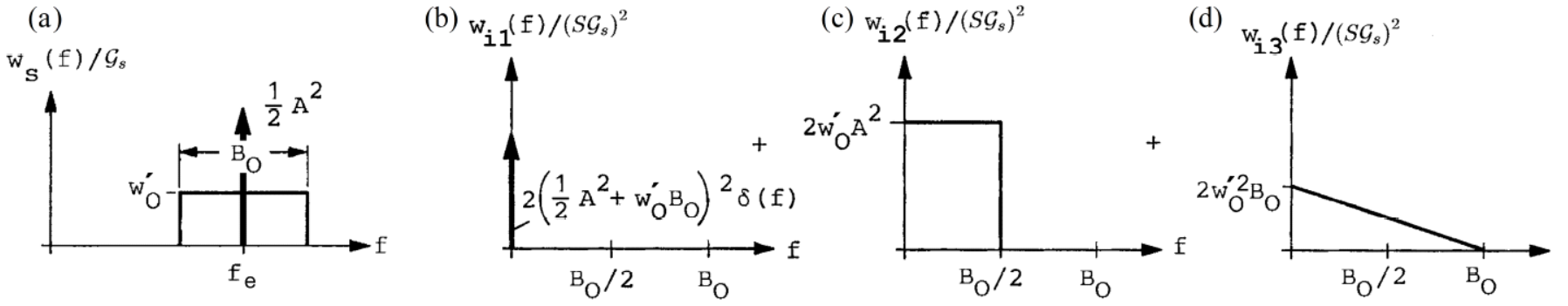

$$F=\frac{\mathrm{SNR}_1}{\mathrm{SNR}_2}=\frac{P_{s1}}{P_{r1}}\Big/\frac{P_{s2}}{P_{r2}}=\frac{P_{r2}}{\mathcal{G}_s P_{r1}}=\frac{\text{polarized output noise power in } B_O}{\text{amplified equiv. pol. input noise power in } B_O}\,. \tag{6.1}$$

SNR_1 at the OA input is

$$\mathrm{SNR}_1=\gamma^{(1)}_{\text{dir qu}}=\gamma_{\text{dir qu}}\big|_{\eta=1}=\frac{P_e}{2w_O B},\qquad w_O=hf_e\,,\qquad S^{(1)}=S\big|_{\eta=1}=\frac{e}{hf_e}\,. \tag{6.2}$$

The approximate SNR at the OA output, Eq. (5.151) on Page 158 is re-written to include also the shot noise term. Taking regard of all OA noise sources $\overline{|i_{RD,1,2,3}|^2}$, we write

$$\mathrm{SNR}_2=\frac{i^2_{S_2}=(S^{(1)}\mathcal{G}_s P_e)^2}{\sum_{i=1}^{3}\overline{|i_{RD,i}|^2}}$$

$$\begin{aligned}\frac{\left(S^{(1)}\mathcal{G}_s P_e\right)^2}{\mathrm{SNR}_2}&=\overline{|i_{RD,1}|^2}+\overline{|i_{RD,2}|^2}+\overline{|i_{RD,3}|^2}\\&=2e\left[S^{(1)}\mathcal{G}_s P_e+S^{(1)}\left(\mathcal{G}_s-1\right)w'_O B_O\right]B+4S^{(1)}\mathcal{G}_s P_e\,S^{(1)}\left(\mathcal{G}_s-1\right)w'_O B\\&\quad+2\left[S^{(1)}\mathcal{G}_s\left(\mathcal{G}_s-1\right)w'_O\right]^2\left(B_O-\tfrac{B}{2}\right)B\end{aligned} \tag{6.3}$$

Noise Figure of Optical Amplifiers (2)

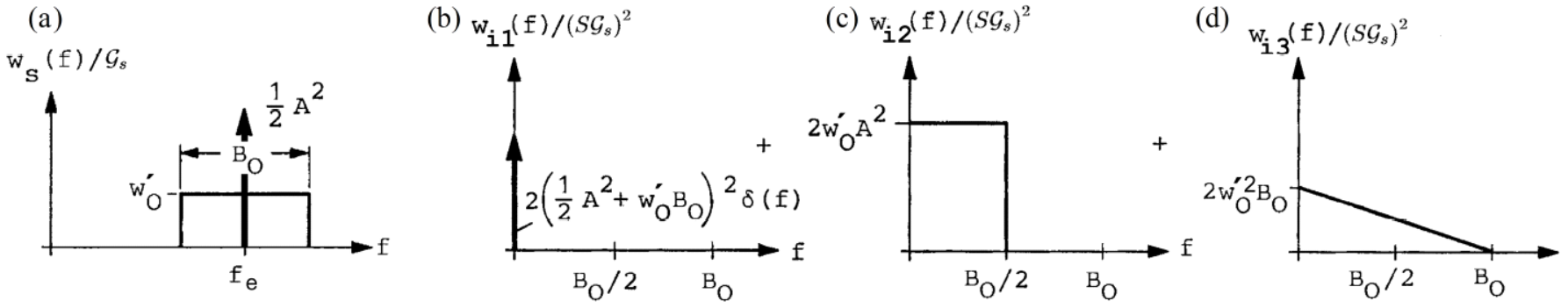

$$F = \frac{\mathrm{SNR}_1}{\mathrm{SNR}_2} = \underbrace{\frac{1}{\mathcal{G}_s}\left[1 + \frac{\mathcal{G}_s - 1}{\mathcal{G}_s}\,\frac{w'_O B_O}{P_e}\right]}_{\text{shot noise: } F_{\mathrm{shot}}} + \underbrace{2\,\frac{\mathcal{G}_s - 1}{\mathcal{G}_s}\,\frac{w'_O}{w_O}}_{\text{signal-noise: } F_{\mathrm{sn}}} + \underbrace{\frac{\mathcal{G}_s - 1}{\mathcal{G}_s}\,\frac{w'_O(B_O - B/2)}{P_e}\,\frac{\mathcal{G}_s - 1}{\mathcal{G}_s}\,\frac{w'_O}{w_O}}_{\text{noise-noise: } F_{\mathrm{nn}}}. \qquad (6.4)$$

SNR_1 at the OA input is

$$\mathrm{SNR}_1 = \gamma^{(1)}_{\mathrm{dir\,qu}} = \gamma_{\mathrm{dir\,qu}}\big|_{\eta=1} = \frac{P_e}{2w_O B}, \qquad w_O = hf_e\,, \qquad S^{(1)} = S|_{\eta=1} = \frac{e}{hf_e}\,. \qquad (6.2)$$

The approximate SNR at the OA output, Eq. (5.151) on Page 158 is re-written to include also the shot noise term. Taking regard of all OA noise sources $\overline{|i_{RD,1,2,3}|^2}$, we write

$$\begin{aligned}\frac{\left(S^{(1)}\mathcal{G}_s P_e\right)^2}{\mathrm{SNR}_2} &= \overline{|i_{RD,1}|^2} + \overline{|i_{RD,2}|^2} + \overline{|i_{RD,3}|^2} \\ &= 2e\left[S^{(1)}\mathcal{G}_s P_e + S^{(1)}\left(\mathcal{G}_s - 1\right)w'_O B_O\right]B + 4S^{(1)}\mathcal{G}_s P_e\, S^{(1)}\left(\mathcal{G}_s - 1\right)w'_O B \\ &\quad + 2\left[S^{(1)}\mathcal{G}_s\left(\mathcal{G}_s - 1\right)w'_O\right]^2\left(B_O - \tfrac{B}{2}\right)B \qquad (6.3)\end{aligned}$$

Noise Figure of Optical Amplifiers (3)

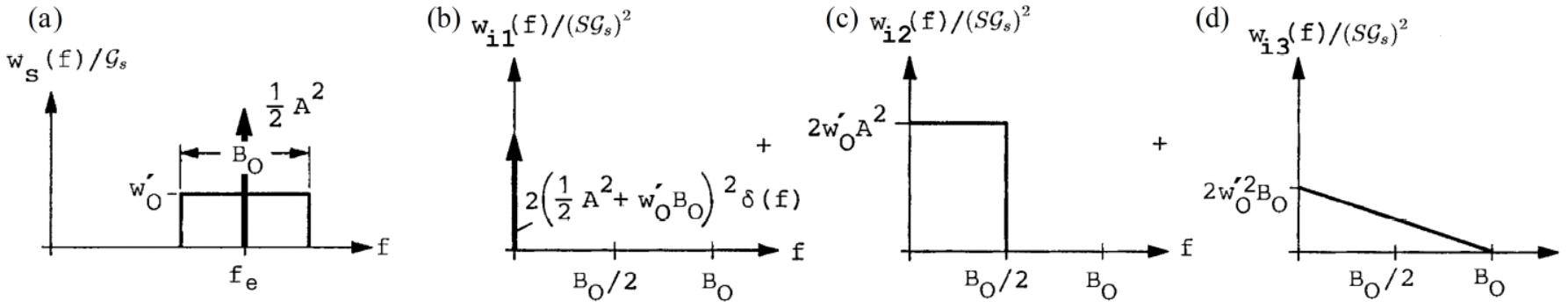

$$F = \frac{\mathrm{SNR}_1}{\mathrm{SNR}_2} = \underbrace{\frac{1}{\mathcal{G}_s}\left[1 + \frac{\mathcal{G}_s - 1}{\mathcal{G}_s}\,\frac{w'_O B_O}{P_e}\right]}_{\text{shot noise: } F_{\mathrm{shot}}} + \underbrace{2\,\frac{\mathcal{G}_s - 1}{\mathcal{G}_s}\,\frac{w'_O}{w_O}}_{\text{signal-noise: } F_{\mathrm{sn}}} + \underbrace{\frac{\mathcal{G}_s - 1}{\mathcal{G}_s}\,\frac{w'_O(B_O - B/2)}{P_e}\,\frac{\mathcal{G}_s - 1}{\mathcal{G}_s}\,\frac{w'_O}{w_O}}_{\text{noise-noise: } F_{\mathrm{nn}}}. \qquad (6.4)$$

For a transparent, i. e., nonexisting OA with $\mathcal{G}_s = 1$, there is no additional noise and $F = 1$. Spontaneous emission factor n_{sp} and gain $\mathcal{G}_s$ are linked. If the gain is larger than but close to one, then the spontaneous emission factor is very large. This expression for the noise factor depends on the input signal power P_e. However, simplifications apply for the following typical data: Signal frequency $f_e = 193.4\,\mathrm{THz}$, OA bandwidth $B_O \approx 3\,\mathrm{THz} \geq 2B$, $w'_O B_O \ll P_e$, noise power $w'_O B_O \approx 2hf_e B_O = 0.77\,\mu\mathrm{W} \mathrel{\widehat{=}} -31\,\mathrm{dBm}$ ($F \approx 4 \mathrel{\widehat{=}} 6\,\mathrm{dB}$), $P_e \gtrapprox -20\,\mathrm{dBm}$, $\mathcal{G}_s \geq 2$. Under these assumptions the red-coloured terms can be neglected, while the blue-coloured terms remain,

$$F \approx F_{\mathrm{shot}} + F_{\mathrm{sn}} \approx \frac{1}{\mathcal{G}_s} + 2\,\frac{\mathcal{G}_s - 1}{\mathcal{G}_s}\,\frac{w'_O}{w_O}, \quad 1 < n_{\mathrm{sp}} < \infty, \quad w'_O = n_{\mathrm{sp}} w_O, \quad w_O = hf_e. \qquad (6.5)$$

Noise Figure of Optical Amplifiers (4)

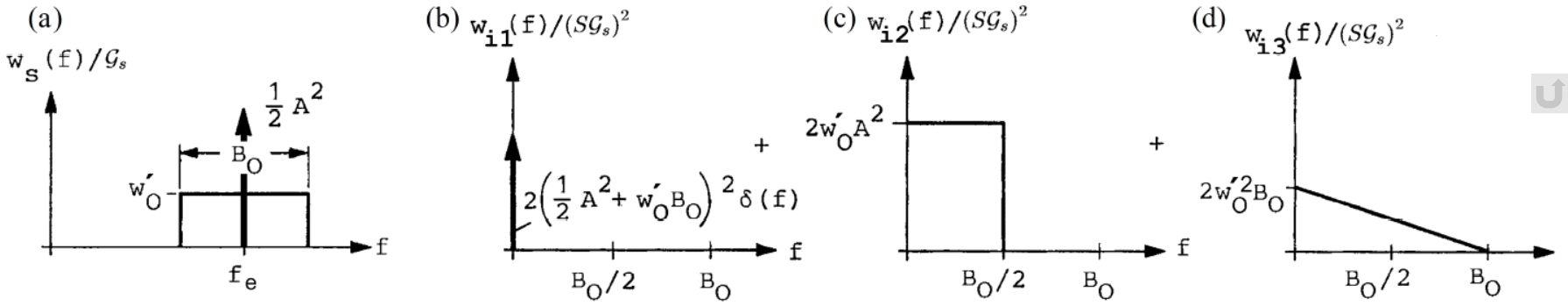

For a transparent, i. e., nonexisting OA with $\mathcal{G}_s = 1$, there is no additional noise and $F = 1$. Spontaneous emission factor n_{sp} and gain $\mathcal{G}_s$ are linked. If the gain is larger than but close to one, then the spontaneous emission factor is very large. This expression for the noise factor depends on the input signal power P_e. However, simplifications apply for the following typical data: Signal frequency $f_e = 193.4\,\mathrm{THz}$, OA bandwidth $B_O \approx 3\,\mathrm{THz} \geq 2B$, $w'_O B_O \ll P_e$, noise power $w'_O B_O \approx 2hf_e B_O = 0.77\,\mu\mathrm{W} \mathrel{\widehat{=}} -31\,\mathrm{dBm}$ ($F \approx 4 \mathrel{\widehat{=}} 6\,\mathrm{dB}$), $P_e \mathrel{\widehat{\approx}} 0\,\mathrm{dBm}$, $\mathcal{G}_s \geq 2$. Under these assumptions the red-coloured terms can be neglected, while the blue-coloured terms remain,

$$F \approx F_{\mathrm{shot}} + F_{\mathrm{sn}} \approx \frac{1}{\mathcal{G}_s} + 2\,\frac{\mathcal{G}_s - 1}{\mathcal{G}_s}\,\frac{w'_O}{w_O}\,, \quad 1 < n_{\mathrm{sp}} < \infty, \quad w'_O = n_{\mathrm{sp}} w_O\,, \quad w_O = hf_e\,. \tag{6.5}$$

If in addition the amplifier gain is large (in practice we have $\mathcal{G}_s \approx 100 \mathrel{\widehat{=}} 20\,\mathrm{dB}$), the noise figure due to shot noise can be neglected, and we end up with the simple relation for the noise figure of an optical amplifier operated at a signal frequency f_e,

$$F \approx F_{\mathrm{sn}} \approx 2n_{\mathrm{sp}}\,, \quad \mathcal{G}_s \gg 1\,, \quad 1 < n_{\mathrm{sp}} < \infty, \quad w'_O = n_{\mathrm{sp}} w_O\,, \quad w_O = hf_e\,. \tag{6.6}$$

For a fully inverted, ideal optical amplifier the minimum noise figure is $F = 2 \mathrel{\widehat{=}} 3\,\mathrm{dB}$. Real-world amplifiers have noise figures of $(4 \ldots 8)\,\mathrm{dB}$.

Noise Figure of Optical Amplifiers (5)

We can apply the recipe Eq. (6.1) for calculating the OA noise figure also for the case of heterodyne reception (Eq. (5.124) on Page 144, Eq. (5.154) on Page 160), and for homodyne reception (Eq. (5.130) on Page 146, Eq. (5.158) on Page 161),

$$\begin{aligned}
&\mathrm{SNR}_1: && \gamma^{(1)}_{\text{dir qu}} = \frac{P_e}{2hf_eB} && \gamma^{(1)}_{\text{BB-het qu}} = \frac{P_s}{hf_OB} && \gamma^{(1)}_{\text{hom qu}} = \frac{P_s}{\frac{1}{2}hf_OB} \\
&\mathrm{SNR}_2: && \gamma_{\text{dir OA qu}} = \frac{1}{2n_{\text{sp}}}\frac{P_e}{2hf_eB} && \gamma_{\text{BB-het OA qu}} = \frac{1}{2n_{\text{sp}}}\frac{P_s}{hf_OB} && \gamma_{\text{hom OA qu}} = \frac{1}{2n_{\text{sp}}}\frac{P_s}{\frac{1}{2}hf_OB}
\end{aligned} \tag{6.8a}$$

and each time we find the same result for the noise figure of an optical amplifier,

$$F = \frac{\mathrm{SNR}_1}{\mathrm{SNR}_2} = 2n_{\text{sp}}\,. \tag{6.8b}$$

6.2.3 Noise figure of a lossy fibre

Finally, we compute the noise figure of a fibre with a power gain factor $0 < g \leq 1$. As before, the quantum-noise limited input SNR is given by Eq. (5.81) on Page 132. The fibre itself does not contribute noise (let aside a negligible amount of thermal noise, because $kT_0 \ll hf_e$), but the output power is reduced to gP_e, and this carries over to the output SNR. The noise figure F_g becomes simply

$$\mathrm{SNR}_1 = \frac{\eta P_e}{2hf_eB}\,, \qquad \mathrm{SNR}_2 = \frac{\eta g P_e}{2hf_eB}\,, \qquad F_g = \frac{1}{g}\,, \qquad 0 < g \leq 1\,. \tag{6.16}$$

But: If SNR_1 *not* given by quantum noise, but classical noise, then signal and noise attenuated alike, and $\mathrm{SNR}_2 = \mathrm{SNR}_1 \rightarrow F_g = 1$.

Noise Figure of Optical Amplifier Link

$$\mathcal{G}_{\text{tot}} = \prod_{n=1}^{N} \mathcal{G}_n\, g_n$$

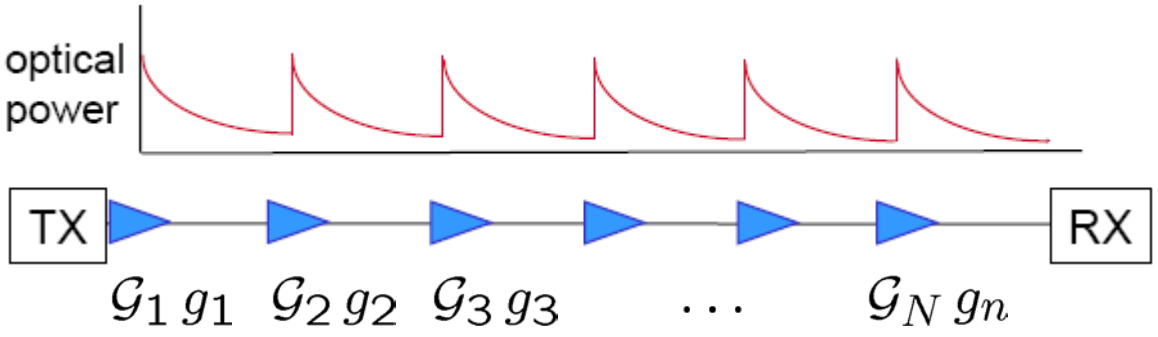

With the partial noise figures $F_{sn}^{(n)}$ as used in Eq. (6.5) on Page 164, we find the total link noise figure

$$F_N^{(\mathcal{G}_n g_n)} = \frac{1}{\mathcal{G}_{\text{tot}}} + \left(F_{\text{sn}}^{(1)} + \frac{F_{\text{sn}}^{(2)}}{\mathcal{G}_1 g_1} + \frac{F_{\text{sn}}^{(3)}}{\mathcal{G}_1 g_1\, \mathcal{G}_2 g_2} + \ldots + \frac{F_{\text{sn}}^{(N)}}{\prod_{n=1}^{N-1} \mathcal{G}_n g_n} \right), \quad F_{\text{sn}}^{(n)} = 2\, \frac{\mathcal{G}_n - 1}{\mathcal{G}_n}\, \frac{w_O^{(n)}}{w_O}\,. \quad (6.12)$$

Equation (6.12) looks very similar to Friis' formula for the noise figure of an electronic amplifier chain for given individual excess noise figures $F_{z\,n}$ and available gains $\Gamma_{v\,n}$, Eq. (5.62b), (5.65) on Page 127,

$$F_N = 1 + \left(F_{z\,1} + \frac{F_{z\,2}}{\Gamma_{v\,1}} + \frac{F_{z\,3}}{\Gamma_{v\,1}\Gamma_{v\,2}} + \ldots + \frac{F_{z\,N}}{\prod_{n=1}^{N-1} \Gamma_{v\,n}} \right) \qquad \text{(noise figure for thermal noise).} \quad (6.13)$$

The difference comes from the fact that Friis' formula Eq. (6.13) describes thermal noise, while Eq. (6.12) specifies shot (quantum) noise and ASE noise.

Noise Figure of Optical Amplifier Link $\mathcal{G}_{\text{tot}} = \prod_{n=1}^{N} g_n \mathcal{G}_n$

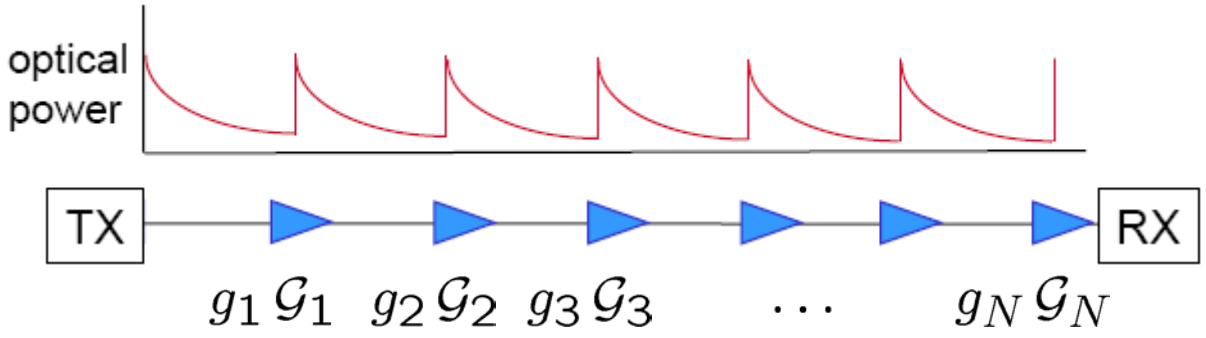

If the sequence of "OA, filter, lossy fibre length" was reversed to "lossy fibre length, OA, filter" in each link, the total link noise figure becomes

$$F_N^{(g_n\mathcal{G}_n)} = \frac{1}{\mathcal{G}_{\text{tot}}} + \frac{1}{g_1}\left(F_{\text{sn}}^{(1)} + \frac{F_{\text{sn}}^{(2)}}{\mathcal{G}_1 g_2} + \frac{F_{\text{sn}}^{(3)}}{\mathcal{G}_1 g_2\,\mathcal{G}_2 g_3} + \ldots + \frac{F_{\text{sn}}^{(N)}}{\prod_{n=1}^{N}\mathcal{G}_{n-1} g_n}\right), \quad F_{\text{sn}}^{(n)} = 2\,\frac{\mathcal{G}_n - 1}{\mathcal{G}_n}\,\frac{w_O^{(n)}}{w_O}\,. \quad (6.14)$$

Frequently, the individual links have virtually identical characteristics, i. e., $\mathcal{G}_n = \mathcal{G}$, $g_n = g$, $w_O^{(n)} = w_O'$, and serve to bridge a total link distance with a net gain of $\mathcal{G}_{\text{tot}} = 1$, i. e., $\mathcal{G}g = 1$. The two arrangements "OA, filter, lossy fibre length" $(\mathcal{G}g)$ and "lossy fibre length, OA, filter" $(g\mathcal{G})$ lead to total noise figures of $F_N^{(\mathcal{G}g)}$ and $F_N^{(g\mathcal{G})}$, respectively,

$$F_N^{(\mathcal{G}g)} = 1 + NF_{\text{sn}}\,, \qquad F_N^{(g\mathcal{G})} = 1 + N\mathcal{G}F_{\text{sn}}\,, \qquad \mathcal{G}_{\text{tot}} = 1\,, \qquad \mathcal{G}g = 1\,, \qquad F_{\text{sn}}^{(n)} = F_{\text{sn}}\,. \quad (6.15)$$

With an OA gain of $\mathcal{G} = 10 \mathrel{\widehat{=}} 10\,\text{dB}$ and an OA noise figure of $F_{\text{sn}} = 4$ $(F = \frac{1}{10} + 4 \approx 4 \mathrel{\widehat{=}} 6\,\text{dB})$ for $N = 10$ links, the arrangement $(\mathcal{G}g)$ has a total noise figure $F_{10}^{(\mathcal{G}g)} = 41$, while an element order with the lossy fibre length in front of the amplifiers shows a *much* larger $\mathcal{G}$-fold noise figure of $F_{10}^{(g\mathcal{G})} = 401$.

Signal Shaping

Elements of a Communications System

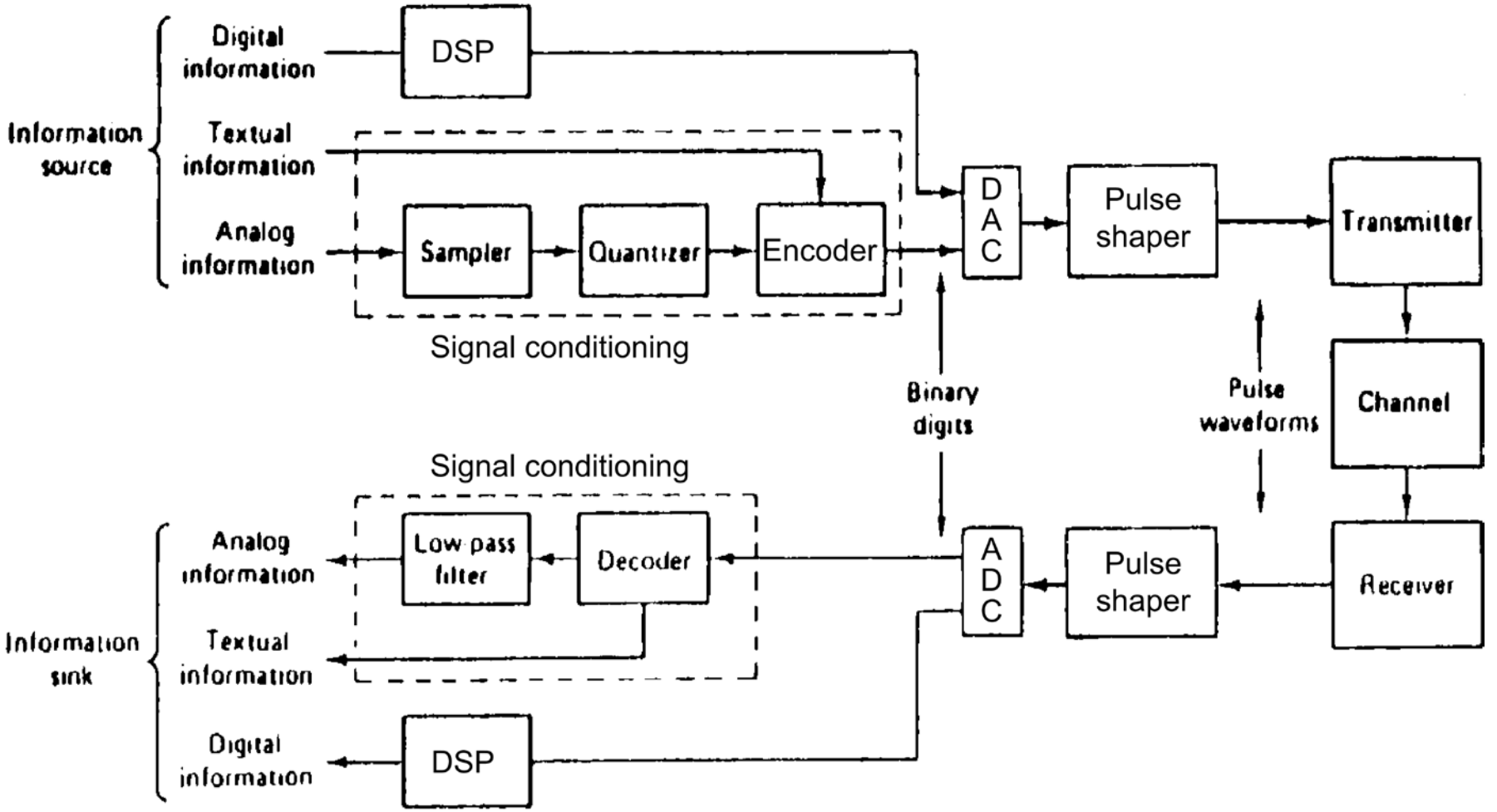

NRZ Spectrum for M-ary Quadrature-Amplitude Modulation

M-QAM power spectrum:

- Rectangular NRZ pulses, therefore
- sinc-shaped spectra for NRZ M-QAM signals.
- Periodic repetition of spectrum due to time-discrete sampling
- Complete signal information contained within Nyquist band

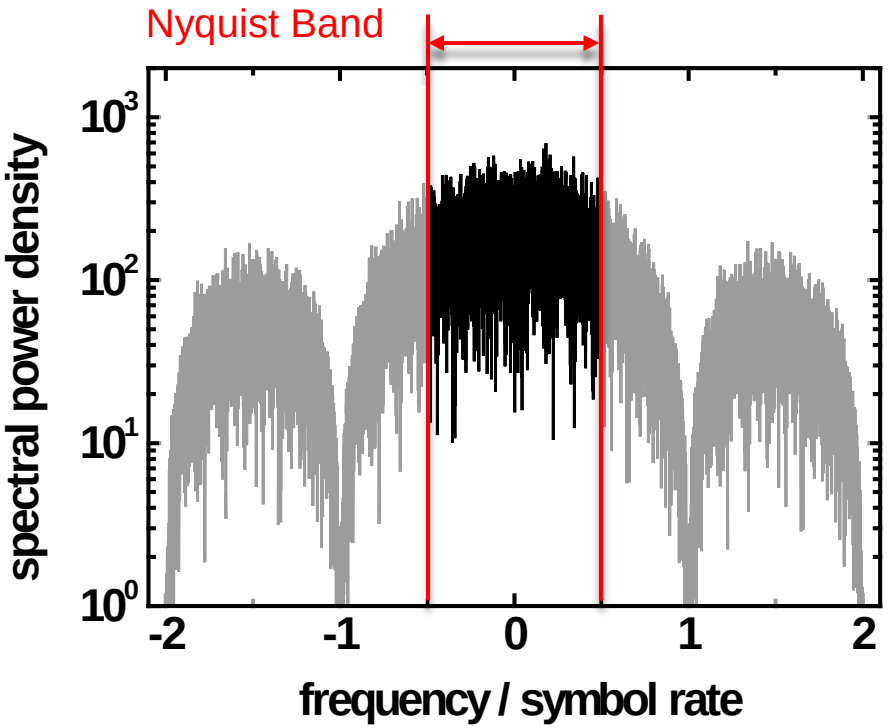

Increasing the Spectral Efficiency for WDM Systems

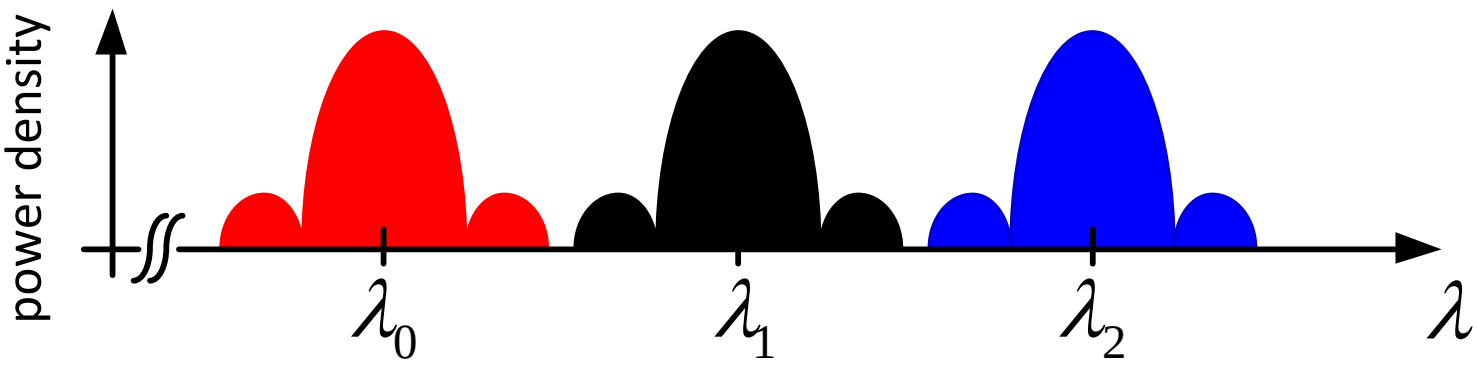

Procedures and their effects:

- Removing spectral redundancies without signal degradation
- Reducing the carrier grid spacing without lowering symbol rate
- Spectrum saving at Tx beneficial for transmission and Rx
- Efficiency limits set by Nyquist rate $\rightarrow$ "Nyquist WDM"
- Analogy to OFDM $\rightarrow$ also known as orthogonal time division multiplexing OTDM

Schmogrow, R.; Winter, M.; Meyer, M.; Hillerkuss, D.; Nebendahl, B.; Meyer, J.; Dreschmann, M.; Huebner, M.; Becker, J.; Koos, C.; Freude, W.; Leuthold, J.: 'Nyquist pulse modulation transmitter generating rectangular spectra of 112 Gbit/s 16QAM in real-time,' *Conf. on Signal Processing in Photonics Communications (SPPCom'11)*, Toronto, Canada, June 12–15, 2011. Paper SPMA5

Enhancement of WDM Systems

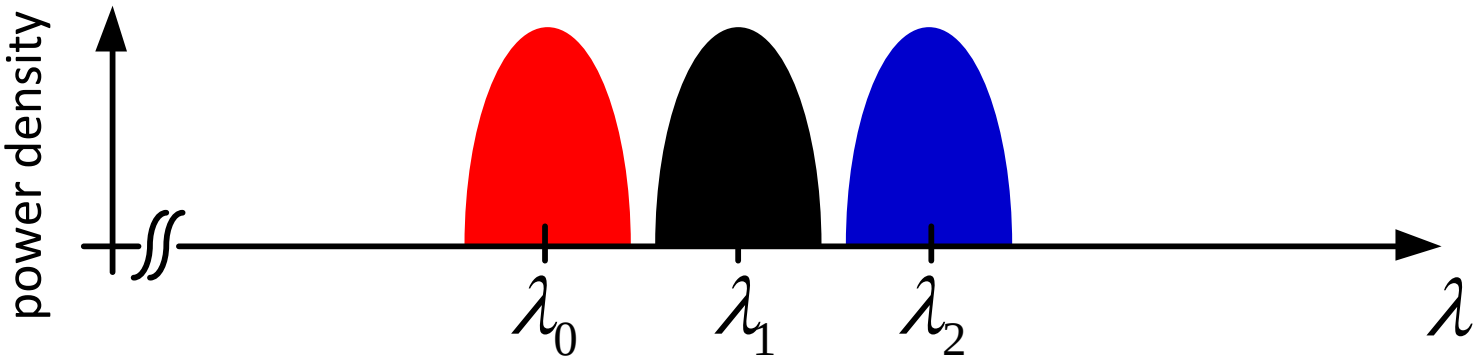

Procedures and their effects:

- Removing spectral redundancies without signal degradation
- Reducing the carrier grid spacing without lowering symbol rate
- Spectrum saving at Tx beneficial for transmission and Rx
- Efficiency limits set by Nyquist rate → "Nyquist WDM"
- Analogy to OFDM → also known as orthogonal time division multiplexing OTDM

Schmogrow, R.; Winter, M.; Meyer, M.; Hillerkuss, D.; Nebendahl, B.; Meyer, J.; Dreschmann, M.; Huebner, M.; Becker, J.; Koos, C.; Freude, W.; Leuthold, J.: 'Nyquist pulse modulation transmitter generating rectangular spectra of 112 Gbit/s 16QAM in real-time,' *Conf. on Signal Processing in Photonics Communications (SPPCom'11)*, Toronto, Canada, June 12–15, 2011. Paper SPMA5

Enhancement of WDM Systems

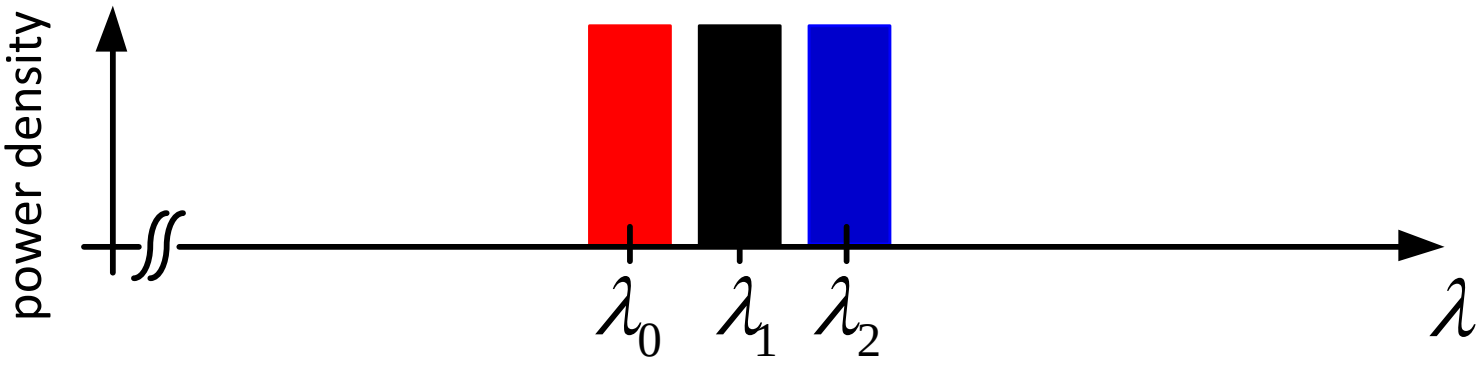

Procedures and their effects:

- Removing spectral redundancies without signal degradation
- Reducing the carrier grid spacing without lowering symbol rate
- Spectrum saving at Tx beneficial for transmission and Rx
- Efficiency limits set by Nyquist rate $\rightarrow$ "Nyquist WDM"
- Analogy to OFDM $\rightarrow$ also known as orthogonal time division multiplexing OTDM

Schmogrow, R.; Winter, M.; Meyer, M.; Hillerkuss, D.; Nebendahl, B.; Meyer, J.; Dreschmann, M.; Huebner, M.; Becker, J.; Koos, C.; Freude, W.; Leuthold, J.: 'Nyquist pulse modulation transmitter generating rectangular spectra of 112 Gbit/s 16QAM in real-time,' *Conf. on Signal Processing in Photonics Communications (SPPCom'11)*, Toronto, Canada, June 12–15, 2011. Paper SPMA5

Enhancement of WDM Systems

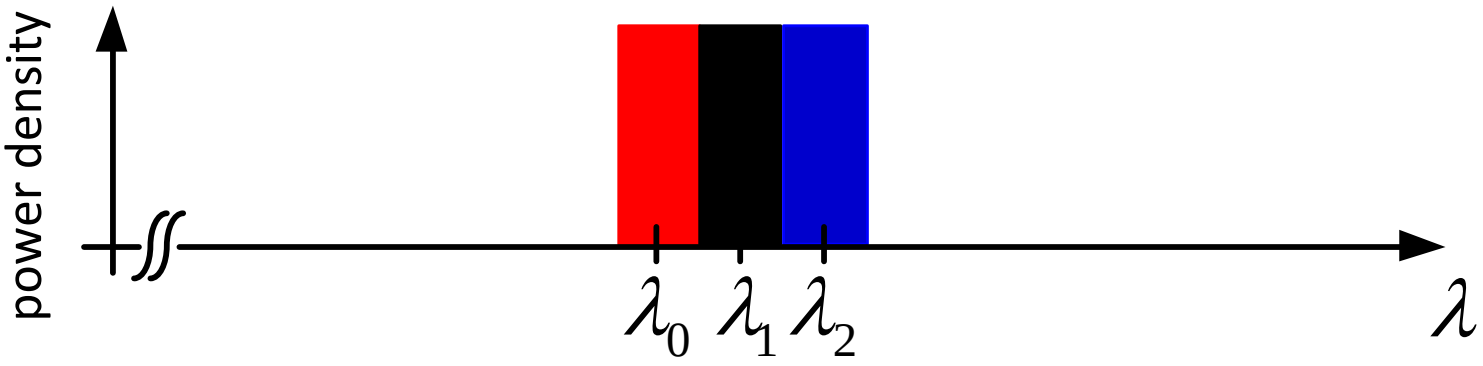

Procedures and their effects:

- Removing spectral redundancies without signal degradation
- Reducing the carrier grid spacing without lowering symbol rate
- Spectrum saving at Tx beneficial for transmission and Rx
- Efficiency limits set by Nyquist rate $\rightarrow$ "Nyquist WDM"
- Analogy to OFDM $\rightarrow$ also known as orthogonal time division multiplexing OTDM

Schmogrow, R.; Winter, M.; Meyer, M.; Hillerkuss, D.; Nebendahl, B.; Meyer, J.; Dreschmann, M.; Huebner, M.; Becker, J.; Koos, C.; Freude, W.; Leuthold, J.: 'Nyquist pulse modulation transmitter generating rectangular spectra of 112 Gbit/s 16QAM in real-time,' *Conf. on Signal Processing in Photonics Communications (SPPCom'11)*, Toronto, Canada, June 12–15, 2011. Paper SPMA5

OTDM (Nyqist-WDM) SDOTx — Experiments at $\lambda = 1.55\,\mu m$

- Optical IQ-modulator for complex real-time Nyquist pulse modulation
- Agilent N4391A optical modulation analyzer for reception using standard M-QAM algorithms

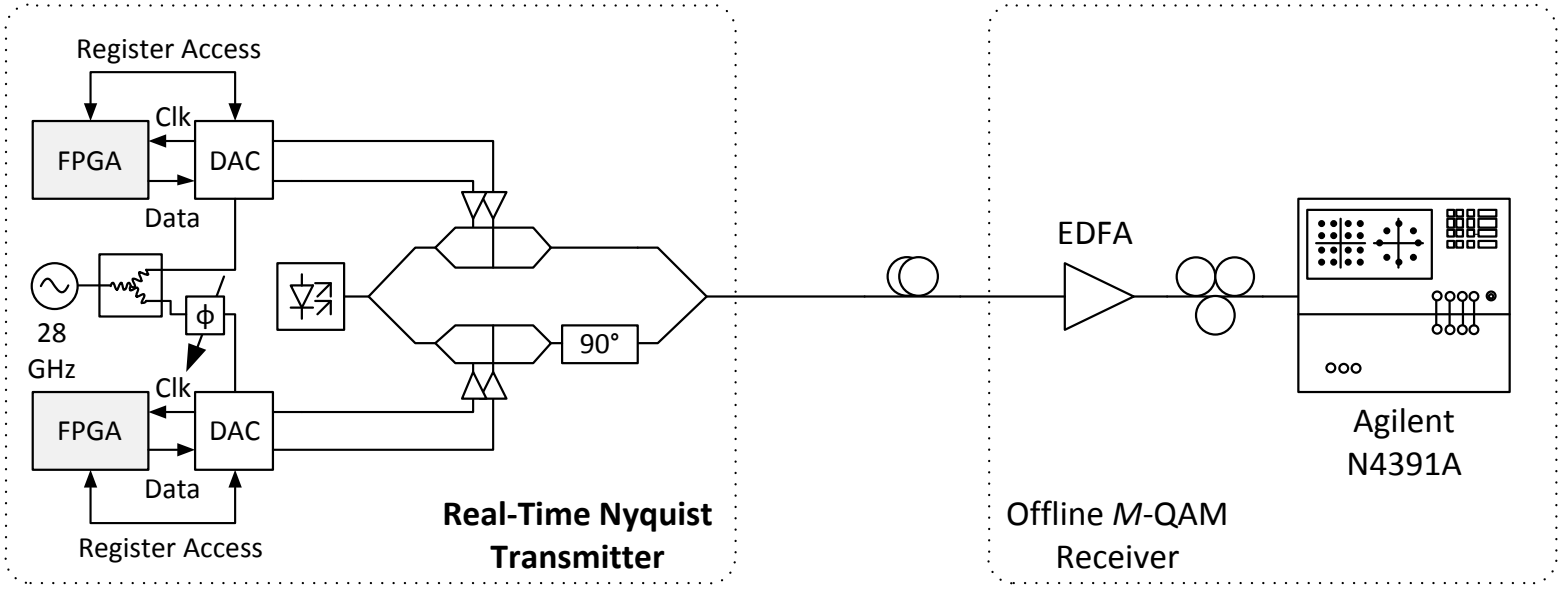

Schmogrow, R.; Winter, M.; Meyer, M.; Hillerkuss, D.; Nebendahl, B.; Meyer, J.; Dreschmann, M.; Huebner, M.; Becker, J.; Koos, C.; Freude, W.; Leuthold, J.: 'Nyquist pulse modulation transmitter generating rectangular spectra of 112 Gbit/s 16QAM in real-time,' *Conf. on Signal Processing in Photonics Communications (SPPCom'11)*, Toronto, Canada, June 12–15, 2011. Paper SPMA5

OTDM (Nyqist-WDM) SDOTx — Experiments at $\lambda = 1.55\,\mu m$

- Optical filter for carving out rectangular spectrum
- Complicated filter, no easy solution

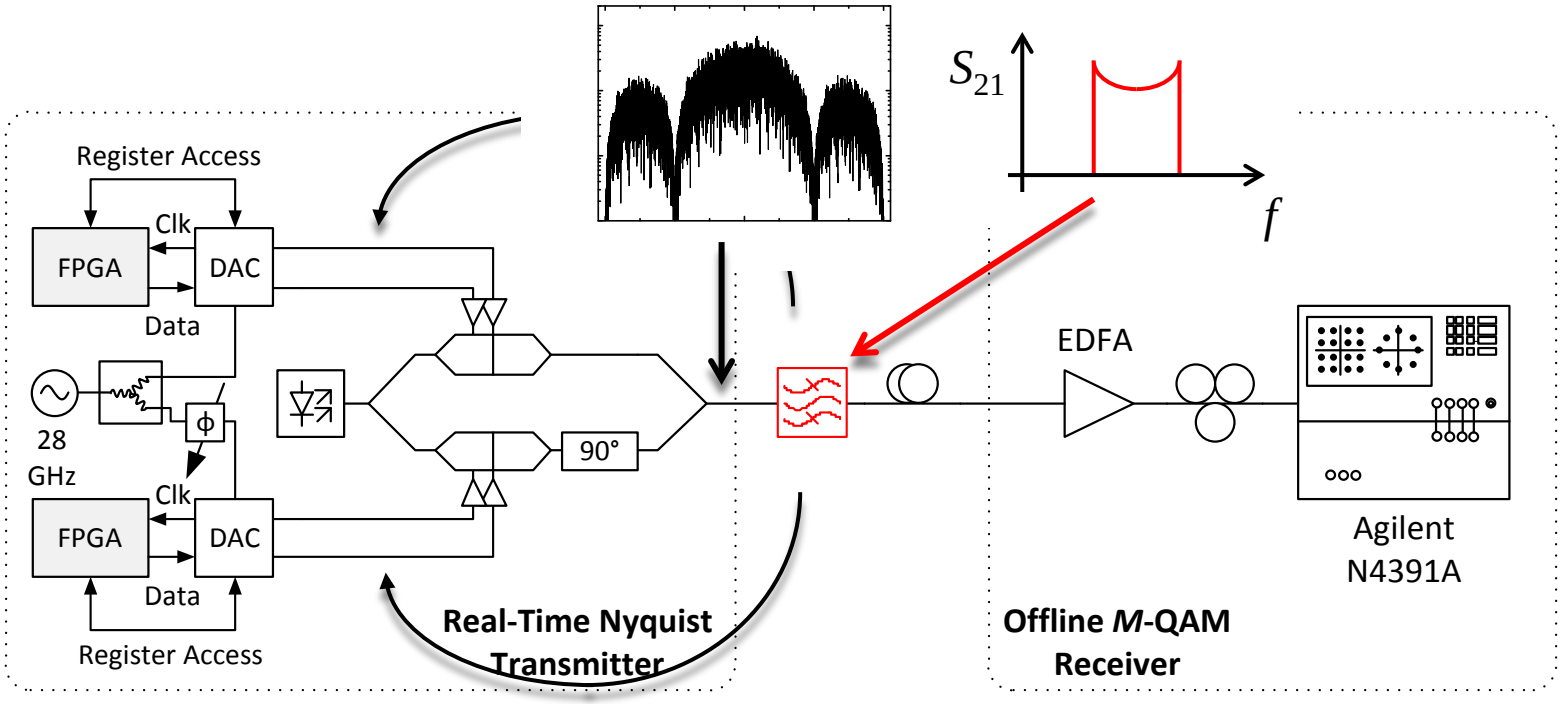

Schmogrow, R.; Winter, M.; Meyer, M.; Hillerkuss, D.; Nebendahl, B.; Meyer, J.; Dreschmann, M.; Huebner, M.; Becker, J.; Koos, C.; Freude, W.; Leuthold, J.: 'Nyquist pulse modulation transmitter generating rectangular spectra of 112 Gbit/s 16QAM in real-time,' *Conf. on Signal Processing in Photonics Communications (SPPCom'11)*, Toronto, Canada, June 12–15, 2011. Paper SPMA5

OTDM (Nyqist-WDM) SDOTx — Experiments at $\lambda = 1.55\,\mu m$

- Electrical filter for carving out rectangular spectrum
- Complicated filter, no easy solution

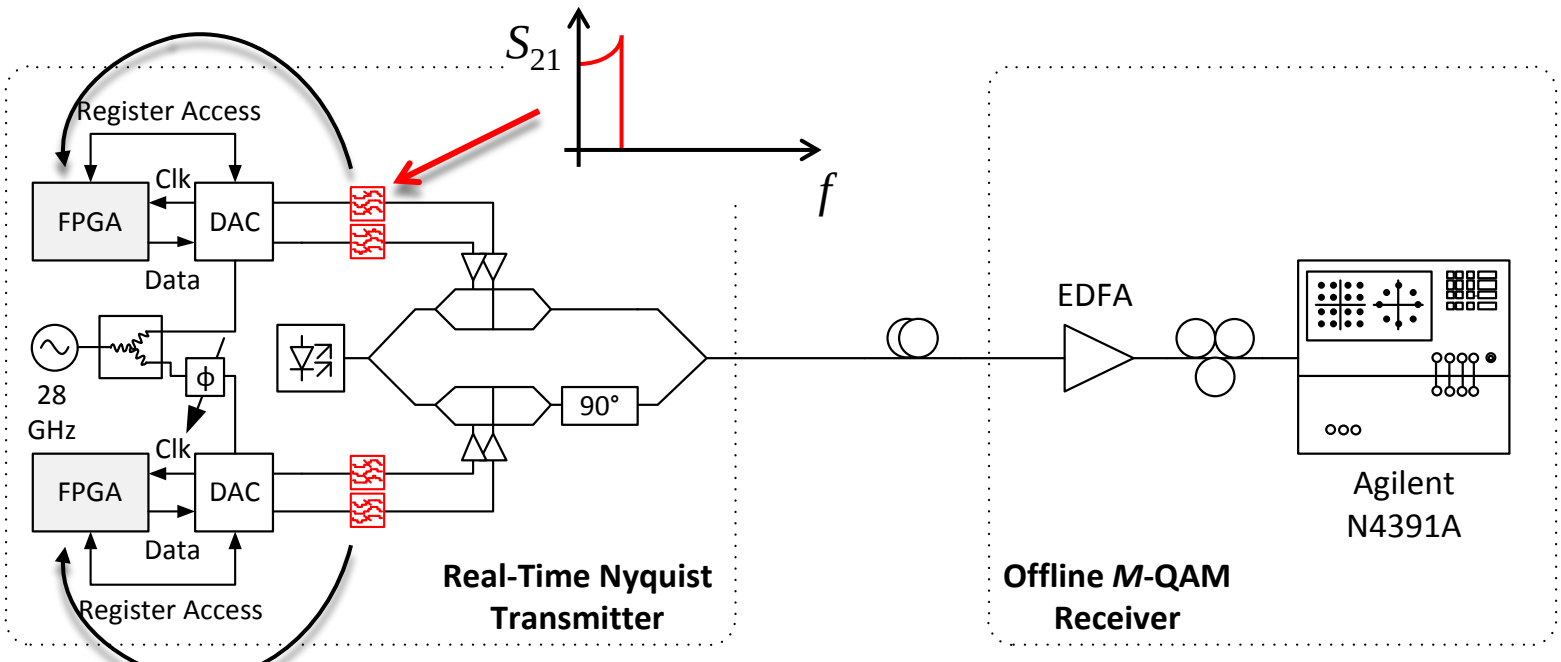

Schmogrow, R.; Winter, M.; Meyer, M.; Hillerkuss, D.; Nebendahl, B.; Meyer, J.; Dreschmann, M.; Huebner, M.; Becker, J.; Koos, C.; Freude, W.; Leuthold, J.: 'Nyquist pulse modulation transmitter generating rectangular spectra of 112 Gbit/s 16QAM in real-time,' *Conf. on Signal Processing in Photonics Communications (SPPCom'11)*, Toronto, Canada, June 12–15, 2011. Paper SPMA5

OTDM (Nyqist-WDM) SDOTx — Experiments at $\lambda = 1.55\,\mu m$

- Digital filter with DSP
- State-of-the-art FPGA for high-performance FIR filters
- Penalty due to finite length of digital filter

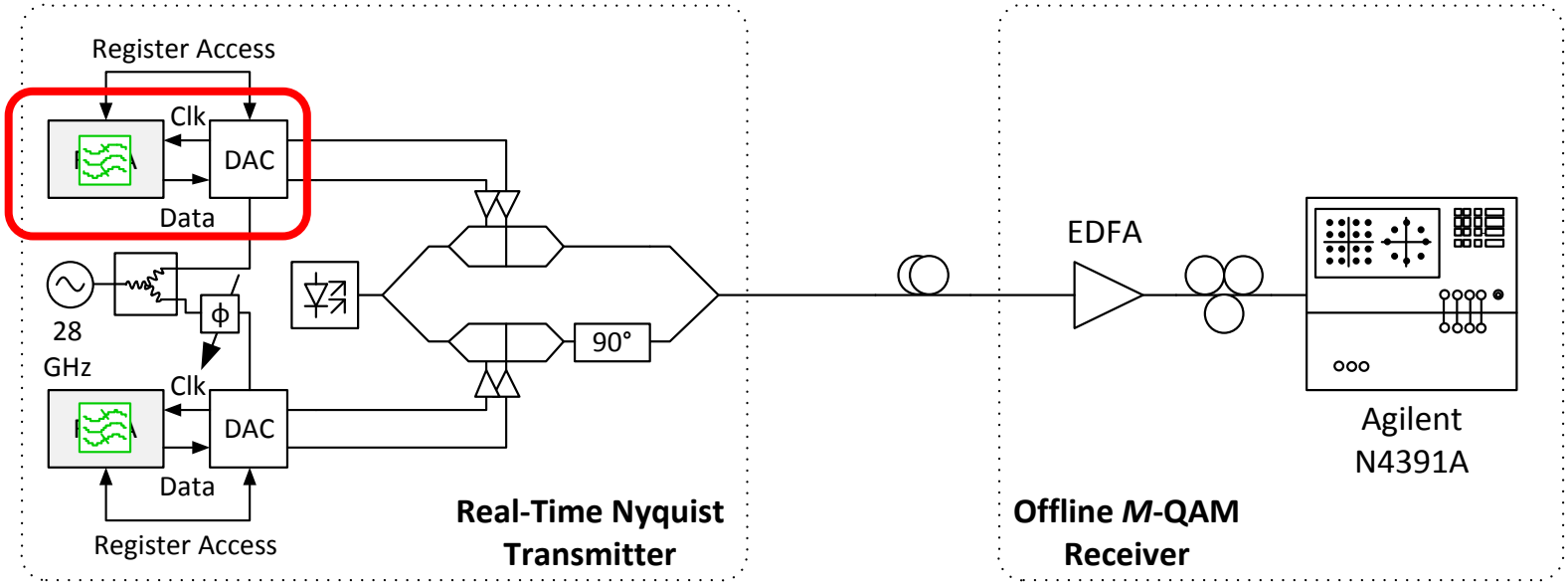

Schmogrow, R.; Winter, M.; Meyer, M.; Hillerkuss, D.; Nebendahl, B.; Meyer, J.; Dreschmann, M.; Huebner, M.; Becker, J.; Koos, C.; Freude, W.; Leuthold, J.: 'Nyquist pulse modulation transmitter generating rectangular spectra of 112 Gbit/s 16QAM in real-time,' *Conf. on Signal Processing in Photonics Communications (SPPCom'11)*, Toronto, Canada, June 12–15, 2011. Paper SPMA5

Signal Impulse Responses and Transfer Functions

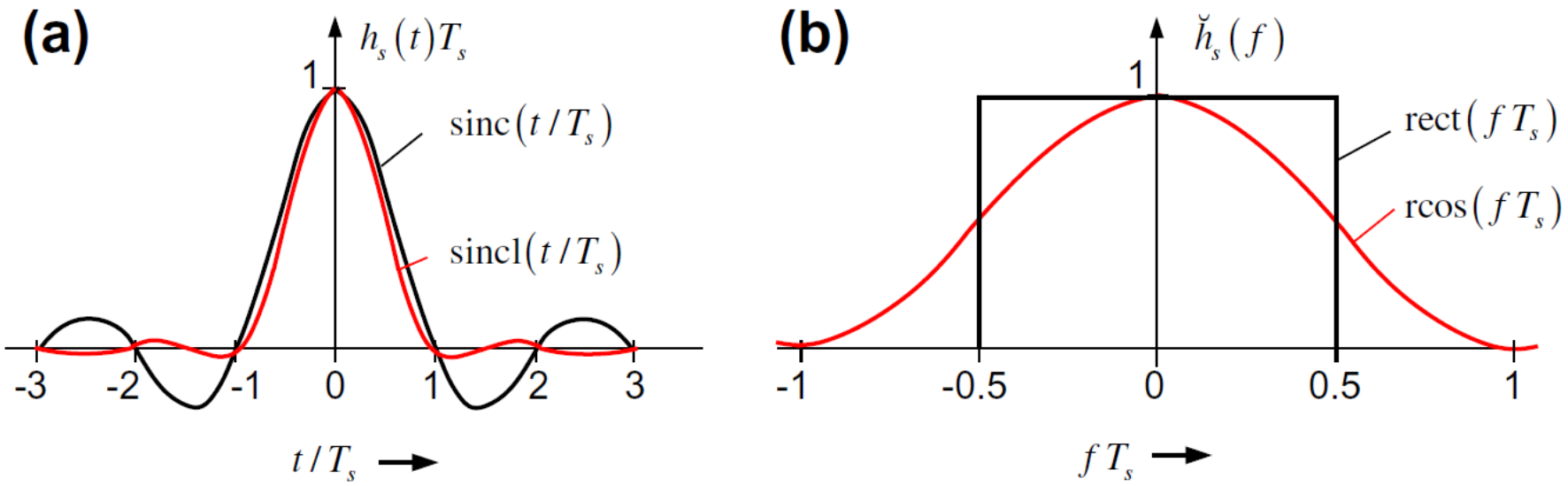

FIGURE 9.6 Impulse responses $h(t)$ and transfer functions $\breve{h}(f)$ of finite length that still provide disappearing inter-symbol interference (ISI). (a) Sinc-function Eq. (9.65) and sinc-like function sincl Eq. (9.66). (b) Spectral rect-function Eq. (9.62) and spectral rcos-function (raised cosine) Eq. (9.63).

Signal Shapes in the Digital, Electrical, and Optical Domain

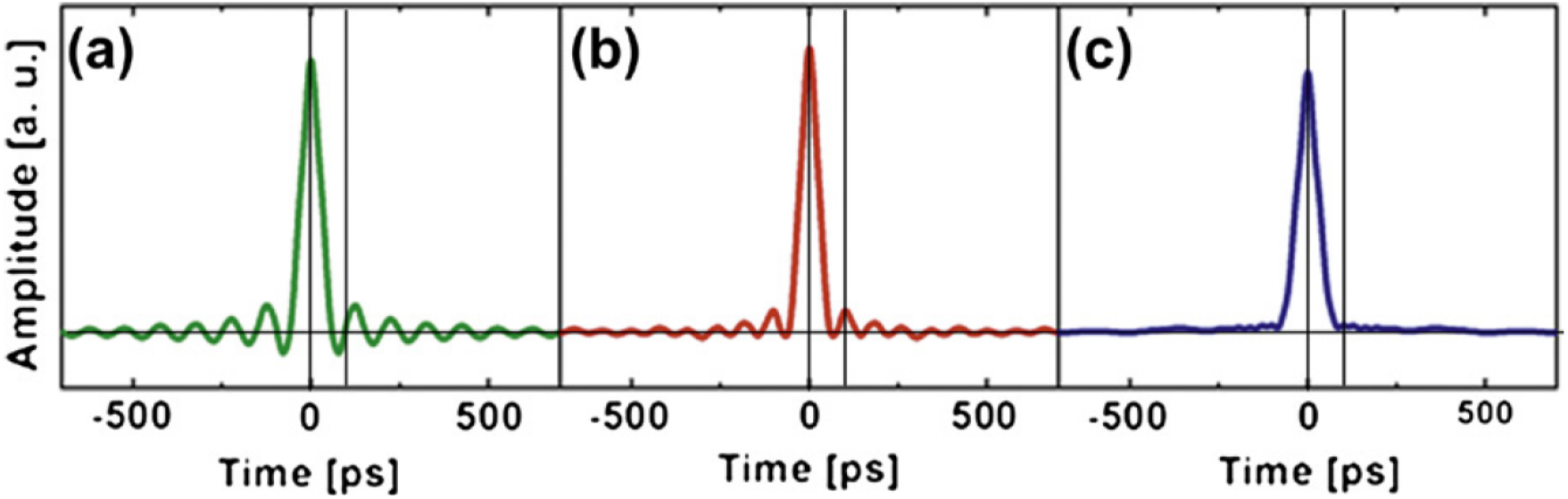

FIGURE 9.8 Different impulse responses measured from received spectra with (a) digital, (b) electrical, and (c) optical pulse-shapers. As expected, the digital pulse-shaper approximates a sinc-function Figure 9.3b closely. The electrical pulse-shaper still produces sinc-typical side lobes, whereas the optical pulse-shaper matches a sinc-function worst. (Figure modified from Ref. [37])

END OF LECTURES